# DEVELOPMENT OF KNOWLEDGE-BASED CRITERIA FOR DESIGNING FOOT ORTHOSES

By

CHEUNG TAK MAN, JASON

*B. Eng., M.Phil.*

A thesis submitted in partial fulfilment of the requirements for the Degree of Doctor of Philosophy in Biomedical Engineering

October 2005

Department of Health Technology and Informatics
The Hong Kong Polytechnic University

# CERTIFICATE OF ORIGINALITY

I hereby declare that this thesis is my own work and that, to the best of my knowledge and belief, it reproduces no material previously published or written, nor material that has been accepted for the award of any other degree or diploma, except where due acknowledge has been made in the text.

(Cheung Tak Man, Jason)

**Abstract of thesis entitled**

"Development of Knowledge-based Criteria for Designing Foot Orthoses"

Submitted by

**Cheung Tak Man, Jason**

for the degree of

Doctor of Philosophy in Biomedical Engineering

at The Hong Kong Polytechnic University

in Oct 2005

Diabetes especially for those with peripheral neuropathy are susceptible for developing neuropathic ulcers on the plantar foot surface, which frequently lead to hospitalization and limb amputations. One of the major causes of diabetic ulceration and plantar foot pain is thought to be the presence of abnormally high plantar foot pressures. Increasing evidence suggests that diabetic feet and painful foot syndrome can be successfully resolved or relieved with a proper foot orthosis, helping to correct ankle-foot abnormalities and to relieve and redistribute elevated plantar pressures.

Numerous *in vivo* experimental studies have been directed to analyze the performance of specific orthosis in terms of subject comfort and disability level, plantar foot pressure relief or redistribution and its functional role in correcting pathological gait and providing good foot support. Owing to the complexity of the ankle-foot structures and experimental difficulties, most studies focused on subjective assessments, gross joint motions and plantar pressure distribution between the foot and supports. The rationale behind the functional role of a foot orthosis on the load distribution and stabilizing ability relies mainly on subjective views, interfacial pressure measurements, or gross motion tracking.

In order to provide a supplement to the experimental inadequacy, many researchers had turned to the computational methods in search of more clinical information.

Computational modeling, such as the finite element (FE) method can be an adjunct to experimental approach to predict the load distribution between the foot and different supports, which offer additional information such as the internal stress and strain of the ankle-foot complex. The FE analyses can allow efficient parametric evaluations for the outcomes of the shape modifications and other design parameters of the orthosis without the prerequisite of fabricated orthosis and replicating patient trials.

Existing FE models of the foot or footwear in the literature were developed under certain simplifications and assumptions including a simplified or partial foot shape, assumptions of linear material properties, infinitesimal deformation and linear boundary conditions without considering friction and slip. Although several 3D foot models were developed recently to study the biomechanical behaviour of the human foot and ankle, a geometrically detailed and material realistic 3D FE model of the human foot and ankle specialized for footwear or orthotic design has not been reported.

In this study, a 3D FE model of the human foot and ankle was developed from 3D reconstruction of Magnetic Resonance (MR) images from the right foot of a male adult subject. The developed FE model, which took into consideration the nonlinearities from material properties, large deformations and interfacial slip/friction conditions consisted of 28 bony structures, 72 ligaments and the plantar fascia embedded in a volume of encapsulated soft tissue. Parametrical studies were conducted to investigate the biomechanical effects of tissue stiffness, muscular reaction, surgical and orthotic performances on the ankle-foot complex. Experimental measurements on cadavers and on the subject who underwent the MR scanning were obtained to validate the FE predictions in terms of plantar pressure distribution, foot arch and joint motion, plantar fascia and ligamentous strains under different simulated weightbearing and orthotic conditions of the foot.

The parametrical analyses showed that increasing soft tissue stiffness led to decreases in total contact area of the foot-support interface and pronounced increases in peak plantar pressure at the forefoot and rearfoot regions. Decreasing the stiffness of plantar fascia would reduce the arch height and increase the strains of the plantar ligaments. In addition, surgical releases of partial and the entire plantar fascia increased the strains of the plantar ligaments and intensified the stresses in the midfoot and metatarsal bones. The FE predictions showed that both the weight on the foot and Achilles tendon loading resulted in an increase in tension of the plantar fascia with the latter showing a two-times larger straining effect. Above all, unloading the posterior tibial tendon was found to increase the arch deformations and strains of the plantar ligaments especially the spring ligament.

The parametrical analyses performed on the foot orthosis showed that the custom-molded shape was a more important design factor in reducing peak plantar pressure than the stiffness of the orthotic material. Besides the use of an arch-supporting foot orthosis, the insole stiffness was found to be the second most important factor for peak pressure reduction. Other design factors contributed to a less pronounced role in peak pressure reduction in the order of insole thickness, midsole stiffness and midsole thickness.

Further investigations on the biomechanical effect of different types of foot orthosis can be used to refine the design principles of orthosis in the CAD/CAM process in terms of appropriate shape and material of the orthosis in order to fit specific functional requirements of the subject and individual foot structure. The ultimate goal of the developed computational system is to establish the knowledge-based criteria to provide systemic guidelines for clinicians to prescribe and fabricate an optimized orthosis to maximize the functions of the foot orthoses as well as the subjects' comfort and gait performance.

# ACKNOWLEDGEMENTS

Day back from my first visit six years ago at the Rehabilitation Engineering Centre, The Hong Kong Polytechnic University, I still remember the scenario that I expressed my keen interests in biomedical research with Dr. Daniel Hung-Kay Chow and Dr. Ming Zhang. During an interview with the faculty members, I had my first meeting with Prof. Arthur Fuk-Tat Mak, Head of our department, who is the one to provide me with the unique opportunity to transform from a mechanical engineer to a biomedical engineer. I would like to take this opportunity to express my deepest gratitude to Prof. Mak for his kind support and encouragement throughout my postgraduate studies.

Not to mention, the most important person in my studies is Dr. Ming Zhang, chief supervisor of my MPhil and PhD studies, who provided me with all the necessary support, guidance, patience, encouragement and constructive advice, which are indispensable to the success of my postgraduate studies. I must also thank Prof. Kai-Nan An, Chair and Professor of Department of Orthopaedic Surgery, Mayo Clinic, my co-supervisor for his invaluable suggestions and inspirations on the clinical and experimental aspects of my studies as well as his constructive comments and recommendations given in my manuscripts.

I would like to express my sincere thanks to my thesis examiners, Prof. You-Lian Hong, Professor of Department of Sports Science and Physical Education, The Chinese University of Hong Kong and Prof. Benno M. Nigg, Professor, Director of Human Performance Laboratory, Faculty of Kinesiology, University of Calgary for their revision and valuable comments on my thesis.

I would like to acknowledge all my fellow students and colleagues who contribute in my research studies. Of particular, I must first extend my sincere thanks to Dr. Ameersing Luximon, who helped me on the programming issue for the geometrical data acquisition and processing, computer-aided design and manufacturing of foot orthoses. I wish to thank Dr. Terry Koo who helped me on the kinematics aspect of my studies. I must also thank Mr. Hok-Sum Man, Mr. Winson Lee, Mr. Xiang Dong, Mr. Cecil Cheng, Ms. Sharon Huang, Ms. Christina Lee, Ms. Bonnie Tsung, Ms. Anita Shum, Mr. CF Tin, Mr. KC Chen, Dr. XQ Dai, Dr. Aaron Leung, Dr. Raymond Tong, Dr. YP Zheng and Dr. Carl W. Imhauser for their suggestions and contributions in specific aspect of my studies.

Graceful thanks to Dr. Jun Ouyang and all the departmental staff of the Institute of Clinical Anatomy, Southern Medical University, Guangzhou, China for providing technical support on the cadaveric studies. I would like to thank Dr. Hector Ma and his departmental staff of the Scanning Department of St. Teresa’s Hospital, Hong Kong for facilitating the MR scanning. Acknowledgments are also given to the Industrial Centre of The Hong Kong Polytechnic University for the provision of computer facilities and operating softwares.

Sincere thanks to all the research staff and fellow students in the Jockey Club Rehabilitation Engineering Centre for giving me a warm, supporting and collaborating research environment throughout my studies.

Last but not the least, I must extend my graceful thanks to my parents, family members for their loving support and patience during my study. I must express my deepest gratitude to my fiancée, Ms. Siu-Cha Tsang for assisting my experimental studies and statistical analyses, sharing my joy and sorrow and for her continual encouragement, loving support and understanding throughout my postgraduate studies.

Finally, the financial support from the Hong Kong Jockey Club endowment, the research grant from The Hong Kong Polytechnic University (A/C No. A-PC91), and the grant from Research Grant Council of Hong Kong (Project No. PolyU 5249/04E & PolyU 5317/05E) are gratefully acknowledged.

# PUBLICATIONS ARISING FROM THE THESIS

## Peer-reviewed Journals

1. Cheung JT, Zhang M, 2006. Consequences of partial and total plantar fascia release – a finite element study. Foot and Ankle International. 27, 125-132.

2. Dai XQ, Li Y, Zhang M, Cheung JT, 2006. Effect of sock on biomechanical responses of foot during walking. Clinical Biomechanics. 21, 314-321.

3. Cheung JT, Zhang M, An KN, 2006. Effect of Achilles tendon loading on plantar fascia tension in the standing foot. Clinical Biomechanics. 21, 194-203.

4. Cheung JT, Zhang M, 2006. A serrated jaw clamp for tendon gripping. Medical Engineering and Physics. 28, 379-382.

5. Cheung JT, Zhang M, Leung AK, Fan YB, 2005. Three-dimensional finite element analysis of the foot during standing – A material sensitivity study. Journal of Biomechanics. 38, 1045-1054.

6. Cheung JT, Zhang M, 2005. A 3-dimensional finite element model of the human foot and ankle for insole design. Archives of Physical Medicine and Rehabilitation. 86, 353-358.

7. Cheung JT, Zhang M, An KN, 2004. Effects of plantar fascia stiffness on the biomechanical responses of the ankle-foot complex, Clinical Biomechanics. 19, 839-846.

8. Cheung JT, Luximon A, Zhang M, 2006. Parametrical design of pressure-relieving foot orthoses using statistical-based finite element method, Journal of Biomechanics, submitted.

## Conference Proceedings

1. Cheung JTM, Zhang M. Finite element modeling of the human foot and footwear. In: Proceedings of the 2006 ABAQUS Users' Conference, Boston, USA, May 23-26, 2006, accepted.

2. Cheung JTM, Zhang M, An KN. Biomechanical effects of plantar fascia release and posterior tibial tendon dysfunction - A finite element and cadaveric foot simulation. In: Proceedings of the International Society of Biomechanics XXth Congress, Cleveland, Ohio, USA, July 31-Aug 5, 2005, pp129.

3. Cheung JTM, Luximon A, Zhang M. Parametrical design of foot orthosis for plantar pressure relieve based on computational modeling. In: Proceedings of the 7th Symposium on Footwear Biomechanics, Cleveland, Ohio, USA, July 27-29, 2005, pp104-105 (RSscan International Pressure Research Award).

4. Zhang M, Cheung JTM, Li Y. Computational modeling of the foot-Insole Interface, In: Proceedings of the 17th IMACS World Congress: Scientific Computation, Applied Mathematics and Simulation, Paris, France, July 11 - 15, 2005

5. Zhang M, Dai XQ, Li Y, Cheung JTM. Computational Simulation of Dynamic Skin and Sock Pressure Distributions, In: Proceedings of the 17th IMACS World Congress: Scientific Computation, Applied Mathematics and Simulation, Paris, France, July 11 - 15, 2005

6. Zhang M, Cheung JTM. Computational models of foot and ankle - Application to foot support design. In: Proceedings of the 2nd World Congress for Chinese Biomedical Engineers, Beijing, China, Sep 27-29, 2004.

7. Cheung JTM, Zhang M. Three-dimensional finite element analysis of human foot and ankle during the stance phases of gait. In: Proceedings of the Conference on Biomedical Engineering, Hong Kong, China. Sep 23-25, 2004, pp112-116.

8. Cheung JTM, Zhang M, Luximon A. Computational model for foot orthosis design. In: Proceedings of the 11th World Congress of the International Society for Prosthetics and Orthotics, Hong Kong, China, 1-6 Aug, 2004, pp202.

9. Luximon A, Cheung JTM, Zhang M. Biomechanical effects of shoe last design on the ankle-foot structures. In: Proceedings of the 11th World Congress of the International Society for Prosthetics and Orthotics, Hong Kong, China, 1-6 Aug, 2004, pp267.

10. Cheung JTM, Zhang M, An KN. Orthopaedic applications of computational model of the human foot and ankle. In: Hong Kong Journal of Orthopaedic Surgery, Abstracts of the 23rd Hong Kong Orthopaedic Annual Congress, 8-9 Nov, 2003, S56.

11. Zhang M, Cheung JTM, Fan YB. A Three-dimensional finite element model of the foot and ankle for foot support design. In: Proceedings of the 7th National Conference on Biomechanics, Xi'an, China, 13-18 Oct, 2003, pp5.

12. Cheung JTM, Zhang M, An KN. Three-dimensional finite element analysis of human ankle-foot complex, World Congress on Medical Engineering and Physics, Sydney, Australia, 24-29 Aug, 2003, WE.TR15, 168.

## Book Chapters

1. Zhang M, Cheung JTM, Li Y. Ch. 26. Computational modeling of the foot-insole interface. In: Computational Textiles, ed Zeng X, Li Y, Ruan D, Koehl L, Springer, 2006, in process.

2. Zhang M, Dai XQ, Li Y, Cheung JTM. Ch. 28. Computational simulation of dynamic skin and sock pressure distributions. In: Computational Textiles, ed Zeng X, Li Y, Ruan D, Koehl L, Springer, 2006, in process.

# ACADEMIC AWARDS

| | |
|---|---|
| 2006 | Distinguish Thesis Award<br>Faculty of Health & Social Science,<br>The Hong Kong Polytechnic University |
| 2005 | RSscan International Pressure Research Award at<br>the 7th Symposium on Footwear Biomechanics by<br>the International Society of Biomechanics Technical Group on<br>Footwear Biomechanics |
| 2004 | Croucher Foundation Scholarship for Conference attendance at<br>the 11th World Congress of the International Society for<br>Prosthetics and Orthotics |

# TABLE OF CONTENTS

# LIST OF FIGURES

# LIST OF TABLES

# CHAPTER I INTRODUCTION

## 1.1 Diabetes Mellitus - A Public Concern

### 1.1.1 What is Diabetes?

Diabetes mellitus is a chronic disease caused by the deficiency of pancreas to produce insulin, a hormone to convert sugar, starches and other food into energy for daily living. Diabetes mellitus may also occur when the body cannot use the insulin produced from the pancreas effectively. Diabetes mellitus results in increased concentrations of glucose in the blood, which in turn damages different organs and systems of the body, in particular the blood vessels and nerves.

There are two principle forms of diabetes. Type 1 diabetes, also known as insulin-dependent diabetes is defined when the pancreas fails to produce enough insulin for survival. According to the Worth Health Organisation (WHO), type 1 diabetes is usually diagnosed in children and young adults but is also increasingly noted later in life. People with type 1 diabetes require daily injections of insulin to survive.

Type 2 diabetes (non-insulin-dependent) results from the body's inability to respond properly to the action of insulin produced by the pancreas. Type 2 diabetes is the most common form of diabetes, which accounts for about 90% of all cases of diabetes (Worth Health Organisation, 2005). It occurs most frequently in adults but is increasingly found in adolescents as well. People with type 2 diabetes can sometimes manage their condition through adapting healthy lifestyles, but oral drugs are often required in order to achieve good metabolic control.

The cause of diabetes is still unknown nowadays, although both genetics and environmental factors such as obesity and lack of exercise appear to be associated with diabetic patients (Worth Health Organisation, 2004). People who are physically inactive, overweight or obese especially for those in urban areas are more susceptible to diabetes. Certain genetic markers have been shown to increase the risk of developing type 1 diabetes. Type 2 diabetes is strongly hereditary, certain genetic characteristics have been suggested recently to be associated with the risk of type 2 diabetes in certain populations. It has been found that type 2 diabetes is more common in African Americans, Latinos, Native Americans, and Asian Americans/Pacific Islanders, as well as the aged population (Worth Health Organisation, 2004).

### 1.1.2 Prevalence of Diabetes

According to the WHO, the latest estimate for the worldwide number of people with diabetes in 2000 is 171 million, which is expected to increase to more than double by 2030 (Wild et al., 2004). Figure 1-1 shows the estimate and distribution for the worldwide number of people with diabetes in 2000 and 2030. The prevalence of diabetes for all age groups was estimated to increase from 2.8% in 2000 to 4.4% in 2030. The global increase in diabetes may be attributed to the ageing and growing population and an increasing trend towards obesity, unhealthy diet and sedentary lifestyle.

Latest demographic projection of diabetes population suggested that the increase in diabetes would be more significant in the developing countries than the developed countries (Fig. 1-2). In developing countries, those most frequently affected are in the middle age and there is a growing incidence of type 2 diabetes at a younger age (Worth Health Organisation, 2004).

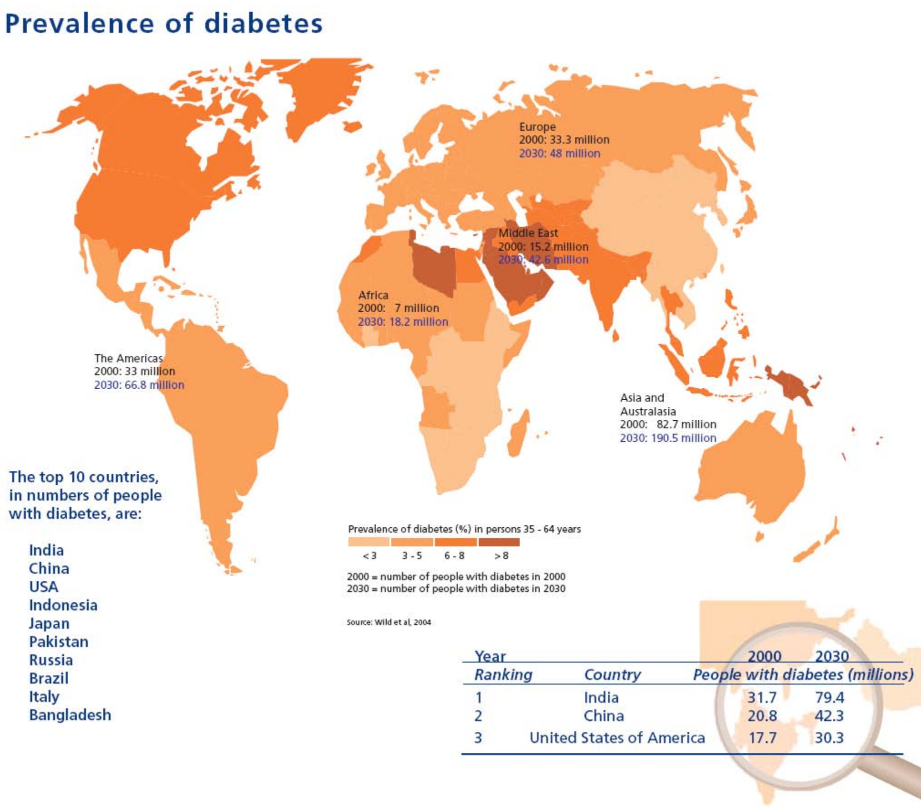


Figure 1-1. The estimate and distribution for the worldwide number of people with diabetes in 2000 and 2030 (World Health Organization, 2004).

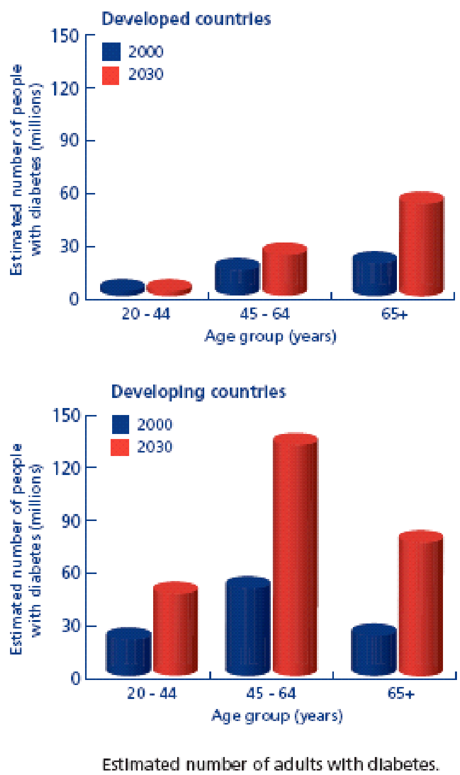


Figure 1-2. The estimated number of people with diabetes in developed and developing countries for the year 2000 and 2030 (World Health Organization, 2004).

A review of epidemiological studies conducted by Cockram (2000) found an increasing rate of diabetes prevalence in the Asia pacific region. The prevalence rates of diabetes in China involving 19 provinces and more than 0.2 million subjects, were 2.5% and 3.2% in year 1994. In Hong Kong, the prevalence rates of diabetes mellitus were 7.7% and 8.9%, respectively in 1990 and 1995. Taking into account the growing and ageing population in addition to the trends in urbanization, the WHO predicted that both India and China might be dealing with at least 122 million diabetes by the year 2030 (Wild et al., 2004). Because of the massive population size of China and India, together with their rapid rates of urbanization and industrialization, the WHO (2004) estimated that the prevalence of diabetes in the Asia-Pacific Region would rise from 48% of global diabetes population in 2000 to 52% in 2030.

Owing to the rising prevalence rate and the earlier onset of the disease in today's population, the prevalence of type 2 diabetes in the younger population now greatly outnumbers those with type 1 diabetes (Cockram, 2000). This phenomenon may be related to westernized and sedentary lifestyle, overnutrition and physical inactivity. These changes in lifestyle have rapidly altered the behavioural patterns of the younger generation and their adverse effects on health will inevitably produce an enormous impact in the new era of population (Cockram, 2000). In fact, WHO has recognized that there is a global epidemic of obesity, which implicates an increasing risk of type 2 diabetes (Sorensen, 2000). In view of the severity of the long-term complications of diabetes, there is an urgent need for all policy-makers especially for the most vulnerable countries to control the threat of diabetes.

### 1.1.3 Cost of Diabetes

Diabetes is the fifth leading cause of death in the United States. In 2000, 3.2 million deaths were attributable to complication of diabetes. About 5% of all deaths are attributable to diabetes contributing to about 8,700 deaths per day in which at least 10% of all deaths with adults aged between 35 and 64 years old (Worth Health Organisation, 2004). Figure 1-3 depicts the estimate and distribution for the worldwide number of deaths attributed to diabetes in 2000. The top 10 countries, in numbers of sufferers, are India, China, USA, Indonesia, Japan, Pakistan, Russia, Brazil, Italy and Bangladesh (Worth Health Organisation, 2004).

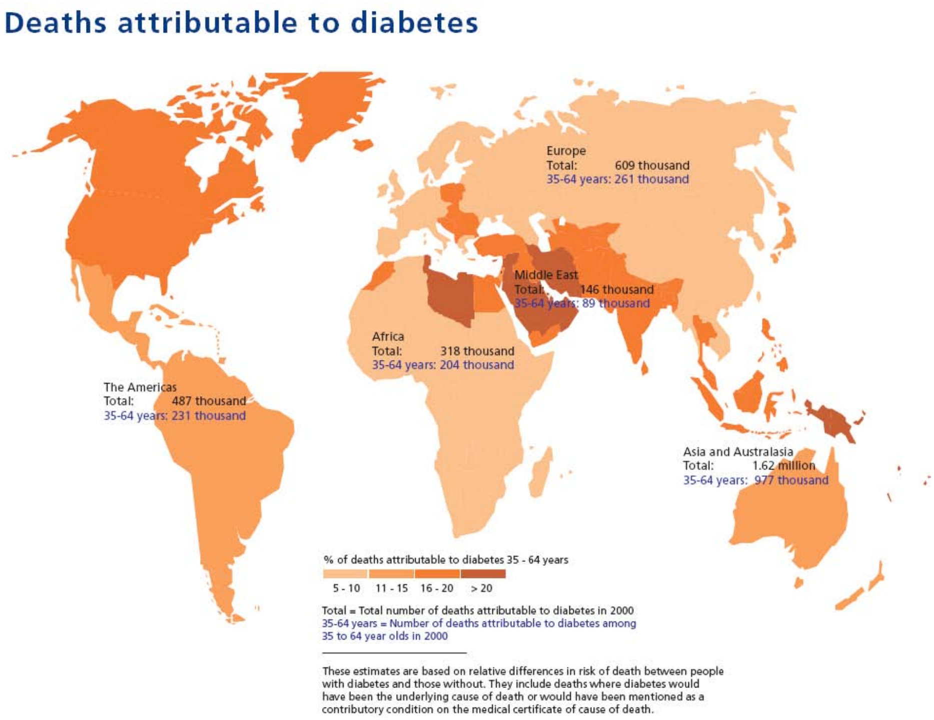


Figure 1-3. The estimate and distribution for the worldwide number of deaths attributed to diabetes in 2000 (World Health Organization, 2004).

Diabetes has become one of the major causes of premature death in most countries, mainly due to the increased risk of cardiovascular disease, which is responsible for 50% to 80% of all deaths in people with diabetes (Worth Health Organisation, 2004). Diabetes contributes to higher morbidity rates of heart disease, blindness, kidney failure, extremity amputations, and other chronic conditions. These complications account for much of the social and financial burden of diabetes.

Because of its chronic nature and the severity of its complications, diabetes is a costly disease affecting individuals, families as well as the health care systems of every nation. The worldwide growing number of diabetes is overwhelming the national economic burden of diabetes. Overall, the direct health care costs of diabetes range from 2.5% to 15% of annual health care budgets, depending on local diabetes prevalence and the available treatment modality (Worth Health Organisation, 2004). The increasing number of premature deaths and increasing diabetic prevalence among the young population further devastate the health care system and the economy of the society.

According to the American Diabetes Association, the total annual economic cost of diabetes in 2002 was estimated to be $132 billion, equivalent to one out of every 10 health care dollars spent in the United States (Hogan et al., 2003). The direct medical expenditure attributable to diabetes was $92 billion while the indirect cost resulting from loss of time from work, permanent disability and premature death due to diabetes was $40 billion. It was speculated that the indirect cost on lost production could be as much as five times the direct health care cost (Worth Health Organisation, 2004). With the projected increase in incidence and prevalence of diabetes in addition to a growing problem of obesity, the annual cost of diabetes in the coming decades could inflate at a tremendous rate (Hogan et al., 2003).

Diabetic foot problems such as foot ulceration and amputation are the leading cause for hospitalization and are the most costly among all medical expenditures. Gordois et al. (2003) estimated that the annual medical cost of peripheral neuropathy and its complications among people with diabetes in the United States at 2001 was 10.9 billion US dollars, accounting for up to 27% of the direct medical cost of diabetes. It has been estimated that medical expenditures for lower-extremity ulcer patients were on average 3 times higher than those for other patients in general (Harrington et al., 2000). In a prospective study, Boyko et al. (1996) found that the mortality rate of diabetic patients with foot ulceration was 2.4 times higher than patients without a foot ulcer.

### 1.1.4 Complications of Diabetes

People with diabetes will develop late complications, including cardiovascular and eyes diseases, progressive kidney failure and nerve damage. Cardiovascular or heart disease accounts for up to 80% of all deaths among people with diabetes (WHO, 2004). Diabetic retinopathy is a leading cause of blindness and visual disability resulting from damages of the blood vessels in the retina.

Diabetic neuropathy is the most common complication affecting up to 50% of all diabetes (Worth Health Organisation, 2004). Young et al. (1993) examined the vibration perception of 6,487 diabetic patients and found that up to 28.5% of all patients were associated with diabetic neuropathy. Neuropathy results in damage of the nerves that run throughout the body, connecting the spinal cord to muscles, skin, blood vessels, and other organs. Neuropathy can lead to sensory loss, damage and amputation of the limbs (Worth Health Organisation, 2004). Peripheral neuropathy is a common form of nerve damage in diabetes that deteriorates the nerve function of the body's extremities. Diabetic neuropathy can cause a variety of symptoms, including a gradual loss of feeling in the feet, shooting pains, or a burning sensation (American Diabetes Association, 2005). Diabetic neuropathy is regarded as a major risk factor of diabetic foot ulceration (Frykberg et al., 1998; Lavery et al., 1998; Pitei et al., 1999; Veves et al., 1992). Because of the vascular and neurological diseases, patients with diabetic neuropathy are susceptible to skin breakdown due to unnoticed and repeated trauma to the plantar surface of the foot during walking (Boulton et al., 1987). Diabetes with peripheral neuropathy especially for those with high plantar foot pressure are at high risk for developing neuropathic ulcers on the plantar surface of their feet (Fig. 1-4) (Boulton et al., 1987; Boyko et al., 1999; Frykberg et al., 1998; Lavery et al., 1998, 2003; Lobmann et al., 2002; Pham et al., 2000; Pitei et al. 1999; Stess et al., 1997), which is often initiated by an untreated cut or fissure and associated skin infection. Untreated ulcers can quickly progress to the gangrene due to infection and poor blood circulation, in which the affected skin begins to die. If the infection progresses deeper into the tissues, it can penetrate into the bones, leading to osteomyelitis, a serious inflammation of the bone marrow. Both gangrene and osteomyelitis often result in amputation of the affected limb.

(a) (b)

Figure 1-4. Diabetic foot ulcers at the (a) midfoot and (b) forefoot.

Diabetic ulceration is the most common cause of non-traumatic amputation of the lower limb (World Health Organization, 2004). About 15% of all diabetes will develop foot ulcers in their lifetime (Boulton, 2000), and approximately 15 to 20% of these ulcers are estimated to result in lower extremity amputation. The global lower extremity amputation study group (Group TG, 2000) reported that diabetes was associated with 25 to 90% of the global incidences of amputation and that the incidence rate rose steeply with age. According to the American Diabetes Association (2005), about 5 to 15% of people with diabetes will ultimately require an amputation and more than 60% of nontraumatic lower-limb amputations in the United States occur among people with diabetes. From 2000 to 2001, about 82,000 nontraumatic lower-limb amputations were performed each year among people with diabetes. Moss et al. (1999) reported a 14-year cumulative incidence of about 8.6% for lower-extremity amputations in 1,890 diabetic patients and found that history of ulcer was a significant risk factor. In Hong Kong, it was estimated that about 30% of the diabetic patients with ulcers required amputations (Leung et al., 2001). A study involving more than 12,000 diabetic patients in Taiwan showed that the lifetime prevalence of diabetic foot problems was 2.9% from which ulcers contributed to 86.7% of all initiating events and approximately 72% of all amputations were preceded with foot ulcers (Tseng, 2003).

### 1.1.5 Prevention and Treatments of Diabetes

Until now, there is still no cure or prevention for type 1 diabetes. The only remedy for this immunal disease is medication. People with type 1 diabetes require daily insulin injections for survival. Although relatively uncommon, people suffering from type 2 diabetes may need insulin for reducing their blood glucose levels. Prevention is the most effective treatment strategy and patients with diabetes should monitor and control blood glucose levels, have a balanced diet and exercise regularly. Good metabolic control including strict controls on high blood glucose, high blood pressure, high serum cholesterol, weight and cigarette smoking are important for preventing the development of diabetes (World Health Organization, 2004). Simple lifestyle measures have been shown to be effective in preventing or delaying the onset of type 2 diabetes.

Screening and early detection of diabetes and its associated diseases are considered as important means for prevention or improvement of the conditions of the diseases. (Worth Health Organisation, 2004). Data from the American Podiatric Medical Association (2005) pointed out that the risk of neuropathy can be reduced by 69% if blood sugar level is well-controlled. Meanwhile, diabetic foot disease can be avoided by regular inspection and good foot care. Effective foot care can reduce not only the frequency of hospitalizations but also the incidence of amputation in diabetes patients by as much as 50% (Humphrey et al., 1996).

Footwear and orthotics play an important role in diabetic foot care. According to the American Podiatric Medical Association (2005), poorly fitted shoes often lead to amputations in diabetic patients. Proper footwear is an important part of an overall treatment program for people with diabetes especially for those with neuropathy, or lack of sensation to prevent diabetic foot complications. Footwear for people with diabetes should reduce shock and shear in addition to the relief of excessive plantar pressure. Footwear should also accommodate, stabilize and support deformities. Deformities resulting from conditions such as Charcot involvement, loss of fatty tissue, hammertoes and amputations must be accommodated.

The excessive pressure and friction from poorly fitting shoes can lead to blisters, calluses and ulcers. Cushioned custom footwear can decrease the risk of developing a foot ulcer. Custom-made orthoses (Fig. 1-5) using soft, shock-absorbing materials may act as a replacement for the thinning fat pad on the bottom of the feet and help to distribute weightbearing pressures over the entire plantar surface of the foot away from the vulnerable bony prominences (Lusardi and Nielsen, 2000). Both prefabricated and custom-made foot orthoses or inserts are commonly prescribed for patients with diabetes to provide comfort and pressure relief. Extra-depth shoes are necessary to provide extra room to accommodate any needed inserts or orthoses, as well as deformities commonly associated with a diabetic foot. Customized insole, healing footwear such as a walking boot, walking cast, a total contact cast, or other post-operative healing shoes can be used especially after surgery or for ulcer treatment. By protecting the skin from excessive bone pressure, these special orthoses can greatly reduce the risk of foot from ulceration or infection.

Figure 1-5. Custom-made foot orthosis.

## *1.2 Objective of this Study*

Many researchers have pointed out that biomechanical factors play an important role on the etiology, treatment and prevention of many foot disorders. Therefore, it is essential to understand the biomechanics associated with the normal foot before any foot orthosis or surgical intervention can be applied. Information on the internal stress and strain of the foot and ankle is essential in enhancing knowledge on the biomechanical behaviour of the ankle-foot complex. Direct measurement of those parameters is difficult, while a comprehensive computational model can acquire those important clinical information.

The biomechanics of the foot and footwear has been better understood owing to the recent scientific advances in both measurement instrumentation and theoretical methodology. In recent literature, many experimental techniques were developed and employed for the quantification of foot biomechanics, such as motion analysis systems, pressure sensing platforms, in-shoe pressure transducers, pressure sensitive films, cadaveric experiments, and *in vivo* force measurements. The above-mentioned measurement techniques are commonly used in predicting joint kinetics and kinematics, and quantifying plantar pressure distributions. However, bones, soft tissue, and associated joint stresses inside the foot are not well addressed and remain unclear. It is very difficult to quantify the *in vivo* bone and soft tissue stress with the existing experimental techniques. As for *in vitro* studies, the loading conditions were often different from the actual physiological loading situation as the foot structure was compromised. Therefore, no overall stress distribution of the whole foot is known using the currently available measuring techniques.

Apart from the experimental approaches, many theoretical models, such kinematics models, mathematical models, and finite element models of the foot has been developed. Finite element (FE) method has been used increasingly in many biomechanical investigations with great success due to its capability of modeling structures with irregular geometry and complex material properties, and the ease of simulating complicated boundary and loading conditions in both static and dynamic analyses. Therefore, it has become a suitable method for the investigation of load distribution of the human foot and ankle. Although many FE analyses of the foot or footwear were performed in the literature, many were 2D approximations with only part of the foot structures considered. Even with 3D FE models, only simplified geometry and loading conditions were used. Therefore, a more detailed FE model is essential to provide an overall representation of the human foot.

The primary objective of this study is to establish a comprehensive FE model of the human foot and ankle to quantify the biomechanical interaction among bones, ligaments, interaction between foot plantar and different supports under various loading conditions. It is expected that the developed FE model can provide quantitative information on joint motion and stress/strain among the bony and soft tissue structures, and pressure distribution between the foot and the support surface. The capability of the model to quantify the biomechanical effects of varying geometrical and material factors of different structures of the foot and to predict different surgical outcomes and orthotic performances will be evaluated.

Nowadays, evaluations of foot orthotic design mainly rely on subjective clinical assessment (subjects' satisfaction, pain and disability symptoms), (Conrad et al., 1996; Hodge et al., 1999; Jordan and Bartlett, 1995; Miller et al., 2000; Mundermann et al., 2001; Pfeffer et al., 1999), plantar pressure measurement (Bus et al., 2004; Hodge et al., 1999; Hosein and Lord, 2000; Jordan and Bartlett, 1995; Lavery et al., 1997; Lobmann et al., 2001; Reiber et al., 2002), and gross motion tracking (Brown et al., 1995; Eng and Pierrynowski 1994; Johanson et al., 1994; Leung et al., 1998;

McCulloch et al., 1993; McPoil and Cornwall 2000; Nawoczenski et al. 1995; Nester et al 2001; Nigg et al., 1998; Nigg et al., 2003; Stacoff et al. 2000) due to experimental difficulties. The biomechanical rationale behind various designs of pressure relief or functional foot orthosis is still unclear. In fact, many suggested there was still a lack of consensus on the appropriate application of shape, material properties and placement of foot orthoses for different foot types or injuries, indicating the knowledge base for these decisions is not fully understood and incomplete (Ball and Afheldt, 2002; Landorf and Keenan, 2000; Nigg et al., 1999; Razeghi and Batt, 2000; Stacoff et al., 2000).

Therefore, the secondary objective of this study is to provide quantitative evaluations of different design parameters of foot orthosis by the developed FE model with an ultimate goal of establishing knowledge-based criteria for the design of foot orthoses. In this study, the structural and material factors of pressure relieving foot orthosis will be investigated with an attempt to provide systematic guidelines on the prescription of foot orthoses for diabetic patients.

## *1.3 Outline of the Dissertation*

Following the introduction chapter, chapter II begins with a review of the functional anatomy of the human foot and ankle. The FE method is then introduced and is followed by a detail review on the existing FE studies on foot and footwear biomechanics.

In chapter III, the development of the FE model and the simulated conditions are presented in details. The geometrical and material properties defined in the FE model are described. The loading and boundary conditions applied for simulating the physiological loading conditions of the human foot and ankle are discussed. The parametrical approaches for simulating the effects of varying soft tissue stiffness, surgical and pathological conditions including plantar fascia release, tight Achilles tendon, posterior tibial tendon dysfunction and the effect of different foot support are presented. The experimental procedures and corresponding measurements of the *in vivo* and cadaveric experiments conducted to validate the FE predictions are described.

Chapter IV presents the results of the FE analysis and experimental studies. This chapter is divided into six sections. The first five sections of the chapter report the findings of the parametrical analyses conducted on the developed FE foot model. The last section presents the results of the parametrical analyses of foot orthosis.

Chapter V starts with the discussion of the findings and relevant clinical implications of the five parametrical analyses performed on the FE foot model. The following section discusses the findings of the sensitivity analyses for different design factors of foot orthosis and a summary about the guidelines on the design of pressure relieving foot orthoses as suggested from the findings of the FE analyses is then introduced. In the last section of this chapter, the limitations of the current FE model are discussed.

Chapter VI summarises the findings in this study and its clinical implications regarding different simulated conditions of the foot. Suggestions on the further development of the FE model and the future research directions of this study are highlighted.

# CHAPTER II LITERATURE REVIEW

## *2.1 Functional Anatomy of the Human Foot and Ankle*

The bones of the feet make up about one-fourth of all the bones in the human body. Each foot contains 26 bones (Fig. 2-1), 33 joints; and more than 100 muscles, tendons and ligaments and a network of blood vessels, nerves, skin, and other surrounding soft tissues. These components work together to provide the body with support, balance, and mobility.

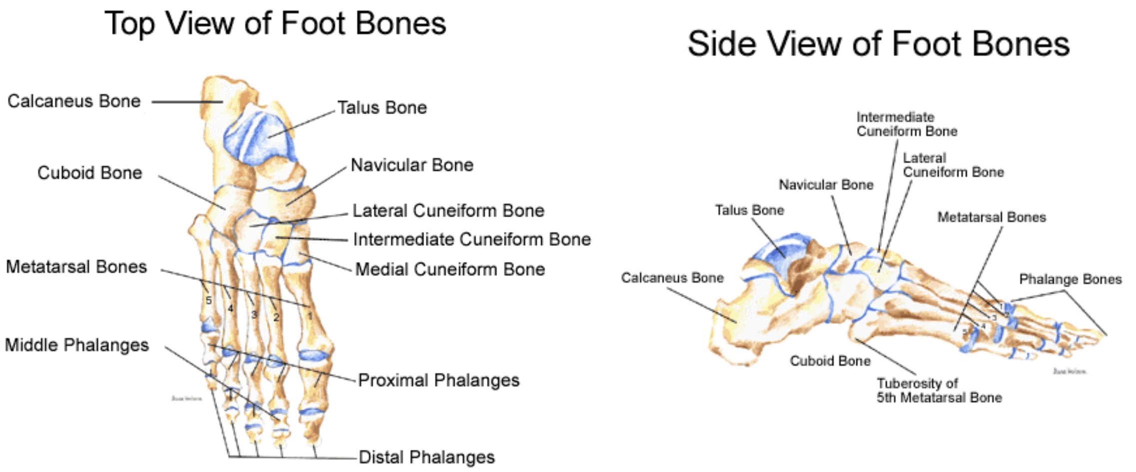


Figure 2-1. The top and side view of the bones in the human foot (Healthcommunities.com, Inc., 2005).

The foot can be divided into three main parts namely forefoot, midfoot, and hindfoot. The forefoot is composed of the five toes called the phalanges and their connecting metatarsals. The big toe (hallux) has two phalanges and two interphalangeal joints. Each of the other four toes has three bones and two joints. The phalanges are connected to the metatarsals by five metatarsophalangeal joints at the ball of the foot. The five tarsal bones of the midfoot are connected to the forefoot and the hindfoot by muscles, plantar fascia and other ligaments, forming the longitudinal foot arch. The hindfoot links to the midfoot via the midtarsal joint. The top of the talus is connected to the tibia and fibula, forming the ankle joint. The calcaneus is the largest bone in the foot that joins the talus to form the subtalar joint. The bottom of the calcaneus is cushioned by a layer of fat so called the heel fat pad, which helps to assimilate plantar pressure and absorb shock during walking, running and jumping. The fat pad of the heel is a fibro-fatty cushion interposed between the skin of the heel and the inferior aspect of the calcaneus.

Articular hyaline cartilage offers a firm, smooth and relatively friction-free surface to facilitate joint movements. The surface of articular hyaline cartilage is lubricated by synovial fluid secreted by the synovial membrane. The compressibility and elasticity of the articular cartilage enable the compressive forces dissipation and permit smooth gliding between the joint surfaces.

The foot is supported and stabilized by about 20 muscles in which the associated tendons provide connection to the bones and joints (Fig. 2-2). The main muscles of the foot are: the anterior tibial which enables the foot to move upward; the posterior tibial which supports the arch; the peroneal tibial which controls movement on the outside of the ankle; the extensors which help the ankle raise the toes to initiate the act of stepping forward; and the flexors which help stabilize the toes against the ground. A number of smaller muscles enable the toes to lift and curl.

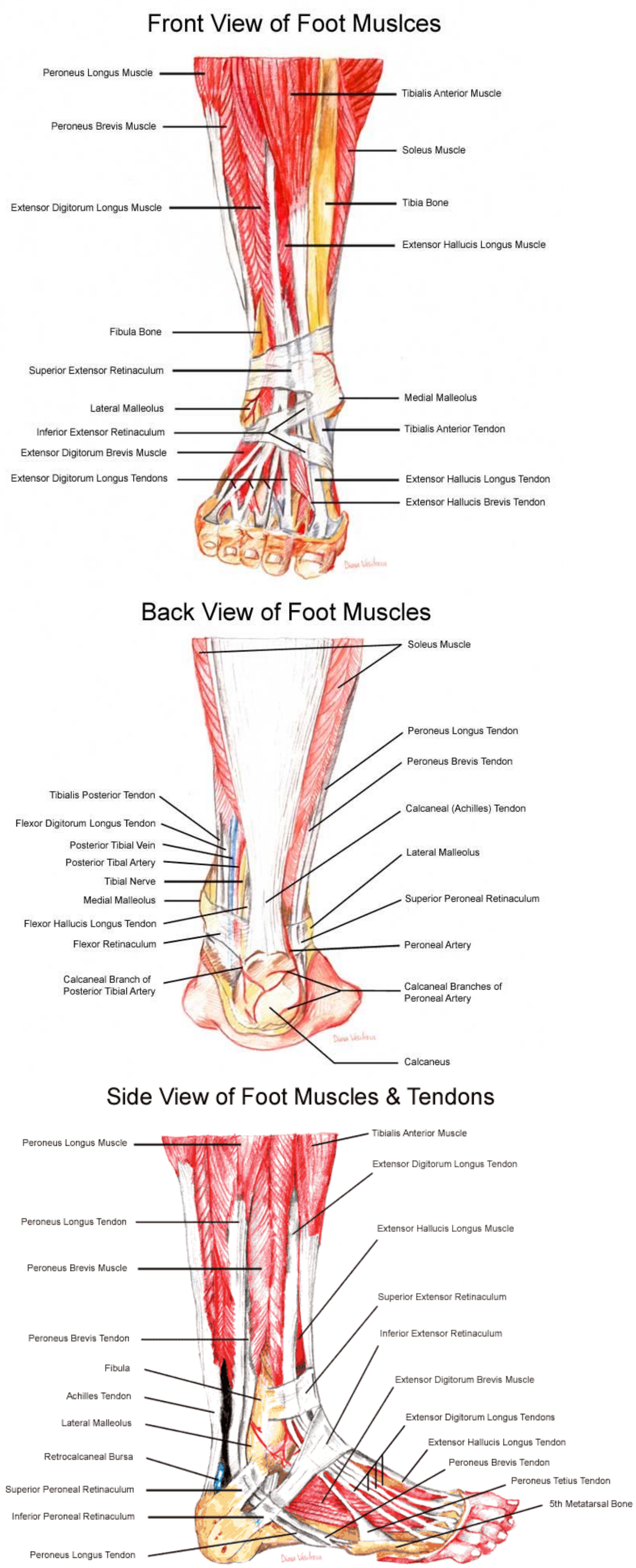


Figure 2-2. The front, back and side view of the foot muscles (Healthcommunities.com, Inc., 2005).

### 2.1.1 Muscles of the Foot and Ankle

*Muscles acting across the ankle and subtalar joints*

Soleus arises from the posterior surface of the tibia, fibula and the deep calf muscles. Its tendon joints the tendons of the gastrocnemius and plantaris to form the Achilles tendon, which inserts into the back of the calcaneus. The Achilles tendon is the largest and strongest tendon of the foot, which extends from the calf muscle to the heel. The gastrocnemius muscle acts to plantarflex the ankle joint. The soleus muscle acts with the gastrocnemius to plantarflex the ankle joint, preventing excessive dorsiflexion during walking. Plantaris is a weak plantar flexor of the ankle, running deep to the gastrocnemius from the lateral condyle of the femur to the calcaneus.

Extensor hallucis longus, extensor digitorum longus and tibialis anterior form the anterior aspect of the tibia and fibula. The extensor hallucis longus acts to dorsiflex the hallux at the interphalangeal and metatarsophalangeal joints. It also assists in dorsiflexing the ankle joint. The extensor digitorum longus extends the lateral four toes at the interphalangeal and metatarsophalangeal joints and assists in dorsiflexion of the ankle. The tibialis anterior is the main ankle dorsiflexor of the ankle joint and invertor of the foot. It is most active during the initial period of stance phase for slowing down ankle plantarflexion and preventing the foot from slapping to the ground. It also prevents the forefoot from scraping the ground during the swing phase.

Flexor hallucis longus, flexor digitorum longus, tibialis posterior, peroneus longus and peroneus brevis are the deep calf muscles and all arise from the tibia and fibula. The former two are flexors of the toes. The flexor hallucis longus flexes the hallux. It acts during final propulsion in gait and assists in the maintenance of the medial longitudinal arch. Peroneus longus everts the foot and is capable of plantarflexing the ankle joint. It also helps to support the lateral longitudinal and transverse arches of the foot. The peroneus brevis, assisted by the peroneus longus tendon, is an evertor of the foot. By exerting a force from the lateral aspect, it helps to stabilize the subtalar and midtarsal joints for propulsion. Tibialis posterior is an invertor of the foot. All the above five muscles are weak ankle plantarflexors.

*Muscles within the foot*

Extensor digitorum brevis and the dorsal interossei are on the dorsum of the foot, the former muscle extends the toes and the latter muscles abduct and flex the toes. Flexor digitorum brevis, abductor hallucis and abductor digiti minimi form the superficial layer of the sole of the foot; they flex the toes and abduct the big toe and the little toe, respectively. Abductor hallucis abducts the hallux at the metatarsophalangeal joint, helping to maintain the transverse arch of the foot. It also assists in flexion of the hallux. Flexor accessories, flexor hallucis brevis and flexor digiti minimi brevis form an intermediate layer in the sole of the foot, which act to flex the five toes. The adductor hallucis adducts the big toe. The plantar interossei and the lumbricals lie in the deepest layer of the foot; the former adducts and flexes the toes whereas the latter assists in flexion of the metatarsophalangeal joints and extension of interphalangeal joints. The above five groups of muscles are the major intrinsic muscles of the foot.

Other intrinsic muscles such as the extensor hallucis brevis, assists the extensor hallucis longus in dorsiflexion of the hallux at the proximal interphalangeal joint and assists the extensor digitorum longus in dorsiflexing the 2nd, 3rd, and 4th toes. The peroneus tertius assists the extensor digitorum longus in extending the fifth metatarsal, helping in dorsiflexion of the ankle joint and eversion of the foot.

### 2.1.2 Joints and Associated Ligaments of the Foot and Ankle

The ankle joint complex comprises the distal tibia and fibula. The tibia and fibula are joined proximally and distally at the proximal and distal tibiofibular joints (Fig. 2-3). The interosseous membrane supports both the proximal and distal tibiofibular joints, which accommodate the rotation of the tibia during knee motion and the triplantar motion of the foot. The primary support of the distal tibiofibular joint is the interosseous tibiofibular ligament that is an extension of the interosseous membrane. It also is supported by the anterior and posterior tibiofibular ligaments as well as by the interosseous membrane. The motion available between the tibia and fibula is quite limited, allowing slight rotation of the fibular about a longitudinal axis as well as slight proximal-distal and medial-lateral translations.

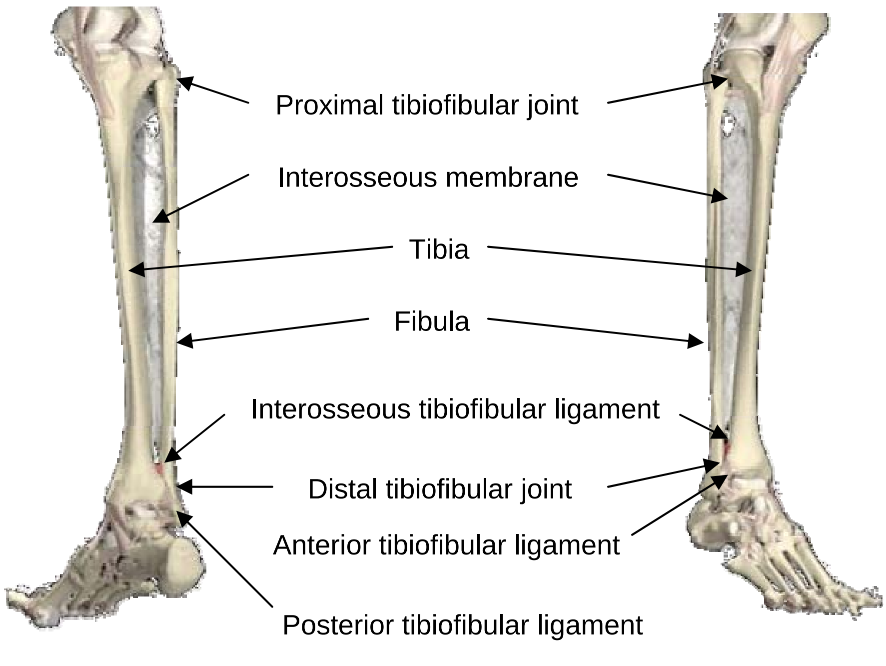


Figure 2-3. The proximal and distal tibiofibular joints and supporting ligamentous structures of the tibia and fibula (Interactive foot and ankle, 1999).

The primary motions of the foot and ankle have often defined with respect to the cardinal axis of the body. These include dorsiflexion and plantarflexion in the sagittal plane about a medial-lateral axis of the ankle joint, eversion and inversion in the frontal plane about the long axis of the foot, which lies with the second metatarsal of the foot, abduction and adduction in the transverse plane about the longitudinal axis of the tibia. Because the actual joint motions of the ankle-foot complex occur about axes that are oblique to the cardinal planes, joints of the foot exhibit triplanar motions. For instance, the most typical motions exhibited by the joints of the ankle and foot combine either dorsiflexion, eversion, and abduction or plantarflexion, inversion, and adduction. These motions are known as pronation and supination, respectively.

*Talocrural joint (Ankle joint)*

The talocrural joint connects the foot to the lower leg via the articulation between the tibia, fibula, and talus. The articulations between the talus and the tibia and fibula bound together to form a mortise for the talus. The primary articular surface is on the superior surface of the talus and on the distal surface of the tibia. The articulating surfaces of the ankle are of similar curvatures, providing joint congruity to allow hinge-like motion and help stabilize and minimize the stress of the ankle. The talocrural joint has a triplanar axis of rotation. Because the lateral malleolus is inferior and posterior to the medial malleolus, the axis of rotation is inclined slightly superior and anterior, as it crosses from the lateral to the medial side of the talus through both malleoli. The axis deviates from medial-lateral axis about 10 degrees in the frontal plane, and 6 degrees in the horizontal plane (Neumann, 2002). Although sagittal plane plantar flexion and dorsiflexion are the primary motions at this joint, the slight inclination of the joint axis of rotation results in transverse and frontal plane motion as well. During plantar flexion, the foot adducts and inverts whereas it abducts and everts with dorsiflexion. The normal range of motion of the talocrural joint is between 12 and 20 degrees of dorsiflexion and 50 and 56 degrees of plantar flexion (Lusardi and Nielsen, 2000).

In addition to the synovial capsule, the primary ligamentous structures for stabilizing and limiting the ankle motion are the medial collateral (deltoid) and lateral collateral ligaments (Fig. 2-4). The collateral ligaments, along with the articular surfaces, help to stabilize the ankle and subtalar joints and guide the motion of the ankle. The deltoid ligaments support the medial side of the ankle and subtalar joint against valgus forces on the foot while the lateral collateral ligaments protect these joints from varus forces on the foot.

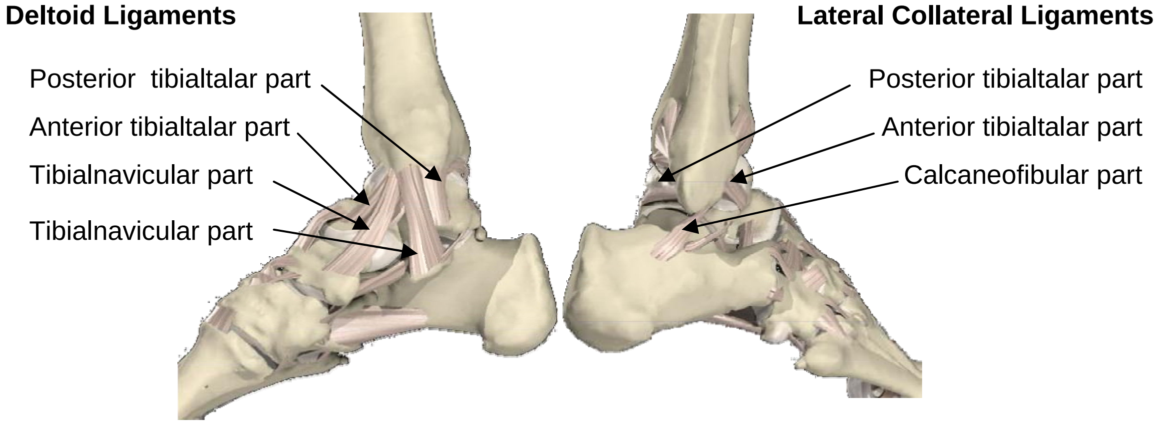


Figure 2-4. The deltoid and lateral collateral ligaments of the ankle joint (Interactive foot and ankle, 1999).

Although the ankle joint functions in general as a hinge joint rotating about an axis aligned between the medial and lateral malleoli, the actual axis of rotation varies throughout the ankle's range of motion. Slight translation usually accompanies with ankle's rotation and the tibia translates anteriorly during dorsiflexion and posteriorly during plantarflexion (Oatis, 2004). Translation of the tibia produces a change in the instant centre of rotation of the ankle joint so that the instantaneous centre moves posteriorly with plantarflexion, anteriorly with dorsiflexion, medially with inversion, and laterally with eversion. Ankle dorsiflexion and plantarflexion also are accompanied by talar rotation and fibular glide and rotation. Both the talus and fibula rotate laterally with respect to the tibia as the ankle dorsiflexes. Despite the translations and rotations of the talus and the variability of the axis during ankle motion, the clinical use of an ankle axis that passes through the two malleoli is generally accepted as a valid simplification.

*Subtalar joint*

The articulation between the calcaneus and talus is the subtalar joint. Three joint surfaces, namely the posterior, anterior, and middle are present in this articulation. The posterior joint surface has a concave talar and convex calcaneal portion, whereas the anterior and middle joint surfaces have convex talar and concave calcaneal arrangements. This structurally based articular geometry, along with the interosseous talocalcaneal ligament and the two joint capsules surrounding the posterior and the anterior facets, limits the amount and type of motion at the subtalar joint (Lusardi and Nielsen, 2000). In addition to the interosseous talocalcaneal ligament, the medial and lateral collateral ligaments, the medial and lateral talocalcaneal ligaments and the cervical ligament also provide support and prevent excessive motion of the subtalar joint (Fig. 2-5).

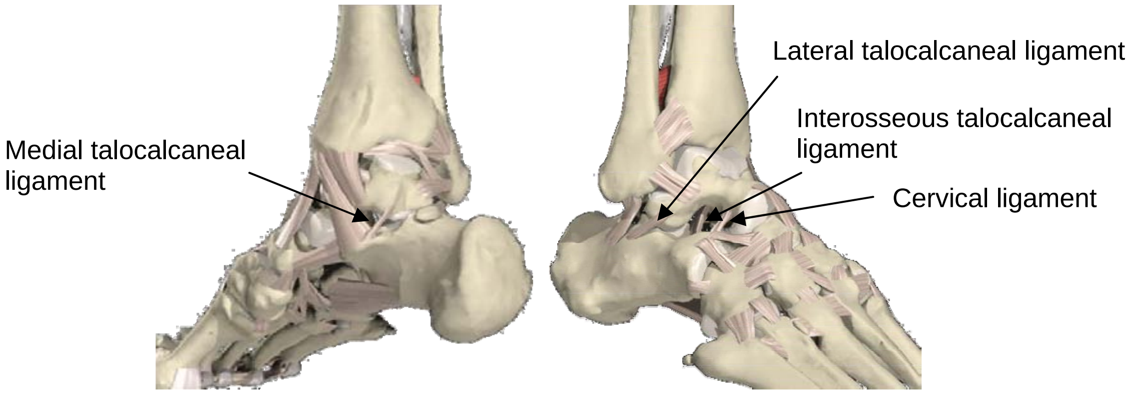


Figure 2-5. Talocalcaneal ligaments supporting the subtalar joint (Interactive foot and ankle, 1999).

The subtalar joint complex has often been described as a hinge joint whose axis lies oblique to both the foot and the leg. The axis of rotation is typically positioned 42 degrees from the horizontal plane and 16 degrees from the sagittal plane (Neumann, 2002). The triplanar motions that occur at the subtalar joint are supination and pronation. When the primary axis lies closer to the long axis of the foot, inversion and eversion constitute the primary components of subtalar motion, but when the axis is close to the long axis of the leg, the adduction and abduction contributions increase. The subtalar joint contributes most of the inversion-eversion and adduction-abduction motion of the hindfoot, while contributing only slightly to plantarflexion and dorsiflexion.

Supination of the weightbearing foot leads to dorsiflexion and abduction of the talus with simultaneous inversion of the calcaneus (Neumann, 2002). Pronation of the weightbearing foot results in plantar flexion and adduction of the talus and eversion of the calcaneus. This variability often has an effect on coupled motion between the joints of the foot and the lower leg. During pronation and supination of the rearfoot, the tibia and fibula rotate internally and externally in the transverse plane. An increase in the frontal plane motion of the rearfoot could cause a simultaneous increase in the transverse plane motion of the lower leg. The subtalar joint acts to translate the motion of the tibia to the foot or conversely to translate the motion of the foot to the tibia, allowing smooth progression of the foot and accommodation of uneven surfaces.

### *Midtarsal joint (Transverse tarsal joint)*

The two articulations between the midfoot and the rearfoot are the talonavicular and calcaneocuboid joints, which form the midtarsal joint or so-called transverse tarsal joint. The articular surfaces of the talonavicular joint are convex-concave, whereas the surfaces of the calcaneocuboid joint are sellar shaped. The midtarsal joint is supported by the bifurcate, short and long plantar, and plantar calcaneonavicular (spring) ligaments and their associated joint capsules (Fig. 2-6). The spring ligament contains a fibrocartilaginous facet for supporting the head of the talus. The short and long plantar ligaments and the spring ligaments also support the longitudinal and transverse plantar arches of the foot. Additional supports include the talonavicular ligament and the capsule that encloses the anterior articulation between the talus and calcaneus.

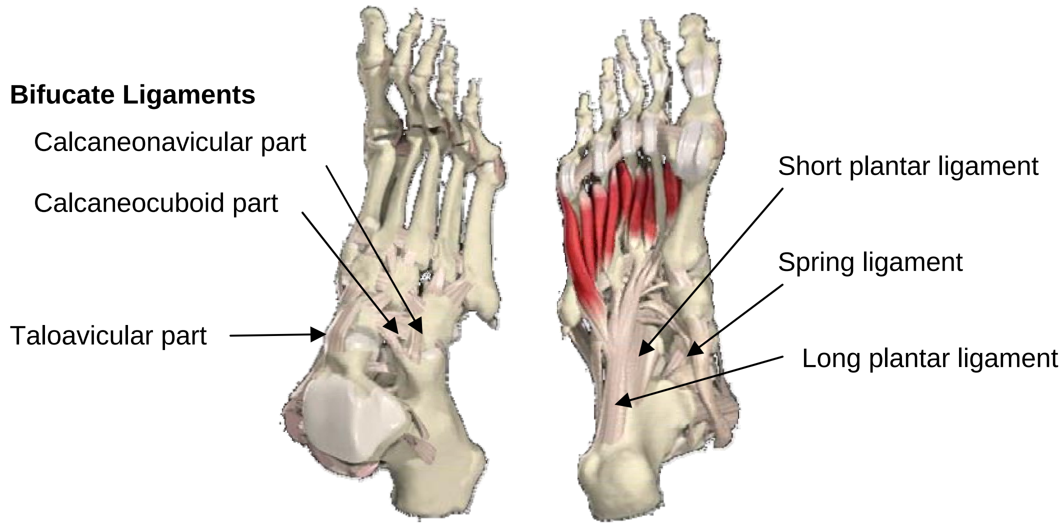


Figure 2-6. Ligaments supporting the midtarsal joint (Interactive foot and ankle, 1999).

The midtarsal joint is a composite joint where motion occurs about two separate triplanar joint axes, namely the longitudinal and the oblique axis. Functionally, movement of the forefoot about each joint axis occurs independently of the other. The predominant motion about the longitudinal axis is frontal plane inversion and eversion. Plantarflexion/dorsiflexion and abduction/adduction are the predominant movements around the oblique midtarsal joint axis. These two joint axes produce the combined motion of supination and pronation of the midtarsal joint. During supination and pronation, the forefoot inverts/everts about the longitudinal axis. The motion around the oblique axis is plantar flexion with adduction, and dorsiflexion with abduction. Fewer motions occur at the calcaneocuboid joint than the talonavicular joint, with the latter generally exhibiting two to three times larger the amount of pronation/supination and dorsiflexion/plantarflexion (Lusardi and Nielsen, 2000). The amount of motion at the two midtarsal joint axes depends on the position of the subtalar joint. With supinated subtalar joint, the two joints axes are nearly perpendicular so that midtarsal joint mobility is restricted. This mechanism helps to convert the forefoot into a rigid structure for propulsion during the push-off phase of gait. When the subtalar joint is pronated, the joint axes are closed to parallel, allowing a greater midtarsal joint mobility for shock absorption of the foot.

*Distal intertarsal and tarsometatarsal joints*

The forefoot comprises of all structures that are distal to the navicular and cuboid bones, which is divided into five rays and toes. The first through third rays consist of a cuneiform and its associated metatarsal bone while the fourth and fifth rays consist of the metatarsals only. The distal intertarsal joints include those between the navicular and the cuneiform bones, between the cuboid and lateral cuneiform, and among the cuneiform bones themselves. These articulations are supported by its surrounding joint capsules and by dorsal and plantar ligaments that run between adjacent bones (Fig. 2-7). The motions of distal intertarsal joints are limited and contribute to pronation and supination of the foot.

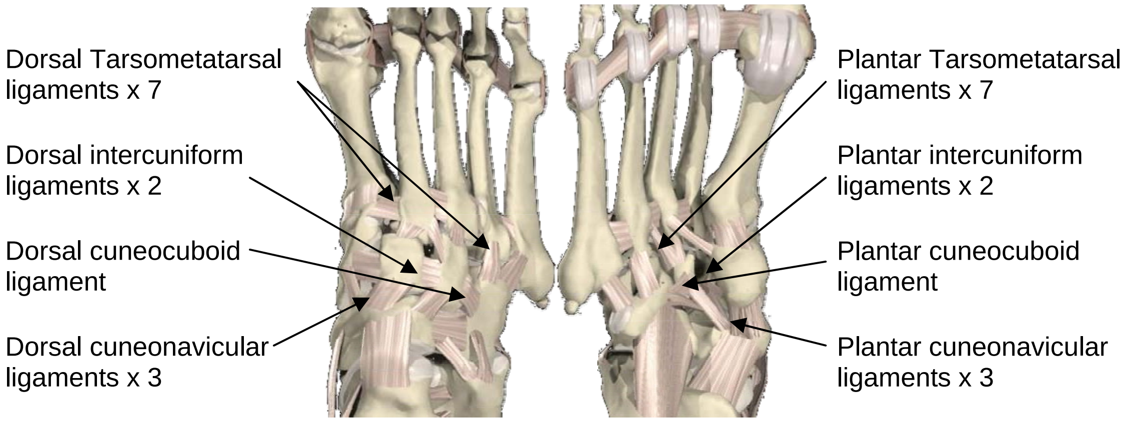


Figure 2-7. Ligaments supporting the distal intertarsal and tarsometatarsal joints (Interactive foot and ankle, 1999).

The tarsometatarsal joints of the toes, also known as the Lisfranc's joint, are gliding joints with limited mobility. These articulations are supported by joint capsules, forming three separate joint spaces: (1) between the medial cuneiform and first metatarsal, (2) between the second and third metatarsals and the middle and lateral cuneiform bones, and (3) between the cuboid and the fourth and fifth metatarsal bones. The cuneometatarsal ligaments of the first and second toes provide the primary support to these joints. The mobility of the tarsometatarsal joints varies across the toes. The first tarsometatarsal joint primarily allows sagittal motion. The motions of the tarsometatarsal joint of the great toe are small in the transverse and frontal planes. Motion at the second tarsometatarsal joint is even more limited than the first. Limited motion results from the tightly wedged base of the second metatarsal among the cuneiforms and first metatarsal. Mobility increases from the third to the fifth tarsometatarsal joints as the bases become progressively less tightly wedged and the articular surfaces become progressively more curved. The relative rigidity of the medial side of the foot provided by the bony surfaces and ligamentous support produces the necessary stability to the foot during foot propulsion.

*Metatarsophalangeal and interphalangeal joints*

The hallux has two bones, namely the proximal and distal phalanx and two corresponding joints known as the metatarsophalangeal and interphalangeal. The lesser toes have three bones, namely the proximal, middle, and distal phalanges and three associated joints. The proximal articular surfaces of metatarsophalangeal and interphalangeal joints are convex, and the distal articular surface is concave. The metatarsophalangeal joints of the toes are supported by joint capsule, collateral ligaments, and a fibrous plantar plate covering the plantar surface of the joints (Fig. 2-8). The metatarsophalangeal joints of the toes exhibit motion primarily in the sagittal plane. The metatarsophalangeal joints have separate vertical and transverse axes of motion. The primary motions are plantarflexion and dorsiflexion with slight eversion and inversion and minimal transverse motion.

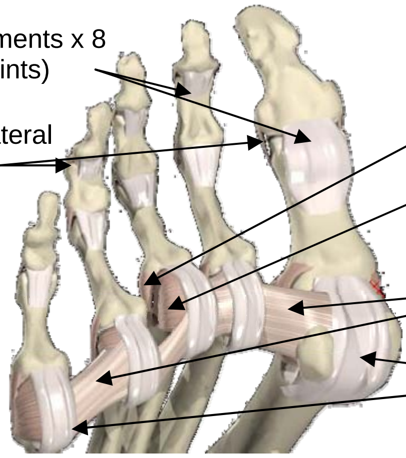


Figure 2-8. Ligaments supporting the metatarsophalangeal and interphalangeal joints (Interactive foot and ankle, 1999).

The interphalangeal joints of the toes are simple hinge joints, supported by a joint capsule, collateral ligaments, and a plantar plate (Fig. 2-8). The proximal interphalangeal joints exhibit flexion motion with minimal extension. Flexion mobility decreases from the second to the fifth toe.

The preceding discussion reveals that most of the joints of the foot contribute to the same triplanar motions of the foot, pronation and supination. Consequently, when the joints move in the same direction, the total motion of the foot is increased. Conversely, individuals with restricted motion at one joint may develop increased mobility at the adjacent joints to maintain overall mobility of the foot. In addition, pronation and supination of the whole foot affect the rigidity of the foot structures. The foot becomes more flexible with simultaneous pronations of the joints while the foot is stiffer with simultaneous supination of the joints. Pronation of the foot during the stance phases of gait allows the foot to accommodate to different conditions of walking surface. Supination of the foot during the later stance phase of gait helps stabilize the foot, which serves as a rigid lever for the body to roll over it.

### 2.1.3 Plantar Fascia (Aponeurosis)

In addition to the ligaments, one of the most functionally important ligamentous structures of the foot is the plantar fascia (aponeurosis). It spans the entire length of the sole, attaching the calcaneal tuberosity proximally and passing distally along the plantar aspect of the foot, and dividing into five slips for its distal attachments at the base of the proximal phalanges (Fig. 2-9). The plantar fascia is composed mainly of longitudinally disposed fibers with a smaller proportion of transversely disposed fibers. The central portion of the length of the plantar fascia is a tough and thick band of tissue, possessing tensile strength of about twice the strength of the ligaments in the foot. The plantar fascia plays an extremely important role in providing the stability and support of the arches of the foot.

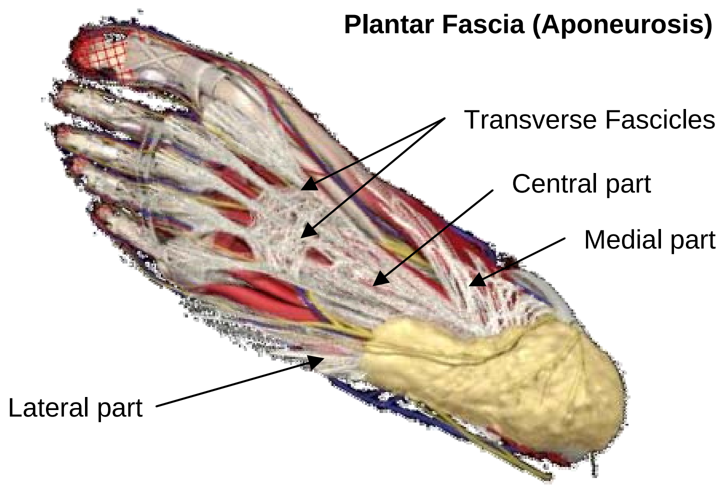


Figure 2-9. Plantar fascia (Aponeurosis) (Interactive foot and ankle, 1999).

### 2.1.4 Arches of the Foot

The articulated foot exhibits three arch-like configurations, medial and lateral longitudinal arches and the transverse arch (Fig. 2-10). The longitudinal and transverse arches are formed by the ligamentous and osseous structures of the foot. The medial longitudinal arch is composed of the calcaneus, talus, navicular, medial cuneiform, and first metatarsal bone. The lateral longitudinal arch consists of the calcaneus, cuboid, and fifth metatarsal bones. The transverse arch can be observed from the interconnecting cuboid and cuneiform bones, which continues at the bases of the metatarsals.

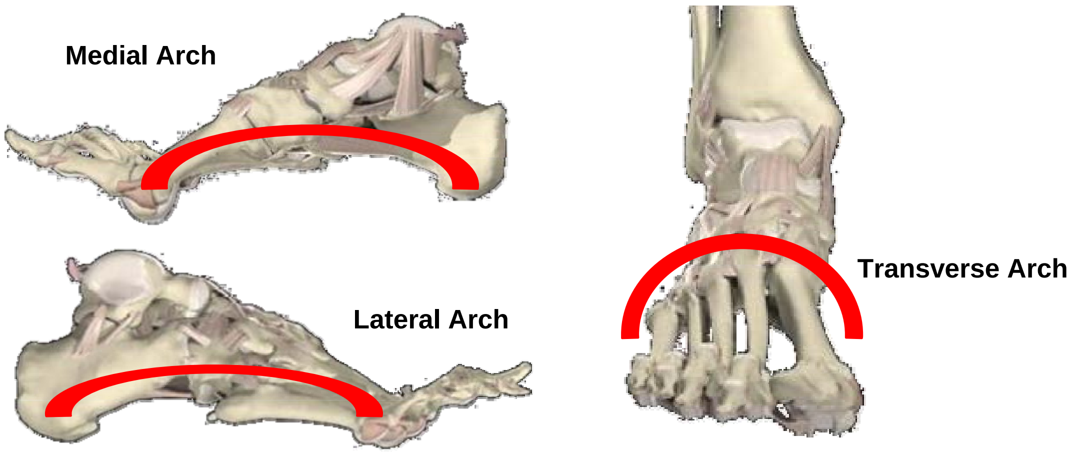


Figure 2-10. Arches of the foot (Interactive foot and ankle, 1999).

Integrity of the arches depends primarily on the ligamentous support with assistance from bony alignment and additional support from the intrinsic and extrinsic muscles of the foot. The plantar fascia, long and short plantar ligaments, the spring ligament, the collateral ligaments of the ankle, and the interosseous ligament of the subtalar joint are important supporting structures for the foot arches. During weightbearing, the height of the arch is reduced as the supporting ligamentous structures are elongated. The foot arches protect the nerves, blood vessels, and muscles on the plantar surface of the foot from compression during weightbearing.

Arch height is measured directly by determining the height of the navicular or the dorsum of the foot from the ground during weightbearing. The arch index provides an indirect measure of the integrity of the arch by examining the amount of contact with the ground made by the midfoot. A flatfoot, or pes planus, refers to a diminished medial longitudinal arch, and a pes cavus indicates an abnormally high medial longitudinal arch.

### 2.1.5 Foot Biomechanics during Gait

*Gait cycle*

The gait cycle can be broken down into two distinct phases namely the stance and swing phases. The foot is in contact with the ground during stance phase while the foot is not in contact with the ground during swing phase. In normal gait, stance phase begins with initial heel contact and ends when the hallux leaves the ground. The swing phase then begins at toe-off and ends with following initial heel contact. The stance phase can be divided into five distinct phases, namely initial contact, loading response, midstance, terminal stance, and preswing. Swing phase consists of three phases, namely initial swing, mid-swing, and terminal swing.

In normal gait, stance is approximately 60% of the gait cycle, and swing is approximately 40% of the gait cycle. Walking velocity will influence the exact distribution of the gait cycle between stance and swing phases. At a higher walking speed, the relative percentage of swing is increased and stance is decreased. In addition, increased walking velocity is associated with increases in both cadence and stride length and a decrease in the absolute time spent in both stance and swing phases.

During the first 10 -12% of the gait cycle after initial contact, the opposite limb remains in contact with the ground and double-limb stance occurs. As the opposite limb leaves the ground and swings forward, the stance limb is in single-limb support. At about 50% of the gait cycle, the opposite foot makes contact with the ground again (opposite initial contact), and a second period of double-limb stance begins.

*Progression of the foot during the gait cycle*

Initial contact occurs at 0% of the gait cycle when the foot contacts the floor. During normal gait, the initial contact by the heel on the ground occurs with the ankle at nearly neutral position or in 3 to 5 degrees of plantar flexion. The position of the foot and limb at initial contact determines the loading response pattern. During normal gait, the heel makes contact first. Loading response occurs from 0% to approximately 10% of the gait cycle.

Midstance occurs from approximately 10-30% of the gait cycle and represents the first half of single-limb support. Midstance begins when the contralateral foot leaves the ground and ends as the centre of mass is aligned over the stance limb. During the midstance, the tibia rotates anteriorly over the stationary foot. Once the forefoot has contacted the ground during midstance, the ankle joint of supporting foot serves as a fulcrum for continuous forward progression of the body. The ankle joint then starts to dorsiflex up to about 10 degrees of ankle dorsiflexion. With the foot fixed on the floor, there is medial rotation about the vertical axis of the leg with respect to the foot.

Terminal stance occurs from about 30-50% of the gait cycle, which begins with heel rise and continues until opposite initial contact. During terminal stance, forward progression of the body continues over the supporting foot with the metatarsophalangeal joints serving as a fulcrum after heel rise. The ankle plantar flexes rapidly during the terminal stance, reaching about 30 degrees of plantarflexion by the end of stance phase. While the toes help to stabilize the foot on the ground, the tibia advances forward proximally with knee flexion to prepare for the swing phase. The leg rotates externally with respect to the plantar flexing foot during the terminal stance.

Preswing occurs from 50-60% of the gait cycle, which concludes with toe-off and marks the onset of swing. During this phase, body weight is shifted to the opposite limb during loading response on the opposite leg. Dorsiflexion of the foot begins at toe-off and the ankle joint reaches its neutral position at mid-swing as the swing limb passes in front of the stance limb.

Initial swing occurs from 60-70% of the gait cycle, which begins at toe-off and ends when the swinging limb is parallel to opposing stance foot. Mid-swing occurs from 73-87% of the gait cycle and ends when the tibia is vertical. Terminal swing (87-100% of the gait cycle) is the last phase and ends with initial contact of the swing limb. Limb advancement is completed at the end of terminal swing, which prepares the limb for the stance. The ankle remains in its neutral position after mid-swing but may return in a slightly plantarflexed position of up 5 degrees during terminal swing before taking the next initial contact for the subsequent gait cycle.

### *Function of the foot during gait*

The foot and ankle complex attenuates the impact forces, maintains equilibrium, and transmits propulsive forces during gait. The elastic properties of the fatty pad under the heel provide an important function to cushion impacts of the foot with the ground. During the initial contact and loading response, the heel helps to absorb and attenuate the shock and impact forces due to landing of the foot on the ground. In addition to transmitting the impact forces to the lower extremities and the rest of the body, the foot help to adapt to different surface conditions during landing.

The elastic properties of the tendon and the ligamentous structures of the arch of the foot provide another important function in human locomotion. During the midstance, the subtalar joint pronates or everts, resulting in a flexible midfoot structure. Deformation of the longitudinal arches of the foot helps to attenuate the forces on the foot in response to the progressive loading of bodyweight. The osseous structures resist the lowering of the arch and protect the foot by sustaining the forces on the foot.

During terminal stance, the arch rises as the supinated subtalar joint, creating a rigid midfoot structure, serving as a rigid lever for propulsion and push-off. The foot and lower leg help to transmit propulsive forces generated by muscles of the lower extremity to the ground. The ability of the foot and lower leg to accomplish aforementioned functions depends on the integrity of the various structures of the foot. When the ankle-foot complex is unable to compensate for deficits in motion or structure, gait abnormalities and painful foot syndromes may occur.

## *2.2 Review on Finite Element Analysis of Foot and Footwear*

### 2.2.1 Why Finite Element Analysis?

Finite element methods were early introduced to analyse structural mechanics problems. Continuous advancement in numerical techniques as well as computer technology has made the FE method a versatile tool for biomechanics applications. Computational method is a viable alternative to experimental studies and is capable of providing a realistic simulation of the *in vivo* conditions. Moreover, a FE simulation can provide a great deal of insight into the internal stress distribution and deformation of the system and can handle complex geometries and material properties encountered in modeling human foot and ankle structures. It allows the investigator to make rapid changes of input parameters to observe their effects on the response. The flexibility in simulation of complex loading and pathological situation of the foot and ankle complex using FE modeling is of great advantage comparing with the use of sophisticated experimental setup.

Many experimental techniques were developed in the literature for the quantification of foot biomechanics, surgical and footwear performances (Hosein and Lord, 2000; Kitaoka et al., 1994b, Leung et al., 1998; Lobmann et al., 2001; Mundermann et al., 2003; Reiber et al., 2002). Experimental studies have often been restricted to study the gross response of the foot and ankle due to the complexity of the ankle-foot structures and the limitations of the experimental setup. Due to the difficulties and lack of technology and the invasive nature of experimental measurements, evaluation of biomechanical parameters such as bone and joint motion, shear and frictional properties and internal stress and strain are relatively sparse (Hosein and Lord, 2000; Kogler et al., 1995, 1999; Stacoff et al., 2000). Cadaveric studies (Ahn et al., 1997; Imhauser et al., 2002; Kim et al., 2003; Kitaoka et al., 1995, 1997a, b, d, 1998, 2000, 2002; Kogler et al., 1995, 1999; Luo et al., 1997; Tochigi, 2003) can provide additional and more accurate measurement of biomechanical parameters and a better control of testing conditions and environment. However, the demand on massive and costly devices and equipment to study human gait or load response of the human foot and ankle is difficult to fulfil. Apart from the issues of reliability and repeatability, experimental measurements are also time consuming and would need to be conducted on a significant amount of patients or specimens with different characteristics to yield generalized and promising results.

In order to provide a supplement to the experimental inadequacy, many researchers have turned to the computational methods in search of more clinical information. The FE method is an adjunct to the experimental approach to predict the load distribution between the foot and different supports, which offer additional information such as the internal stress and strain of the foot structures. The FE method has been used increasingly and with great success in biomechanical research due to its capability of modeling structures with irregular geometry and complex material properties, and the ease of simulating complicated boundary and loading conditions in both static and dynamic analyses. Further, its proficiency to monitor the parametrical effects of different structural, material and testing conditions makes it an ideal tool to investigate the underlying functional biomechanics of different foot structures, pathologies, surgical and orthotic treatment.

### 2.2.2 Introduction to Finite Element Method

*General procedures of finite element analysis*

Finite element analysis usually consists of three stages: pre-processing, solution, and post-processing. In pre-processing, the model of the physical problem is defined. This includes geometrical structures, material properties, loading and boundary conditions of the problems. The solution is the stage in which the numerical problem defined in the pre-processor is solved. This can be an automatic step performed by the computer with the use of commercial package such as ABAQUS (Hibbitt, Karlsson and Sorensen Inc, Pawtucket, RI, USA) and the users need minimal participation unless solution controls involving user-defined time stepping or increment is required. Computational time depends on the increment size, iteration times, mesh density and degree of nonlinearity of the analysis. In postprocessing, the results obtained from the solution stage is interpreted and displayed. The results obtained, such as displacements, stresses, and strains or other fundamental variables of the model can be viewed either in tabular or graphical format. The user can analyse the results in each part of the model and validate the prediction by all means to see how closely the FE model reflect the actual response of the physical problem. The user may go through the above three steps again and again in order to refine the model to get the best solution from the FE analysis. It should be noticed that the solution obtained from the FE analysis is generally an approximation. How well the numerical simulation matches the physical problem depends on the assumptions made in the model's geometry, material behaviour, boundary and loading conditions.

In the FE analysis, a structure is divided into a finite number of “elements” which interact at their points of attachment, called “nodes”. The relation between load and deformation in the FE model is governed by the stiffness matrix of each single element, which is defined by the material properties prescribed by the user. Since the accuracy of the material variables defined in the FE model depends on the input data, the predictions at each step of model development need to be validated in terms of experimentally measured parameters. It is imperative to remember that the accuracy of FE predictions directly depends on assumptions made in the development of the model. Validation of a model by comparison of its predictions with experimental results should be taken as seriously as the development of the model itself. Such comparisons should be used in fine-tuning a model that replicates the essential features of the musculoskeletal system. Experimental data are also required for the adequate development and implementation of constitutive equations as well as the identification of failure modes of biological tissues in order to enhance the accuracy and value of model predications.

*Defining geometrical properties*

The geometric data of a model can be created either by internal model configuration using own FE software, model transfer from computer-aided design systems or automatic surface data acquisition from commercial digitising tools or computer topography scans. Once geometric data are obtained, the data should be processed to create a FE mesh. The first step of developing a FE mesh is to discretize the actual geometry of the structure using appropriate types of finite elements. Each element represents a discrete portion of the physical structure and elements are joined by shared nodes. The collection of nodes and elements is called mesh. The number of elements used in a particular mesh is referred to as the mesh density. The element type, shape, and location as well as the overall number of elements used in the mesh affect the results obtained from a simulation. The accuracy of the solution is primarily dependent on the quality of the mesh. Generally speaking, the greater the mesh density, the more accurate the results. As the mesh density increases, the analysis results converge to a unique solution but the computer time required for the analysis increases.

### *Defining material properties*

Once the mesh is created, material models can be associated with the elements in the mesh. In most commercial FE package, a large number of material behaviour can be defined for the modeled structures. The users must define the values of the governing material parameters for the material model (For example the values of Young's Modulus and Poisson's ratio must be provided when using linearly elasticity model). The reliability of the FE model to represent the physical problem depends strongly on the accuracy of the material parameters defined.

### *Loading and boundary conditions*

The degree of reality of the load application to the actual system is essential in having a realistic simulation of the problem. The most common forms of loading include concentrated loads, distributed loads and thermal loads. Boundary conditions are used to constrain portions of the model to remain fixed or to move by a prescribed amount and must be given to prevent a rigid body motion to occur. In a static stress analysis, the unrestrained rigid body motion will cause singularity of the governing stiffness matrix, lead to a solver problem during the solution stage and cause the simulation to terminate and stop prematurely. Displacements are applied to those parts of the model where displacements are known. Such parts may be constrained to remain fixed during the simulation or may have specified nonzero displacements. In either situation, the constraints are applied directly to the nodes of the model to specify the degree of freedom of the node.

### *Sources of nonlinearity*

Finite element analysis is often subject to sources of nonlinearity. There are three main sources of nonlinearity, namely geometric nonlinearity, material nonlinearity and boundary nonlinearity.

Geometric nonlinearity occurs whenever the magnitude of the displacements affects the response of the structure, resulting in a nonlinear strain-displacement relationship. It is possible to define a problem as a small displacement problem, ignoring the large deformation effect. However, such an approximation causes an error whenever large deformation occurs. It is obvious that the foot and ankle structures will undergo large amount of deformations. Hence, the common assumption of small deformation in linear FE analysis will lead to incorrect motion segment response. Most commercial FE analysis packages provide the capability to take into account the large deformation effect through the iteration process and the geometric relationship is refreshed for each new iteration. In this case, the change in geometry of the modeled structures is taken into account when forming the strain-displacement and the equilibrium equations.

Material nonlinearity occurs where the material stress-strain relationship is nonlinear. In this case, the material behaviour depends on current deformation state and possibly the history of the deformation. Material nonlinearity can be observed in structures undergoing nonlinear elasticity, plasticity or viscoelasticity. Material nonlinearity is commonly observed in the mechanical behaviour of biological tissue. A wide range of capability is offered in most FE packages for incorporating material nonlinearity, these include hyperelasticity, viscoelasticity or poroelasticity.

Boundary condition nonlinearity occurs whenever the displacement boundary conditions depend on the deformation of the structure. Contact problem is the most common forms of boundary nonlinearity. Finite element package such as ABAQUS provides wide range of contact and interface elements for modeling point-to-point contact or surface-to-surface contact problem. Contact problem often subjects to sources of nonlinearity including open and close condition of the contact pairs and the change in degree of rigidity of the contact problem. The articulating surfaces of the foot joints as well as the plantar foot and its support may or may not come into contact with each other under various loading and boundary conditions and the nonlinearities resulting from this are referred as contact nonlinearities.

*Solution of nonlinear problems*

Nonlinear problems require the solution of nonlinear equilibrium equations, and Newton’s method with implicit integration is used in the ABAQUS standard package (ABAQUS, 2004). Many problems involve history-dependent response; therefore, the solution is usually obtained as a series of increments, with iterations to obtain equilibrium within each increment. Increments should sometimes be kept small to assure correct modeling of history-dependent effects.

The general analysis procedures in ABAQUS offer two approaches for controlling incrementation. Direct user control of increment size is one choice, whereby the user specifies the incrementation scheme. Automatic control is the alternative approach in which the user can specify certain tolerances or error measures. By default, ABAQUS automatically chooses appropriate load increments and convergence tolerances in a nonlinear analysis. Not only does it choose the values for these parameters, it also continually adjusts them during the analysis to ensure that a solution is obtained efficiently. ABAQUS automatically selects the increment size as it develops on the response in the step. Automatic control allows nonlinear analysis to be run with confidence without extensive experience with the problem.

### *Convergence of solution*

The iteration scheme and solution control as described in ABAQUS (2004) are summarised as followed. Consider the external forces, **P**, and the internal nodal forces, **I**, acting on a body (Fig. 2-11), which are caused by the stresses in the elements that are attached to that node, the net force acting at every node must be zero for the body to be in equilibrium. The basic statement of equilibrium is that the internal forces, **I**, and the external forces, **P**, must balance each other with **P – I = 0**.

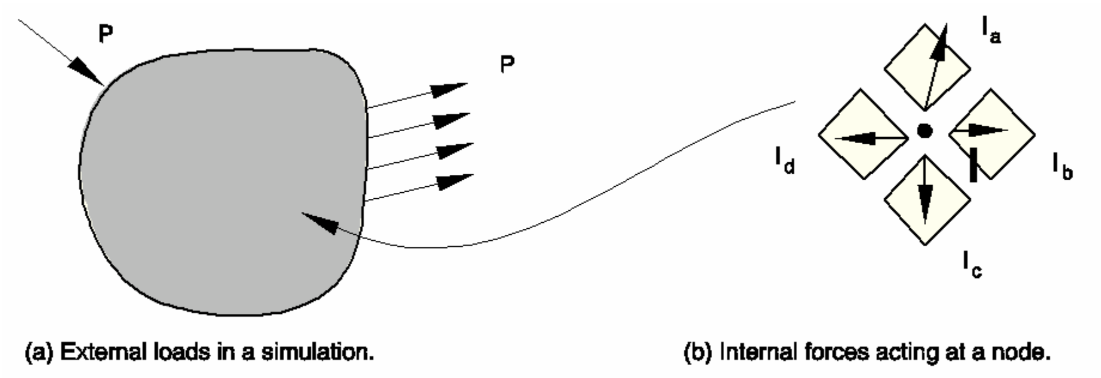


Figure 2-11. (a) External and (b) Internal loads on a body (ABAQUS, 2004).

The nonlinear response of a structure to a small load increment, $\Delta$**P**, is shown in Figure 2-12. ABAQUS uses the structure's tangent stiffness, $\mathbf{K_0}$, which is based on its configuration at $\mathbf{u_o}$, to calculate a displacement correction, $\mathbf{c_a}$, for the structure. Using $\mathbf{c_a}$, the structure's configuration is updated to $\mathbf{u_a}$. ABAQUS then calculates the structure's internal forces, $\mathbf{I_a}$, in this updated configuration. The difference between the total applied load, **P**, and $\mathbf{I_a}$ can now be calculated as $\mathbf{R_a = P - I_a}$, where $\mathbf{R_a}$ is the force residual for the iteration.

If $\mathbf{R_a}$ is zero at every degree of freedom in the model, point **a** in Figure 2-12 would lie on the load-deflection curve and the structure would be in equilibrium. In a nonlinear problem $\mathbf{R_a}$ will never be exactly zero, so ABAQUS compares it to a tolerance value. If $\mathbf{R_a}$ is less than this force residual tolerance at all nodes, ABAQUS accepts the solution as being in equilibrium. By default, this tolerance value is set to 0.5% of an average force in the structure, averaged over time. ABAQUS automatically calculates this spatially and time-averaged force throughout the simulation.

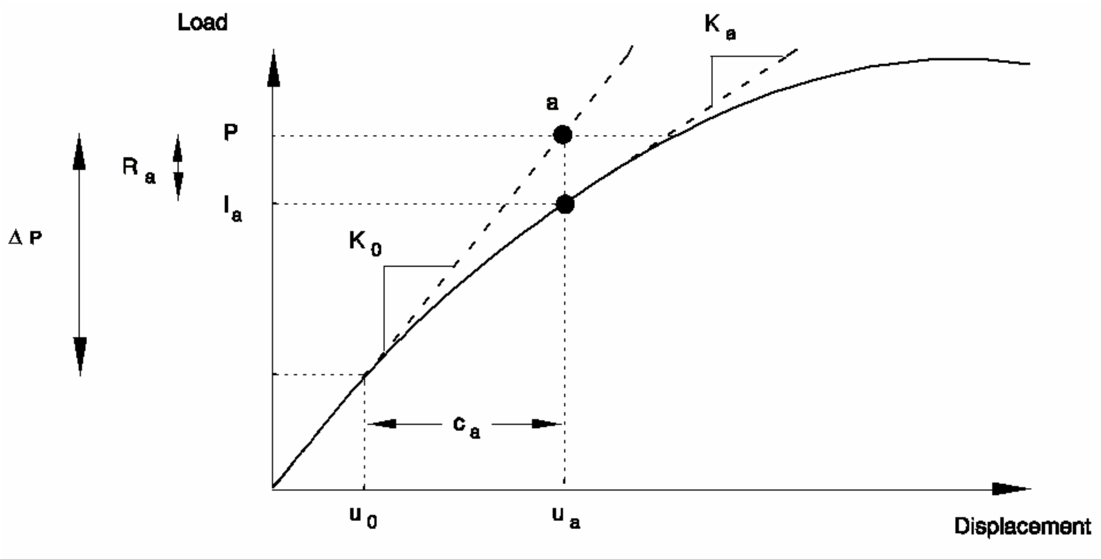


Figure 2-12. First iteration scheme in an increment (ABAQUS, 2004).

If $\mathbf{R_a}$ is less than the current tolerance value, $\mathbf{P}$ and $\mathbf{I_a}$ are considered to be in equilibrium and $\mathbf{u_a}$ is a valid equilibrium configuration for the structure under the applied load. However, before ABAQUS accepts the solution, it also checks that the last displacement correction, $\mathbf{c_a}$, is small relative to the total incremental displacement, $\Delta\mathbf{u_a} = \mathbf{u_a} - \mathbf{u_o}$. If $\mathbf{c_a}$ is greater than a fraction (1% by default) of the incremental displacement, ABAQUS performs another iteration. Both convergence checks must be satisfied before a solution is said to have converged for that time increment.

If the solution from an iteration is not converged, ABAQUS performs another iteration to try to bring the internal and external forces into balance. First, ABAQUS forms the new stiffness, $\mathbf{K_a}$, for the structure based on the updated configuration, $\mathbf{u_a}$. This stiffness, together with the residual $\mathbf{R_a}$, determines another displacement correction, $\mathbf{c_b}$, that brings the system closer to equilibrium (point **b** in Figure 2-13).

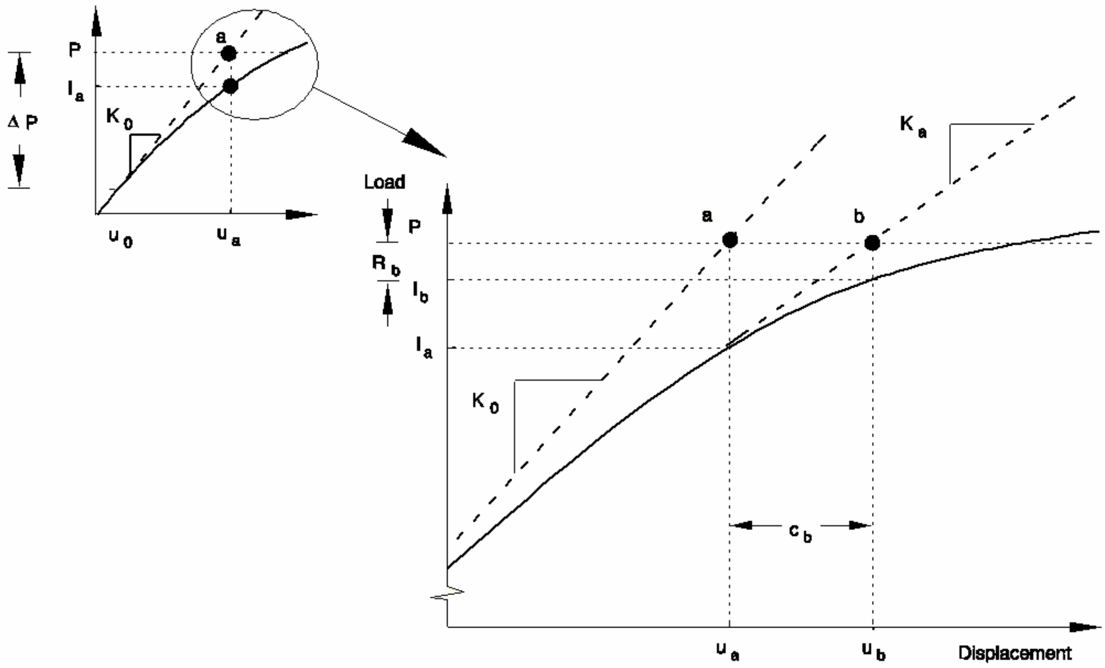


Figure 2-13. Second iteration scheme in an element (ABAQUS, 2004).

ABAQUS calculates a new force residual, $\mathbf{R_b}$, using the internal forces from the structure's new configuration, $\mathbf{u_b}$. Again, the largest force residual at any degree of freedom, $\mathbf{R_b}$, is compared against the force residual tolerance, and the displacement correction for the second iteration, $\mathbf{c_b}$, is compared to the increment of displacement, $\Delta\mathbf{u_b}$. If necessary, ABAQUS performs further iterations. For each iteration in a nonlinear analysis, ABAQUS forms the model's stiffness matrix and solves a system of equations. Therefore, the computational cost of each iteration is close to the cost of conducting a complete linear analysis, making the computational expense of a nonlinear analysis become many times greater than the cost of a linear analysis.

By default, ABAQUS automatically adjusts the size of the time increments to solve nonlinear problems (ABAQUS, 2004). The user needs to suggest the size of the first increment in each step of the simulation, after which ABAQUS automatically adjusts the size of the increments. If the user does not provide a suggested initial increment size, ABAQUS will attempt to apply all of the loads defined in the step in a single increment. The increment size may have to be reduced repeatedly to obtain a solution for highly nonlinear problems. Besides, the number of iterations needed to find a converged solution for a time increment will vary depending on the degree of nonlinearity in the system.

### 2.2.3 History of Finite Element Analysis on Foot and Footwear Research

Computational methods such as the FE approach have been widely used in studying a variety of biomechanical systems such as the intervertebral joint, knee and hip joint. However, the development of detail finite element foot model has just been sparked off in the late 90's due to the complexity of the ankle-foot structures. In the following, the current establishment of FE models for the biomechanical research of human foot and footwear is reviewed.

*Finite element analysis of foot biomechanics research*

Computational modeling of the human foot and ankle in the past has often been restricted to the conventional modeling approach due to the limitation of computer capability. Conventional computational models consider the skeletal structures as series connections of rigid segments with prescribed degrees of freedom of the joints and the soft tissue constraint and behaviour modeled by spring and damper model. Scott and Winter (1993) developed a biomechanical model of the human foot in which the foot was represented as eight rigid segments and eight monocentric, single-degree-of-freedom joints. The soft tissue under the foot was divided into seven independent sites of contact, or loading, and each of these was modeled as a nonlinear spring and a nonlinear damper in-parallel. The computational foot model was used to quantify the contributions of individual muscles in supporting the body during normal gait based on a dynamic optimization approach. Recently, a computational model of the foot considering the role of muscles, tendons, and ligaments was developed by Salathe and Arangio (2002) to determine the distribution of support under the metatarsal heads, the tension in the plantar aponeurosis, and the bending moment at each of the joints of the foot. Although the conventional models can provide important information in terms of the kinematics and kinetics of the foot during the stance phase of walking, and are computationally more efficient for dynamic simulation and optimization of solution, they have difficulties in incorporating the realistic structural deformation and interaction especially for the highly deformed soft tissue components and obtaining an analytical solution. Alternatively, the numerical approach used by the FE technique enables efficient estimation of an approximated solution of complicated problems simulating complex structural, material and loading properties.

With the fast expanding computer technology, FE model of the human foot and ankle having complex and irregular geometrical structures can be established in the late 90's. Over the past decade, both two and three-dimensional models have been built to explore the biomechanics of the ankle-foot structures (Bandak et al., 2001; Camacho et al., 2002; Chen et al., 2001; Erdemir et al., 2006; Gefen et al., 2000; Gefen, 2001, 2002, 2003a; Giddings et al., 2000; Jacob and Patil 1999; Kitagawa et al., 2000; Spears et al., 2005; Thomas et al., 2004). Table 2-1 summarizes the model characteristics and applications of existing FE foot models in the literature.

Table 2-1. Summary of the configurations of existing FE foot models in the literature

| Years | Authors | Geometrical Properties | Material and Loading Conditions | Parameters of interest |
|---|---|---|---|---|
| 2000 | Kitagawa et al. | 3D, CT images of cadaveric foot<br>(ankle-foot bones) | Bones, ligaments, plantar tissue (linearly elastic)<br>Contact simulation of major joints & plantar support<br>Static & impact compression on foot | Force & deformation of foot under static & dynamic compression load |
| 2000 | Giddings et al. | 2D, CT image of subject<br>(foot bones) | Bones, cartilages, ligaments, tendon (linearly elastic)<br>Contact simulation of major joints<br>Ground reaction forces to simulate 6 stance phases | Load distribution of foot joints & ligamentous structures during stance phases of gait |
| 2001 | Bandak et al. | 3D, CT images of cadaveric foot<br>(ankle-foot bones, plantar soft tissue) | Bones, cartilage, plantar tissue (viscoelastic)<br>ligaments (linearly elastic)<br>Contact simulation of major joints & plantar support<br>Vertical impact load at various initial velocities | Stress distribution of rearfoot bones & ankle ligaments under impact loading |
| 2001 | Chen et al. | 3D, CT images of subject<br>(ankle-foot bones,<br>encapsulated soft tissue) | Bones, ligaments, cartilages, soft tissue (linearly elastic)<br>Contact simulation of plantar support<br>Displacement control between plantar foot & ground support to simulate midstance to push-off phases | Plantar foot pressure & bone stress during simulated stances |
| 2002 | Camacho et al. | 3D, CT images of cadveric foot<br>(ankle-foot bones, plantar soft tissue) | - | Relative positions of foot bones |
| 2000<br>2001<br>2002b | Gefen et al.<br>Gefen<br>Gefen | 3D, MR images of subject<br>(foot bones, plantar soft tissue) | Bones, cartilage (linearly elastic)<br>Ligaments, plantar tissue (nonlinearly elastic)<br>Ankle joint & major muscular forces to simulate 6 stance phases | Stress distribution of foot bones & soft tissues during simulated stances with varying ground reaction forces locations & muscle forces |
| 2002a<br>2003 | Gefen<br>Gefen | 2D, MR images of subject<br>(foot bones, plantar soft tissue) | Bones, cartilage (linearly elastic)<br>Ligaments, plantar tissue (nonlinearly elastic)<br>Ankle joint & Achilles tendon forces to simulate balanced standing | Partial and complete plantar fascia release<br>Plantar soft tissue stiffening |
| 1999a<br>1999b<br>2004 | Jacob & Patil<br>Jacob & Patil<br>Thomas et al. | 3D, X-rays of subject<br>(foot bones, plantar soft tissue) | Bones, cartilages, ligaments, plantar tissue (linearly elastic)<br>Ankle joint & major muscular forces to simulate heel strike, midstance & push-off | Dysfunction of peroneal & dorsiflexor muscles<br>Reduction in midfoot cartilage thickness<br>Plantar soft tissue stiffening, varying plantar tissue thickness & hardness |
| 2005 | Spears et al. | 3D, CT images of cadveric foot<br>(heel bone, heel pad tissue) | Heel bones (rigid), plantar heel pad (hyperelastic & viscoelastic)<br>Contact simulation of heel support<br>Vertical ground reaction force to simulate heel strike | Heel tissue stress with varying force, loading rates & foot-ground inclination |
| 2006 | Erdemir et al. | 2D, MR image of subject<br>(heel bone, heel pad tissue) | Bone (rigid), heel pad (hyperelastic)<br>Contact simulation of foot-support interface<br>Vertical load on heel bone to simulate loading on heel | 5 heel pad thickness & 40 subject-specific stress-strain properties on peak heel pressure |

Giddings et al. (2000) developed a 2D FE model of the foot from a sagittal CT image of the foot to study the loading on the joint, ligaments and calcaneus. The model was divided into the talus, calcaneus and the fused midfoot and forefoot bony structures connected by the major plantar ligaments and the Achilles tendon. All structures were defined as linearly elastic and the interactions of the calcaneotalar and calcaneocuboid joints were defined as contacting articulating surfaces. The ground reaction forces and major ankle moments obtained from the force platform were applied to simulate walking and running at speeds of of 1.6 and 3.7 m/s, respectively. Maximum joint forces of the hindfoot were predicted at 70% and 60% of the stance phase, respectively during walking and running. The tension on the Achilles tendon and the plantar fascia were found to increase with gait velocities in similar scales. The trajectories of the predicted principal stresses were found to qualitatively correspond to the calcaneal trabecular architecture.

Gefen (2002a) built five 2D models from MR images to represent the five rays of the foot to study the effects of partial and complete plantar fascia release on arch deformation and soft tissue tensions during standing. Bony elements and cartilage were idealized to linearly elastic and isotropic materials, while the ligaments, fascia and the soft tissue fat pad were defined as nonlinearly elastic materials. The ankle joint force and Achilles tendon reaction along with constrained plantar surface displacements were applied to simulate balanced standing. Simulation of partial and total release of the plantar fascia was carried out by gradually decreasing the fascia's thickness in intervals of 25%, until it was completely detached. The change in the vertical height of the arch that occurred with the application of body weight increased from 0.3 mm to about 3 mm when the plantar fascia was released completely. Removal of the plantar fascia increased about two to three times the tensions of the long plantar ligament and up to 65% of metatarsal stress from the model predictions.

Using the same 2D FE model, Gefen (2003a) investigated the biomechanical effects of soft tissue stiffening in the diabetic feet. The models predicted about 50% increase in forefoot contact pressure of the standing foot with 5 times the stiffness of normal tissue. Increasing soft tissue stiffness was found to increase the peak plantar pressure but with minimal effect on the bony structures. Gefen (2003a) further speculated from the FE predictions that the development of diabetic foot related infection and injury was more likely initiated by micro-damage of tissue from intensified stress in the deeper subcutaneous layers rather than the skin surface.

Erdemir et al. (2006) studied the effect of five different heel pad thicknesses and the nonlinear stress-strain properties of 40 normal and diabetic subjects on the predicted peak heel pressure using a 2D hyperelastic FE model of the heel. The subject-specific mechanical properties of heel pad tissues were calculated using a combined FE and ultrasound indentation technique to allow the true stress-strain behaviour of heel pad tissue to be predicted. The heel pad thickness and stiffness of diabetic subjects were not significantly different from normal subjects. By comparing the predicted peak plantar pressure obtained from the average and subject-specific hyperelastic material models during simulated heel weightbearing, root mean square errors of up to 7% were reported from the FE analyses. The highly individualized heel pad material properties suggested that the importance of acquiring subject-specific descriptions of the nonlinear elastic behaviour.

Spears et al. (2005) developed a viscoelastic 3D FE model of the heel from CT images to quantify the relationship between magnitude of force, time to peak force, and sole angle with internal stresses in the heel. The material model was based on force-displacement data derived from *in vitro* experiments. Internal stresses and external plantar pressures were investigated for different forces, loading rates and angles of foot inclination in the sagittal plane. The greatest internal compressive stress was predicted in the heel pad inferior to the calcaneal tuberosity. Peak internal compressive stress was greater than external plantar pressure. Increasing the loading rate caused plantar pressure to increase to a greater extent than internal stress. The general levels of stress were higher when the heel was loaded in an inclined position. Increasing the loading rate caused a decrease in contact area, strains and an increase in plantar pressure and internal compressive stress. During simulated heel strike, the internal stresses were generally greater than the external plantar pressures. Increasing the sole angle caused increases in both external pressure and internal stress and a posterior shift of induced stress.

Jacob and Patil (1999b) developed a 3D two-arch model of the foot from X rays of subject, taking into consideration bones, cartilages, ligaments and major muscle forces, and foot sole soft tissue, which were defined as linearly elastic material. The simulation of quasi-static response such as heel strike, midstance and push-off were achieved by applying the ankle joint forces and predominant muscle forces on the foot at the points of insertion. The model structure was modified for the push-off phase by aligning the metatarsophalangeal joint angle together with the associated plantar soft tissue. The response of Hansen’s disease with muscle paralysis was studied by reducing the thickness of the cartilages between the talus, navicular and the cuneiforms and by neglecting the action of the peroneal and dorsiflexor muscles. Highest stress was predicted during push-off in the dorsal central part of the lateral and medial metatarsals, the dorsal junction of the calcaneus, and the cuboid and plantar central part of the lateral metatarsals in the foot. The stresses in the tarsal bone regions during push-off increased with muscle paralysis simulation. The predicted peak normal stresses at the plantar soft tissue were comparable with corresponding pressure measurement by the pedobarograph.

The same model was employed by Jacob and Patil (1999a) to study the effect of soft tissue stiffening with diabetic neuropathic foot on stress distribution of the foot. The elastic moduli of the normal and stiffened soft tissue were taken as 1 MPa and 4 MPa, respectively. The maximum normal stresses of the plantar foot in diabetic neuropathy were higher and the forefoot region increased with a larger extent compared to the heel region. The simulation of diabetic neuropathy with soft tissue stiffening was found to have negligible effect on stress distribution of the foot bones. Thomas et al. (2004) further utilized the same FE model to study the effect of foot sole tissue thickness and hardness in diabetes on the stress distribution of the plantar foot during push-off. Comparing to the normal forefoot sole of thickness 13 mm, the predicted normal and shear stress of the foot sole increased more than 50% in the diabetic forefoot sole of thickness 7.8mm.

A 3D FE model of the human foot and ankle was developed by Chen et al. (2001) using CT images of 2mm intervals to demonstrate the capability of the FE model to estimate the plantar foot pressure and bone stresses. The model consisted of the bony structures, encapsulated soft tissue and the major plantar ligamentous structures. The joint spaces of the metatarsophalangeal joints and the ankle joint were fused with layers of cartilage elements while the rest of the bony structures were merged. All the structures were assumed to be homogeneous and linearly elastic. Interfacial contact with a frictional coefficient of 0.3 between the plantar foot and a rigid ground support was established to simulate heel-off and push-off phases during normal walking. The peak stress region was shifted from the second metatarsal to the other metatarsal from the midstance to push-off. The predicted plantar stress distribution was found to agree with the reported plantar pressure measurements.

Gefen et al. (2000) developed a 3D model of the foot, including cartilage and ligament connection for 17 bony elements. Each toe was unified as a single unit and 38 major ligaments and the plantar fascia were incorporated. A pad of soft tissue, covering the plantar aspects of the foot was included. Bony elements and cartilage were idealized as linearly elastic and isotropic materials, while the ligaments, fascia and the soft tissue fat pad were defined as nonlinearly elastic material. The ankle joint forces and the major muscular reactions were applied to represent the physiological loading condition of 6 different stance phases. The model structure was adapted for each stance phase by alternating the inclination of the foot and alignment of the phalanges together with associated plantar soft tissue pad. The displacement of the contacting plantar surface in corresponding stance phases was constraint. The model predicted the highest stress values to appear in the dorsal part of the mid-metatarsals from midstance to toe-off. Other high stress regions were found during these sub-phases at the posterior aspect of the calcaneus. The predicted plantar stress distribution was found to be comparable to the plantar pressure measurement during natural gait.

Using the same FE model, Gefen (2001) investigated the change in location of centre of pressure under the heel during foot placement with forces reductions in tibialis anterior and extensor digitorum longus. Reductions of greater than 50% in the tibialis anterior force were found to cause a medialization of centre of pressure, which was thought to compromise stability and a possible cause of falling in the elderly. Gefen (2002b) also examined the changes in tissue deformations and stresses with muscle fatigue and suggested a possible cause of stress fractures in military recruits. It was found that a 40% reduction in pretibial muscle force resulted in a 50% increase in peak calcaneal stress, and that a similar force reduction in triceps surae force during push-off increased metatarsal stresses by 36%.

Bandak et al. (2001) investigated the response of the lower leg and foot to impact loading. Three-dimensional models were constructed from CT scans of cadaver specimen and the same specimens were subjected to impulsive axial impact loading.

Distinction between the material stiffness of cortical and cancellous bone was taken into accounted for the tibia, fibula, calcaneus and talus, and these bones were defined as linearly viscoelastic material. The rest of the midfoot and forefoot bone were fused and modeled as rigid bodies. Bone interactions were allowed through contacting surfaces and ligament connections. The major ligamentous structures, the plantar soft tissue and the cartilages were also defined as viscoelastic. Forces and accelerations measured at the impactor were generally comparable to those predicted by the simulation, especially at lower impact velocities. Examination of the internal stress distributions in the model showed localizations of stress at the attachment sites of the anterior talofibular ligament and the deltoid ligament, which were consistent with clinical reports of injuries sites and calcaneal fractures. A similar 3D FE model of the human foot and ankle was developed by Kitagawa et al. (2000) to study the static and impact response of the foot under compression. They concluded from their experimental validation on cadavers that the ligamentous and tendon structures were important in achieving a realistic simulation of the foot response in both static and dynamic loading conditions.

Camacho et al. (2002) described a method for creating an anatomically detailed, 3D FE model of the foot, which included descriptions of bones, plantar soft tissue, and cartilage. The employed contact modelling technique permitted calculation of the relative orientations of the bones based on the principal axes for individual bones, which were established from the inertia matrix. The developed model can provide an objective quantification of the stress/strain distribution and joint motions of the foot under different loading and boundary conditions.

### *Finite element analysis of footwear research*

Apart from the FE models for studying the foot biomechanics, several 2D or simplified 3D FE analyses were conducted to study the biomechanical effect of footwear (Barani et al., 2005; Chen et al., 2003; Chu and Reddy, 1995, Chu et al., 1995; Erdemir et al., 2005; Goske et al., 2006; Lemmon et al., 1997; Lewis, 2003; Nakamura et al., 1981; Shiang, 1997; Syngellakis et al., 2000). Table 2 summarizes the model characteristics and applications of existing FE analysis on footwear in the literature.

Table 2-2. Summary of the configurations of existing FE footwear models in the literature

| Years | Authors | Geometrical Properties | Material and Loading Conditions | Parameters of interest |
|---|---|---|---|---|
| 1981 | Nakamura et al. | 2D (unified foot bones, plantar soft tissue, shoe sole) | Bones (linearly elastic), plantar tissue (nonlinearly elastic)<br>Shoe sole (linearly / nonlinearly elastic)<br>Ankle joint & Achilles tendon forces to simulate midstance | Shoe sole stiffness on stress in plantar tissue |
| 1995<br>1995 | Chu et al.<br>Chu & Reddy | 3D (unified ankle-foot bones, encapsulated soft tissue, ankle-foot orthosis) | Bones, ligaments, encapsulated tissue, orthosis (linearly elastic)<br>Ground reaction, Achilles, flexor, extensor tendons forces to simulate heel strike & toe-off | Drop foot, stiffness of orthosis & soft tissue on stress distribution in ankle-foot orthosis |
| 1997 | Shiang | 3D (insole, midsole) | Insole (linearly elastic), midsole (nonlinearly elastic)<br>Vertical heel pressure & shear to simulate loading on heel | Different cushioning configurations of insole & midsole on plantar pressure relief |
| 2000 | Syngellakis et al. | 3D shell (ankle-foot orthosis) | Ankle-foot orthosis (nonlinearly elastic)<br>Uniform pressure at distal orthosis to simulate plantar & dorsiflexion | Thickness on stiffness characteristics of plastic ankle foot orthosis |
| 2003 | Lewis | 2D (rocker sole footwear) | Shoe surface, insole, midsole, outsole (linearly elastic)<br>Vertical loads on insole surface to simulate loading on shoe | Material of midsole & outsole on stress & displacement of shoe |
| 2003 | Chen et al. | 3D (ankle-foot bones, encapsulated soft tissue, foot orthosis) | Bones, ligaments, cartilages, encapsulated tissue, (linearly elastic), insole, midsole (hyperelastic)<br>Contact simulation of foot-support interface<br>Displacement control of plantar support to simulate midstance | Flat & total-contact insole with different material on plantar pressure distribution |
| 2004 | Verdejo & Mills | 2D (heel bone, heel pad, midsole) | Bone (linearly elastic), heel pad, midsole (hyperelastic)<br>Contact simulation of heel-support interface<br>Vertical deformation on plantar heel to simulate heel strike | Stress distribution in heel pad with & without midsole support |
| 2005 | Barani et al. | 3D (insole) | Insole (hyperelastic)<br>Vertical pressure on insole at 6 locations to simulate midstance | Insole material on stress distribution in insole |
| 1997<br>2005 | Lemmon et al.<br>Erdemir et al. | 2D (metatarsal bone, encapsulated soft tissue, insole, midsole) | Bone (linearly elastic)<br>Encapsulated tissue, insole, midsole (hyperelastic)<br>Contact simulation of foot-support interface<br>Vertical load on metatarsal bone to simulate push-off | 6 insole thicknesses, 2 tissue thicknesses, 36 plug designs of midsole (3 materials, 6 geometries, 2 locations of placement) on peak plantar pressure |
| 2006 | Goske et al. | 2D (heel bone, heel pad, shoe heel counter, insole, midsole) | Bone (Rigid), heel counter (linearly elastic)<br>heel pad, insole, midsole (hyperelastic)<br>Contact simulation of foot-shoe interface<br>Vertical load on heel bone to simulate heel strike | 3 insole conformity levels, 3 different materials, 3 insole thicknesses on heel pressure distribution |

In the early 80's, Nakamura et al. (1981) developed a 2D FE foot model, reporting the first FE analysis for footwear design. This pioneer FE model consisted of a unified bony structure of the foot, plantar soft tissue and a shoe sole layer. The foot bone was defined as linearly elastic while the plantar soft tissue and the shoe sole were defined as either linearly or nonlinearly elastic. The body weight and Achilles tendon forces were applied on the bony structure to simulate midstance. A sensitive analysis on the linearly elastic shoe sole material with Young's modulus varied from 0.08 MPa to 1000 MPa suggested an optimum range of 0.1 to 1 MPa for stress reduction in the plantar soft tissue. The stress reduction predicted from the FE model with a nonlinearly elastic foamed shoe sole was comparable to the optimized linearly elastic shoe material.

Lemmon et al. (1997) investigated alterations in pressure under the second metatarsal head as a function of 6 different insole thicknesses and 2 different tissue thicknesses using a 2D model considering the sagittal section of the second metatarsal bone with encapsulated soft tissue. Hyperelastic material models were employed to represent the material behaviour of plantar soft tissue, polyurethane insole and cloud crepe foamed midsole. Two-dimensional sliding interface elements were considered for the contact simulation between foot and footwear with a coefficient of friction of 0.5. The loading applied on the second metatarsal was calculated from plantar pressure measurement at push-off. Orthoses with relatively soft material was found to reduce peak plantar pressures. The predicted peak pressure decreased with an increase in insole thickness but the efficiency reduced with an increasing insole thickness. The pressure decrease for a given increase of insole thickness was greater when plantar tissue thickness was less. Tissue thickness was found to have a dominant effect on the plantar pressure. The predicted plantar pressure was found to resemble the corresponding measured pressure.

Using a similar 2D FE model as Lemmon et al. (1997), Erdemir et al. (2005) investigated the effects of 36 plug designs of a midsole (Microcell Puff) including a combination of three materials (Microcell Puff Lite, Plastazote medium, Poron), six geometries (straight or tapered with different sizes), and two locations of placement. Plugs that were placed according to the most pressurized area were more effective in plantar pressure reduction than those positioned based on the bony prominences. Large plugs (40mm width) made of Microcell Puff Lite or Plastazote Medium, placed at peak pressure sites, resulted in the highest peak pressure reductions of up to 28%.

A 2D FE model of the heel developed by Goske et al. (2006) was used to investigate the material and structural insole design factors on pressure distribution. Combinations of three insole conformity levels (flat, half conforming, full conforming), three insole thickness values (6.3, 9.5 and 12.7 mm) and three insole materials (Poron Cushioning, Microcel Puff Lite and Microcel Puff) were simulated during heel strike. Conformity of the insole was found to be a more important design factor than insole material in terms of peak pressure reduction. The FE model predicted a 24% reduction in peak plantar pressure compared to the barefoot condition using flat insoles while the pressure reduced up to 44% for full conforming insoles. In addition, increasing the insole thickness was found to provide pressure reduction.

Shiang (1997) introduced a 3D FE model of the shoe soles, composing of the insole and midsole with measured heel pressure applied as the loading condition at the heel region. Nonlinear elasticity was defined for the soft tissue and insole/midsole properties. The mean peak plantar pressure of the running situation was found to be higher than that of the walking situation as predicted and that the present of an insole provided better cushioning effect. The results showed that nonlinear stress/strain curve and compressibility offered by the nonlinear hyperfoam approach provided a better approximation of the behaviour of footwear material because of large deflections of structures. Addition of an insole layer especially with a contoured surface on top of the midsole was found to provide better cushioning performance for plantar pressure relief.

Verdejo and Mills (2004) studied stress distribution of the heel pad during simulated bare heel running and with EVA foamed midsole using a 2D hyperelastic FE model. The heel pad was found to have a higher order of nonlinearity but a lower initial stiffness than the foam material. The predicted peak plantar pressure with bare heel strike was about two times the pressure during shod condition.

A 3D hyperelastic FE model of a full-length insole was developed by Barani et al. (2005) to study the effect of different insole materials including silicon gel, Plastozot, polyfoam, and ethylene vinyl acetate (EVA). Discrete pressures were applied at the forefoot and heel regions to simulate the loading on the insole surface during midstance. They concluded from the stress analysis of the insole that most of the materials especially Silicon Gel were effective in plantar stress reduction.

Chu et al. (1995) developed a 3D FE with simplified geometrical features of the foot and ankle and material model of linear elasticity to study the loading response of ankle-foot orthoses. With simulated heel strike and toe-off, peak compressive and tensile stress were found to concentrate at the heel and neck region of the ankle-foot orthosis, respectively. The neck region of the ankle-foot orthosis experienced the largest amount of stress, which was consistent with the common clinical observation of orthoses break down. The peak compressive stress in the orthosis was found to increase with increasing Achilles tendon force whereas the peak tensile stress decreased with increasing stiffness of the ankle ligaments. Further parametric studies on the same FE model (Chu and Reddy, 1995) suggested that the stress distribution in the orthosis is more sensitive to the stiffness of the orthosis than to the stiffness of the soft tissue.

Syngellakis et al. (2000) studied the stiffness characteristics of the plastic ankle foot orthoses using a 3D model of shell elements. Nonlinear elasticity was considered along with geometrical nonlinearity. It was found that thickness of ankle foot orthoses have a pronounced effect on the deflection of the ankle-foot orthosis. Both the material and geometrical nonlinearity were found to be essential in obtaining a realistic simulation of the stress distribution of the ankle foot orthosis.

Lewis (2003) used a 2D FE model to perform a sensitive study of the effect of the materials used for the midsole and outsole of a solid rocker bottom design of a therapeutic shoe on the stress and displacement of a model of the shoe. Linear elasticity was considered for all structures and concentrated loadings were applied on the insole surface. There were noticeable differences in the displacement and distribution of the von Mises stress at the interface between the bottom of the foot and the top of the top layer of the insole in the therapeutic shoe, as a consequence of a change in the material selected for the two layers of the midsole and outsole. The von Mises stress at the heel region was 62% higher with a relatively rigid midsole to the outsole.

Chen et al. (2003) used their previously developed 3D FE model to study the effect of flat and total-contact insole on plantar pressure distribution. The efficacies of stress reduction and redistribution by flat and total contact insoles with different material combinations were compared. Nonlinear elasticity was defined for the insoles and the frictional contact behaviour of the foot and support were considered. The results showed that the peak and average pressure normal stresses were reduced in most of the plantar regions except the midfoot and the hallux region with total contact insoles compared with the use of a flat insole. The percentage of pressure reduction by total-contact insoles with different combination of material varied with plantar foot region and the difference was not pronounced and preference could not be decided.

*Limitation of existing finite element models*

A number of FE models have been setup to quantify the motion of the foot and ankle joint and the loading on the ligamentous structures. Those models have been developed under certain simplifications and assumptions. These simplifications included assumptions of geometrical simplification, linearly elastic material properties, infinitesimal deformation and simplified loading and boundary conditions.

(a) Geometrical simplification

Some of the foot models in the literature were based on a simplified or partial foot shape. For instance, the model developed by Giddings et al. (2000) and Gefen (2002, 2003a) was in two-dimension and the out of plane loading and joint movement cannot be accounted. Even for the 3D models in the literature, they are subjected to certain geometrical simplification. For example, Jacob and Patil (1999) and Thomas et al. (2004) considered only simplified foot bone structures representing the medial and lateral arch without differentiation of individual metatarsal bones in the medial-lateral directions. The three medial metatarsals and the two lateral metatarsals were combined to represent the medial and lateral foot arch. Meanwhile, the 3D geometrical accurate model employed by Chen et al. (2001) was subjected to similar simplification with the tarsal bones modeled with two rigid columns.

In many of the 3D foot models, only the major ligaments were considered and the whole encapsulated soft tissue was not included (Bandak et al., 2001; Chen et al., 2001; Gefen et al., 2000; Jacob and Patil, 1999; Kitagawa et al., 2000). The ignorance of these structures may affect the representation of accurate structural integrity and stiffness of the ankle-foot complex. In addition to geometrical simplification, many of the FE models for footwear or insole design incorporated only parts (Erdemir et al., 2005; Goske et al., 2006; Lemmon et al., 1997), symmetric (Chu and Reddy, 1995; Chu et al, 1995) or even did not include the foot structures (Barani et al., 2005; Lewis, 2003; Shiang, 1997; Syngellakis et al., 2000). Until recently, Chen et al. (2003) employed a 3D ankle-foot model to investigate the effects of various insole designs on plantar pressure distribution.

Although there were 3D FE models in the literature (Camacho et al., 2002; Chen et al., 2001), accurate geometrical representation of the plantar foot contour, which is an important element for foot orthotic design, is still lacking. The encapsulated soft tissue modeled by Chen et al. (2001) consisted of an observable medial foot arch; however, the simulation was not able to differentiate the distinct load-bearing feature shared by individual metatarsals as can be seen from the plantar pressure predictions. The quality of the FE mesh probably needs further improvement to have a better representation of the plantar foot contour. Above all, incorporation of the surrounding shoe structures into the ankle-foot model has not been attempted for all the FE models in the literature, and the effects of motion control and pressure distribution by the shoe, insole and foot interactions cannot be addressed.

(b) Material simplification

The material behaviour of the structural components was assumed to be homogeneous, isotropic and linearly elastic in some of the foot models (Chen et al., 2001; Chu and Reddy, 1995; Chu et al., 1995; Giddings et al., 2000; Jacob and Patil 1999; Thomas et al., 2004). This is surely an approximated situation of the biological tissues, which exhibit non-homogeneous, nonlinear, inelastic, or viscoelastic behaviour. In fact, assumptions of linear material properties in early model often accompanied with the consideration on infinitesimal deformation, which further deviated from the accurate representation of the actual situation. In addition, the justification of some of the parameter selection was not provided and the values assumed deviated from experimental observation (Bandak et al., 2001; Chen et al., 2001; Chu and Reddy, 1995; Chu et al., 1995; Jacob and Patil, 1999; Thomas et al., 2004).

Improvements have been made by incorporating nonlinear analysis, taking into consideration the nonlinearities, resulting from geometric nonlinearity mainly from large deformation of materials and material nonlinearity. Several foot models have considered the use of nonlinear elasticity and viscoelasticity models in modeling the material behaviour of ligaments (Bandak et al., 2001; Gefen et al., 2000; Gefen, 2001, 2002, 2003), plantar soft tissue (Erdemir et al., 2005, 2006; Gefen et al., 2000; Gefen, 2001, 2002, 2003; Lemmon et al., 1997; Nakamura et al., 1981), bony structures (Bandak et al., 2001) and various insole material (Barani et al., 2005; Chen et al., 2003; Erdemir et al., 2005; Lemmon et al., 1997; Shiang, 1997; Syngellakis et al., 2000). However, some of the material models or parameters were not extracted from the ankle-foot structures and were originally from other parts of the body instead.

(c) Simplification of loading and boundary conditions

Only a limited number of FE analysis of the foot in the literature considered the physiological loading conditions (Gefen et al., 2000; Jacob and Patil, 1999; Thomas et al., 2004). In these models, force vectors were applied according to the points of insertion and line of action of the muscular force and the ground reaction forces. Muscles forces were approximated by normalized electromyography (EMG) data by assuming a constant muscle gain and cross-sectional area relationship and by force equilibrium consideration.

In the rest of the FE models, only the ground reaction forces or vertical compression forces were considered (Bandak et al., 2001; Chen et al., 2001; Chu and Reddy, 1995; Erdemir et al., 2005, 2006; Goske et al., 2006; Lemmon et al., 1997) with the stabilizing muscular forces ignored or lumped as a resulting ankle moment (Giddings et al., 2000). Apart from some of the simplified impact loading model in the literature, most models ignored the dynamic or inertia effects of the ankle-foot motion. The quasi-static simulation may hinder the dynamic biomechanical behaviour of the foot whenever acceleration of the lower limb especially at the instance of heel strike and push-off is significant.

In many of the foot models (Chen et al., 2001; Chu and Reddy, 1995; Gefen et al., 2000; Jacob and Patil, 1999), finite joint and bone movements have not been accounted with difficulties in simulating complex boundary and loading conditions. In these models, the adjacent articulating surfaces were fused by layer of connective tissue without considering the relative movement between the articulating joints (Chen et al., 2001; Gefen et al., 2000; Jacob and Patil, 1999). Although relative articulating surfaces movements were allowed in some models (Bandak et al., 2001; Giddings et al., 2000), these models consisted of only reduced number of distinct bony segments. Consequently, many of the existing models would not be able to capture the relative articulating joint movements during gait. These models were limited in predictions of relatively small ankle-foot motions and should have resulted in a representation of an overly-stiffened ankle-foot structure. For instance, the high stress values predicted in push-off phase (Chen et al., 2001) may be contributed to the reduced flexibility of the fused metatarsophalangeal joints and an abnormal stress concentration of the foot bones.

Unrealistic boundary condition with constrained plantar surface displacement of the foot was prescribed in some of the foot models (Chu and Reddy, 1995; Gefen et al., 2000; Jacob and Patil, 1999; Nakamura et al., 1981). This assumption prevents the realistic simulation of the friction and slip behaviour in contact with the foot support and results in unrealistic stress concentration and reduced deformation at the plantar foot. Chen et al. (2003) considered the frictional contact between the foot and support in their model; however, the normal stress instead of the contact pressure of the plantar foot reported in their simulation, obstructing direct comparison between predicted and measured in-shoe plantar pressure.

(b) Insufficient model validation

Model validation being done for the FE models in the literature relied on gross plantar pressure measurement or foot arch deformation. Model validation on multi-segmental joint motions and strain of the ligamentous structures has not been reported and therefore to what extent the existing FE models can predict the actual biomechanics of the ankle-foot complex is still unknown. To evaluate the reliability of the model to predict the biomechanical behaviour of the human foot and ankle, experimental validation should be done based on plantar pressure measurement, motion analysis as well as cadaveric experiment to compare the relevant biomechanical parameters.

### 2.2.4 Summary of Existing Finite Element Analysis

Previous FE foot models have shown their contributions to the understanding of biomechanical behaviour and performance of foot supports (Barani et al., 2005; Chen et al., 2003; Chu and Reddy, 1995; Chu et al., 1995; Erdemir et al., 2005; Goske et al., 2006; Lemmon et al., 1997; Lewis, 2003; Shiang, 1997; Syngellakis et al., 2000). However, more realistic geometry and mechanical properties of both bony and soft tissue components in addition to realistic physiological loadings are required in the FE analysis to provide a better representation of the foot and the supporting conditions. Having this type of comprehensive model is certainly a prerequisite to achieve objective and quantitative evaluations of the biomechanical effect of different orthotic designs. Currently, the major drawbacks for the existing foot models are the inability of accurate representation of the geometrical features of the encapsulated soft tissue and the plantar foot, realistic material behaviour, joint and foot-ground contact conditions.

With an experimentally validated FE model, it is possible to predict the plantar foot pressure, internal stress and strain of the bony and ligamentous structures under normal, pathological and various surgical conditions. The biomechanical effects of different orthotic designs on different simulated conditions can be investigated. The effects of different design parameters such as shape and material variation of different foot orthoses can be documented through a series of factorial analyses. Design parameters such as a custom-molded support, degree of heel elevation, rearfoot and forefoot posting, height of the arch support and metatarsal pad and the material stiffness of specific region of the orthosis can be considered. A number of standard and optimized designs of orthosis can be evaluated in terms of the performance on plantar pressure redistribution, alignment and stabilization of foot joints and motions.

Because of the high demanding accuracy for simulation of geometry, material behaviour, loading and boundary conditions, improvements on certain categories for the existing FE models are needed in order to be able to serve for the parametric design of foot orthoses. With the fast expanding computational and experimental techniques and equipments, a combined experimental and computational approach should provide fruitful information on the design principle of foot orthotics so as to enhance the orthotic performance and reliability.

By and large, most of FE analyses of foot or footwear in the literature (Bandak et al., 2001; Barani et al., 2005; Camacho et al., 2002; Chen et al., 2001, 2003; Chu and Reddy, 1995; Chu et al., 1995; Erdemir et al., 2005, 2006; Gefen et al., 2000; Gefen, 2001; 2002, 2003; Giddings et al., 2000; Goske et al., 2006; Jacob and Patil 1999; Kitagawa et al., 2000; Lemmon et al., 1997; Lewis, 2003; Nakamura et al., 1981; Shiang, 1997; Spears et al., 2005; Syngellakis et al., 2000; Thomas et al., 2004; Verdejo et al., 2004), were developed under certain geometrical and material simplifications. A detailed FE model of the human foot and ankle, incorporating realistic geometrical and material properties of both bony and soft tissue components is needed to provide a more realistic representation of the foot and the supporting conditions.

# CHAPTER III METHODS

The discussion of the methodology of this study is divided into three main sections. In the first section, the development of the FE model of the human foot and ankle and foot orthosis is introduced. The procedures for obtaining the geometries, material properties, loading and boundary conditions for the FE model are described. In the second section, the methods for establishing the FE simulations for individual parametrical analysis of the FE foot model are described in the order of parametrical analyses for bulk soft tissue stiffening, plantar fascia stiffness, partial and total plantar fascia release, Achilles tendon loading and posterior tibial tendon dysfunction. The cadaveric studies on six foot specimens for validating the parametrical analyses on Achilles tendon loading and posterior tibial tendon dysfunction are described. For the last section, the methods for establishing the FE simulations for different parametrical designs of foot orthosis and the *in vivo* plantar pressure measurements of the subject are described.

## *3.1 Development of the Finite Element Model*

### 3.1.1 Geometrical Properties of the Finite Element Model

*FE model of human foot and ankle*

The geometry of the human foot and ankle for building the FE model was obtained from 3D reconstruction of coronal Magnetic Resonance (MR) images from the right foot of a normal male subject of age 26, height 174 cm and weight 70 kg in the neutral foot position (Fig. 3-1). The neutral position was defined by the Standardization and Terminology Committee of the International Society of Biomechanics, who proposed a reporting standard for joint kinematics based on the joint coordinate system (Wu et al., 2002). A custom ankle-foot orthosis fabricated during upright sitting of the subject was used to maintain the neutral foot position of the supine lying subject during MR scanning. The undeformed arch height of the subject was 55 mm during upright sitting. The arch height was defined as the height of the medial navicular cortex to the ground support. For the sake of maintaining image quality and avoiding unnecessary details of the surface texture of the foot bones, MR images with 2mm intervals were chosen.


Figure 3-1. Acquisition of coronal MR images of the foot and ankle in the neutral foot position.

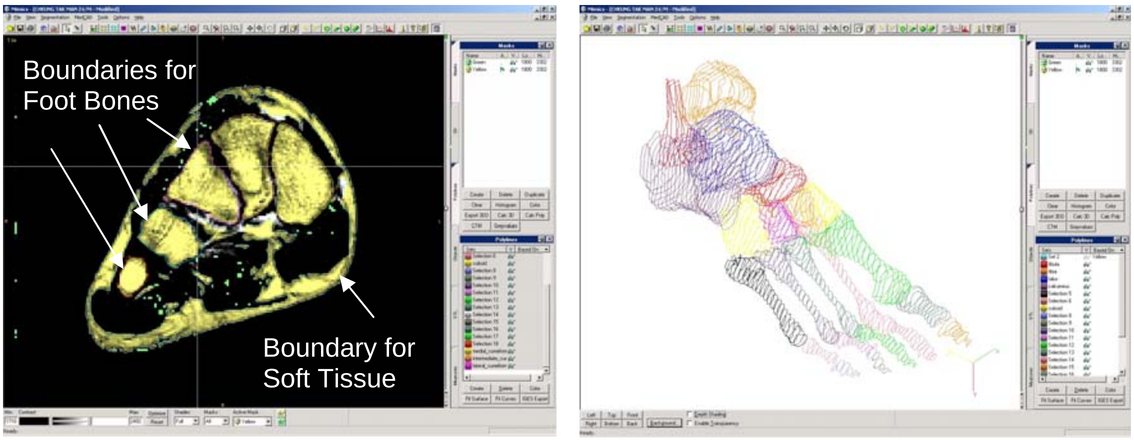


Figure 3-2. Segmentation of MR images using MIMICS v7.10 (Materialise, Leuven, Belgium).

The MR images were segmented using MIMICS v7.10 (Materialise, Leuven, Belgium) to obtain the boundaries of skeleton and skin surface (Fig. 3-2). For the sake of simplification, the articular cartilages of the bones were fused with their corresponding bone surfaces in the segmentation process. The boundary surfaces of the skeletal and skin components (Fig. 3-3) were processed using SolidWorks 2001 (SolidWorks Corporation, Massachusetts, USA) to form solid models for each bone and the whole foot surface. The solid model was then imported and assembled in the FE package, ABAQUS (version 6.4, Hibbitt, Karlsson and Sorensen, Inc., Pawtucket, RI, USA).

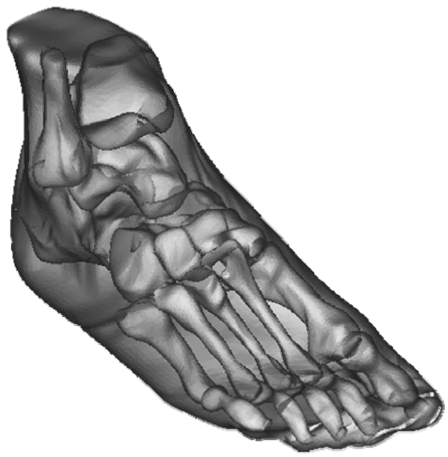

Figure 3-3. Surface model for foot bones and encapsulated soft tissue.

The FE model of the human foot and ankle, as shown in Fig. 3-4, consisted of 28 bony segments, including the distal segments of the tibia and fibula and 26 foot bones: talus, calcaneus, cuboid, navicular, 3 cuneiforms, 5 metatarsals and 14 components of the phalanges embedded in a volume of encapsulated bulk soft tissue. The phalangeal bones were connected together and spaced by 2 mm using solid elements, which represented the thickness of the articulating cartilage layers and simulated the connection of the cartilage and other connective tissues. The interactions among the metatarsals, cuneiforms, cuboid, navicular, talus, calcaneus, tibia and fibula were defined as contacting elastic bodies to allow the simulation of relative bone movement.

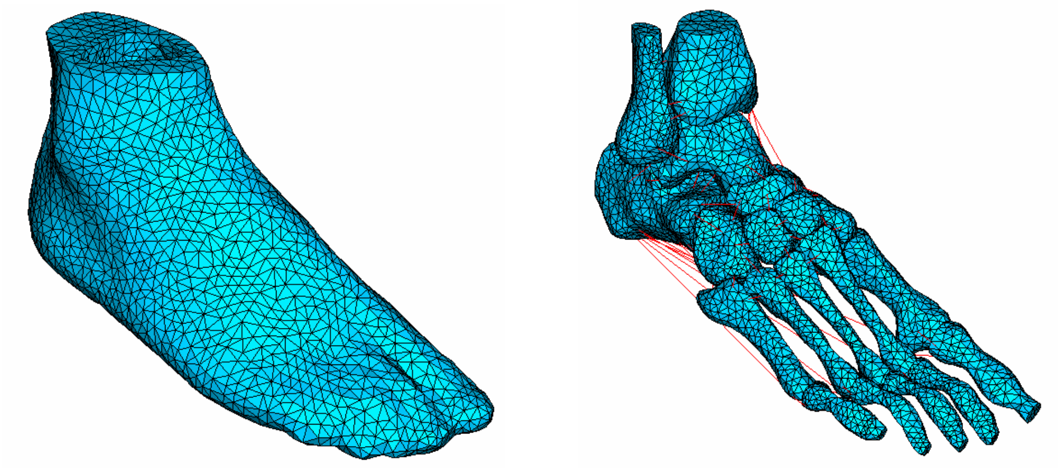

(a)

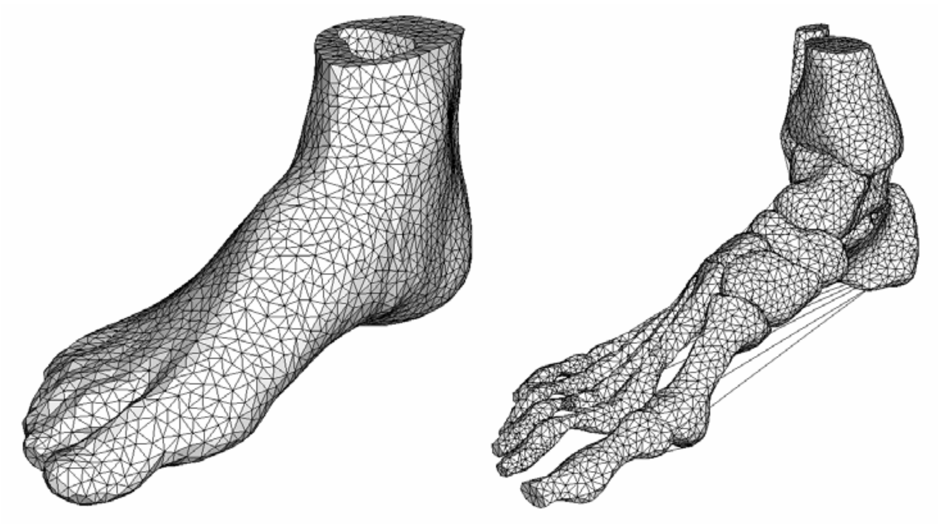

(b)

Figure 3-4. The FE meshes of the encapsulated soft tissue and bony structures in the (a) lateral and (b) medial view.

Except the collateral ligaments of the phalanges and other connective tissue, a total number of 72 ligaments and the plantar fascia were included and defined by connecting the corresponding attachment points on the bones. Information on the attachment regions of the ligamentous structures (Fig. 3-5) was obtained from the Interactive foot and ankle, 1999 (Primal Picture Ltd., London, UK, 1999). All the bony and ligamentous structures were embedded in a volume of soft tissues.

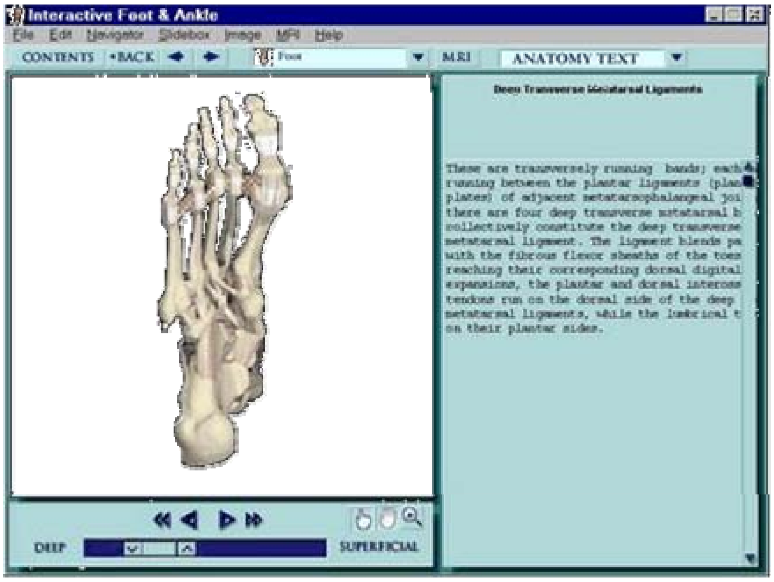


Figure 3-5. Attachments points of the ligamentous structures (Interactive foot and ankle, 1999).

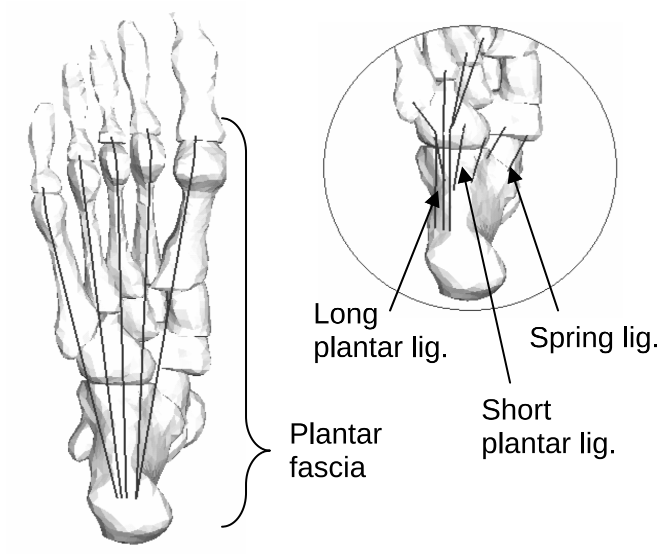


Figure 3-6. The attachment points of the plantar fascia, spring ligaments, long and short plantar ligaments of the FE model.

The attachment points of the major plantar ligamentous structures such as the plantar fascia, long plantar ligament, short plantar ligament and spring ligament are depicted in Figure 3-6. The number of attachment points defined for individual ligaments depended on the width of the ligamentous structures. For instance, the plantar fascia was divided into 5 rays of separate sections, linking the insertions between the calcaneus and the metatarsophalangeal joints (Fig. 3-6). The plantar ligaments and spring ligament were defined by 3 and 2 rays of separate sections while only a single ray was defined for those small ligaments. The attachments points were defined close to the geometrical centre of the insertional regions of the ligamentous structures.

A variety of solids elements in ABAQUS package can be used to model the foot and ankle structures. Among all the continuum elements, the hexahedra (brick) elements usually provide solution with a higher accuracy at less cost especially with analysis considering geometrically complex structure undergoing large deformations. However, because of the limitation for the automatic-meshing algorithms in ABAQUS to produce hexahedral meshes (brick elements) for those irregularly shaped structures, tetrahedral elements were used for meshing the foot bones and encapsulated soft tissue. The bony and encapsulated soft tissue structures were meshed with 4-noded tetrahedral elements.

For the sake of geometrical simplification, truss elements were chosen to model the ligaments of the FE model. Truss elements are typically designated to model slender, line-like structures that can only transmit force along the axis or the centreline of the element. Truss elements cannot resist loading perpendicular to their axis. The distance between the two connecting nodes defines the length of each truss element and the cross-sectional area is specified by the user. As the ligaments were assumed to sustain tensile force only, the No-Compression option in ABAQUS was used to modify the elastic behaviour of the material so that compressive stress cannot be generated. In the current FE model, a total number of 98 tension-only truss elements were used to represent the ligaments and the plantar fascia.

To simulate the surface interactions among the bony structures, ABAQUS automated surface-to-surface contact algorithm was used. In ABAQUS, a pair of contacting surfaces consisted of a master and a slave surface. The contact algorithm for establishing the contact pair in ABAQUS is described in Figure 3-7. For each contact pair, Normal vectors ($N_2$) are computed for all nodes on the master surface by averaging the normal vectors of outward edges (1-2 and 2-3 segments) making up the master surface and additional normal vectors ($N_{L/2}$) are computed at the middle of each segment. Those normal vectors together with the element size and function are used to define a set of smooth varying normal vectors on the whole master surface. An "anchor" point on the master surface $X_0$ is calculated for each slave node on the slave surface so that the vector formed by the slave node and $X_0$ coincided with the normal vector $N(X_0)$ of the master surface. A tangent plane is found at every "anchor" point that is perpendicular to the normal vector. Under the master-slave contact algorithm in ABAQUS, surface contact is detected with a prescribed tolerance and the slave nodes are automatically constrained not to penetrate into their tangent planes on the master surface when two surfaces come into contact.

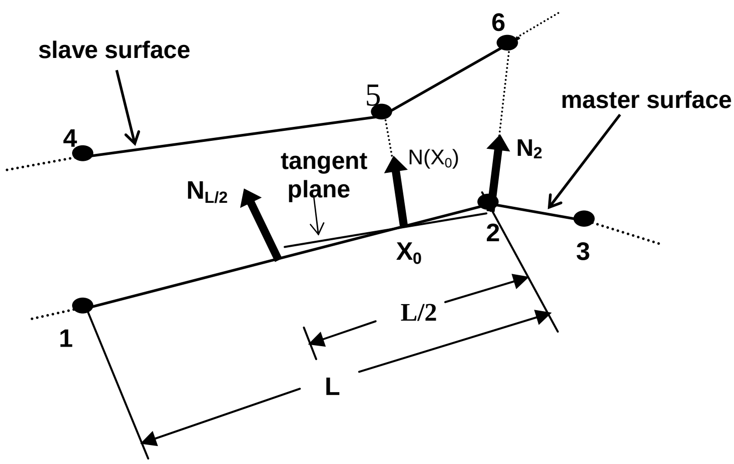


Figure 3-7. Master slave contact algorithm. Anchor point ($X_0$) and tangent plane are computed for every slave node based on the computed normal vectors. Each slave node (e.g. node 5) is constrained not to penetrate its tangent planes.

Depending on the segmented surface model of the bony structures, initial slave nodal penetration between the contact pair may exist at the initial neutral position of the FE mesh. An automatic slave node adjustment option is used to eliminate the node penetration and any pre-contact stress before the analysis. During the analysis, the solver continuously detects contact between the contact surfaces and calculates the contact stress by initiating constraints on the penetrating slave nodes on their corresponding master surface.

Because of the lubricating nature of the articulating surfaces, the contact behaviour between the articulating surfaces can be considered frictionless. The overall joint stiffness against shear loading was assumed to be governed by the surrounding ligamentous and encapsulated soft tissue structures together with the contacting stiffness between the adjacent contoured articulating surfaces. Frictionless surface-to-surface contact behaviour was defined between the contacting bony structures. Contact stiffness resembling the softened contact behaviour of the cartilaginous layers (Athanasiou et al., 1998) was prescribed between each pair of contact surfaces to simulate the covering layers of articular cartilage.

To simulate barefoot stance, a horizontal plate consisting of an upper concrete layer and a rigid bottom layer was used to establish the foot-ground interface. The horizontal ground support was meshed with hexahedral elements. The same contact modeling algorithm was used to establish the contact simulation of the foot-ground interface with an additional frictional property assigned to model the frictional contact behaviour between the foot-support interface. During the contact phase, sliding was allowed only when the shear stress exceeded the critical shear stress value $\tau > \tau_{crit} = \mu p$, where $p$ is the value of normal stress. During the sliding phase, if the shear stress was reduced and lower than the critical shear stress value, sliding stopped. It was assumed that the static and kinetic coefficients of friction were the same in this model. The coefficient of friction ($\mu$) between the foot and ground was taken as 0.6 (Zhang and Mak, 1999).

### *FE model of foot orthosis*

The geometry of the foot orthosis was obtained from the barefoot shape of the same subject who underwent the MR scanning for the development of the aforementioned foot and ankle model. The 3D foot shape of the subject was obtained from surface digitization via a 3D laser scanner (INFOOT Laser Scanner, I-Ware Laboratory Co. Ltd.) (Fig. 3-8). The foot shape was obtained under three different weightbearing conditions: single-limb standing (full-weightbearing), double-limb standing (semi-weightbearing), and upright sitting (non-weightbearing) (Fig. 3-9). Algorithms were established in MATLAB v7.0 (MATLAB, Mathworks, Inc) to create surface models for the insole and midsole from the digitized foot surface (Fig. 3-10) for each scanning position. The surface models were transferred to SolidWorks software (SolidWorks 2001, SolidWorks Corporation, Massachusetts USA) for creation of solid models of variable thicknesses.

Figure 3-8. INFOOT Laser Scanner, I-Ware Laboratory Co. Ltd.

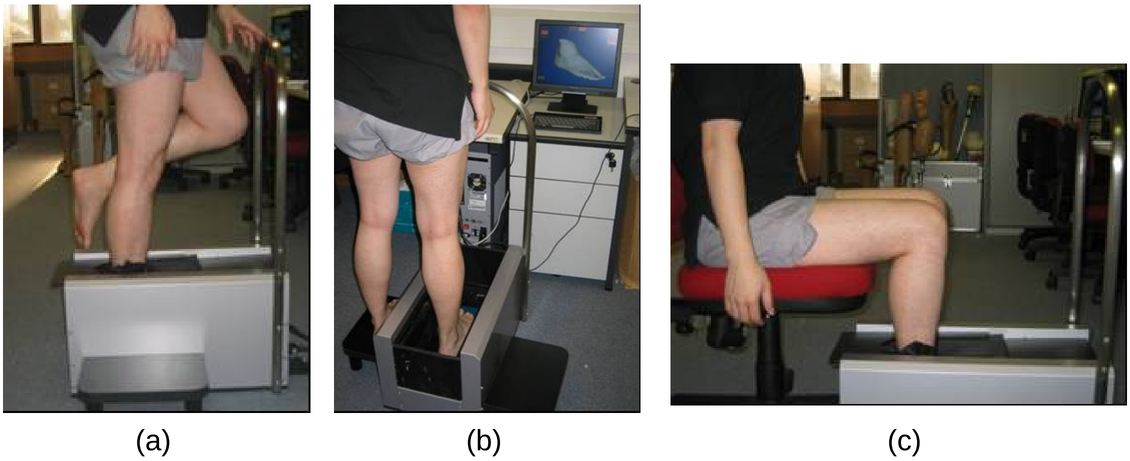


Figure 3-9. Digitization of the subject's foot during (a) single-limb standing, (b) double-limb standing, and (c) upright sitting.

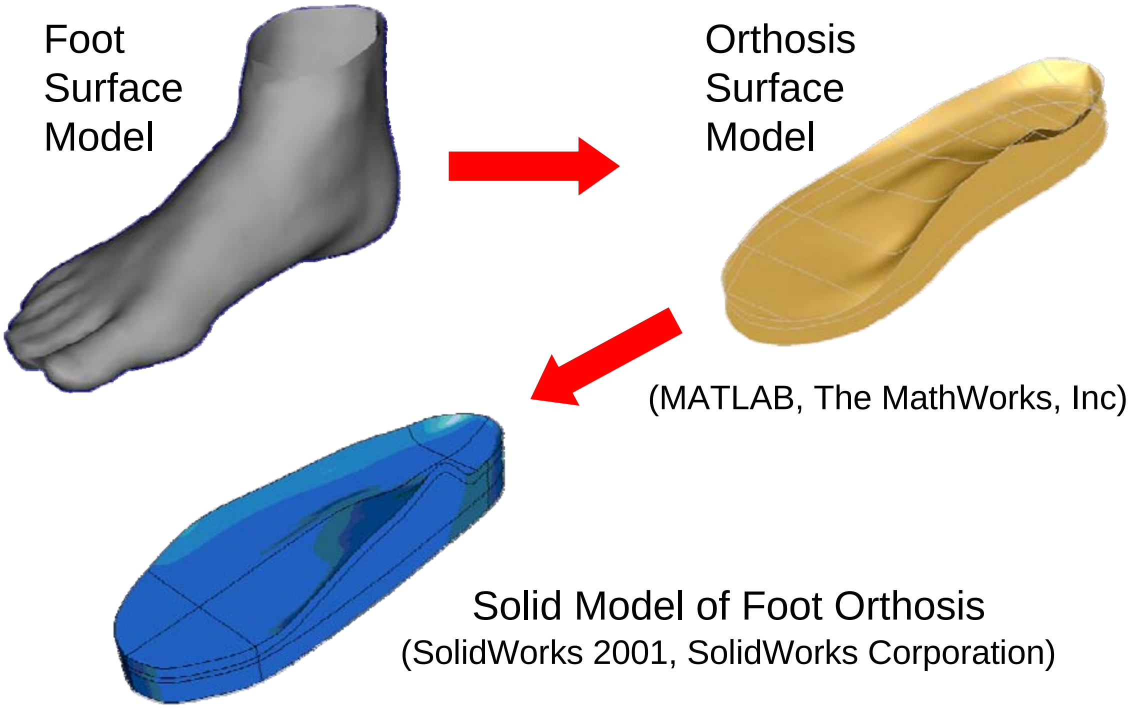


Figure 3-10. Procedures for creating the foot orthosis model.

The solid model of the foot orthosis was then imported into ABAQUS for the creation of FE mesh. In order to enhance the accuracy of the FE analysis, the foot orthosis was properly partitioned for the creation of a FE mesh of hexahedral elements. The FE mesh of the foot orthosis (Fig. 3-11) composed of an insole layer, a midsole layer and an outsole layer. The same frictional contact modeling approach was used to establish the contact simulation of the foot-insole interface.

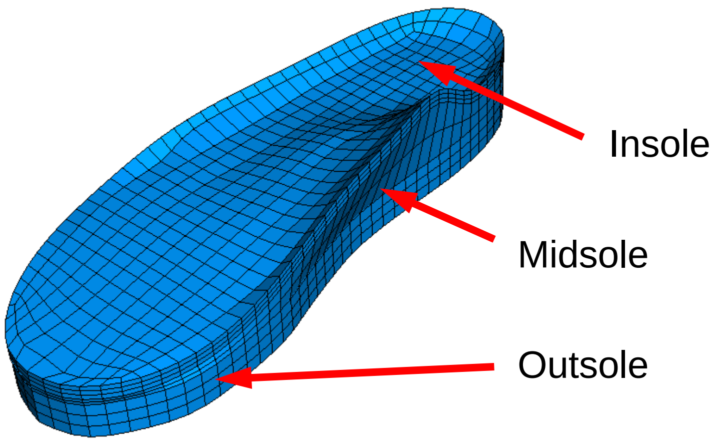


Figure 3-11. The FE mesh of the foot orthosis.

### 3.1.2 Material Properties of the Finite Element Model

*Foot and Ankle Model*

To reduce the complexity and the size of the problem, linearly elastic materials were chosen to represent the mechanical properties of the bony, ligamentous and cartilaginous structures and the ground support of the FE model. The linearly elastic properties were defined by giving the Young's modulus, $E$, and the Poisson's ratio, $\nu$. As the shear modulus, $G$, can be expressed in terms of $E$ and $\nu$ as $G = E / 2(1 + \nu)$, only two distinct constants were needed to be defined.

Except for the encapsulated soft tissue, all other tissues were idealized as homogeneous, isotropic and linearly elastic (Table 3-1). The Young's modulus and Poisson's ratio for the bony structures were assigned as 7300 MPa and 0.3, respectively, according to the model developed by Nakamura et al. (1981). The effective Young's modulus and Poisson's ratio for foot bony structures were obtained by averaging the elasticity values of cortical and trabecular bones in terms of their volumetric contribution. The Young's modulus of the cartilage (Athanasiou et al., 1998), ligaments (Siegler et al., 1988) and the plantar fascia (Wright and Rennels, 1964) were selected from the literature. The cartilage was assigned with a Poisson's ratio of 0.4 for its nearly incompressible nature. The ligaments and the plantar fascia were assumed to be incompressible.

Table 3-1. Material properties and element types defined in the FE model

| Component | Element Type | Young's Modulus E (MPa) | Poisson's Ratio $v$ | Cross-sectional Area ($mm^2$) |
|---|---|---|---|---|
| Bony Structures | 3D-Tetrahedra | 7,300 | 0.3 | - |
| Encapsulated Soft Tissue | 3D-Tetrahedra | Hyperelastic | - | - |
| Cartilage | 3D-Tetrahedra | 1 | 0.4 | - |
| Ligaments | Tension-only Truss | 260 | - | 18.4 |
| Fascia | Tension-only Truss | 350 | - | 58.6 |
| Ground Support | 3D-Brick | 17,000 upper layer<br>1,000,000 lower layer | 0.1 | - |

Bones (Nakamura et al., 1981); Cartilage (Athanasiou et al., 1998); Ligaments (Siegler et al., 1988); Plantar fascia (Wright and Rennels, 1964).

The encapsulated soft tissue of the FE model was defined as nonlinearly elastic. The stress–strain data on the plantar heel pad (Fig. 3-12) were adopted from the *in vivo* ultrasonic measurements (Lemmon et al., 1997) to represent the varying stiffness of the encapsulated soft tissue.

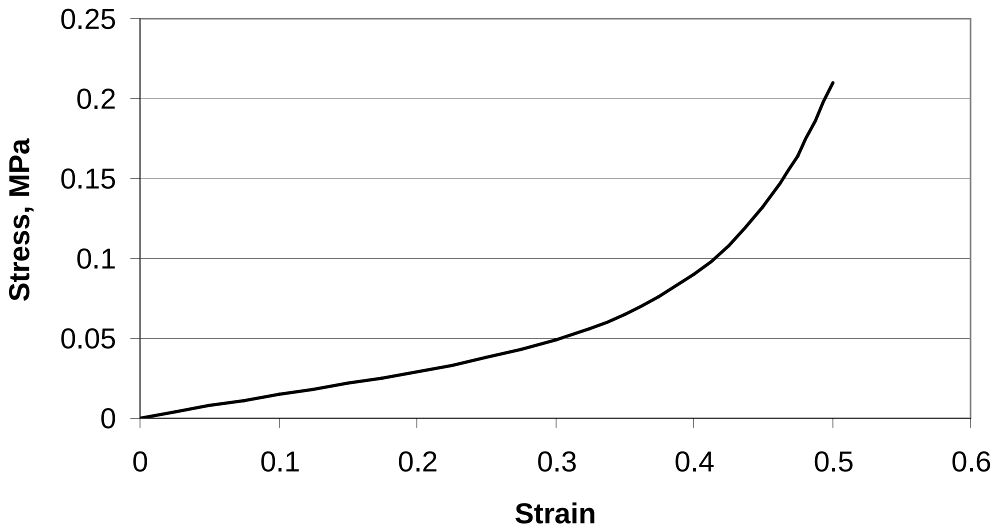


Figure 3-12. Stress-strain curve for plantar foot tissue obtained from indentation test (Lemmon et al., 1997).

ABAQUS offers a hyperelastic material model to simulate highly incompressible, elastic materials. The hyperelastic material model defined in ABAQUS is isotropic and nonlinear, which is especially useful in representing materials that exhibit instantaneous elastic response up to large strains (such as rubber, bulk soft tissue). Given isotropy and additive decomposition of the deviatoric and volumetric strain energy contributions in the presence of incompressible or almost incompressible behaviour, we can represent the strain energy potential with a polynomial expression. A second-order polynomial strain energy potential (ABAQUS, 2004) was adopted with the form

$$U = \sum_{i+j=1}^{2} C_{ij}(\bar{I}_1 - 3)^i(\bar{I}_2 - 3)^j + \sum_{i=1}^{2}\frac{1}{D_i}(J_{el} - 1)^{2i} \tag{3-1}$$

where $U$ is the strain energy per unit of reference volume; $C_{ij}$ and $D_i$ are material parameters (Table 3-2); $\bar{I}_1$ and $\bar{I}_2$ are the first and second deviatoric strain invariants defined as

$$\bar{I}_1 = \bar{\lambda}_1^2 + \bar{\lambda}_2^2 + \bar{\lambda}_3^2 \tag{3-2}$$

$$\bar{I}_2 = \bar{\lambda}_1^{(-2)} + \bar{\lambda}_2^{(-2)} + \bar{\lambda}_3^{(-2)} \tag{3-3}$$

with the deviatoric stretches $\bar{\lambda}_i = J_{el}^{-1/3}\lambda_i$. $J_{el}$ and $\lambda_i$ are the elastic volume ratio and the principal stretches, respectively.

Table 3-2. The coefficients of the hyperelastic material model used for the encapsulated soft tissue

| $C_{10}$ | $C_{01}$ | $C_{20}$ | $C_{11}$ | $C_{02}$ | $D_1$ | $D_2$ |
|---|---|---|---|---|---|---|
| 0.08556 | -0.05841 | 0.03900 | -0.02319 | 0.00851 | 3.65273 | 0.00000 |

### *Foot orthosis model*

Most elastomers have very little compressibility and their mechanical behaviour can be accurately modeled by the hyperelastic material model. However, rubber-like material for the fabrication of foot orthosis such as elastomeric foam is elastic but very compressible and a different strain-energy function is needed to describe the mechanical behaviour of this elastomeric material.

Common examples of elastomeric foam materials are cellular polymers such as cushions, padding, and packaging materials that utilize the excellent energy absorption properties of foams. Three distinct stages can be distinguished during compression of an elastomeric foam (Fig. 3-13). Within small strains of about 5%, the foam deforms in a linear elastic manner due to cell wall bending. The next stage is a plateau of deformation at almost constant or with a slowly increasing stress, caused by the elastic buckling of cell edges or walls. Finally, a region of densification occurs, where the cell walls crush together, resulting in a rapid increase of compressive stress. The ultimate compressive nominal strain usually ranges from 0.7 to 0.9.

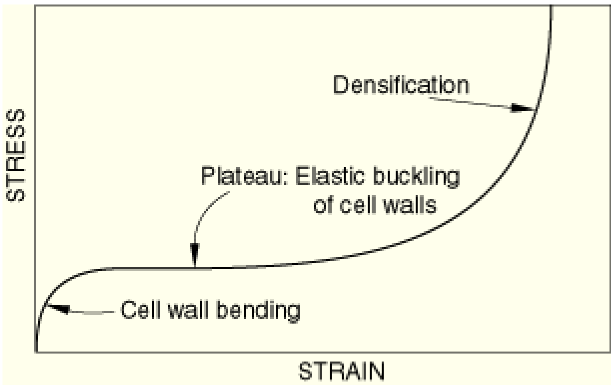


Figure 3-13. A typical stress-strain curve for elastomeric foam.

The elastic foam energy function (ABAQUS, 2004) is used for describing highly compressible elastomers. This energy function has the form

$$U = \sum_{i=1}^{2} \frac{2\mu_i}{\alpha_i^2}\left[\hat{\lambda}_1^{\alpha_i} + \hat{\lambda}_2^{\alpha_i} + \hat{\lambda}_3^{\alpha_i} - 3 + \frac{1}{\beta_i}(J_{el}^{-\alpha_i \beta_i} - 1)\right] \tag{3-4}$$

where U is a second order, isotropic hyperfoam strain energy potential per unit of reference volume; $\hat{\lambda}_i$ are principal stretches and $J_{el}$ is the elastic volume ratio with

$\hat{\lambda}_1\hat{\lambda}_2\hat{\lambda}_3 = J_{el}$. $\mu_i$, $\alpha_i$ and $\beta_i$ are material parameters with $\mu_i$ related to the initial shear modulus, $\mu_0$, by

$$\mu_0 = \sum_{i=1}^{2} \mu_i \tag{3-5}$$

and the initial bulk modulus, $K_0$ defined by

$$K_0 = \sum_{i=1}^{2} 2\mu_i\left(\frac{1}{3} + \beta_i\right) \tag{3-6}$$

The coefficient $\beta_i$ determines the degree of compressibility, which is related to the Poisson's ratio, $v_i$, by

$$\beta_i = \frac{v_i}{1-2v_i} \tag{3-7}$$

Figure 3-14. Shore A type durometer.

In this study, two commonly used elastomeric foam materials for fabricating foot orthosis in our research centre: Poron® (Rogers Corporation, Connecticut, USA) and Nora® (Freudenberg, Germany), were analyzed. Poron® (Rogers Corporation, Connecticut, USA) is open-cell polyurethane foams, which are commonly used for cushioning in footwear or insole. Nora® (Freudenberg, Germany) is close-cell ethylene vinyl acetate (EVA) foam, which is available in wide range of densities and stiffness for fabricating insole, midsole or outsole of the shoes. Two different grades of Poron® with Shore A hardness $10^0$ (Poron_L24) and $20^0$ (Poron_L32) and three different Nora® material of hardness $30^0$(Nora_SLW), $40^0$(Nora_SL), and $50^0$(Nora_AL) were used. Hardness of orthotic material was measured using a Shore A type durometer (Fig. 3-14).

Figure 3-15. Compression test for different orthotic materials.

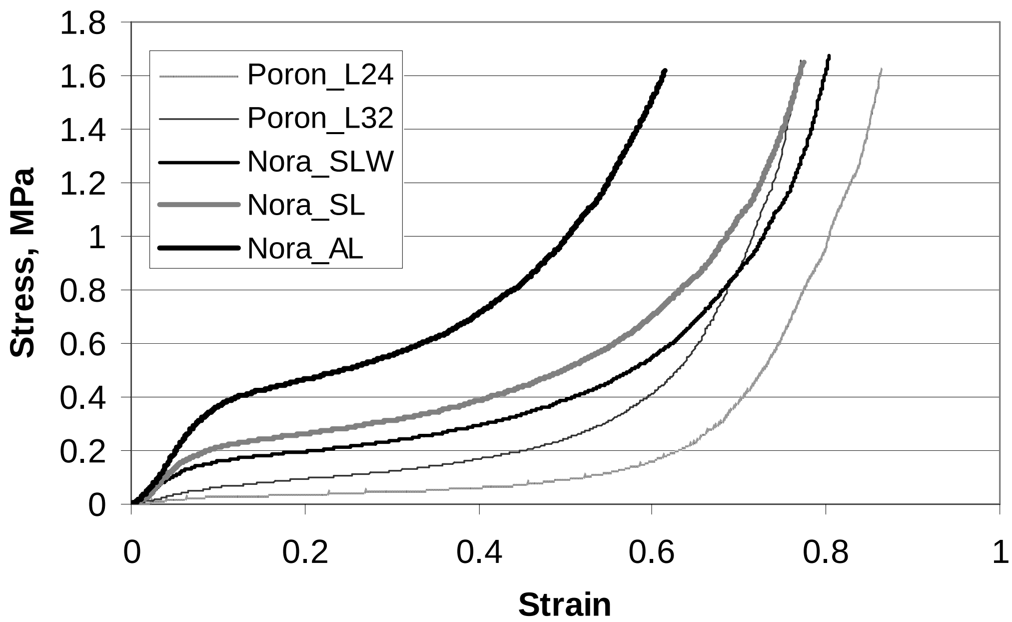


Figure 3-16. Compression curve for different orthotic materials.

Each orthotic material was tested in a Hounsfield material testing machine (Model H10KM, Hounsfield Test Equipment, UK) with a 1 kN load cell (Fig. 3-15). Samples with 20 mm in diameter and 6 mm in thickness were tested under uniaxial compression of up to 500 N with a testing speed of 1 mm/s. The stress–strain data for different hardnesses of Poron and Nora materials (Fig. 3-16) was used to extract the material parameters of the hyperfoam material model (Table 3-3) in ABAQUS.

Table 3-3. The coefficients of the hyperfoam material model used for orthotic materials.

| **Orthotic Material** | $\mu_1$ | $\mu_2$ | $\alpha_1$ | $\alpha_2$ | $\beta_1$ | $\beta_2$ |
|---|---|---|---|---|---|---|
| Poron_L24 | 0.213 | -0.06209 | 10.3 | -3.349 | 0.32 | 0.32 |
| Poron_L32 | -0.3365 | -0.08731 | 7.272 | -2.391 | 0.32 | 0.32 |
| Nora_SLW | 0.9754 | -0.2914 | 8.87 | -2.884 | 0.32 | 0.32 |
| Nora_SL | 1.037 | -0.3044 | 7.181 | -2.348 | 0.32 | 0.32 |
| Nora_AL | 8.874 | -7.827 | 2.028 | 1.345 | 0.32 | 0.32 |

### 3.1.3 Loading and Boundary Conditions of the Finite Element Model

In order to simulate the physiological loading on the foot, accurate ground reaction and muscle forces must be applied. In this study, double-limb balanced standing and midstance were simulated. In order to establish the above loading conditions, information on the centre of pressure, total ground reaction forces and foot-shank position, which can be measured from the plantar pressure measuring system and human motion analysis system, should first be known.

For a subject with body mass of 70 kg, a vertical force of approximately 350N is applied on each foot during balanced standing. According to Opila et al. (1988), the standing line of gravity was about 6 cm in front of the ankle. Therefore, the plantar flexors must act to balance the forward moment of the body about the ankle in order to achieve an equilibrium balanced standing position. Basmajian and Stecko (1963) found that the triceps surae provided the major stabilization role of the foot during balanced standing and the reactions of all other intrinsic and extrinsic muscles were minimal. Therefore, only the Achilles tendon loading was considered during simulated balanced standing while other intrinsic and extrinsic muscle forces were neglected.

For simulated balanced standing, force vectors, corresponding to half of the body weight, and the reaction of the Achilles tendon were applied. Five equivalent force vectors representing the Achilles tendon tension were applied at the points of insertion by defining contraction forces via five axial connector elements (Fig. 3-17). The ground reaction force was applied as a concentrated force underneath the ground support. The superior surface of the soft tissue, distal tibia and fibula was fixed throughout the analysis. The ankle joint was assumed to be in its neutral position during balanced standing. The Achilles tendon forces required for simulating the upright balanced standing posture were estimated by matching the FE predictions with the measured plantar pressure distribution and location of centre of pressure of the same subject who volunteered for the MR scanning.

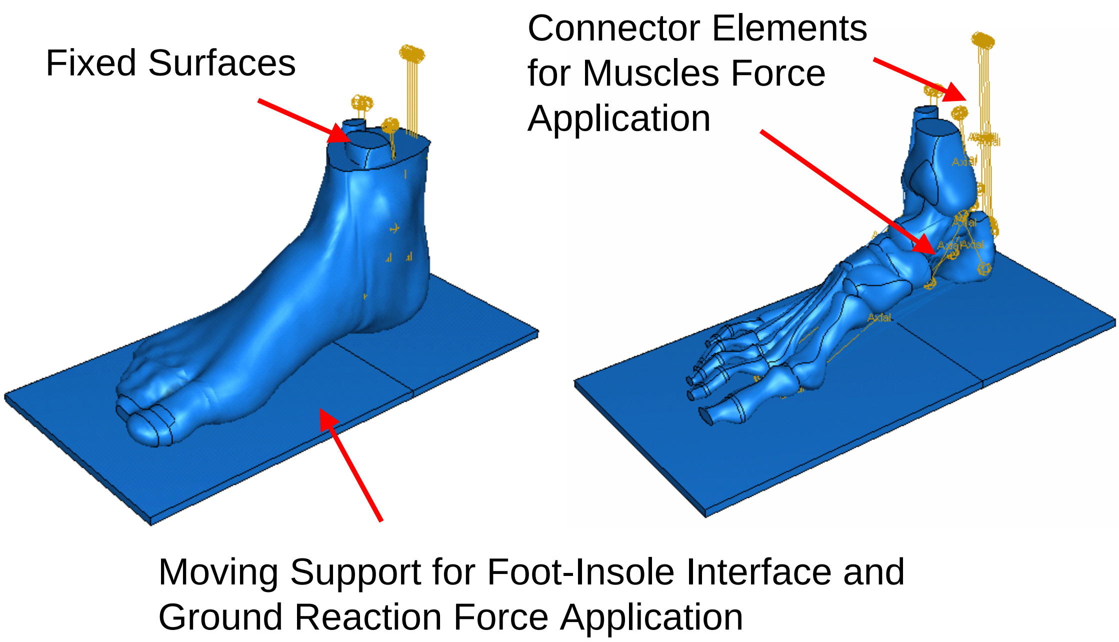


Figure 3-17. Loading and boundary conditions for simulating the physiological loading on the foot.

For simulated midstance, the ground reaction and the active extrinsic muscle forces were applied. The geometrical information of the muscular insertion points (Fig. 3-18) were obtained from the Interactive Foot and Ankle, 1999 (Primal Picture Ltd., London, UK, 1999). The extrinsic muscles forces during midstance were estimated from the physiological cross-sectional area (PCSA) of the muscles muscles (Dul, 1983) and normalized electromyography (EMG) data during normal walking (Perry, 1992) assuming a linear EMG-force relationship with a muscle gain of 25 N/cm$^2$ (Kim et al., 2001). Fine adjustments on the applied muscles forces were made to match the measured centre of pressure of the subject. Musculotendon forces were applied at their corresponding points of insertion by defining contraction forces via axial connector elements (Fig. 3-17). Again, the ground reaction force was applied as a concentrated force underneath the ground support and the superior surface of the soft tissue, distal tibia and fibula was fixed throughout the analysis. The foot-shank position during midstance was measured from the subject.

Figure 3-18. Insertion points of the extrinsic muscles (Interactive foot and ankle, 1999).

## *3.2 Parametrical Studies of the Foot and Ankle Structures*

The FE model developed in this study provides the first model in the literature to take into account the actual 3D ankle-foot geometry and nonlinearities from material properties, large deformations and interfacial slip/friction conditions. Throughout the development process of the FE model, parametrical analyses were done to evaluate the sensitivity of different model parameters such as the stiffness of encapsulated bulk soft tissue and plantar fascia, and Achilles tendon forces. The ability of the FE model to simulate different surgical and pathological conditions including plantar fasciotomy, posterior tibial tendon dysfunction and the interactions with different foot supports was evaluated by comparing the FE predictions to the experimental measurements conducted in the current and literature studies.

Upon the above parametrical studies, parametrical analyses were conducted to evaluate the effect of different design parameters such as arch height, thickness and material stiffness of foot orthosis on its pressure-relieving capability. A statistically-based factorial analysis was conducted to evaluate the sensitivity of different design parameters of foot orthoses. The predicted biomechanical effects of different design parameters such arch height, thickness and material stiffness of foot orthosis were used to establish the knowledge-based guidelines for designing pressure-relieving foot orthoses.

### 3.2.1 Effects of Varying Bulk Soft Tissue Stiffness

A sensitivity analysis on the biomechanical effect of varying stiffness of the encapsulated bulk soft tissue was conducted using the developed FE model. Except the encapsulated soft tissue, all other tissues were idealized as homogeneous, isotropic and linearly elastic as described in the previous section. An increase in bulk soft tissue stiffness from 2 and up to 5 times the normal values were used to approximate the pathologically stiffened tissue behaviour with increasing stages of diabetic neuropathy (Klaesner et al., 2002; Gefen et al., 2001a; Zheng et al., 2000). The nominal stress values at corresponding nominal strains were multiplied by a factor of 2, 3 and 5 (Fig. 3-19) to investigate the biomechanical effect of soft tissue stiffening. The coefficients of the hyperelastic material model used for the encapsulated soft tissue were calculated in ABAQUS (Table 3-4).

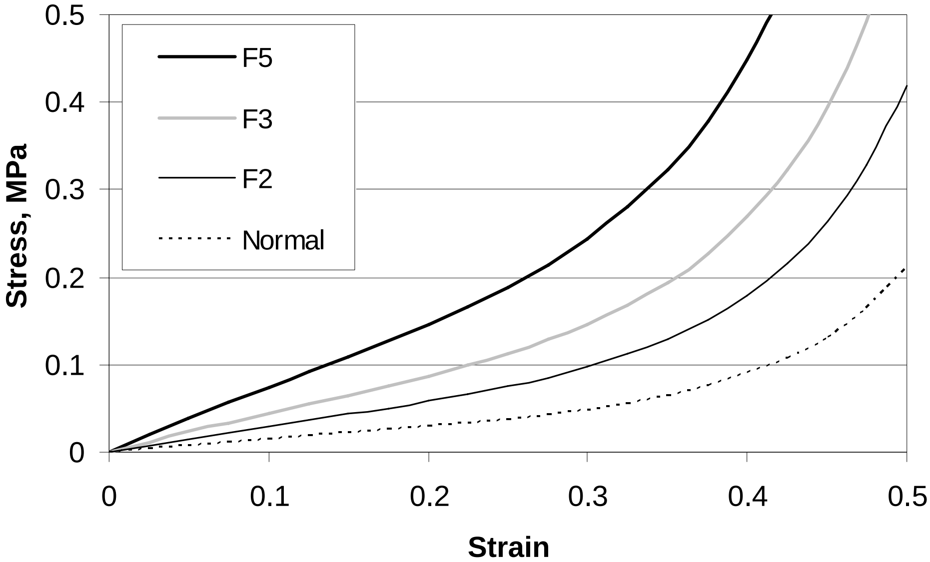


Figure 3-19. Nonlinear stress–strain response of soft tissue adopted for the FE model. The nominal stress values at corresponding nominal strains adopted from the *in vivo* measurements (Lemmon et al., 1997) were multiplied by factors of 2, 3 and 5 to simulate stiffening of soft tissue. F2, F3 and F5 correspond to simulations of two, three and five times the stiffness of normal tissue.

Table 3-4. The coefficients of the hyperelastic material model used for the encapsulated soft tissue

| Coefficients | Normal | F2 | F3 | F5 |
|---|---|---|---|---|
| $C_{10}$ | 0.08556 | 0.17113 | 0.25669 | 0.42782 |
| $C_{01}$ | -0.05841 | -0.11683 | -0.17524 | -0.29207 |
| $C_{20}$ | 0.03900 | 0.07800 | 0.11700 | 0.19499 |
| $C_{11}$ | -0.02319 | -0.04638 | -0.06957 | -0.11594 |
| $C_{02}$ | 0.00851 | 0.01702 | 0.02553 | 0.04256 |
| $D_1$ | 3.65273 | 1.82636 | 1.21758 | 0.73055 |
| $D_2$ | 0.00000 | 0.00000 | 0.00000 | 0.00000 |

Units are $Nmm^{-2}$ for $C_{ij}$ and $mm^2N^{-1}$ for $D_i$. Values for these coefficients for the encapsulated soft tissue were calculated by ABAQUS based on uniaxial stress-strain data in Figure 3-10. F2, F3 and F5 correspond to simulations of two, three and five times the stiffness of normal tissue.

A horizontal ground support (Fig. 3-20a) was used to establish the simulation of balanced standing. The ground support was properly aligned such that an initial foot-ground contact was established with minimal induced stress before the application of the ground reaction forces and Achilles tendon loading (Fig. 3-20b). Assuming a subject with body mass of 70 kg, force vectors, corresponding to half of the body weight (350 N), and the reaction of the Achilles tendon (175 N) were applied. The magnitude of the Achilles tendon loading was adopted according to the study by Simkin (1982), who calculated that the Achilles tendon force was approximately 50% of the force applied on the foot during balanced standing using a three-dimensional biomechanical model. The superior surface of the soft tissue, distal tibia and fibula was fixed throughout the analysis while the point of load application at the centre of pressure was allowed to move in the vertical direction only.

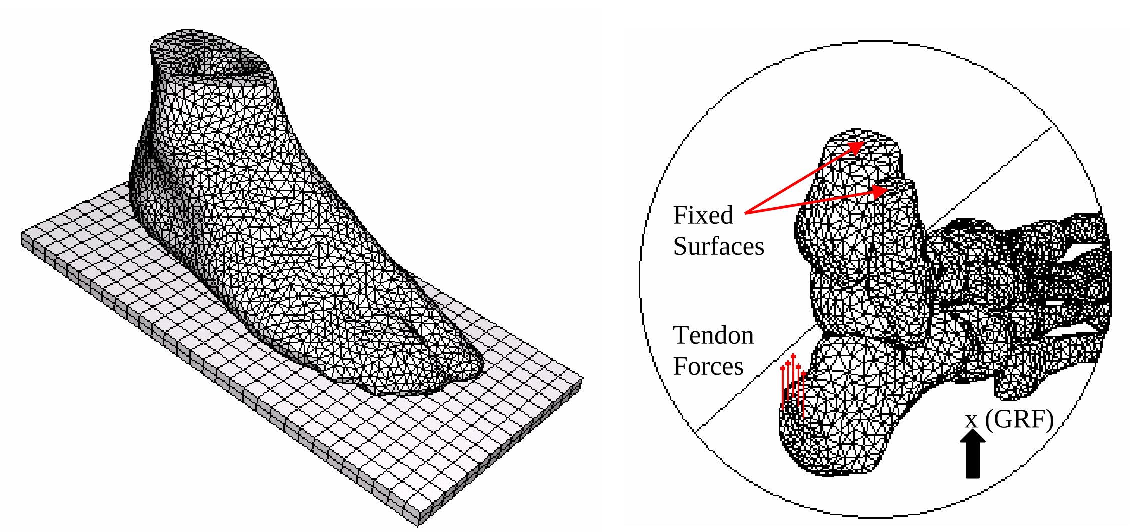


(a) (b)

Figure 3-20. (a) The FE meshes of the foot and the horizontal foot support and (b) the loading to simulate balanced standing.

The normal ground reaction force was applied at the location of the centre of pressure of the inferior surface of the ground support. The F-scan system (Tekscan Inc., Boston, USA) was used to measure the plantar pressure of the subject during balanced standing. The F-scan pressure sensor (Fig. 3-21) has a spatial resolution of 4 sensors per $cm^2$.

Figure 3-21. F-scan pressure sensor (Tekscan Inc., Boston, USA)

The measured plantar pressures were used to calculate the centre of pressure on the foot and to compare the FE predicted plantar pressure distribution. For this subject, the centre of pressure was 90 mm from the posterior extreme of the foot and 30 mm from the medial heel extreme. The predicted plantar foot pressure, contact area and von Mises stress of the foot bones with different degree of soft tissue stiffening were compared.

### 3.2.2 Effects of Varying Plantar Fascia Stiffness

A sensitivity study was conducted on the stiffness of the plantar fascia to evaluate its load-bearing role of the weightbearing foot. To reduce the complexity of the problems, all the bony and soft tissue structures were idealized as homogeneous, isotropic and linearly elastic (Table 3-5). The average elastic modulus of soft tissue at various sites of subject's foot was measured using the ultrasonic indentation system (Zheng et al., 2000). The Young's modulus of varied values ranging from 0 to 700 MPa were assigned to the plantar fascia to investigate the effect of its stiffness on the load distribution of the foot. Young's modulus of 350 MPa (Wright and Rennels, 1964) was chosen as a reference value to represent the normal plantar fascia stiffness and the cross-sectional area of the fascia was kept unchanged in all simulated cases. The same loading and boundary conditions for simulating the balanced standing position were prescribed as described in the previous sensitivity study on the bulk soft tissue.

The predicted arch height and length, plantar pressure, ligaments strain/tension and von Mises stress of the foot bones with different stiffness of the plantar fascia were compared.

Table 3-5. Material properties and element types of the FE model.

| Component | Young's Modulus E (MPa) | Poisson's Ratio *v* |
|---|---|---|
| Bony Structures | 7,300 | 0.3 |
| Soft Tissue | 0.15 | 0.45 |
| Cartilage | 1 | 0.4 |
| Ligaments | 260 | - |
| Fascia | 0 - 700 | - |

### 3.2.3 Effects of Partial and Complete Plantar Fascia Release

The biomechanical effects of surgical releases of partial and the entire plantar fascia were investigated by the FE model. To reduce the complexity of the problems, the material properties of all structures were idealized as homogeneous, isotropic and linearly elastic as described in the sensitivity analysis on the plantar fascia. The Young's modulus of the plantar fascia was taken as 350 MPa (Wright and Rennels, 1964). Balanced standing position was simulated as described in the previous sensitivity studies.

Five different cases of plantar fascia release and the intact condition were simulated by deleting the corresponding structures from the model. Partial plantar fascia releases of 20%, 40%, 60% and complete fascia release with and without dissection of the long plantar ligament were simulated. Simulation of partial release considered only the medial portion of the fascia, which is the common surgical procedure to relieve the medial calcaneal insertion pain associated with plantar fasciitis. The location of centre of pressure was assumed unchanged with the simulations of different fascia stiffness. The predicted arch height and length, plantar pressure, ligaments strain/tension and von Mises stress of the foot bones with different types of fascia release were compared.

### 3.2.4 Effects of Varying Achilles Tendon Loading

A sensitivity analysis was conducted to investigate the biomechanical effect of varying Achilles tendon forces during upright, balanced standing. The nonlinear FE model with the encapsulated bulk soft tissue defined as hyperelastic was used for this sensitivity study. The rest of the structures were simplified as homogeneous, isotropic and linearly elastic. A horizontal plate assigned with the properties of Aluminium (Young's modulus: 70000 MPa; Poisson's ratio: 0.3) was used to simulate the ground support. A coefficient of friction of 0.6 was assumed for the foot-support interface (Zhang and Mak, 1999). The ground support was properly aligned such that an initial foot-ground contact was established with minimally induced stress before the application of the loading conditions. The superior surface of the soft tissue, distal tibia and fibula was fixed throughout the analysis.

Two different loading conditions namely pure compression and balanced standing were simulated. For pure compression, a vertical compression force of up to 700 N was applied to the plantar foot via the ground support. To establish the loading conditions for a subject weighing 70 kg in double-limb, balanced standing posture, vertical ground reaction forces of 350 N and Achilles tendon forces were applied at the inferior ground support and at the insertion of the posterior calcaneus, respectively. Five equivalent force vectors representing the Achilles tendon tension were applied at the points of insertion by defining contraction forces via five axial connector elements.

To provide a sensitivity analysis of Achilles tendon loading, a varying Achilles tendon force from 0 to 700 N was applied while maintaining the ground reaction force at 350 N.

From the sensitivity analysis, the Achilles tendon forces required for simulating the upright, balanced standing posture were estimated by matching the FE predictions with the measured plantar pressure distribution and location of centre of pressure of the same subject who volunteered for the MR scanning. The plantar pressure distribution of the standing subject was measured by the F-scan pressure sensors (Tekscan Inc., Boston, USA). The predicted foot deformation, load distribution of the plantar foot and the strain/tension of the plantar fascia with different magnitudes of Achilles tendon loading were compared.

### *Compression test on the cadaveric foot*

Apart from validating the FE predictions under simulated balanced standing from the *in vivo* pressure measurements of the standing subject, the FE-predicted foot responses under simulated pure compression were compared to the cadaveric measurements. Six nonpaired fresh cadaveric ankle-foot specimens at the mid-shank level were obtained from middle-aged adult male donors. The body masses were unknown and the specimens had an average foot length and width measuring 24.2 cm with a standard deviation of 0.82 cm and 9.4 cm with a standard deviation of 0.69 cm, respectively. All foot specimens were kept under -20 degrees Celsius before the experiments.

Before thawing the foot specimen at room temperature on the day of the experiment, the foot specimen was unfrozen in 4 degrees Celsius for about 12 hours. While thawing the foot specimen at room temperature for about 3 hours, the skin, subcutaneous tissues and muscles above the ankle joint level were dissected, leaving the distal fibula and tibia and all the muscular tendons (Fig. 3-22). The ankle-foot specimens were amputated at the junction of mid-shank level of the lower leg and the 9 major tendons of the extrinsic muscles were exposed.

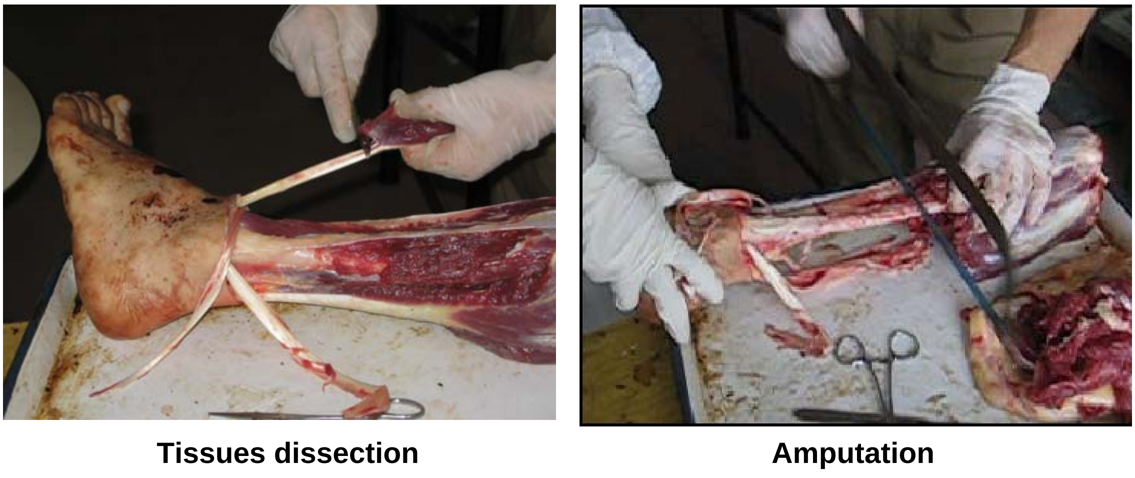


Figure 3-22. Preparation of cadaveric foot specimen.

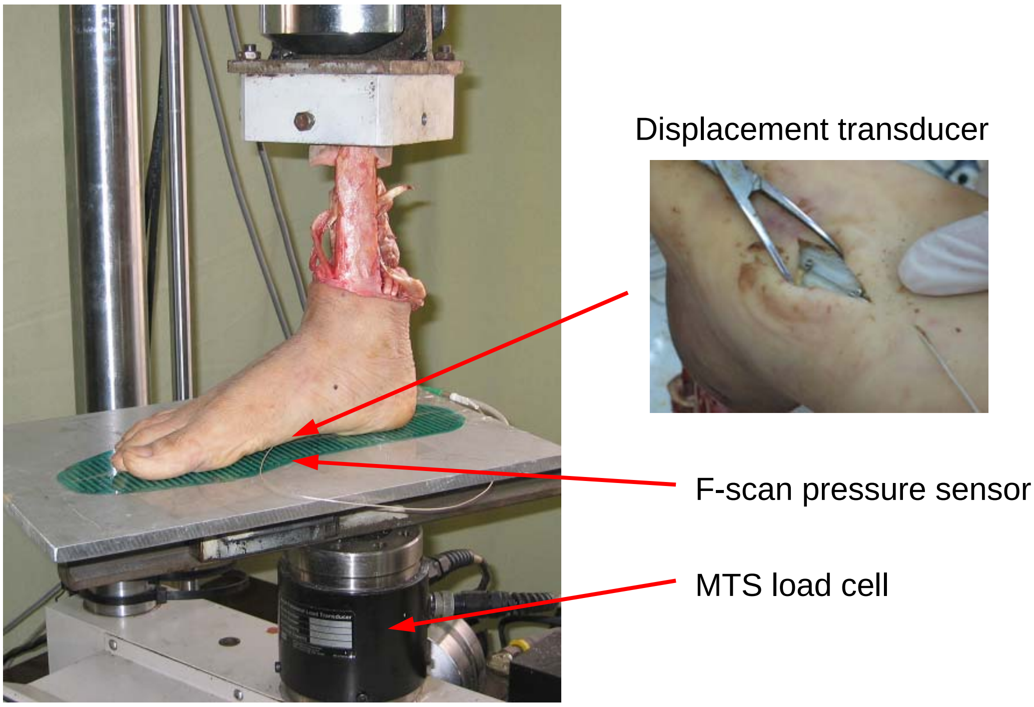


Figure 3-23. Experimental setup for the vertical compression test of cadaveric foot specimen.

The fibula and tibia were then potted in acrylic resin and a 3 cm incision at 2 cm proximal to the medio-inferior heel region was made for implantation of a 3-mm stroke differential variable reluctance transducer (DVRT) (Microstrain, Inc, Williston, Vermont, USA). The transducer was aligned parallel to the fiber orientation of the plantar fascia and secured to the tissue using two barbed prongs (Fig. 3-23). The connector lead exited from the plantar surface at the medial arch of the foot. This Hall Effect transducer calculates axial displacement by reading the voltage change that is proportional to the change in the magnetic field. The DVRT (Model: M-DVRT-3) has a resolution of 1.5 microns. The strain of the plantar fascia was calculated from the measured initial gauge length at the beginning of the compression test. The initial gauge length of the transducer was calculated from a reference gauge length (~1.8 cm) relative to the neutral position of the transducer measured before the implantation.

The specimen was mounted on a material testing unit (858 Mini Bionix, MTS Systems, Minnesota, USA) for application of vertical compression forces up to 700 N (Fig. 3-23). A F-scan pressure sensor was placed on the Aluminium foot support. Compression tests preceded by 10 cycles of preconditioning trials were conducted at a loading rate of 200 N/s (~10 mm/s). The total vertical forces and displacements, strains of the plantar fascia, the plantar pressure distributions and contact areas were measured simultaneously during the compression test. The data from the MTS unit, DVRT and F-scan sensor was acquired at a frequency of 50Hz. Because of a limitation in the experimental testing apparatus, the loading of the Achilles tendon could not be performed in the cadaver experiments. Therefore, the cadaveric measurements were compared to the FE predictions under pure vertical compression only.

### 3.2.5 Effects of Posterior Tibial Tendon Dysfunction

*Finite Element Simulation*

The biomechanical effects of posterior tibial tendon loading on the foot during midstance were investigated. The FE model considering the nonlinear material properties of soft tissue was used for this sensitivity study. The encapsulated bulk soft tissue was defined as hyperelastic while the rest of the structures were simplified as homogeneous, isotropic and linearly elastic. A horizontal plate assigned with the properties of Aluminium was used to simulate the ground support.

To establish the loading and boundary conditions for late midstance (50% of the stance phase cycle), the plantar pressure, ground reaction forces and foot-shank positions during normal walking (1.1s / gait cycle) of the same subject who underwent the MR scanning was measured in a human motion analysis laboratory. The barefoot plantar pressure distribution was measured by a pedobarograph (Tekscan Inc., Boston, USA) (Fig. 3-24). The foot-shank position and the total ground reaction forces were measured by the Vicon motion analysis system (Oxford Metrics, UK) and an AMTI force platform (Advanced Mechanical Technology, Inc., MA, USA) (Fig. 3-25). The extrinsic muscles forces during late midstance were estimated from the physiological cross-sectional area (PCSA) of the muscles (Dul, 1983) and normalized EMG data during normal walking (Perry, 1992) (Table 3-6). A linear EMG-force relationship with a muscle gain of 25 $N/cm^2$ (Kim et al., 2001) was assumed with Muscles forces = Muscle gain x PCSA x Normalized EMG.

Figure 3-24. Barefoot plantar pressure measurement using pedobarograph (Tekscan Inc., Boston, USA).

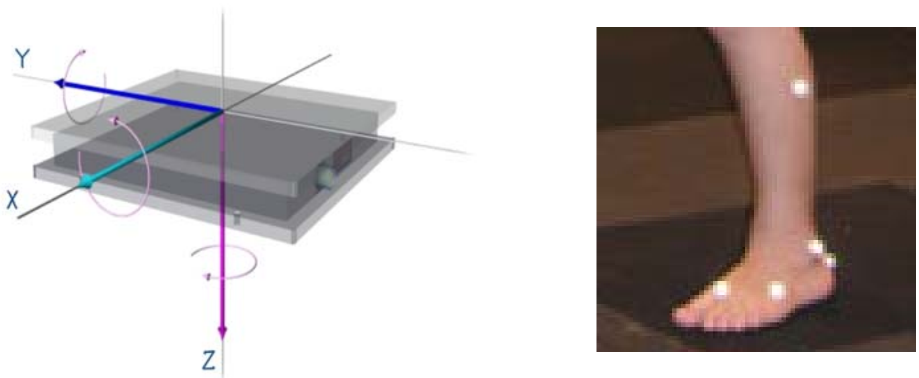


Figure 3-25. Ground reaction forces measurement using AMTI force platform (Advanced Mechanical Technology, Inc. MA, USA) and motion capture using the Vicon motion analysis system (Oxford Metrics, UK).

From the motion analysis measurement, the foot-shank position of the subject during late midstance (50% of stance phase cycle) was about 10 degrees relative to the ground. The estimated musculotendon forces were slightly adjusted until a reasonable match between the FE predicted and measured normal ground reaction forces and location of centre of pressure was achieved. The musculotendon and ground reaction forces for simulating late midstance were tabulated in Table 3-7. The reactions forces for the lateral and medial retinaculum were estimated according to the tendon forces of the peroneal and flexor group muscles, respectively.

Table 3-6. Physiological cross-sectional area (PCSA) and normalized EMG data of the extrinsic muscles during midstance assuming a muscle gain of 25 N/cm$^2$.

| **Tendon/External Forces** | **PCSA (cm$^2$)** | **EMG (%)** |
|---|---|---|
| Tibialis Anterior | 14 | 0 |
| Extensor Hallucis Longus | 3 | 0 |
| Extensor Digitorum Longus | 8 | 0 |
| Soleus | 67 | 54.3 |
| Gastrocnemius | 35 | 57.1 |
| Tibialis Posterior | 17 | 14.2 |
| Flexor Hallucis Longus | 11 | 20 |
| Flexor Digitorum Longus | 4 | 22.8 |
| Peroneus Brevis | 8 | 17.1 |
| Peroneus Longus | 11 | 14.2 |

Table 3-7. Muscles and ground reaction forces for midstance simulation.

| **Muscles** | **FE Simulation** | **Cadaveric Simulation** |
|---|---|---|
| Tibialis Anterior | - | - |
| Extensor Hallucis Longus | - | - |
| Extensor Digitorum Longus | - | - |
| Achilles | 750N | 750N |
| Tibialis Posterior | 70N | 70N |
| Flexor Hallucis Longus | 59N | 75N |
| Flexor Digitorum Longus | 16N | |
| Peroneus Brevis | 37.5N | 75N |
| Peroneus Longus | 37.5N | |
| Reaction of Lateral Retinaculum | 50N | - |
| Reaction of Medial Retinaculum | 60N | - |
| Vertical Ground Reaction | 558N | 558N |

The late midstance position was established in a quasi-static manner. To simulate the foot-shank position at late midstance, the ground support was initially inclined at 10 degrees relative to the plantar foot. An ankle-foot position at 10-degrees dorsiflexion was established before the application of the ground reaction and muscles forces. The superior surface of the soft tissue, distal tibia and fibula was fixed throughout the analysis while the ground support was constrained to move in the same direction of ground reaction force vector, which was applied perpendicularly at the inferior ground support. The musculotendon and ground reaction forces were applied simultaneously in a step-by-step approach.

The effect of posterior tibial tendon dysfunction (PTTD) on intact and low-arched foot structures was investigated during simulated midstance. Five different cases namely intact, plantar fascia release (PFR), posterior tibial tendon dysfunction (PTTD) and plantar fascia release with posterior tibial tendon dysfunction (PFR+PTTD) were simulated. Simulation of PFR and PTTD were done by removing the plantar fascia structures and the posterior tibial tendon forces from the FE model. The predicted arch height and length, plantar pressure, ligaments strain/tension and von Mises stress of the foot bones with different types of fascia release were compared.

### *Cadaveric Foot Simulation*

The FE predicted biomechanical foot responses during simulated late midstance were compared to the experimental measurements in cadaveric specimens. The six nonpaired fresh cadaveric ankle-foot specimens for the compression test described in the previous section were used. Static experimental loading tests were done to simulate the loading response of the foot during a single instance of the midstance phase. The junction of the fibula and tibia that were potted in acrylic resin, was mounted on a loading frame in an inverted position with the shank aligned in a vertical position (Fig. 3-26).

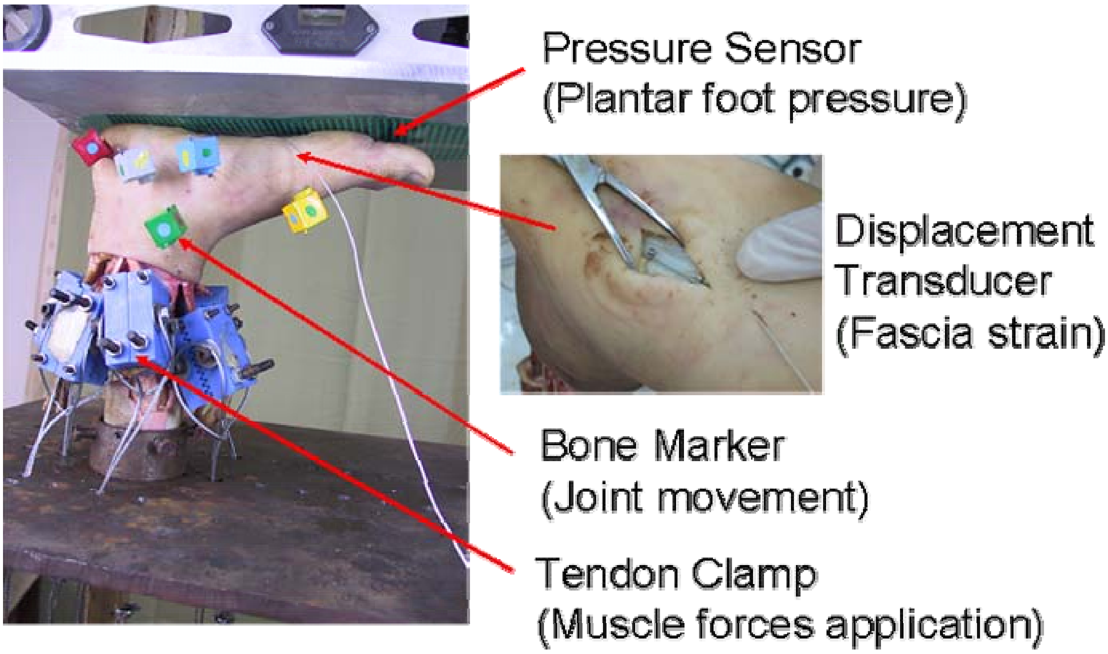


Figure 3-26. Cadaveric experimental setup for midstance simulation.

An Aluminium plate was used to simulate the ground support. The foot support allowed adjustments in vertical displacement and inclination in the sagittal plane. An F-scan pressure sensor (Tekscan Inc., Boston, USA) was affixed on the Aluminium ground support for plantar pressure measurement. The implanted displacement transducer (Microstrain, Inc, Williston, Vermont, USA) (Fig. 3-26) used in the previous compression test was kept for the strain measurement of the plantar fascia.

Simulations of muscular tendon forces were done by applying death weights on the designated tendon clamps via metal wire and hook (Fig. 3-27). The muscle tendons were gripped by custom-made serrated jaw clamps fabricated from plastic racks (Kohara Gear Industry Co., Ltd, Japan) (Appendix A). Due to the size of the tendon clamp, the nine muscle tendons were lumped in six functional tendon groups: Achilles (gastrocnemius and soleus), posterior tibial (tibialis posterior), flexor (flexor digitorum longus and flexor hallucis longus), extensor (extensor digitorum longus and extensor hallucis longus), peroneal (peroneous brevis and peroneous longus), and anterior tibial (tibialis anterior) (Fig. 3-26). The applied tendon forces (Table 3-7) for simulating the late midstance position was verified using the location of the centre of pressure as the primary feedback mechanism as suggested by Imhauser et al. (2004).

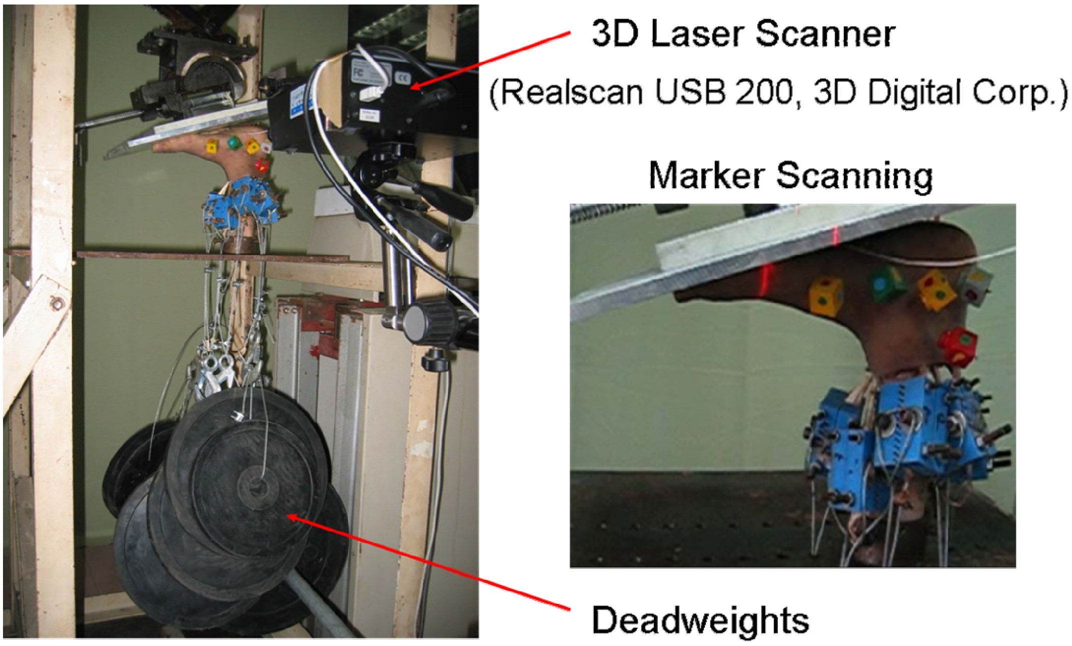


Figure 3-27. Midstance simulation for the vertical compression test of cadaveric foot specimen.

Bone markers were attached to the tibia, talus, calcaneus, navicular and first metatarsal for position tracking using a 3D laser scanner (Realscan USB 200, 3D Digital Corp, Danbury, CT, USA) (Fig. 3-27). The laser scanner has an accuracy of 0.2 mm at 300 mm, and resolution of 512 x 1000. A global coordinate system was assumed at the fixed tibia and fibular junction. The vertical x-axis was oriented along the tibial shaft through the ankle centre; the y-axis was oriented in a mediolateral direction; and z-axis had an anteroposterior orientation, with the right foot as a reference. The anteroposterior axis was parallel to the projection of a line connecting the centre of the heel and the second metatarsal on the horizontal plane. Abduction-adduction was defined as movement in the transverse plane, dorsiflexion-plantarflexion as movement in the sagittal plane, and eversion-inversion as movement in the coronal plane.

For each loading condition, digitized marker images of four tracked bone (talus, calcaneus, navicular, first metatarsal) and one reference bone (tibia) were obtained. The digitized data were used to reconstruct the 3D surface model of each bone marker in the image analysis software, Geomagic Studio 5.0 (Raindrop Geomagic, Inc. NC, USA). The 3D relative position of digitized bone markers were calculated using the projection matching technique performed by Geomagic Studio software. This image registration process was done by matching the surface normal from the over lapping region in the two scanned images of the same bone marker from different loading conditions. Before the calculation of the marker position of each of the four tracked bones, the image of the tibia bone marker in the four midstance simulations were first aligned to the tibia bone marker in the reference neutral foot position to establish a reference coordinate system. The 3D movements of each of the four tracked bone markers in the four midstance simulations relative to the neutral position were then calculated. The relative bone movements calculated for each of the tracked bone markers can then be used to calculate the relative joint movements for each loading condition. The relative orientations of the bones were expressed as joint angles measured using Cardan angle convention.

Before the loading simulation, 5 cycles of preconditioning loading cycles up to compression of 350 N were done. The neutral or unloaded position was achieved with the foot in contact with the foot support under Achilles tendon forces of 50 N and F-scan measured total ground reaction forces of about 10 N. For midstance simulation, an initial foot-support contact was established with the ground support inclined at 10 degrees relative to the plantar foot. In order to standardize the experimental procedures, the musculotendon forces were applied one by one in the following sequence: Achilles tendon (750 N), flexor tendons (75 N), peroneal tendons (75 N), and posterior tibial tendon (70 N). After the tendon forces were applied, further compression of the Aluminium foot support was applied to the foot until the location of centre of pressure and magnitude total ground reaction forces were consistent with the experimental measurements of the subject during normal walking.

Four conditions of the late midstance phase were simulated accordingly from intact foot condition, PTTD, PFR, and PFR with PTTD. For the simulation of PTTD and PFR, the dead weights on the posterior tibial tendon were removed while the plantar fascia was completely detached proximally to the medial inferior heel region. Specimens were preloaded for at least 10 seconds for each loading condition before data collection. The relative bone rotations in the global coordinate system, strains of the plantar fascia (for intact fascia condition only) and the plantar pressure were measured. Throughout the experiments, the room temperature was kept at approximately 25 Degree Celsius and the tissue was moistened with saline to avoid tissue desiccation. The measured plantar fascia strain, plantar pressure, and joint rotations in different loading conditions were compared to the FE predictions.

## *3.3 Parametrical Analysis of Foot Orthosis*

### 3.3.1 Effects of Foot Orthosis on the Loading Response of the Foot

A preliminary parametrical analysis on foot orthosis was conducted to examine the ability of the FE model in quantifying the biomechanical effect of a custom-molded foot orthosis on the foot during balanced standing. For the sake of simplification, all the bony and soft tissue structures were assigned to be homogeneous, isotropic and linearly elastic.

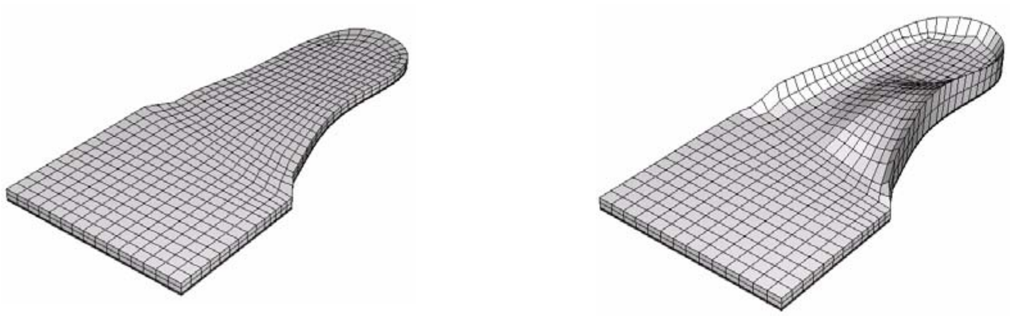

Figure 3-28. The FE meshes of flat and custom-molded insoles.

The geometry of a simplified insole model was extracted from the plantar foot shape of the same subject who underwent the MR scanning for the development of the FE model. An impression cast with the subject sitting in the neutral position was obtained using liquid dental plaster (Tsung et al., 2004) and a positive cast was created and digitized. A surface model of the insole (SURFACER; Imageware Inc., Ann Arbor, MI, USA) was developed and imported into SolidWorks, 2001 to form the solid model of the insole. A 5 mm thick insole was meshed into 3D brick elements (Fig. 3-28) with a Poisson's ratio of 0.4 and a varied Young's modulus of 0.3 (soft), 1 (firmer), and 1000 MPa (rigid) for simulation of (1) open-cell polyurethane foams, such as Professional Protective Technology's PPT material (Professional Protective Technology, Deer Park, NY, USA); (2) high-density ethylene vinyl acetate (EVA); and (3) polypropylene materials, respectively (Lemmon et al., 1997; Syngellakis et al., 2000). A relatively rigid, 1 mm thick bottom layer was used to simulate the ground support and to facilitate the application of concentrated ground reaction forces. The foot-insole interface was modeled using contact surfaces with a friction coefficient of 0.6 (Zhang and Mak, 1999).

To validate the model, the plantar pressure measurement of the subject during barefoot standing was used to calculate the centre of pressure and to compare the plantar pressure distribution predicted by the FE model. Interfacial pressures between the foot and standing support were measured using the F-scan system (Tekscan Inc, Boston, USA). The insole was properly aligned in a way that permitted an initial foot-insole contact to be established, with minimal induced stress and contact pressure, before ground reaction forces (350 N) and Achilles tendon loading (175 N) were applied. The superior surface of the soft tissue, distal tibia, and fibula was fixed throughout the analysis, while the point of load application at the centre of pressure was allowed to move in the vertical direction only.

### 3.3.2 Parametrical Analysis on Pressure-Relieving Foot Orthoses

A statistical-based parametrical analysis was conducted to investigate the effect of different design parameters such as arch height, thickness and material stiffness of a foot orthosis on its pressure-relieving capability. The FE model considering the nonlinear material properties of the foot and foot orthosis was used in this parametrical study. The effect of different structural and material combination of foot orthoses on the plantar pressure distribution during simulated midstance was investigated. The validated FE predictions were used to establish the knowledge-based guidelines for designing pressure-relieving foot orthoses.

To establish the loading and boundary conditions for midstance at neutral ankle position (45% of the stance phase cycle), the plantar pressures and foot-shank positions (Tekscan Inc., Boston, USA) during normal walking of the same subject who underwent the MR scanning were measured. The extrinsic muscles forces during midstance were estimated from the physiological cross-sectional area (PCSA) of the muscles (Dul, 1983) and normalized EMG data during normal walking (Perry, 1992) assuming a linear EMG-force relationship with a muscle gain of 25 N/cm$^2$ (Kim et al., 2001). Table 3-8 shows the muscle and ground reaction forces for simulating midstance. The loading and boundary conditions for simulation of shod and with different design of foot orthosis were assumed to be identical.

Table 3-8. Normalized EMG data and ground reaction and extrinsic muscles forces applied for midstance simulation.

| Muscles | EMG (%) | Applied Forces (N) |
|---|---|---|
| Tibialis Anterior | 0 | - |
| Extensor Hallucis Longus | 0 | - |
| Extensor Digitorum Longus | 0 | - |
| Achilles (Soleus, Gastrocnemius) | 48.6, 45.7 | 700 |
| Tibialis Posterior | 17.1 | 70 |
| Flexor Hallucis Longus | 20 | 40 |
| Flexor Digitorum Longus | 14.2 | 30 |
| Peroneus Brevis | 14.2 | 30 |
| Peroneus Longus | 14.2 | 40 |
| Reaction of Lateral Retinaculum | - | 50 |
| Reaction of Medial Retinaculum | - | 50 |
| Vertical Ground Reaction | - | 550 |

A foot orthosis composing of insole, midsole and outsole layers and a horizontal concrete ground support (Fig. 3-29) was used to establish the foot-support interface. The foot-insole interface was modeled using contact surfaces with a friction coefficient of 0.6 (Zhang and Mak, 1999) while the foot orthosis and ground support were rigidly tied together. The concrete ground support was defined with a very rigid bottom layer to facilitate the application of concentrated ground reaction force.

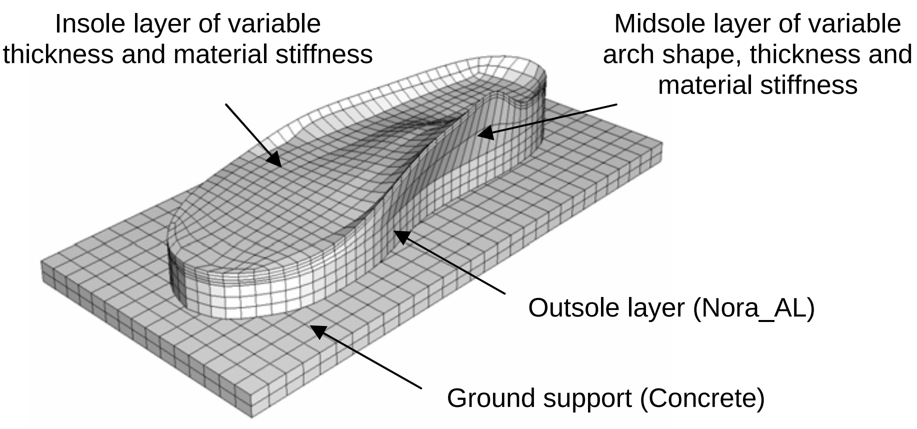


Figure 3-29. The FE meshes of custom foot orthosis and ground support.

The insole was defined as a uniform layer of varied thickness (3mm, 6mm, 9mm, and 12mm) to simulate a cushioning layer of polyurethane (Poron_L24, Poron_L32) or EVA (Nora_SL, Nora_SLW) foam. The midsole composed of an upper layer of the custom-molded foot shape of the subject and a flat bottom layer. Varied thickness (3 mm, 6 mm, 9 mm, and 12 mm) and material stiffness (Poron_L32, Nora_SL, Nora_SLW, Nora_AL) were also defined for the midsole layer. The outsole was defined as a uniform layer of 12 mm thick with properties of high-density EVA foam (Nora_AL). Before the application of the muscle and ground reaction forces, an initial foot-insole contact was established with minimal plantar pressure. The superior surface of the soft tissue, distal tibia and fibula was fixed throughout the analysis while the ground support was allowed to move in the vertical direction only.

Robust Design method, also called the Taguchi Method, pioneered by Dr. Genichi Taguchi was used to study the sensitivity of different structural and material parameters of pressure-relieving foot orthosis. Five design factors of foot orthosis namely, the arch shape, insole thickness, midsole thickness, insole stiffness, and midsole stiffness were selected for evaluation. Each factor was assigned with four levels (Table 3-9). Four different arch shapes namely Flat (F), Full-weightbearing (FWB), Half-weightbearing (HWB) and Non-weightbearing (NWB) were considered. Insole and midsole thickness from 3 to 12 mm was considered. Insole and midsole material of hardness ranging from Shore A value of 10 to 50 degree was considered.

Table 3-9. Design factors and their levels of Taguchi method.

| **Design factor** | **Level** | | | |
|---|---|---|---|---|
| | Level 1 | Level 2 | Level 3 | Level 4 |
| Arch Type | F | FWB | HWB | NWB |
| Insole Thickness (mm) | 3 | 6 | 9 | 12 |
| Midsole Thickness (mm) | 3 | 6 | 9 | 12 |
| Insole Material (Hardness) | 10 | 20 | 30 | 40 |
| Midsole Material (Hardness) | 20 | 30 | 40 | 50 |

F: Flat, FWB: Full-weightbearing, HWB: Half-weightbearing, NWB: Non-weightbearing. Hardness values of 10, 20, 30, 40 and 50 correspond to Poron_L24, Poron_L32, Nora_SLW, Nora_SL, Nora_AL, respectively.

An orthogonal array is used in a Taguchi design experiment. The columns of an orthogonal array are mutually orthogonal in which for any pair of columns, all combinations of factor levels occur at an equal number of times. The L16 orthogonal array (Taguchi, 2005) was used for the current experimental design and the configurations of the foot orthoses for each simulation were shown in Table 3-10. It can be seen in Table 3-10 that only sixteen simulations were required to identify the relative significance of the design factors using the Taguchi method. A total number of total number 1024 ($4^5$) analyses are required using full factorial approach.

Table 3-10. L16 orthogonal array table (the numbers under design factors indicate the levels assigned to each design factor)

| **Trial number** | **Factors** | | | | |
|---|---|---|---|---|---|
| | Arch Type (A) | Insole Thickness (IT) | Midsole Thickness (MT) | Insole Stiffness (IS) | Midsole Stiffness (MS) |
| 1 | 1 | 1 | 1 | 1 | 1 |
| 2 | 1 | 2 | 2 | 2 | 2 |
| 3 | 1 | 3 | 3 | 3 | 3 |
| 4 | 1 | 4 | 4 | 4 | 4 |
| 5 | 2 | 1 | 2 | 3 | 4 |
| 6 | 2 | 2 | 1 | 4 | 3 |
| 7 | 2 | 3 | 4 | 1 | 2 |
| 8 | 2 | 4 | 3 | 2 | 1 |
| 9 | 3 | 1 | 3 | 4 | 2 |
| 10 | 3 | 2 | 4 | 3 | 1 |
| 11 | 3 | 3 | 1 | 2 | 4 |
| 12 | 3 | 4 | 2 | 1 | 3 |
| 13 | 4 | 1 | 4 | 2 | 3 |
| 14 | 4 | 2 | 3 | 1 | 4 |
| 15 | 4 | 3 | 2 | 4 | 1 |
| 16 | 4 | 4 | 1 | 3 | 2 |

The peak plantar pressure at the forefoot, midfoot and rearfoot from the 16 FE analyses were predicted. The mean effect of each level of the four design factors on the mechanical responses was computed. For example, the mean response of arch type at level 1 [$R(A_1)$] on peak plantar pressure was calculated as the mean plantar pressure over trial 1 to trial 4. An analysis of variance (ANOVA) was performed for the sum of squares of each design factor to determine the sensitivity of each design parameter. For example, the sum of squares due to arch type are equal to

$$4[R(A_1)-R_m]^2+4[R(A_2)-R_m]^2+4[R(A_3)-R_m]^2+4[R(A_4)-R_m]^2 \quad (3\text{-}8)$$

where $R(A_1)$, $R(A_2)$, $R(A_3)$ and $R(A_4)$ are the mean response of arch type at level 1 to 4, respectively and $R_m$ is a balanced overall mean response over the entire 16 experimental trials.

The mechanical response of any combination of levels among the design factors can be predicted using a superposition model (Phadke, 1989), which assume that the total effect of several factors is equal to the sum of the individual factor effect. A superposition model for the mechanical response (R) of any combination of levels among the design factors can be described as:

$$R(A_a, IT_b, MT_c, IS_d, MS_e) = R_m + [R(A_a) - R_m] + [R(IT_b) - R_m] + [R(MT_c) - R_m] + [R(IS_d) - R_m] + [R(MS_e) - R_m] \quad (3\text{-}9)$$

where design factors: arch type (A), insole thickness (IT), midsole thickness (MT), insole stiffness (IS), midsole stiffness (MS) are set at levels as indicated with their subscripts (a, b, c, d and e). The mechanical response (R) of any combination is equal to the mean response of all 16 runs ($R_m$) plus the deviations from $R_m$ caused by setting the five factors at the levels. Finite element analysis was carried out for each of the 16 configurations of foot orthoses. Using the results of the superposition model and the sensitivity analysis of each factor, levels of each factor can be manually adjusted such that the pressure-relieving effect of the foot orthosis is maximized.

*Plantar pressure measurement*

Plantar pressure measurement was conducted to validate the FE predictions of the sensitivity analysis on the design factors. Flat and custom-molded foot orthoses were fabricated for plantar pressure measurement during normal walking of the same subject for FE model development. Three custom-molded shapes namely full-weightbearing, half-weightbearing and non-weightbearing were considered. Poron_L32 and Nora_SL were chosen to fabricate the insole and midsole layers, respectively. Two different thicknesses (3 & 6 mm) were considered for the insole layer while the thickness of 3 mm was considered for the midsole layer.

The custom-molded foot orthoses were fabricated using a computerized numerical control (CNC) milling machine (LeadWell CNC Machines MFG. CORP.) (Fig. 3-30). The machine code for the CNC machining was created for the surface models of the foot orthoses using a custom MATLAB program. A ball nose shape milling head of 16 mm in diameter was used. The milling and feeding speed were 6000 rpm (clockwise) and 1000 mm/min, respectively. The tool path was programmed with three rough cut (8 mm intervals) along the longitudinal direction of the foot orthosis and one fine cut (1 mm interval) along the transverse direction. The milling time for a single foot orthosis was about one hour.


**CNC Machine** **Insole Milling**

Figure 3-30. Computerized numerical control (CNC) machining (LeadWell CNC Machines MFG. CORP.)

The cut-out for the foot orthosis was manually trimmed by an Orthotist to fit the size of the shoes (size 41 for men) for the subject (Fig. 3-31). The covering insole layer (Poron_L32) was then glued to the midsole layer (Nora_SL). A pair of canvas shoes with a flat outsole of 12 mm thick was used for the experiments. The 2 mm thick insoles that come with the shoes were removed.

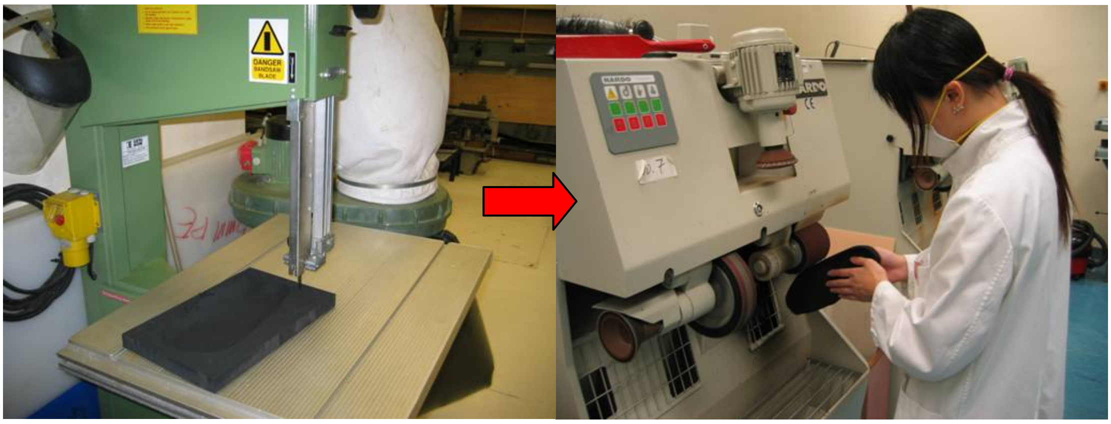

**Rough Trimming of midsole layer** **Fine Trimming of midsole layer**

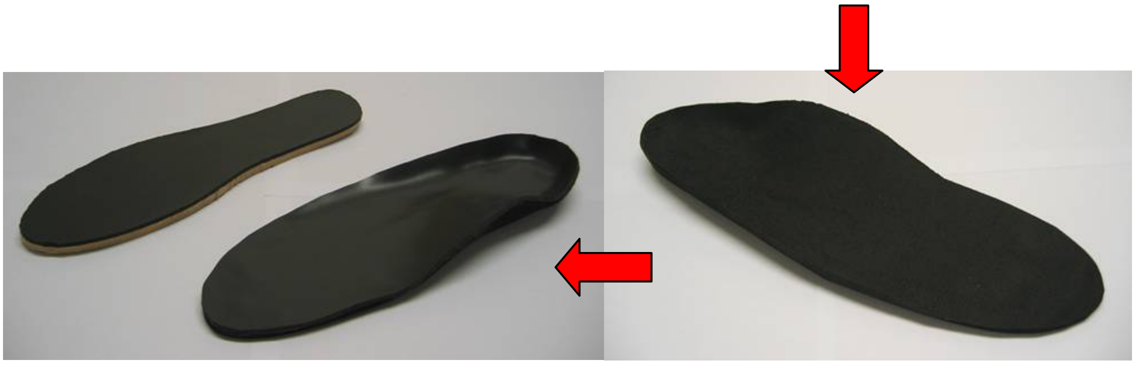

**Flat and Custom-molded Foot orthoses** **Custom-molded midsole layer**

Figure 3-31. Fabrication process of the custom foot orthoses

In-shoe plantar pressures during shod and with different prescribed foot orthoses were measured using the F-scan system (Tekscan Inc., Boston, USA). The F-scan sensors were trimmed to fit the shoes (Fig. 3-32). The F-scan sensors were calibrated by the subject's body weight (700 N) during single-leg standing (Fig. 3-32). The video measurement for the foot-shank position and the plantar pressure data were collected at a sampling frequency of 25Hz and 100Hz, respectively. The plantar pressure measurement was done in a human motion analysis laboratory with the subject walking at a comfortable pace (1.15s / gait cycle) on a walkway of about 10 m. The measured plantar pressure distribution of the right foot of the subject at neutral ankle position during midstance was compared to the aforementioned FE predictions. The pressure measurement of the second step after gait initiation was used (Bus and Lange, 2005).

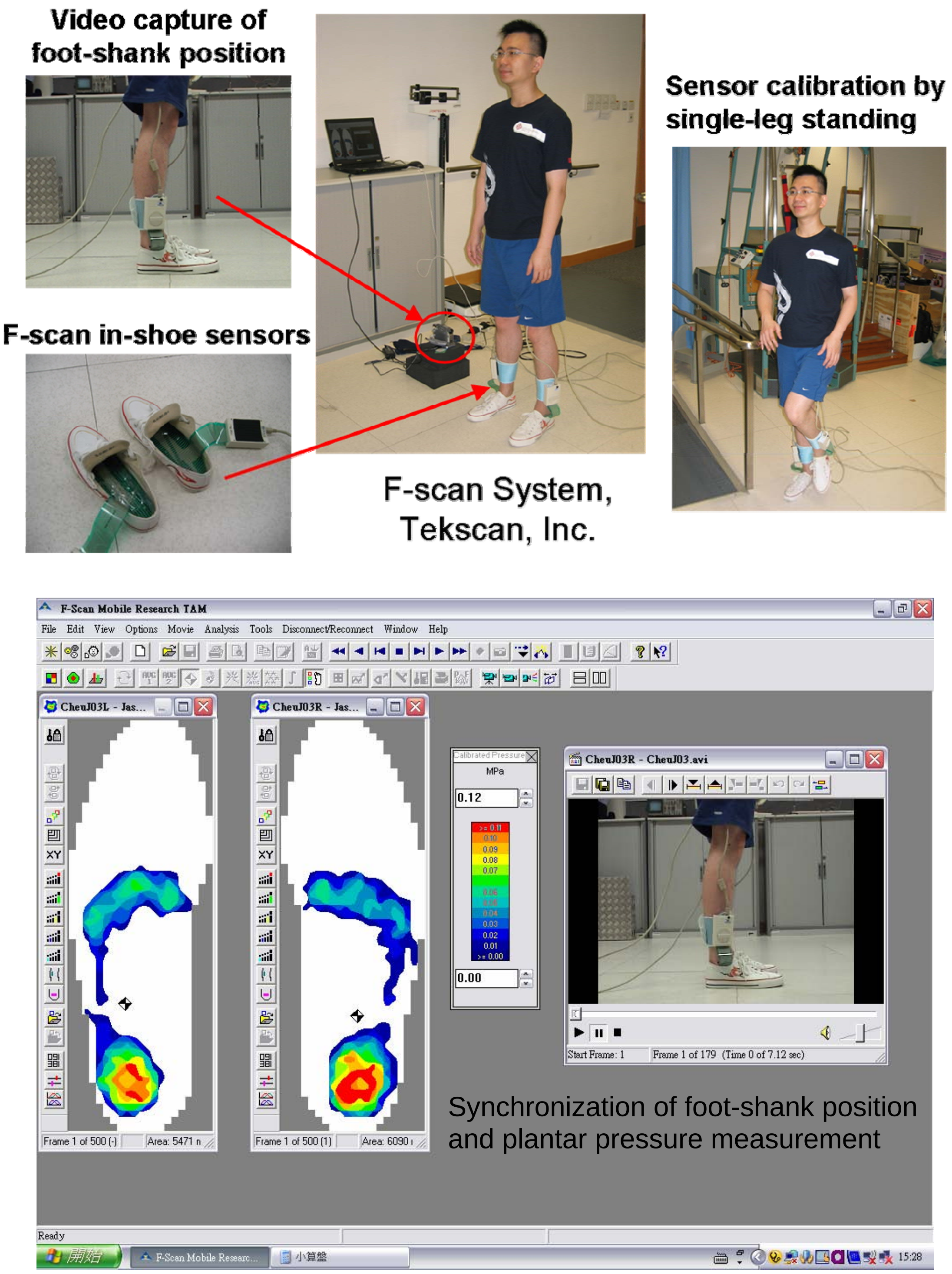


Figure 3-32. Experimental setup and calibration of the F-scan system for in-shoe plantar pressure measurement (Tekscan Inc., Boston, USA).

# CHAPTER IV RESULTS

## 4.1 Effects of Varying Bulk Soft Tissue Stiffness

In this sensitivity study, the developed FE model was used to document the effect of varying bulk soft tissue stiffness on the plantar pressure distributions and the internal load during weightbearing of the foot. Figure 4-1 depicts the plantar pressure distribution obtained from F-scan measurements and the plantar pressure and shear stress distributions and von Mises stresses in the foot bones predicted by the FE simulation during balanced standing. The von Mises stress ($\sigma_{VM}$) is derived from the distortion energy theory to weighs the effects of principal stresses ($\sigma_1$, $\sigma_2$ and $\sigma_3$) according to the relation:

$$\sigma_{VM} = \sqrt{\frac{1}{2}\left[(\sigma_1 - \sigma_2)^2 + (\sigma_2 - \sigma_3)^2 + (\sigma_3 - \sigma_1)^2\right]} \qquad (4\text{-}1)$$

The model predicted peak pressures of about 0.23, 0.097, 0.112, 0.095, 0.044 and 0.025 MPa, accordingly at the heel region and from the first to the fifth metatarsal head regions, while the corresponding peak pressures measured by the F-scan sensors were about 0.17, 0.06, 0.09, 0.07, 0.06 and 0.08 MPa. Peak anterior–posterior shear stress of about 0.06 MPa was predicted at the posterior heel region and the soft tissue beneath the third metatarsal head (Fig. 4-1c). The contact areas predicted by the FE model was about 68 $cm^2$, compared to about 70 $cm^2$ from F-scan measurement during balanced standing.

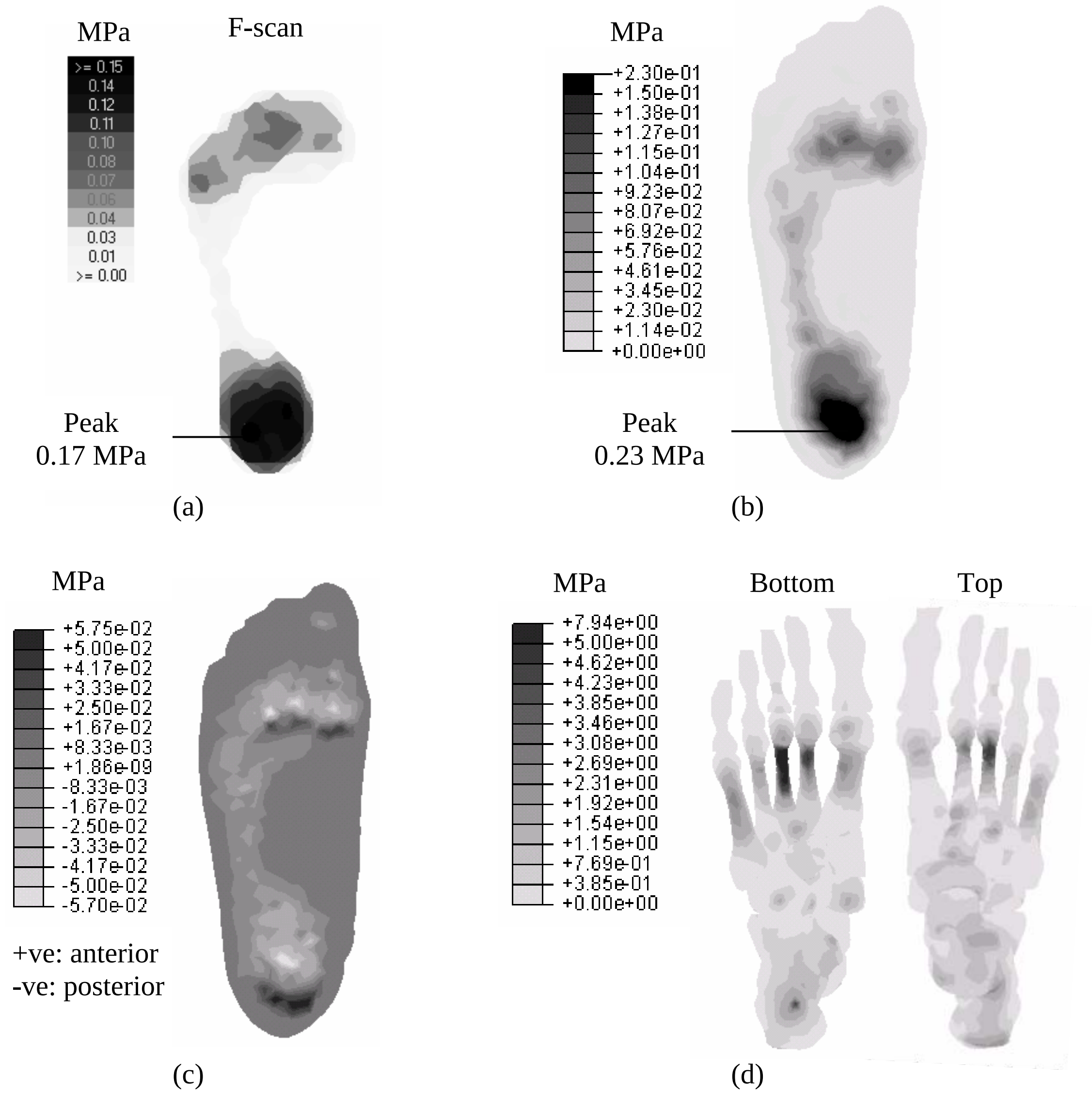


Figure 4-1. (a) The pressure distribution from F-scan measurements during balanced standing, (b) FE predicted plantar pressure distribution, (c) FE predicted plantar anteroposterior shear stresses, and (d) FE predicted von Mises stress in the foot bones, with normal soft tissue stiffness.

During balanced standing, relatively high von Mises stresses were predicted at the mid-shaft of metatarsals especially in the third metatarsal (Fig. 4-1d). The insertion sites of the plantar fascia at the inferior calcaneus and the metatarsal heads experienced large stress as a result of tension in the plantar fascia. The ankle and subtalar joints junctions together with the dorsal junction of calcaneal-cuboid joint also sustained high stresses. The predicted peak von Mises stresses in specific foot bones were tabulated in Table 4-1. With normal soft tissue stiffness, peak von Mises stress of 7.94 MPa was predicted at the third metatarsal, followed by the second metatarsal (4.47 MPa), the calcaneus (3.94 MPa), and the talus (2.89 MPa). Peak bone stress was found at the third metatarsal in all calculated cases with a minimal increase of about 7% with soft tissue stiffening. With a five-fold increase in tissue stiffness, a stress reduction and an increase of up to 50% (lateral cuneiform) and 26% (fourth metatarsal), respectively, were predicted in the major foot bones. Maximum stress reduction of about 1.13 MPa was predicted at the lateral cuneiform, which was followed by reduction at the calcaneus (0.95 MPa), talus (0.78 MPa) and the first metatarsal (0.69 MPa). Meanwhile, a maximum stress increase of about 1.37, 0.60 and 0.56 MPa were predicted at the cuboid, fourth and third metatarsals, respectively. The changes in peak von Mises stress were less than 0.2 MPa in the medial cuneiform, the second metatarsal and the five toes.

Table 4-1. Peak von Mises stresses in the foot bones during balanced standing with different degrees of soft tissue stiffening. F2, F3 and F5 correspond to simulations of two, three and five times the stiffness of normal tissue.

| **Bone** | **Peak von Mises stress, MPa** | | | |
|---|---|---|---|---|
| | Normal | F2 | F3 | F5 |
| Talus | 2.89 | 2.47 | 2.33 | 2.11 |
| Calcaneus | 3.94 | 3.50 | 3.27 | 2.99 |
| Navicular | 1.47 | 1.18 | 1.10 | 0.96 |
| Cuboid | 1.58 | 2.06 | 2.11 | 1.88 |
| Medial Cuneiform | 0.63 | 0.69 | 0.71 | 0.70 |
| Intermediate Cuneiform | 1.42 | 1.29 | 1.18 | 1.01 |
| Lateral Cuneiform | 2.22 | 1.84 | 1.54 | 1.09 |
| 1st Metatarsal | 2.30 | 2.02 | 1.84 | 1.61 |
| 2nd Metatarsal | 4.47 | 4.20 | 4.20 | 4.28 |
| 3rd Metatarsal | 7.94 | 8.40 | 8.50 | 8.33 |
| 4th Metatarsal | 2.32 | 2.62 | 2.79 | 2.92 |
| 5th Metatarsal | 2.42 | 2.57 | 2.76 | 2.82 |
| 1st Toe | 0.46 | 0.37 | 0.33 | 0.28 |
| 2nd Toe | 0.34 | 0.40 | 0.43 | 0.43 |
| 3rd Toe | 0.63 | 0.62 | 0.65 | 0.70 |
| 4th Toe | 0.16 | 0.26 | 0.26 | 0.21 |
| 5th Toe | 0.10 | 0.11 | 0.08 | 0.05 |

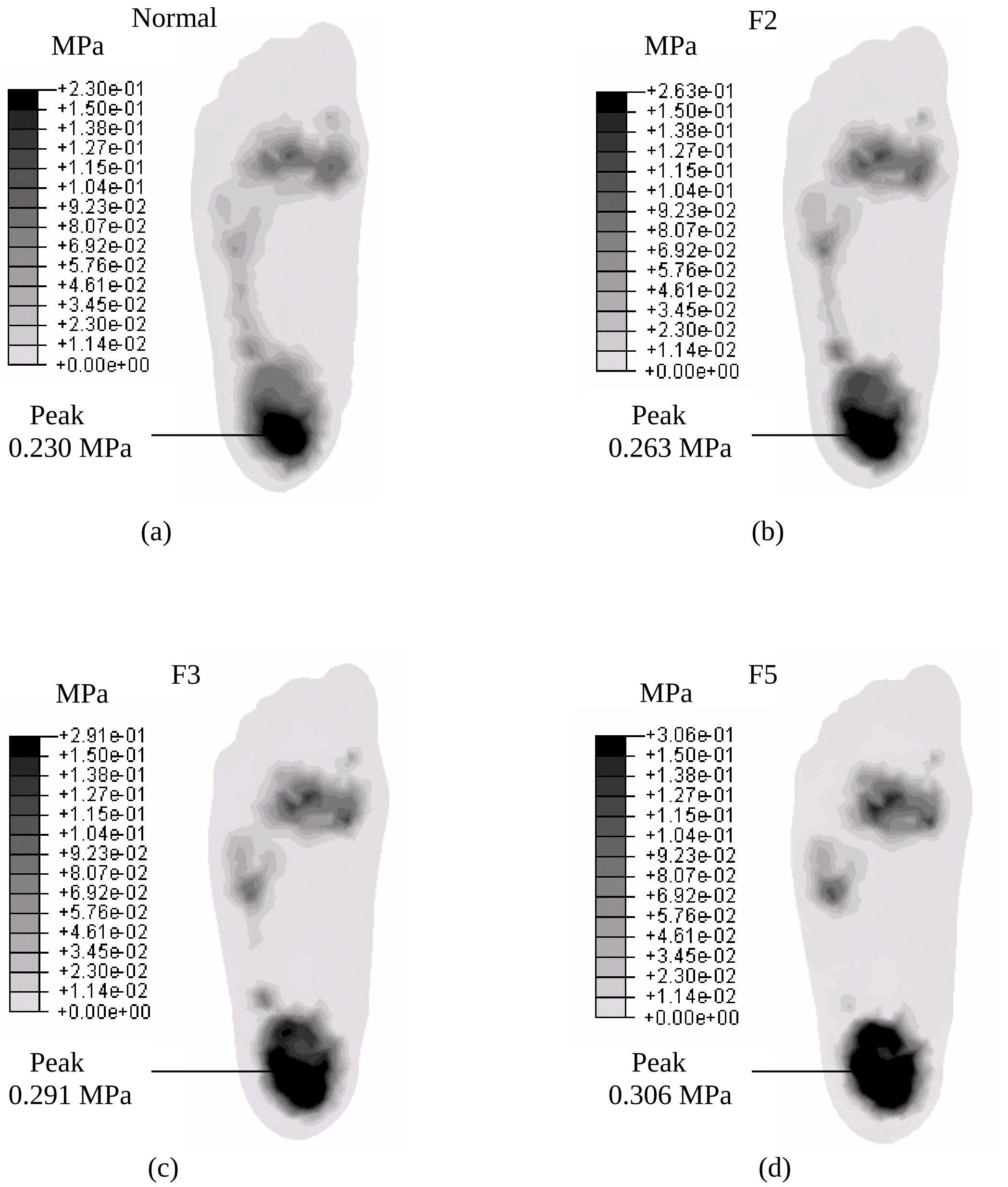


Figure 4-2. Plantar pressure distributions with different degrees of soft tissue stiffening. F2, F3 and F5 correspond to simulations of two, three and five times the stiffness of normal tissue.

Figure 4-2 shows the FE predicted plantar pressure patterns with different stress–strain behaviour assigned for soft tissues. Under the identical loading conditions, an increase in soft tissue stiffness would increase the peak plantar pressure. The plantar pressure tended to intensify at the heel and beneath the metatarsal heads except the fourth metatarsal with increasing soft tissue stiffness. A maximum pressure of 0.31 MPa corresponding to about 33% increase was predicted at the heel with soft tissue stiffness of five times the normal values. With a five-fold increase in tissue stiffness, the peak plantar pressure from beneath the first, second, third and the fifth metatarsal heads increased by about 35%, 35%, 57% and 64%, respectively while a decrease in pressure of about 16% was predicted beneath the fourth metatarsal heads. The posterior shear stress beneath the heel and third metatarsal head increased by about 82% and 14% to peak values of 0.104 and 0.064 MPa, respectively.

Figure 4-3 shows the effects of soft tissue stiffness on the plantar peak pressure (Fig. 4-3a), the contact area between the plantar foot and the support (Fig. 4-3b) in the forefoot, midfoot and rearfoot regions, divided with an equal length of the pressurized area. During balanced standing, the rearfoot experienced the highest plantar pressure, followed by the forefoot. Peak plantar pressure increased by about 1.14 and 1.33 times, respectively with two- and five-fold increases in soft tissue stiffness (Fig. 4-3a). The forefoot and midfoot experienced larger increases of up to about 1.35 and 2.19 times to peak values of 0.151 and 0.114 MPa, respectively.

The contact area between the plantar foot and the floor reduced with high soft tissue stiffness especially at the midfoot area (Fig. 4-3b). The forefoot and the rearfoot areas become the major support of the foot with increased tissue stiffness. The contact area between the plantar surface and the support reduced by about 47% upon five times stiffening of normal soft tissue behaviour. This corresponded to reductions of about 39%, 78% and 41%, respectively, at the forefoot, midfoot and rearfoot regions.

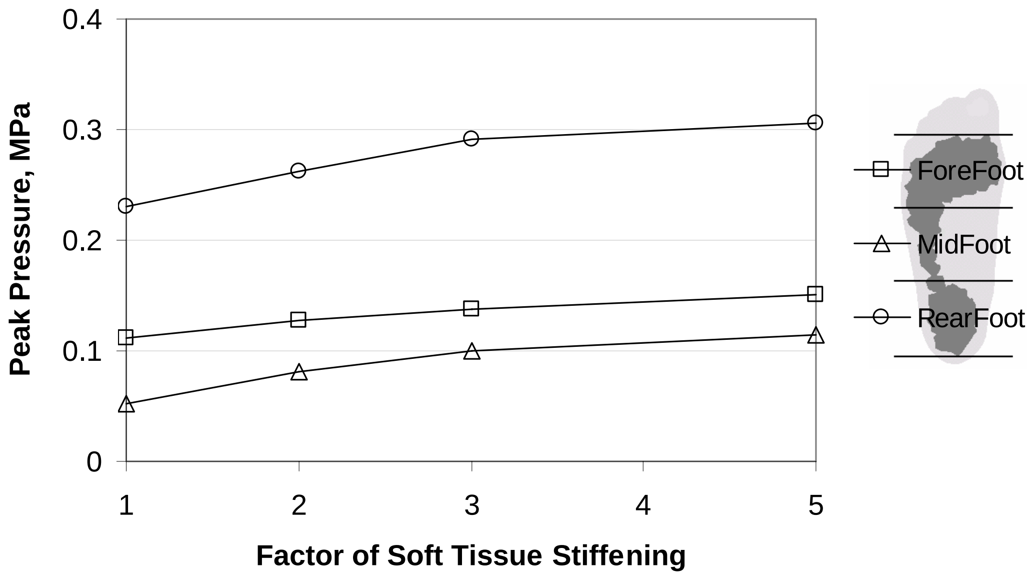


(a)

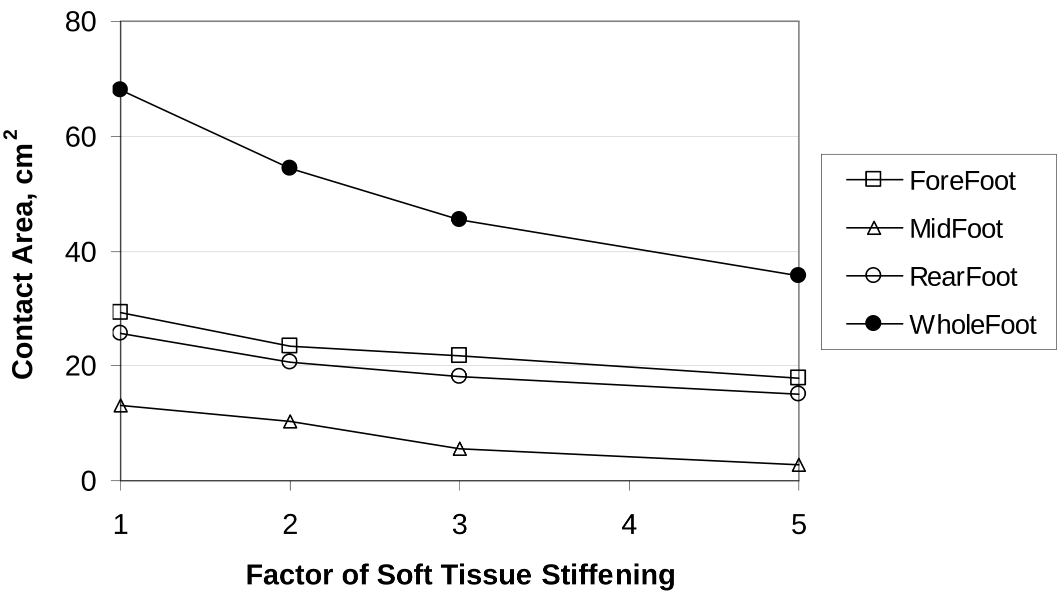


(b)

Figure 4-3. Effects of soft tissue stiffening on (a) peak plantar pressure, and (b) contact area between the plantar foot and the support. The soft tissue stiffening was represented by a scale factor from 1 to 5 to represent simulations of up to five times the stiffness of normal tissue.

## *4.2 Effects of Varying Plantar Fascia Stiffness*

In this sensitivity study, the developed 3D FE model was used to investigate the effects of plantar fascia stiffness on the plantar foot pressure and the biomechanical responses among the bony and ligamentous structures under weightbearing. Figure 4-4 shows the F-scan measured and FE predicted plantar pressure distribution during balanced standing. With a reference value, E = 350 MPa for Young's modulus of fascia, peak plantar pressure of about 0.19 and 0.26 MPa were predicted as compared to the F-scan measurement of 0.07 and 0.15 MPa, respectively. Contact areas of 69.4 $cm^2$ were measured comparing to 63.5 $cm^2$ predicted by the model.

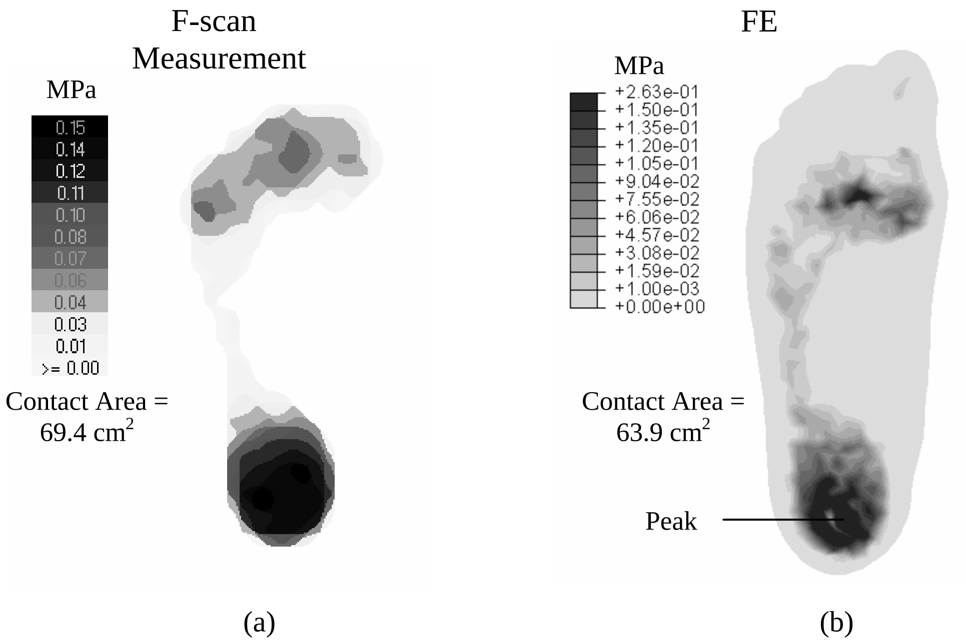


Figure 4-4. The pressure distribution from pedobarographic measurements during balanced standing and (b) FE predicted plantar pressure distribution with Young's modulus of fascia, E = 350 MPa.

There was a general peak pressure increase at the rearfoot and a decrease at the forefoot, respectively with increasing Young's modulus of fascia (Fig. 4-5a). Comparing to the reference value, E = 350 MPa, a decrease of about 6.9% in peak heel pressure and a 10.1% increase in peak forefoot pressure were predicted with simulated fasciotomy (Young's modulus of fascia, E = 0 MPa), while a change of less than 1% was predicted with half or twofolds the reference value.

There was a general increase in total forces on the rearfoot and forefoot region and a decrease on the midfoot, respectively with increasing Young's modulus of fascia (Fig. 4-5b). With Young's modulus of fascia, E = 350 MPa, the forefoot, midfoot and rearfoot sustained 33%, 8% and 59% of the total forces, respectively. With fasciotomy, about 50% increase in total forces on the midfoot was predicted, which was accompanied with a 7% and 2.5% decrease at the forefoot and rearfoot, respectively.

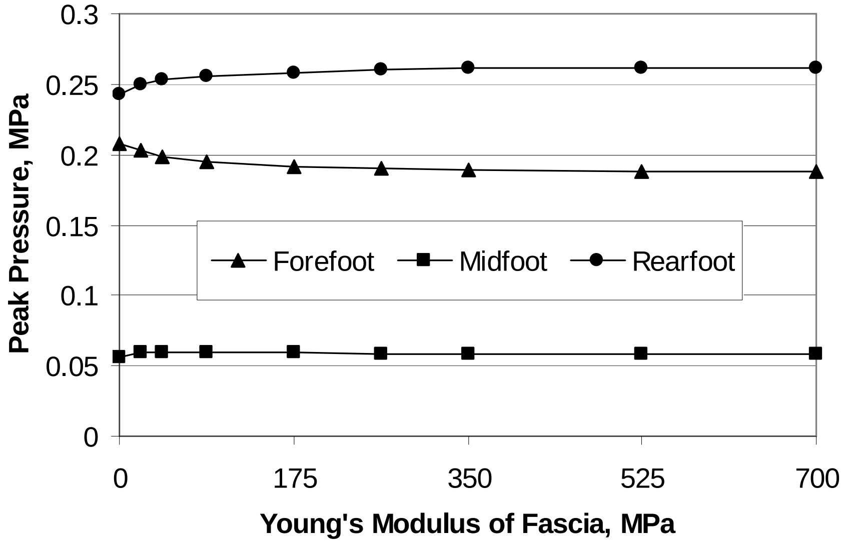


(a)

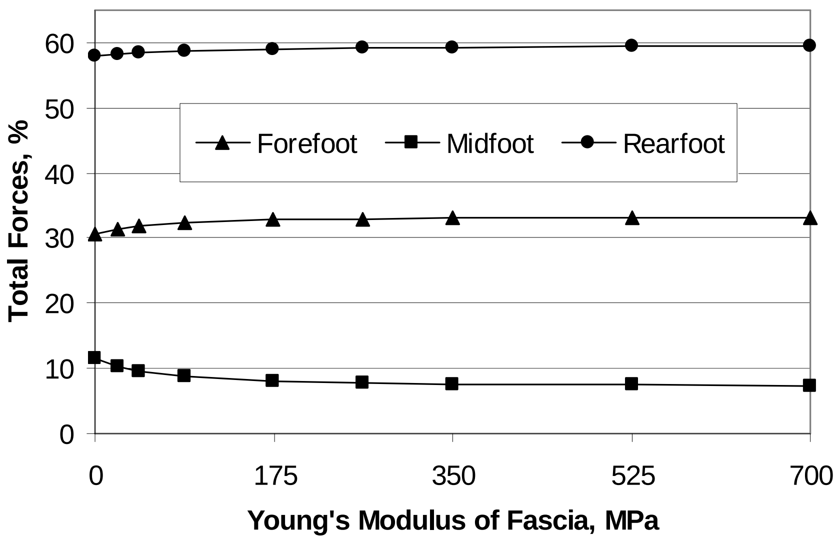


(b)

Figure 4-5. Effects of varying Young's modulus of fascia on (a) peak pressure and (b) total forces on the plantar foot during balanced standing.

The undeformed arch height of the subject was 52.5 mm by measuring the height of the medial navicular cortex to the ground support. During balanced standing, the arch height decreased by 16.2% to 44 mm. The arch height of the model was 52 mm at unloaded state and decreased 18.3% to 42.5 mm. Comparing to the reference Young's modulus value, E = 350 MPa, arch height had only about 3% less decrease with twofolds the reference value (Fig. 4-6a). An arch height reduction of 50% more was predicted with fasciotomy.

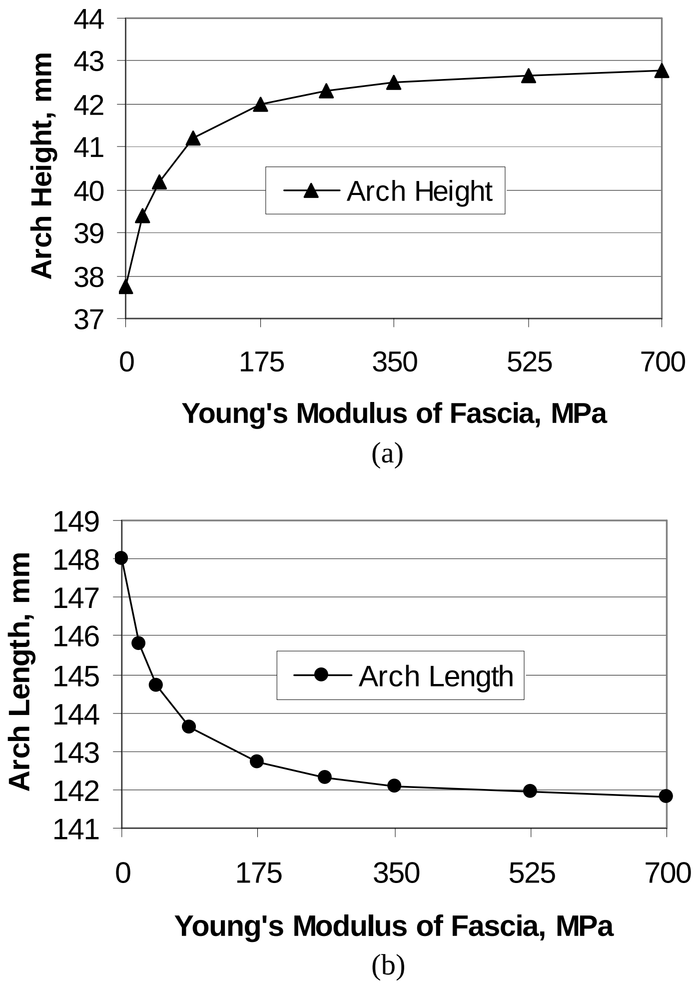


Figure 4-6. Effects of varying Young's modulus of fascia on changes in (a) arch height and (b) arch length during balanced standing.

The undeformed arch length, measuring from the longitudinal distance from the base of the proximal first metatarsal and the base of the calcaneus cortex, was 142.5 mm. With a normal and stiffened fascia (Fig. 4-6b), a decrease of less than 0.4% in arch length was predicted during balanced standing. The arch length increased by about 4% with fasciotomy.

The maximum strain of the plantar fascia decreased and it corresponding tension increased with increasing Young's modulus of fascia (Fig. 4-7). With the reference fascia Young's modulus (E = 350 MPa), the tension of the fascia during balanced standing was about 44.6% of the applied body weight, which corresponded to a maximum strain of 0.4%. With twofolds and half of the reference value, the fascia sustained about 3.2% increases and 7.7% decreases in tension, respectively.

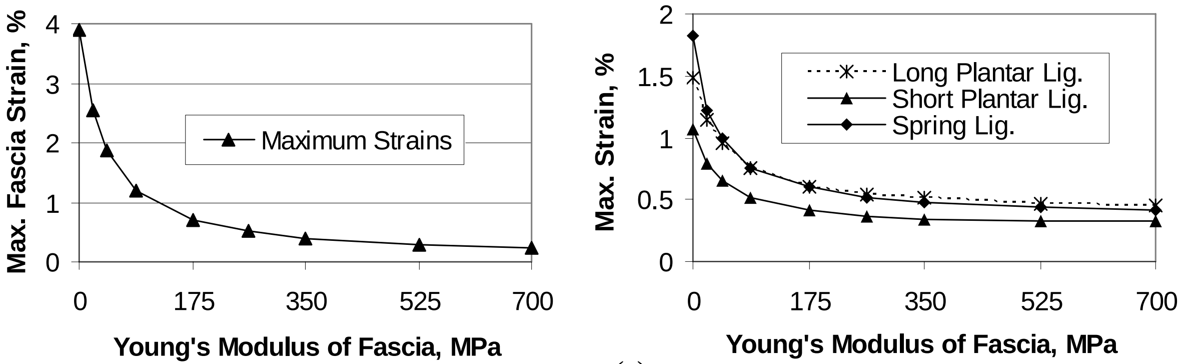


(a)

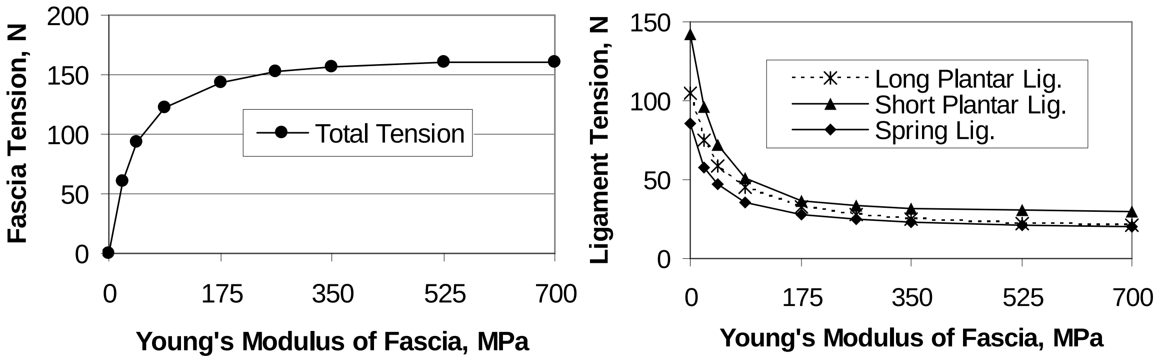


(b)

Figure 4-7. Effects of varying Young's modulus of fascia on changes in (a) maximum strains and (b) tensions of the fascia and the major plantar ligaments during balanced standing.

With twofolds the reference fascia Young's modulus, a decrease of about 16%, 6.3% and 13% in tensions of the long plantar, short plantar and spring ligaments, respectively was predicted (Fig. 4-7). Decreasing half of the reference value resulted in an increase of about 32%, 15.6% and 21.7% in tensions. Fasciotomy resulted in a pronounced increase in tensions of 228%, 344% and 274%, respectively. These corresponded to maximum ligament strains of 1.5%, 1.1% and 1.8%, respectively.

There was a general increase in maximum von Mises stress of all the metatarsal bones (Fig. 4-8) with increasing Young's modulus of fascia from one-fourths of reference value, E = 350 MPa. With twofolds of normal Young's modulus of fascia, an increase of 9.3%, 6.6%, 6.9%, 1.2% and 18.8% was predicted from the first to the fifth metatarsal bones, respectively. The changes in maximum bone stresses in the major midfoot and rearfoot were minimal with Young's modulus of fascia ranged from one-fourths to twofolds the reference value. Reducing the Young's modulus of fascia to zero resulted in a pronounced increase in maximum von Mises stress in the cuboid (136%), navicular (83%), second (53%) and fourth (154%) metatarsals (Fig. 4-8). Meanwhile, a decrease of 49%, 44% and 56% was predicted in the first, third and fifth metatarsal bones, respectively. With fasciotomy, there was a shift of peak von Mises stress from the plantar mid-shaft of third metatarsal to the dorsal mid-shaft of second metatarsal. With the reference fascia Young's modulus (E = 350 MPa), the predicted von Mises stress at the calcaneal insertion was 1.97 MPa. It decreased to 1.78, 1.53, 1.09 and 0.68 MPa, respectively with half, one-fourths, one-eighths of the reference value and with fasciotomy. Increasing twofolds the Young's modulus of fascia from reference value increased the stress to 2.12 MPa.

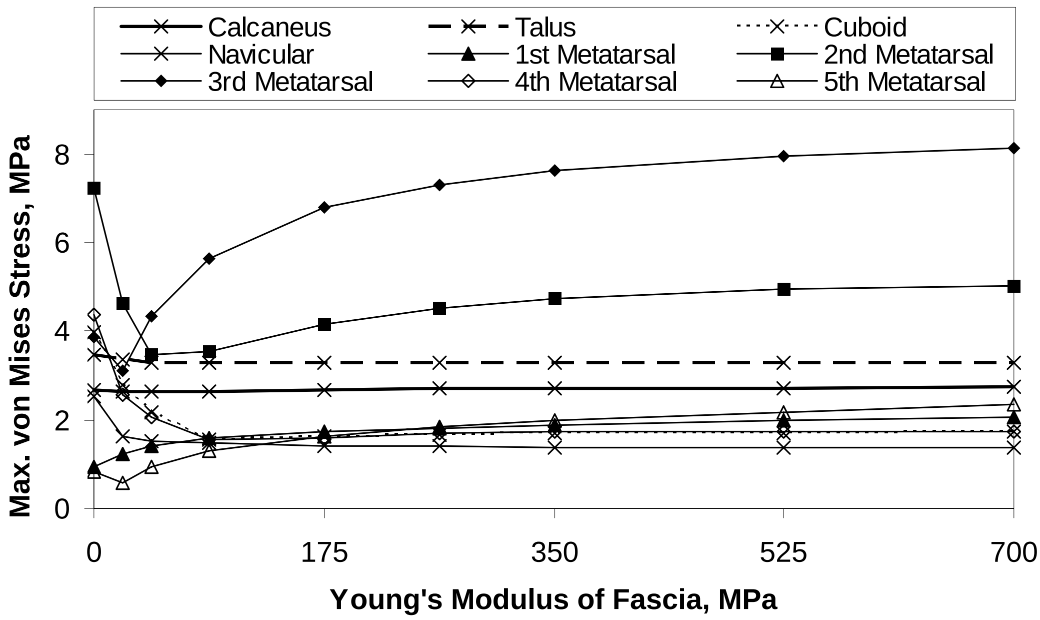


Figure 4-8. Effects of varying Young's modulus of fascia on maximum von Mises stress of the major foot bones during balanced standing.

In all simulated cases, the maximum von Mises stress of the calcaneus and talus were located at the posterior junction of the subtalar joint. With Young's modulus of fascia below one-fourths of reference value, pronation of the midfoot tended to shift the maximum metatarsal stresses from the plantar mid-shaft to the dorsal midshaft and proximal regions. The corresponding maximum von Mises stresses of the cuboid and navicular were shifted from the joint junction to the attachment regions of the plantar ligaments.

## 4.3 Effects of Partial and Complete Plantar Fascia Release

The biomechanical effects of partial and total plantar fascia release were quantified using the developed 3D FE model. Figure 4-9 shows the F-scan measured and FE predicted plantar pressure distribution during balanced standing. With plantar fascia intact, peak plantar pressure of about 0.188 MPa and 0.263 MPa at the metatarsals and heel regions were predicted as compared to the F-scan measurement of 0.07 MPa and 0.15 MPa, respectively. The patterns of the predicted plantar pressure distribution and contact area were comparable to the F-scan measurement (Fig. 4-9). Relatively higher peak pressures were predicted comparing to the measured values, which were probably due to the differences in resolution of peak pressure measurement and prediction. Contact areas of 69.4cm$^2$ were measured comparing to 63.9cm$^2$ predicted by the model.

Plantar fascia release was not found to pose a tremendous impact in redistribution of plantar pressure. There was a general peak pressure increase at the forefoot and a decrease at the rearfoot of up to 19.7% and 8.4%, respectively with sequential plantar fascia release starting from 40% of the medial sections (Fig. 4-10a). This redistribution of pressure was probably a result of the flattened and pronated foot, which increased the load bearing percentage of the midfoot and the medial forefoot. Unexpectedly, maximum peak pressure increase of 60% at the forefoot and a slight increase of about 1% at the rearfoot were predicted with 20% release of the fascia. The increased peak pressure was a result of midfoot pronation which unloaded the lateral midfoot.

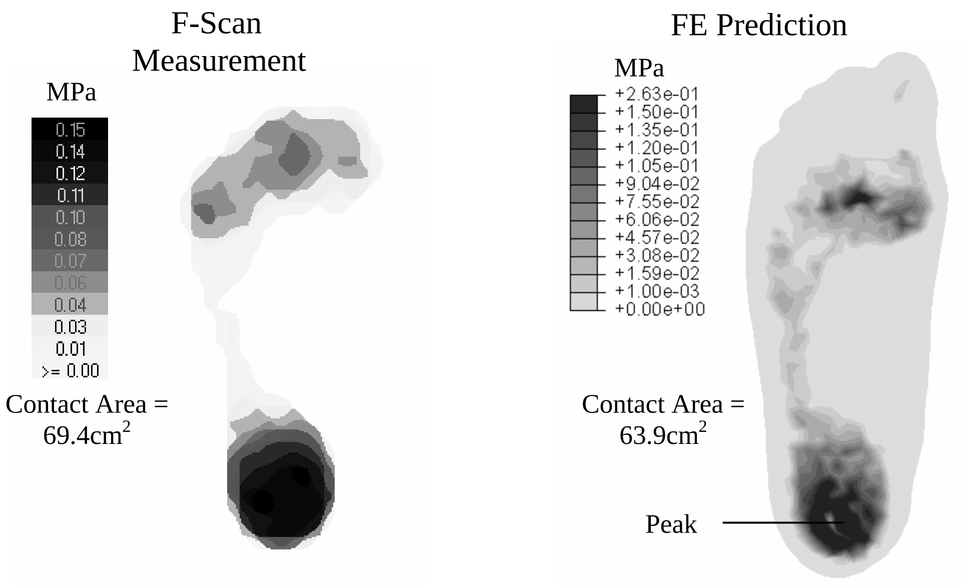


Figure 4-9. The plantar pressure distribution and total contact areas from F-scan measurements and FE predictions with intact fascia during balanced standing.

With intact fascia, 31.3%, 8.9% and 59.8% of the total forces were sustained by the forefoot, midfoot and rearfoot, respectively (Fig. 4-10b). With medial 20% and 40% release of the plantar fascia, slight increases of up to 2% in total forces bearing percentage on the rearfoot and forefoot regions and a decrease of less than 3% on the midfoot were predicted. Starting from the medial 60% release, there was a general shift of load-bearing percentage from the forefoot and rearfoot to the midfoot. With complete fascia release, about a 4.4% increase in total forces bearing percentage on the midfoot was predicted, which was accompanied with a 2.6% and 1.8% decrease at the forefoot and rearfoot, respectively (Fig. 4-10b).

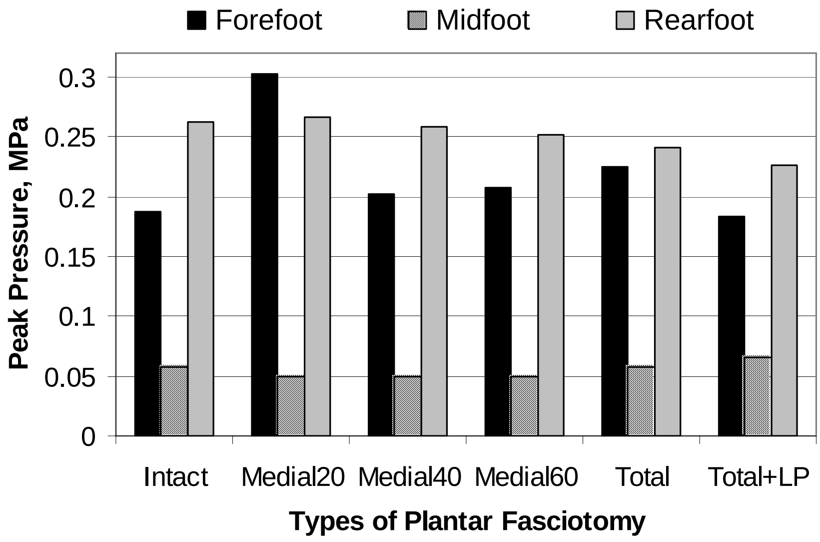


(a)

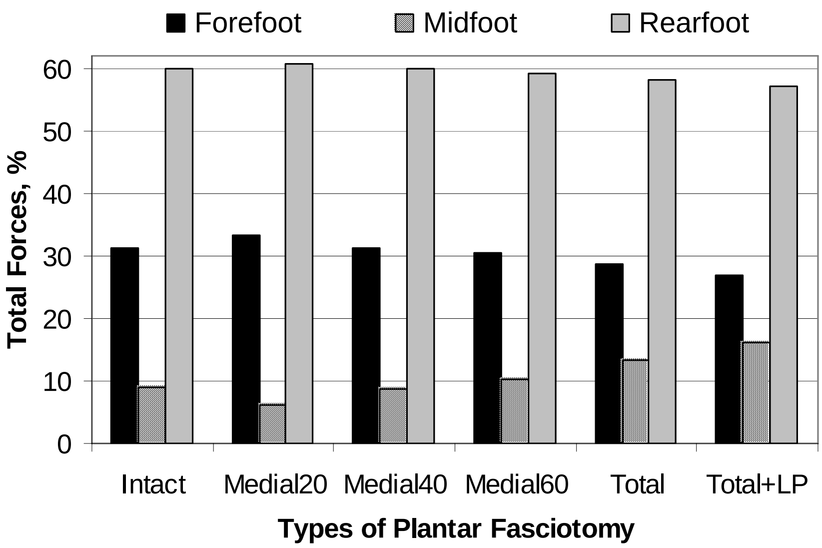


(b)

Figure 4-10. Effects of different types of fasciotomy on (a) peak pressure and (b) total forces on the forefoot, midfoot and rearfoot region during balanced standing.

The undeformed arch height of the subject and the model at unloaded state was 55 mm, measuring from the medial navicular cortex to the ground support. The measured arch height reduced to 46 mm during balanced standing, corresponding to a 16.3% decrease. The model predicted an 18.9% decrease in arch height featuring a deformed arch height of 44.6 mm during simulated balanced standing. The FE model predicted 10.4 mm and 15.1 mm arch deformation with normal fascia stiffness and with fasciotomy, corresponding to a 45% increase. Comparing to the intact fascia condition

(Fig. 4-11), the medial arch height decreased up to 6 mm from the case of medial 20% fascia release to total release of plantar fascia and long plantar ligament. The corresponding increases in medial arch length (measuring from the longitudinal distance from the base of the proximal first metatarsal and the base of the calcaneus cortex) were up to 7.4 mm.

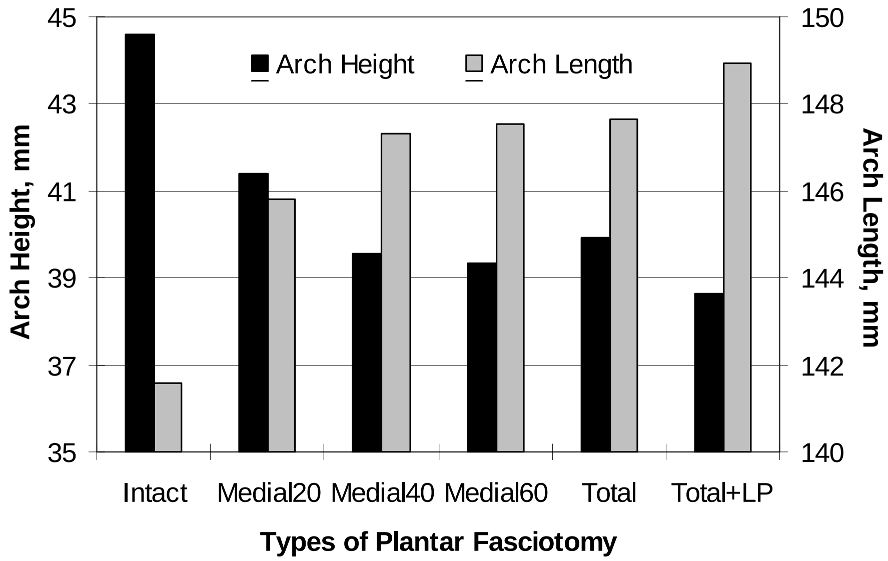


Figure 4-11. Effects of different types of fasciotomy on changes in arch height and arch length during balanced standing.

With intact fascia condition, the total tension (150 N) of the fascia during balanced standing was about 42.9% of the applied body weight (Fig. 4-12). The maximum strains of the plantar fascia decreased 0.04%, 0.03% and 0.08%, respectively with medial 20%, 40% and 60% of plantar fascia release. These corresponded to a decrease of 16.7%, 34.7% and 52%, respectively in total tensions of the plantar fascia. With medial sequential release of the plantar fascia, the maximum strains and total tensions of the plantar ligaments generally increased with sectioned portion of the fascia (Fig. 4-12). Comparing to the intact conditions, complete plantar fascia release resulted in an increase of about 228%, 155% and 72% in tensions of the long plantar (105 N), short plantar (135 N) and spring ligaments (86 N), respectively. These corresponded to maximum strains of 1.6%, 1.1% and 1.8%, respectively. Additional dissection of the long plantar ligaments enhanced the increased total tensions of the short plantar and spring ligaments to 296% and 134%, respectively. Among the four cases of plantar fascia releases, the medial 60% release of fascia produced the largest strains and total tensions of the spring ligament. However, the largest difference in total tensions of the spring ligament between the four cases was only about 10%.

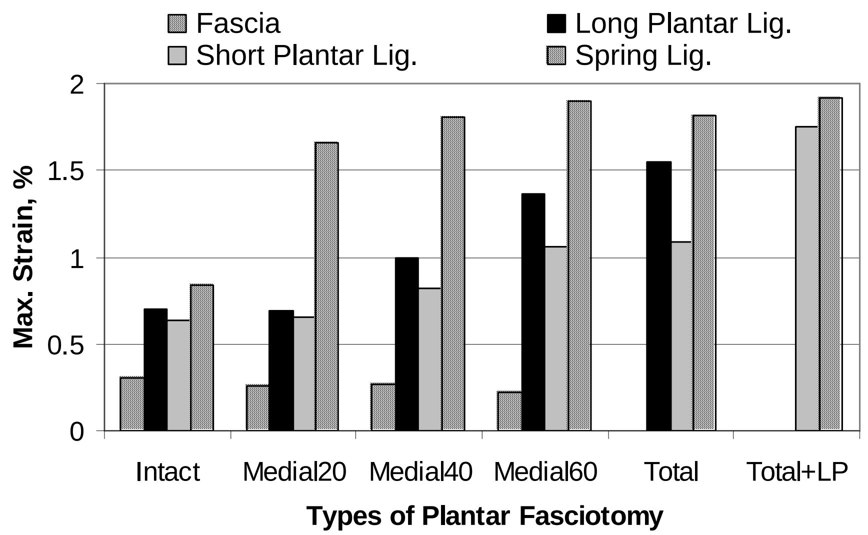


(a)

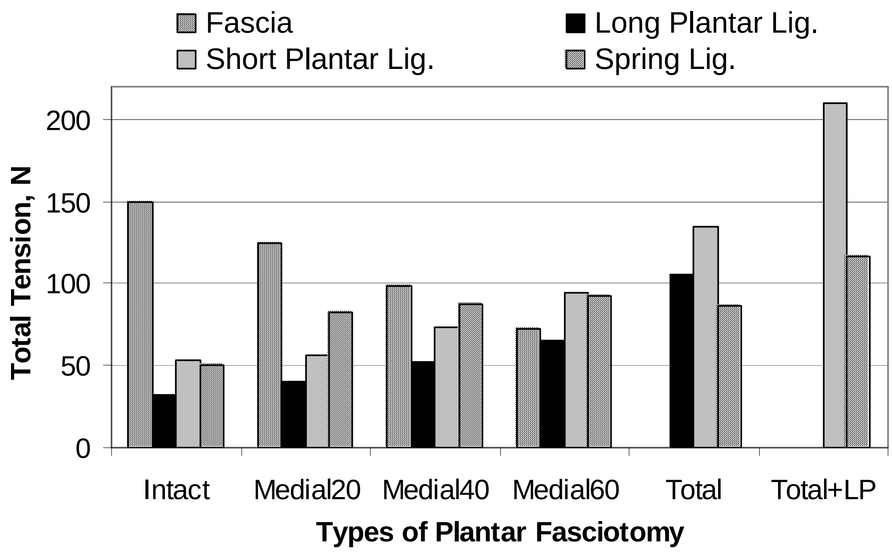


(b)

Figure 4-12. Effects of different types of fasciotomy on changes in (a) maximum strain and (b) total tension of the plantar fascia and the major plantar ligaments during balanced standing.

Among all the simulated cases, peak von Mises stress of about 9 MPa was predicted at the plantar mid-shaft surface of the third metatarsal with medial 40% release of the fascia (Fig. 4-13). With the intact fascia condition, peak von Mises stress of about 4.6 MPa was predicted at the plantar mid-shaft surface of the third metatarsal. With medial 20% release of the plantar fascia, there was an increase in maximum von Mises stress in the plantar mid-shafts of the second and third metatarsals to values of 6.3 MPa and 6.7 MPa, respectively. With the medial 40% release of the fascia, peak von Mises stress at plantar mid-shaft of third metatarsal intensified and a noticeable increase in stress at the dorsal mid-shaft of the second metatarsal were predicted. With medial 60% and complete plantar fascia release, there was a shift of peak metatarsal stress from the third metatarsal to the dorsal mid-shaft of the second metatarsal. The corresponding peak von Mises stresses of about 4.9 MPa and 5.6 MPa, respectively were predicted at the dorsal mid-shaft of second metatarsal. Additional dissection of the long plantar ligament shifted the peak von Mises stresses to the mid-shafts of the fourth (8.1 MPa) and third (5.8 MPa) metatarsals.

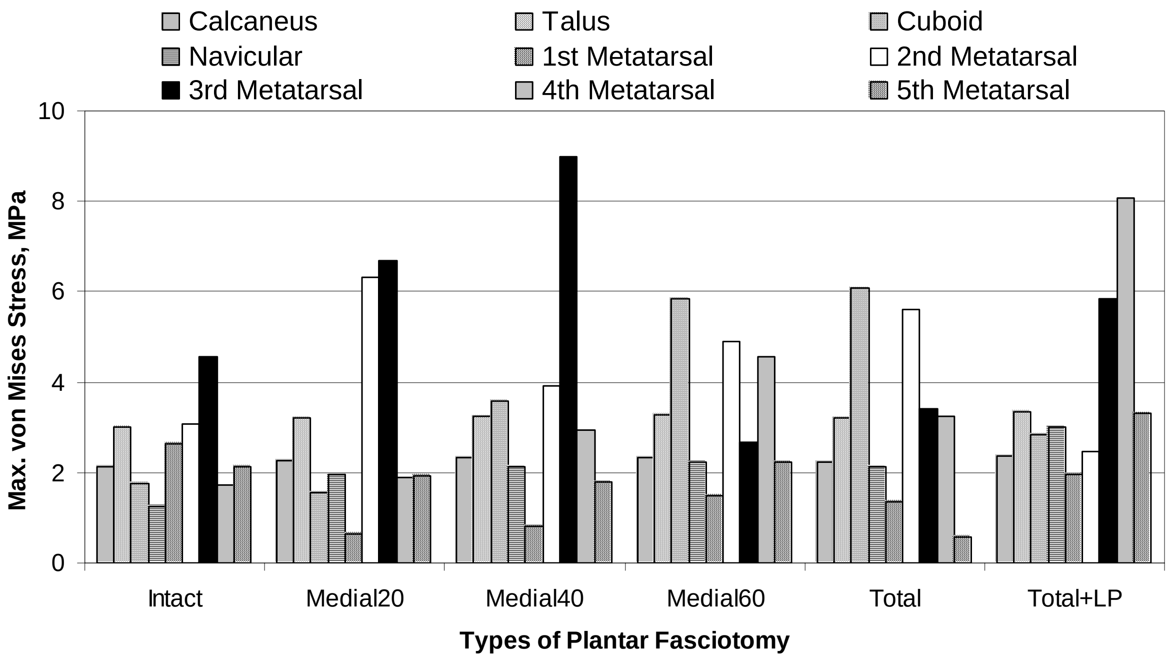


Figure 4-13. Effects of different types of fasciotomy on maximum von Mises stress of the major foot bones during balanced standing.

The changes in maximum von Mises stresses in the calcaneus and talus bone stresses were minimal in all simulated cases of fascia release, having changes of less than 0.4 MPa. With the intact fascia condition, the predicted peak von Mises stress at the calcaneal insertion was 1.84 MPa. It decreased to 1.53 MPa, 1.82 MPa, 1.73 MPa, 0.56 MPa and 0.55 MPa, respectively with partial plantar fascia releases of 20%, 40%, 60% and complete fascia release with and without dissection of the long plantar ligament.

Comparing to the intact fascia condition, there was a shift of peak von Mises stress from the centralized metatarsals to the cuboid bone with medial 60% and complete fascia release. A pronounced increase in cuboid stress to about 5.8 MPa and 6.1 MPa was predicted, respectively. The navicular stress increased with sequential sectioning of the fascia, however, the difference among the four cases of plantar fascia releases was less than 14%. With complete plantar fascia release, the maximum von Mises stresses increased about 246% and 70%, respectively in the cuboid and navicular bones.

In all the simulated cases, the maximum von Mises stress of the calcaneus and talus were located at the posterior junction of the subtalar joint. There was an anterior shift in peak von Mises stress at the calcaneal insertion with complete plantar fascia release. Sectioning of the plantar fascia tended to shift the maximum stresses of the corresponding metatarsals from the plantar mid-shaft to the dorsal mid-shaft and proximal regions. With plantar fascia release, the maximum von Mises stresses of the cuboid and navicular were shifted from the joint junction to the attachment regions of the plantar ligaments.

## 4.4 Effects of Varying Achilles Tendon Loading

In this sensitivity study, the developed FE foot model was employed to quantify the biomechanical effect of varying Achilles tendon loading on the plantar fascia, longitudinal arch deformation and plantar pressure distribution of the standing foot.

*FE predictions and cadaveric foot measurements under pure compression*

The load-deformation curve of the six foot specimens exhibited an increasingly stiffening response under vertical compression (Fig. 4-14a). The FE predictions also characterised a nonlinear load-deformation response, but with a larger magnitude of vertical deformation. The average vertical deformation of the six specimens under a compression force of 700 N was 5.6 mm while the FE model predicted a value of 10.6 mm. The intraclass correlation coefficient (ICC) for evaluating the consistency between the FE predicted and experimentally measured (averged) vertical foot deformation under vertical compression was 0.892.

The plantar fascia experienced increasing strains with the increased vertical compression forces (Fig. 4-14b). The measured strain in the plantar fascia was observed to increase linearly with increasing vertical compression load. Under a compression force of 700 N, an average plantar fascia strain of 1.98% with a range from 0.8 to 3.6% was measured in the cadaveric specimens. The FE model predicted maximum and average strains of 0.97% and 0.61%, respectively in the five rays of plantar fascia segments. The ICC for evaluating the consistency between the FE predicted (FE_Max) and experimentally measured (averged) plantar fascia strain under vertical compression was 0.880. A higher ICC of 0.994 was found when considering only the strain response of the fascia beyond a vertical load of 100 N.

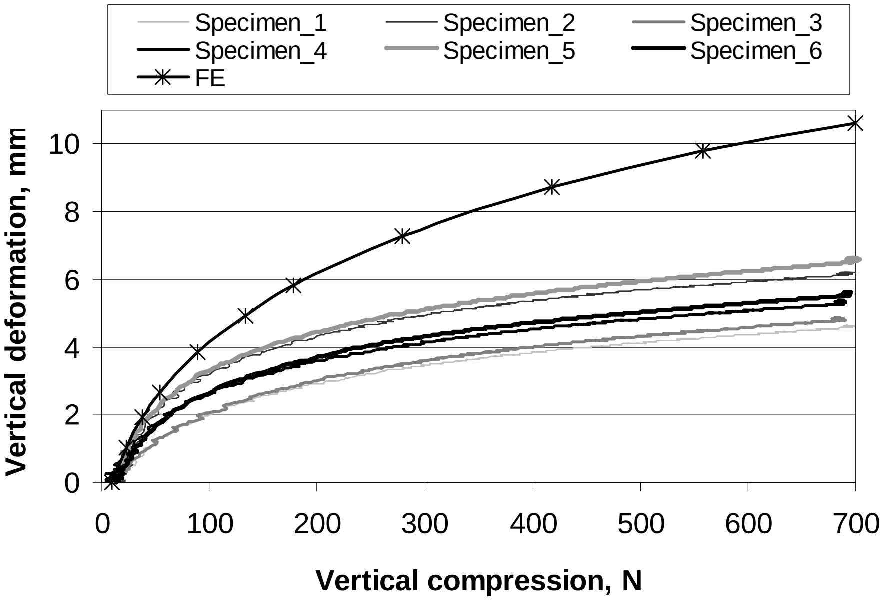


(a)

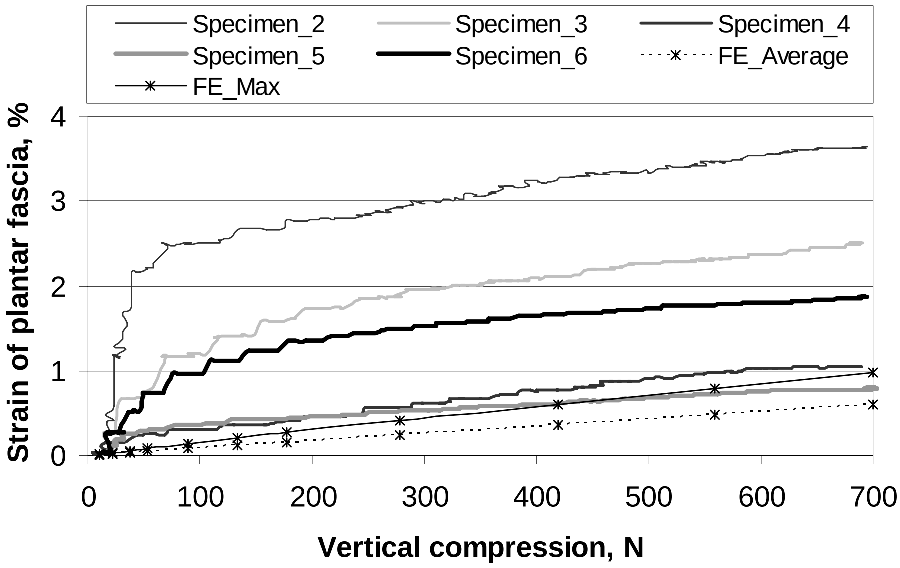


(b)

Figure 4-14. The (a) vertical deformation and (b) plantar fascia strain under vertical compression loading obtained from experimental measurements and FE predictions.

The FE model predicted a larger rearfoot to forefoot load distribution ratio of 4.3 with compression of 700 N, comparing to the average value (3.7) of the F-scan measurements on the cadaveric specimens. Peak plantar pressures of 0.65 MPa and 0.14 MPa were predicted at the heel and metatarsal regions under a vertical compression force of 700 N, which were larger than the average experimental measurements of 0.38 MPa and 0.06 MPa, respectively. Meanwhile, a total contact area of 74.9 $cm^2$ was predicted comparing to an average experimental measurement of 91.5 $cm^2$. Relatively higher peak pressures were predicted comparing to the measured values, which were due probably to the lower resolution of F-scan sensors and the numerical errors resulted from pressure concentration at the contact interface between the foot and support.

### *FE predictions and subject measurements during balanced standing*

With a constant ground reaction force of 350 N, the centre of pressure shifted anteriorly with an increasing Achilles tendon force (Fig. 4-15a). From the FE predictions, the Achilles tendon force required to produce the measured centre of pressure and forefoot to rearfoot force distribution of the standing subject was around 75% of the total weight on the foot. The predicted tendon force might be an overestimation of the actual tendon forces because the reactions of other intrinsic and extrinsic muscles were neglected due to their minimal contributions (Basmajian and Stecko, 1963). With the simulated balanced standing, the FE model predicted a rearfoot to forefoot load distribution ratio of 1.55 and the centre of pressure located at 93 mm anterior and 3 mm lateral to the posterior heel extreme. The F-scan measurements on the standing subject were consistent with the predicted load distribution. Contact areas of 68.8 $cm^2$ were measured comparing to the FE predictions of 68.3 $cm^2$. Peak plantar pressure of about 0.136 MPa and 0.2 MPa at the metatarsals and heel regions were predicted as compared to the F-scan measurements of 0.08 MPa and 0.16 MPa, respectively. The FE model predicted a larger arch deformation (9.9 mm) during simulated balanced standing than the measured value (7.5 mm) of the subject.

### *FE predictions of the effect of Achilles tendon tension on the standing foot*

With the total ground reaction forces maintained at 350 N, an increase in Achilles tendon loading from 0 to 700 N resulted in a general increase in forefoot load-bearing and a decrease in rearfoot load-bearing (Fig. 4-15b). The total force and peak plantar pressure at the forefoot increased about 250% with an Achilles tendon loading of 700N. Meanwhile, there was a lateral and anterior shift of centre of pressure (Fig. 4-15a) with an increasing Achilles tendon loading, which agreed with the reported experimental findings (Kim et al., 2003).

With the total ground reaction forces maintained at 350 N, the total foot deformation reduced with increasing Achilles tendon loading (Fig. 4-15c). However, the arch height decreased until the Achilles tendon loading increased to beyond 1.5 times the weight on the foot (525 N), which tended to lift the heel. Apart from increasing the load on the forefoot, an increase in Achilles tendon loading was found to reduce the calcaneal inclination. The arch height reduced with increasing Achilles tendon loading until the tendon forces were large enough to lift the heel (Fig. 4-15c). The predicted arch-deforming effect of the Achilles tendon was consistent with the experimental findings by Thordarson et al. (1995) who measured an increased arch flattening of the vertically loaded cadaveric feet after additional pulling of the Achilles tendon.

The strain and tension of the plantar fascia increased with either the increase of vertical compression alone or the tension of the Achilles tendon (Fig. 4-16). The Achilles tendon loading were found to produce a greater straining effect on the plantar fascia. With the total ground reaction forces maintained at 350 N, an increase in Achilles tendon loading of 350 N resulted in an increased of about 120 N in fascia tension while a further increase of pure compression (from 350 N to 700 N) produced a fascia tension increase of only 60 N.

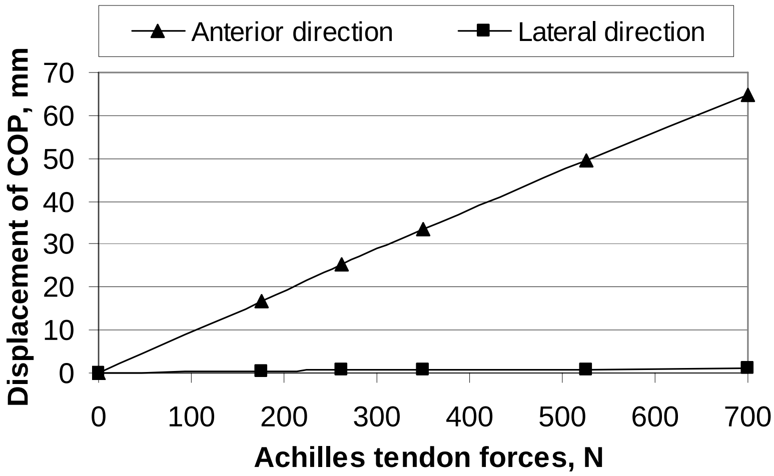


(a)

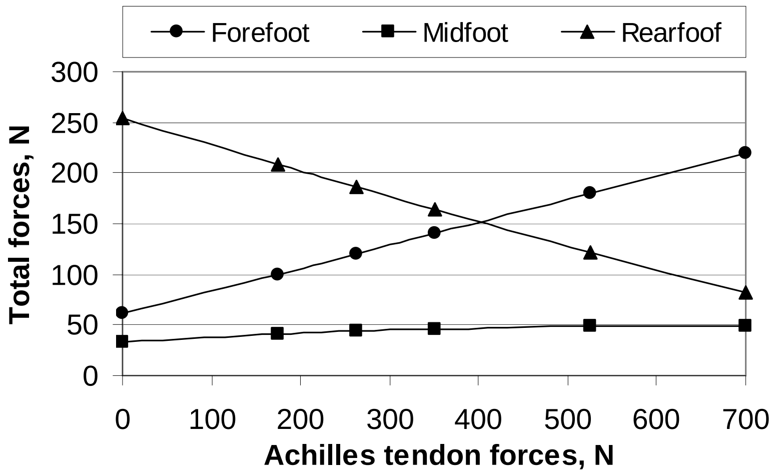


(b)

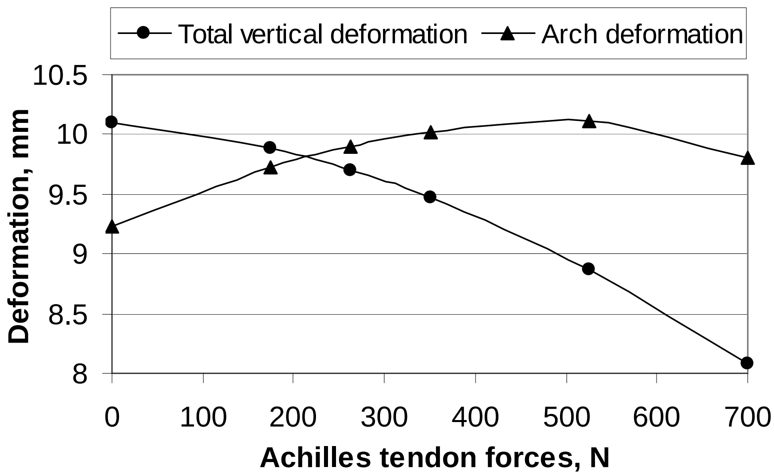


(c)

Figure 4-15. The effects of Achilles tendon loading on the predicted (a) displacement of centre of pressure (COP), (b) load distribution of the plantar foot and (c) vertical and arch deformation of the standing foot under compression preload of 350 N.

Among the five rays of plantar fascia, the first ray segment sustained the largest strain and loading in all simulated cases. There was a general decrease in the load-bearing from the medial to the lateral segments. During simulated balanced standing, the five rays of plantar fascia sustained about 28.2%, 18.9%, 19.8%, 16.6% and 16.5% of the total fascia tension, respectively from the medial first segment to the fifth lateral segment. From Figure 4-16a, a linear force relationship to approximate the total tension of the plantar fascia ($F_f$) during weightbearing can be established with

$$F_f = 0.1762F_w + 0.3285F_a \quad (4\text{-}2)$$

where $F_w$ is the total weight on the foot and $F_a$ is the tension of the Achilles tendon.

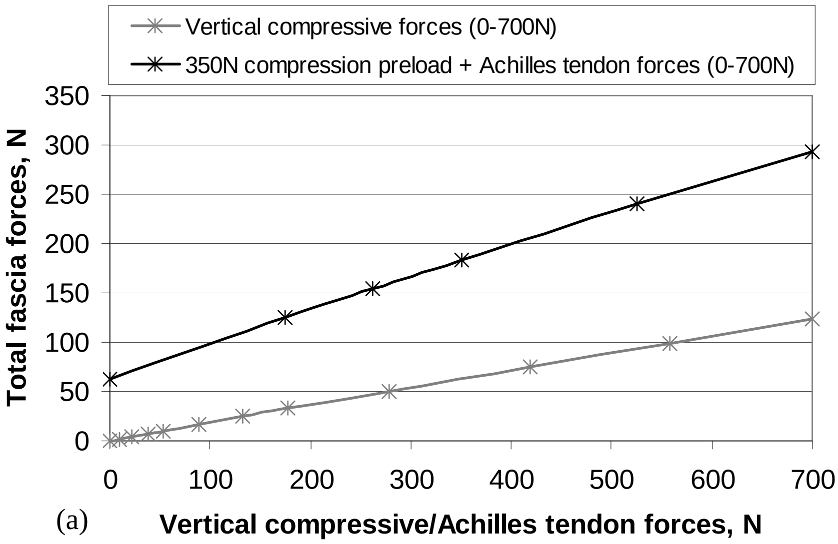

(a)

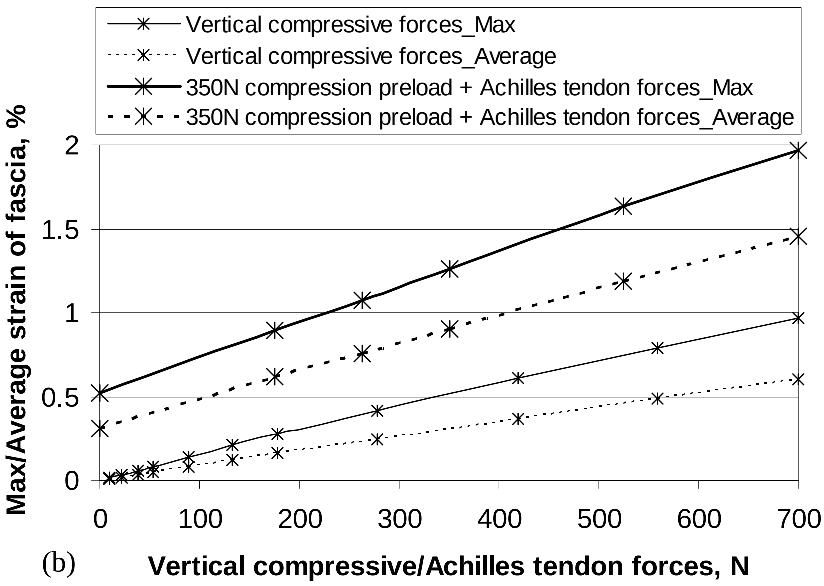

(b)

Figure 4-16. The effects of Achilles tendon loading on the predicted (a) tension and (b) strain of the plantar fascia of the standing foot under compression preload of 350 N.

## *4.5. Effects of Posterior Tibial Tendon Dysfunction*

In this sensitivity study, the developed 3D FE model of the human foot and ankle was employed to quantify the biomechanical effect of PTTD on the intact foot and with fasciotomy. The predicted arch deformation, plantar pressure, strain/tension of the plantar fascia and ligaments, and von Mises stress of the bones were compared during simulated late midstance. Figure 4-17 shows the F-scan measurement of the cadaveric foot simulation and FE predicted plantar pressure distribution during four simulated late midstance conditions, namely intact, PTTD, plantar fascia release (PFR) and PFR with PTTD. For intact condition, peak plantar pressure of about 0.447 MPa, 0.082 MPa and 0.144 MPa at the metatarsals, midfoot and heel regions were predicted as compared to the average F-scan measurements of 0.167 MPa (SD: 0.066 MPa), 0.075 MPa (SD: 0.024 MPa), and 0.080 MPa (SD: 0.045 MPa), respectively. Among the six foot specimens, peak plantar foot pressure was located beneath either the first, second or fifth metatarsal head during simulated midstance. The FE model predicted peak plantar pressure beneath the second metatarsal head region for the intact, PTTD and PFR conditions. The FE predicted peak plantar pressure shifted to the third metatarsal head region with simulated PFR with PTTD.

With PFR or PTTD, a medial shift of plantar pressure at the metatarsal region was measured in the cadaveric specimens and fasciotomy consistently produced a more pronounced effect. Posterior tibial tendon dysfunction resulted in a decrease in total contact forces of the plantar foot in the cadaveric experiments. From the FE predictions, unloading the PTT in both the intact and PFR conditions resulted in a decrease in peak plantar pressure at the second metatarsal head region while a slight increase in peak plantar pressure was predicted in the rest of the metatarsal head regions (Fig. 4-18). The FE model predicted an increase in peak plantar pressure of the midfoot and a decrease in the rearfoot region with PFR.

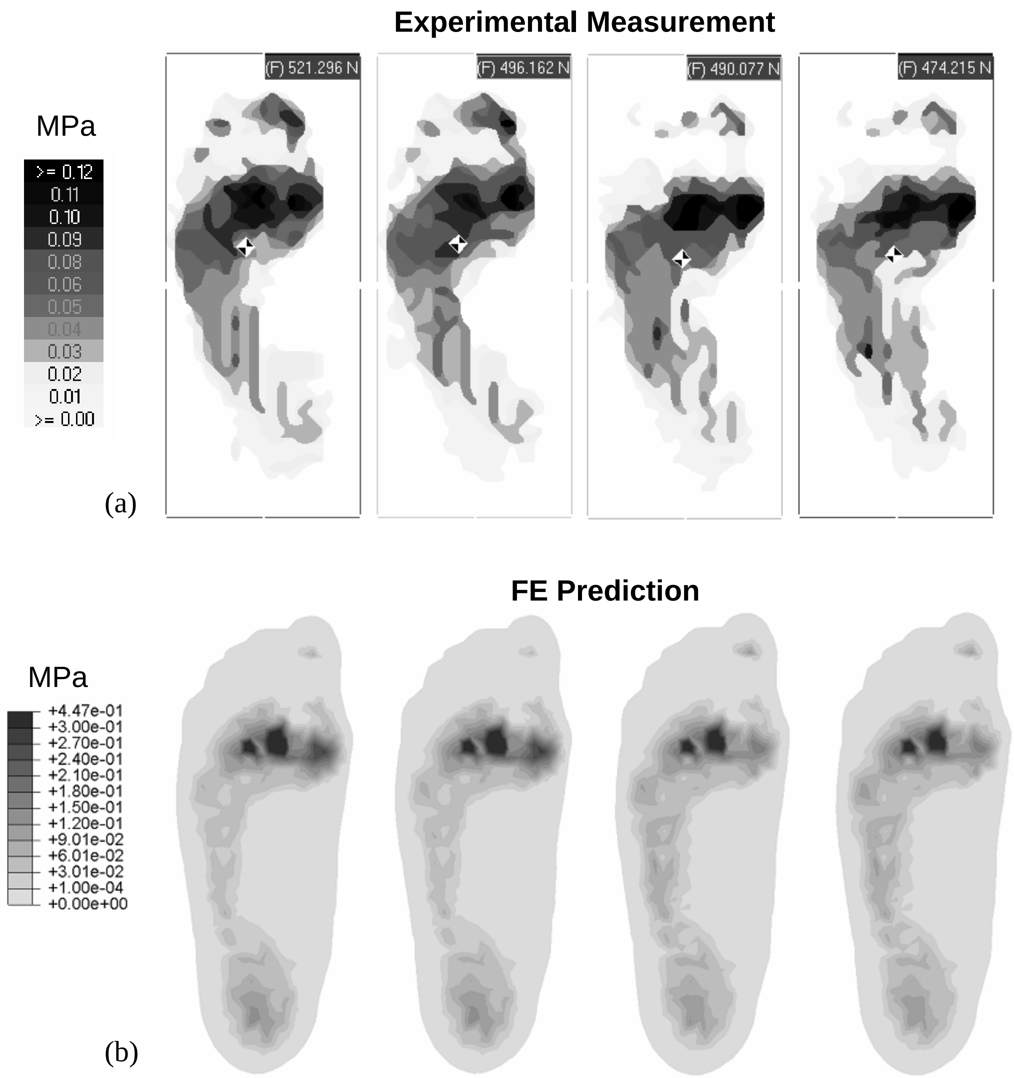


Figure 4-17. The (a) F-scan measured and (b) FE predicted plantar pressure distribution during four simulated late midstance conditions, namely intact, posterior tibial tendon dysfunction (PTTD), plantar fascia release (PFR) and plantar fascia release with posterior tibial tendon dysfunction (PFR + PTTD).

From the cadaveric and FE simulations (Fig. 4-17), PFR was found to increase and decrease the contact area of the midfoot and heel regions, respectively while PTTD produced negligible effect. Comparing to the intact condition, the FE model predicted an 8.86% increase in contact area between the foot-ground interface with PFR (Fig. 4-19a). The FE predicted arch height, defined as the height of the medial navicular cortex to the ground support was found to decrease with either PFR and PTTD (Fig. 4-19b). Comparing to the intact condition, the FE model predicted 1.88% and 5.63% decreases in arch height with PTTD and PFR. Unloading the PTT in addition to simulated PFR further decreased the arch height by 2.24% to a total decrease of 7.75% comparing to the intact condition (Fig. 4-19b).

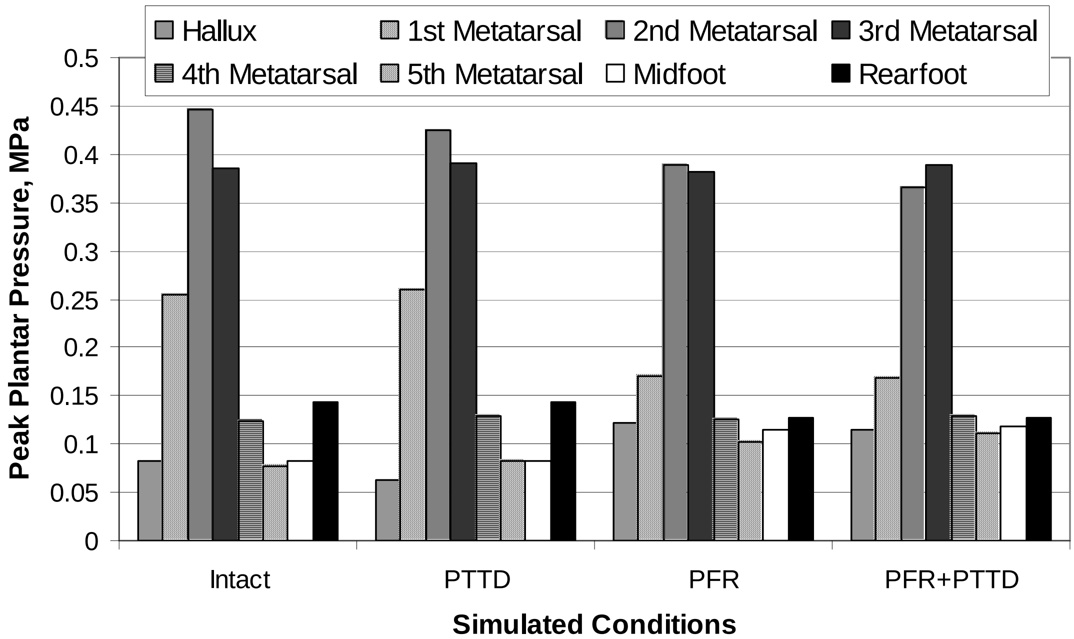


Figure 4-18. Effects of plantar fascia release (PFR) and posterior tibial tendon dysfunction (PTTD) on the peak plantar pressure during simulated midstance.

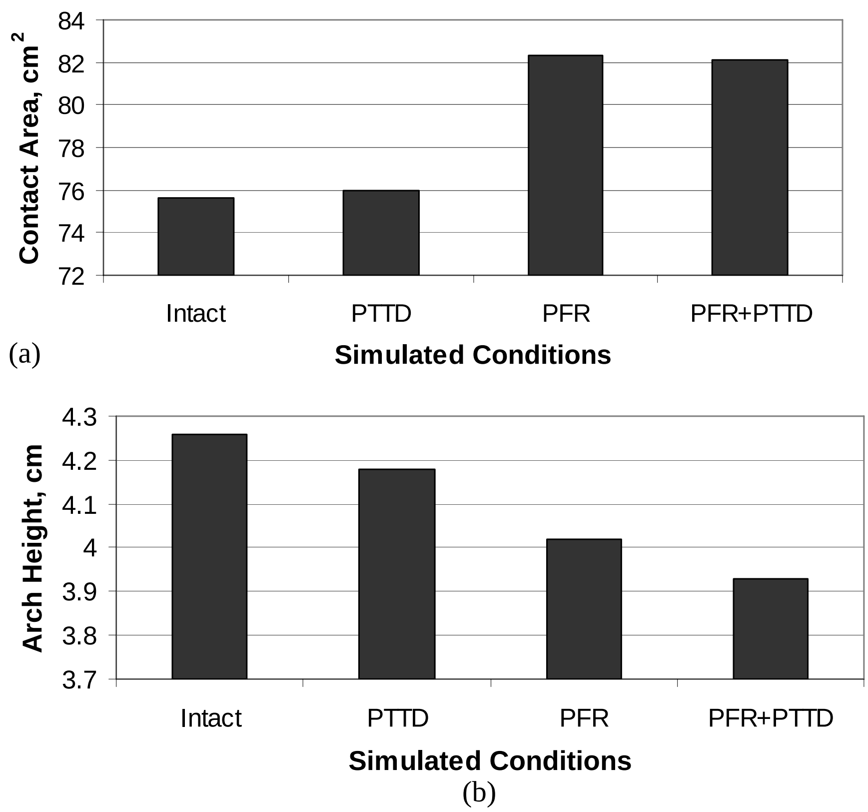


Figure 4-19. Effects of plantar fascia release (PFR) and posterior tibial tendon dysfunction (PTTD) on the predicted (a) contact area and (b) arch height during simulated midstance.

With PTTD, the strain of the plantar fascia was found to increase by 6.7% and 2.4% (SD: 4.7%) from the cadaveric measurements and FE predictions, respectively (Fig. 4-20). In the intact condition, the FE predicted total tension (330.2 N) of the plantar fascia during simulated midstance was about 59.2% of the total weight on the foot (Fig. 4-21). With PTTD, the tension of the plantar fascia and the spring ligament increased about 5.6% and 3.4% while slight decreases in tension of about 1.1% and 2.4% were predicted for the long and short plantar ligaments.

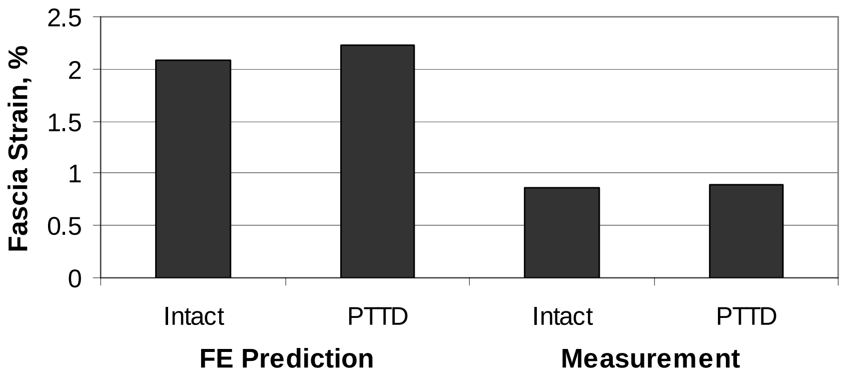


Figure 4-20. Effects of posterior tibial tendon dysfunction (PTTD) on the FE predicted and measured plantar fascia strain during simulated midstance.

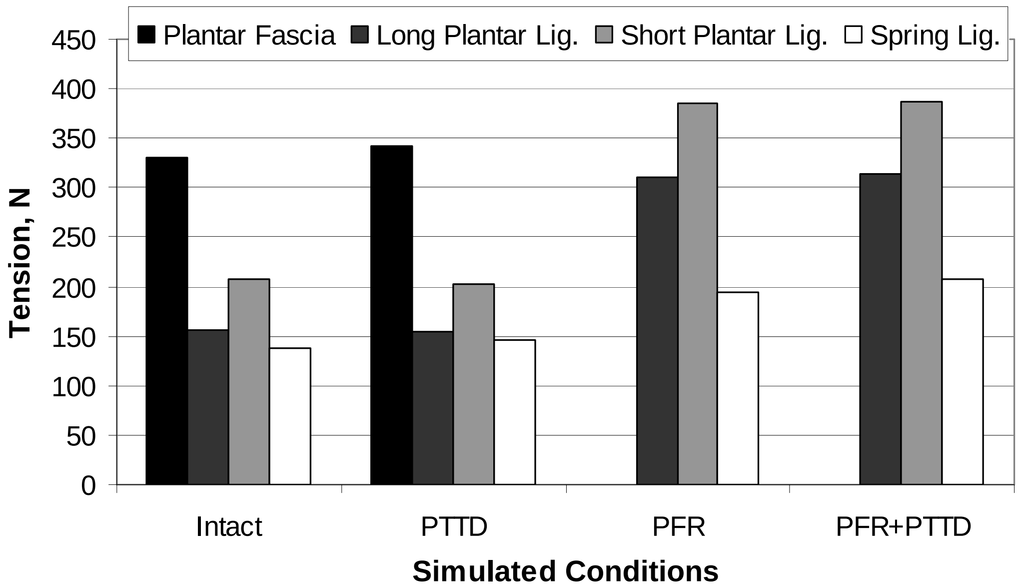


Figure 4-21. Effects of plantar fascia release (PFR) and posterior tibial tendon dysfunction (PTTD) on the total tension of the plantar fascia and the major plantar ligaments during simulated midstance.

The predicted increase in strain of the spring ligament with PTTD was larger than the experimental measurement (1.82%) by Hansen et al. (2001). Comparing to the intact condition, the tension of the spring, long and short plantar ligaments increased about 40%, 98.7% and 86.9%, respectively with PFR (Fig. 4-21). Unloading the PTT in addition to PFR further enhanced the tension of the spring ligament by 7.3% while less than 1% increase was predicted for the long and short plantar ligaments. Unlike PFR which resulted in a larger increase in the long and short plantar ligaments, PTTD induced a larger straining effect on the spring ligament.

The effect of PTTD and PFR during simulated midstance on the change in 3D rotation was shown in Table 4-2. With PTTD, the FE predicted talotibial (Talus to Tibia) rotations were $0.161^0$ in plantar flexion, $0.072^0$ in eversion and $0.016^0$ in external rotation. The corresponding average measurements on the cadaveric foot were $1.875^0$ in plantar flexion, $0.718^0$ in eversion and $0.02^0$ in internal rotation. The FE predicted calcaneotalar (Calcaneus to Talus) rotations were $0.043^0$ in dorsiflexion, $0.219^0$ in eversion and $0.199^0$ in external rotation. The corresponding average measurements on the cadaveric foot were $1.543^0$ in dorsiflexion, $0.155^0$ in eversion and $1.722^0$ in internal rotation. For the talonavicular joint (Navicular to Talus), the FE predicted rotations were $0.329^0$ in dorsiflexion, $0.961^0$ in eversion and $0.511^0$ in external rotation. The corresponding average measurements on the cadaveric foot were $0.008^0$ in plantarflexion, $0.205^0$ in inversion and $0.048^0$ in external rotation. For the metatarsonavicular joint, the FE predicted (1$^{st}$ Metatarsal to Navicular) rotations were $0.272^0$ in plantarflexion, $0.413^0$ in inversion and $0.555^0$ in internal rotation. The corresponding average measurements on the cadaveric foot were $0.617^0$ in dorsiflexion, $0.132^0$ in eversion and $0.765^0$ in external rotation. The FE predicted metatarsotalar (1$^{st}$ Metatarsal to talus) rotations were $0.422^0$ in dorsiflexion, $0.416^0$ in eversion and $0.071^0$ in external rotation. The corresponding average measurements on the cadaveric foot were $0.608^0$ in dorsiflexion, $0.073^0$ in inversion and $0.813^0$ in external rotation.

Table 4-2. Effects of posterior tibial tendon dysfunction (PTTD) and plantar fascia release (PFR) on the joint motion during simulated midstance.

| | | **FE (degree)** | | | **Mean Experiment (degree)** | | |
|---|---|---|---|---|---|---|---|
| **Relative Bones** | **Relative Conditions** | **Dorsi-flexion** | **Eversion** | **Internal Rotation** | **Dorsi-flexion** | **Eversion** | **Internal Rotation** |
| Talus to Tibia | PTTD / Intact | -0.161 | 0.072 | -0.016 | -1.875 (5.818) | 0.718 (1.477) | 0.020 (1.243) |
| | PFR / Intact | -1.506 | 0.061 | -0.007 | -1.62 (3.222) | 1.572 (2.262) | 2.123 (2.013) |
| | PFR+PTTD / PFR | -0.574 | 0.285 | 0.172 | -1.348 (2.449) | 2.145 (4.806) | -2.253 (4.176) |
| | | | | | | | |
| Calcaneus to Talus | PTTD / Intact | 0.043 | 0.219 | -0.199 | 1.527 (6.788) | 0.155 (1.989) | 1.702 (4.152) |
| | PFR / Intact | -0.182 | 0.9163 | -0.307 | -0.790 (2.312) | 0.108 (3.274) | -0.427 (3.009) |
| | PFR+PTTD / PFR | 0.091 | -0.384 | -0.247 | 1.405 (4.432) | -2.932 (6.257) | 2.378 (3.637) |
| | | | | | | | |
| Navicular to Talus | PTTD / Intact | 0.329 | 0.961 | -0.511 | -0.032 (4.222) | -0.205 (1.405) | -0.462 (1.449) |
| | PFR / Intact | 0.178 | 1.201 | -0.992 | -0.765 (2.660) | -0.228 (1.925) | -1.037 (1.932) |
| | PFR+PTTD / PFR | 0.511 | -1.265 | -0.935 | 1.060 (2.076) | -1.947 (4.749) | 1.745 (2.567) |
| | | | | | | | |
| 1st Metatarsal to navicular | PTTD / Intact | -0.272 | -0.413 | 0.555 | 0.243 (1.380) | 0.132 (2.000) | -0.505 (1.545) |
| | PFR / Intact | 3.075 | -4.118 | -0.453 | 2.765 (3.182) | -2.422 (2.215) | 1.440 (1.068) |
| | PFR+PTTD / PFR | 0.247 | -0.957 | 0.405 | -0.445 (2.097) | 0.338 (0.919) | -0.775 (1.151) |
| | | | | | | | |
| 1st Metatarsal to Talus | PTTD / Intact | 0.422 | 0.416 | -0.071 | 0.212 (3.995) | -0.073 (2.024) | -0.967 (1.712) |
| | PFR / Intact | 5.156 | -1.086 | 0.390 | 2.000 (2.551) | -2.650 (2.652) | 0.403 (1.251) |
| | PFR+PTTD / PFR | 1.496 | 0.518 | -0.211 | 0.615 (2.823) | -1.608 (5.346) | 0.970 (3.102) |

Values in ( ) are standard deviations for the experimental measurements

Because of the scattered experimental measurements in cadaveric specimens and a qualitative comparison was done to compare directional changes of the FE predicted and experimentally measured 3D joint motions. The overall percentages of agreement of the directional changes of joint motion were 67% (Talus to Tibia), 78% (Calcaneus to Talus), 44% (Navicular to Talus), 22% (1st Metatarsal to navicular), 56% (1st Metatarsal to Talus), respectively at the five designated joints. The percentages of agreement of the directional changes of joint motion in the sagittal, coronal, transverse planes were 73%, 60% and 27%, respectively. Although there were large variations between the FE predicted and experimentally measured joint rotations, unloading the PTT of intact foot in general resulted in plantarflexed and everted talotibial joint, dorsiflexed and everted calcaneotalar joint, dorsiflexed metatarsotalar joint.

Among all the simulated cases, peak von Mises stresses were predicted at the lateral region of the talar dome surface (Fig. 4-22). Peak von Mises stresses of 21.7, 22.3, 20.9 and 21.2 MPa were predicted for intact, PTTD, PFR and PFR with PTTD conditions, respectively (Fig. 4-23). With, PFR, the cuboid and navicular sustained an increased stress of 18% and 48%, respectively. Except the second metatarsal, all the metatarsal bones were found to sustain an increased stress up to 160% at the second metatarsal with PFR. Comparing to the effect of PFR, the effect of PTTD on the stress distribution of the foot bones was minimal. Except with a 20% increase in maximum von Mises stress of the navicular at the medial talonavicular joint junction with PTTD conditions in addition to PFR, the effect of PTTD on the stress distribution of the foot bones was negligible or less than 5%.

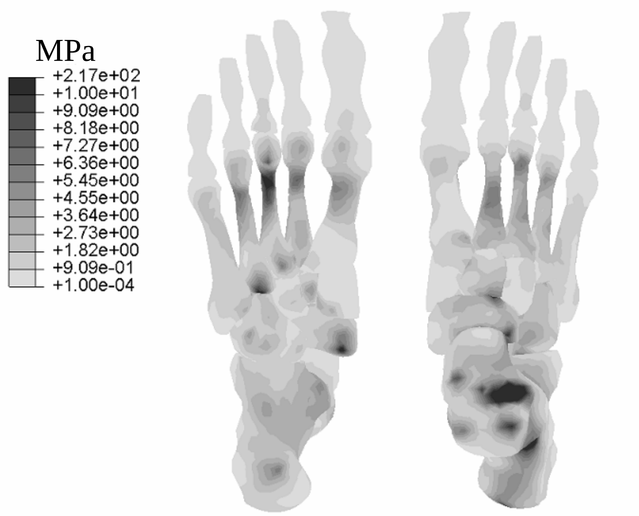


Figure 4-22. Von Mises stress distribution of the foot bones during simulated midstance for the intact condition.

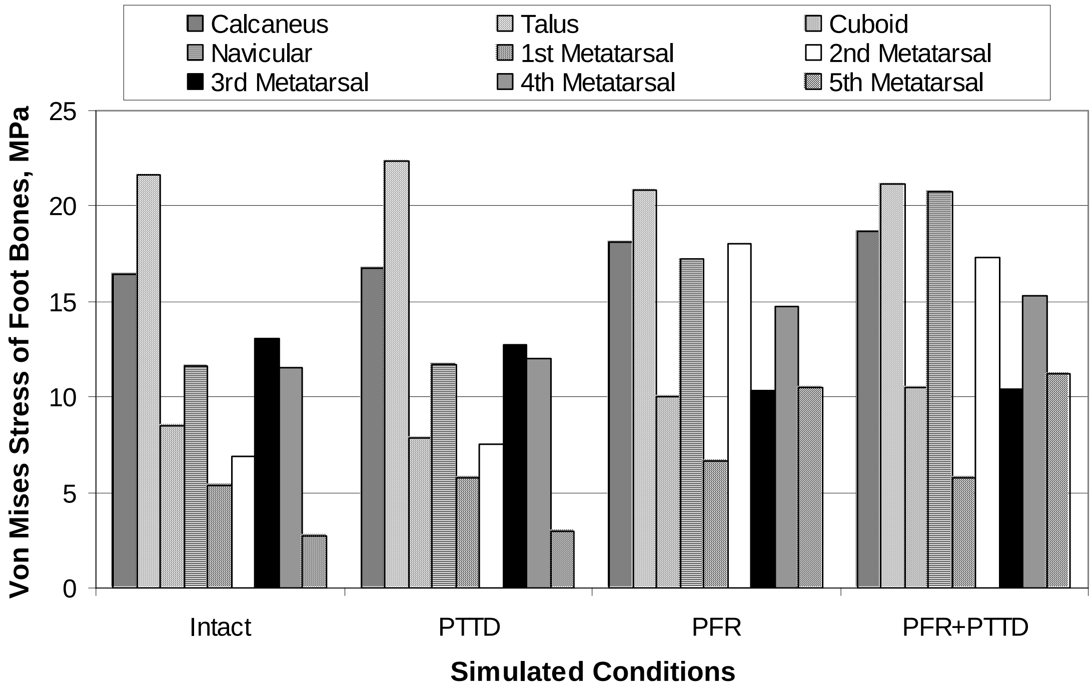


Figure 4-23. Effects of plantar fascia release (PFR) and posterior tibial tendon dysfunction (PTTD) on the maximum von Mises stress of the major foot bones during simulated midstance.

## *4.6. Effects of Foot Orthoses*

### 4.6.1 Effects of Foot Orthosis on the Loading Response of the Foot

In this preliminary analysis, the ability of the developed 3D FE model of the human foot and ankle to quantify the effect of different foot orthoses on the biomechanical foot responses was investigated. The FE model of the human foot and ankle and a preliminary foot orthosis model were used to study the effects that stiffness and shape of foot insole have on plantar pressure distribution, and to study the internal stresses in the bones during balanced standing. Figure 4-24 depicts the plantar pressure distribution obtained from the F-scan measurements and Figure 4-25 gives the pressure distribution predicted by FE simulation during balanced standing. Both the measured and predicted values showed high pressures around the soft tissue beneath the calcaneus and the metatarsal heads, especially the second metatarsal head (Figs. 4-24, 4-25). The model predicted a peak pressure of 0.266 and 0.194 MPa at the heel and metatarsal region, respectively, with a flat, rigid (E = 1000 MPa) insole. With a flat, soft (E = 0.3 MPa) insole, the peak pressures were 0.214 and 0.162 MPa, respectively. The corresponding peak pressure measured with the F-scan sensors were 0.14 and 0.09 MPa with the polypropylene platform and 0.13 and 0.07 MPa with the PPT platform.

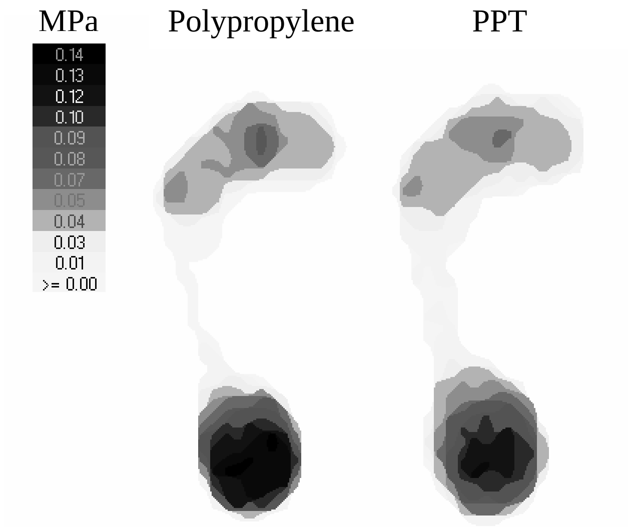


Figure 4-24. The pressure distribution from F-scan measurements during barefoot standing on 5 mm of polypropylene and PPT flat support.

Figure 4-25 shows the predicted plantar pressure patterns with flat and custom-molded insoles of different Young modulus ratings of 0.3, 1.0, and 1000 MPa. Under the same loading condition, use of a custom-molded and a softer insole would reduce the peak plantar pressure and increase the contact area between the plantar foot and the insole. The efficiency of specific insoles in redistributing the plantar foot pressure can be further seen in Figure 4-26.

Figure 4-26 displays 3 features: (1) the effects of stiffness of the flat and custom-molded insoles on the peak pressure (Fig. 4-26a), (2) effects on the contact area between the plantar foot and the insoles (Fig. 4-26b), and (3) the von Mises stress distribution in the bony structures (Fig. 4-26c). During balanced standing, the heel region experienced the highest plantar pressure. Compared with a flat, rigid (E = 1000 MPa) insole, reductions of about 16.5% and 19.5% in peak plantar pressure over the metatarsal and heel regions were predicted with the use of a flat and soft (E = 0.3 MPa) insole. Use of the custom-molded insole had a pronounced effect on pressure reduction. The custom-molded, rigid insole reduced the peak plantar pressure by about 23.2% and 24.4% over the metatarsal and heel regions, respectively. The soft custom-molded insoles provided pressure reduction of 40.7% and 31.6%, respectively. The rigid and soft custom-molded insoles enabled increases of peak plantar pressures of about 68.8% and 22.2% in the midfoot, respectively, compared with the use of a flat, rigid insole.

The contact area between the plantar foot and the insole increased with use of the custom-molded insole (Fig. 4-26b). This increase mainly resulted from the increase over the midfoot contact. Compared with a flat, rigid insole, in the custom-molded insoles the contact area of the plantar foot increased by 51.5% for rigid and 59.7% for soft orthotics. A 13.5% increase in contact area was noted with a softer insole, but the effect was less pronounced than that found with custom-molded insoles.

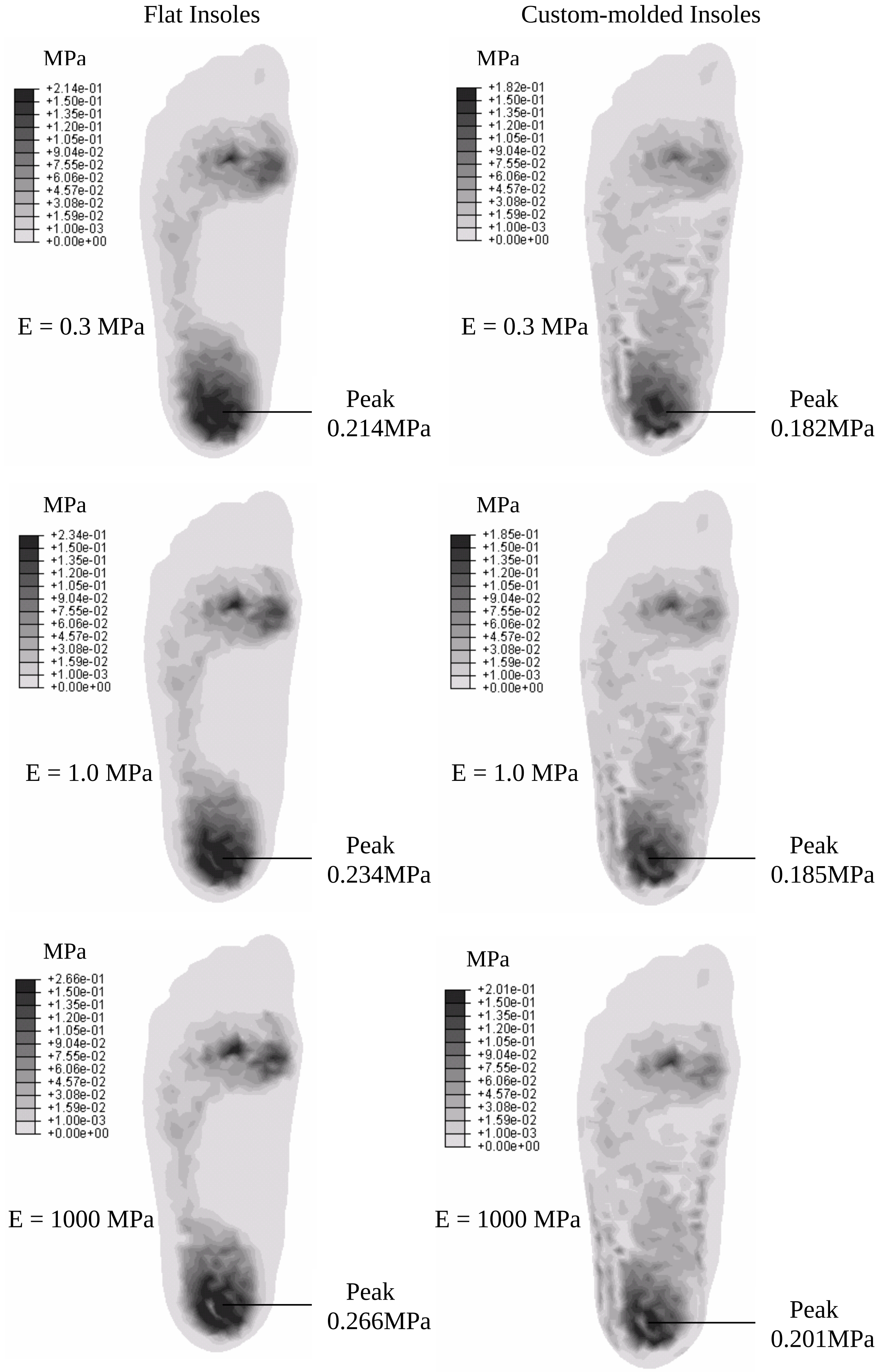


Figure 4-25. The FE predicted plantar pressure distributions supported by a flat or custom-molded insole with different material stiffness.

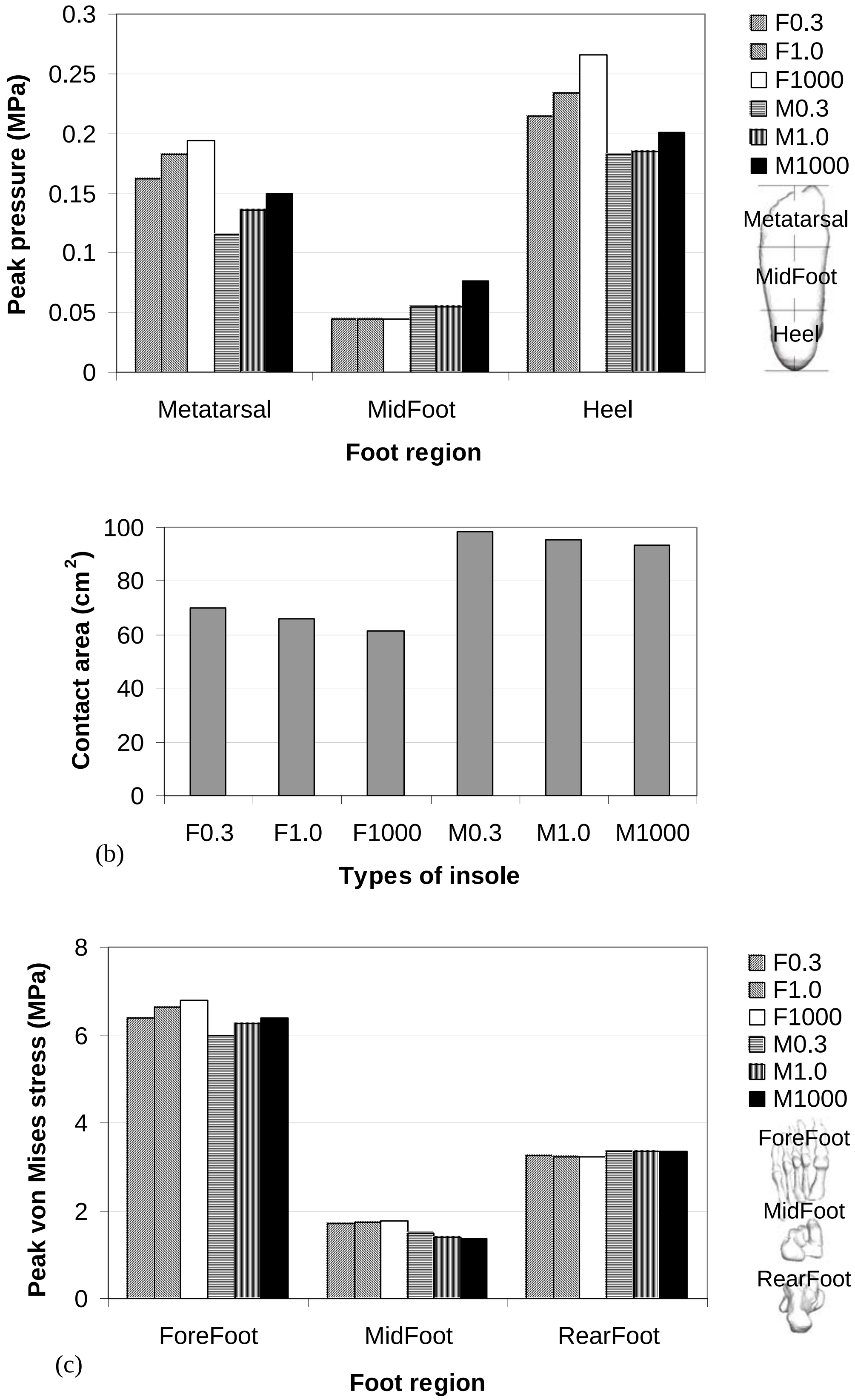


Figure 4-26. Effects of stiffness of flat and custom-molded insoles on (a) peak plantar pressure, (b) contact area between the plantar foot and the insoles, and (c) peak von Mises stress in the bony structures. The key indicates insole type (F, flat; M, custom-molded) and rigidity (0.3, soft; 1.0, firmer; 1000, rigid).

During balanced standing, the highest von Mises stress in the bony structures was predicted to occur in the forefoot region in all the cases calculated (Fig. 4-26c). Over the forefoot, relatively high von Mises stresses were predicted at the midshaft of the second and third metatarsals. The calcaneocuboid joints and the posterior articulation of the subtalar joint sustained relatively large stresses in the midfoot and rearfoot regions, respectively. In general, use of the softer and custom-molded insole reduced the stress on the bony structures. The stress reduction was more pronounced in the forefoot and midfoot and with use of the custom-molded insoles (Fig. 4-26c). Compared with the flat, rigid insole, the forefoot experienced a 5.6% and 11.7% peak stress reduction with use of soft, flat and soft, custom-molded insoles, respectively. The corresponding decreases in the midfoot were 3.4% and 16.8%. Interestingly, the rearfoot experienced a small increase in peak von Mises stress with use of softer insoles.

During balanced standing, we found that the plantar fascia sustained a maximum strain of about 0.49% and 0.37%, respectively, with use of flat insoles and custom-molded, rigid insoles. Use of softer material had a negligible effect on strain of the plantar fascia.

### 4.6.2 Parametrical Analysis on Pressure Relieving Foot Orthoses

In this parametrical analysis, the sensitivity of five design factors of pressure-relieving foot orthosis, namely arch type, insole stiffness, midsole stiffness, insole thickness and midsole thickness were investigated using the developed FE model of the human foot and foot support. Figure 4-27 depicts the foot-support interaction during simulated midstance and the deformed plot of the soft tissue and bony structure, showing the deformed medial longitudinal arch of the foot during weightbearing.

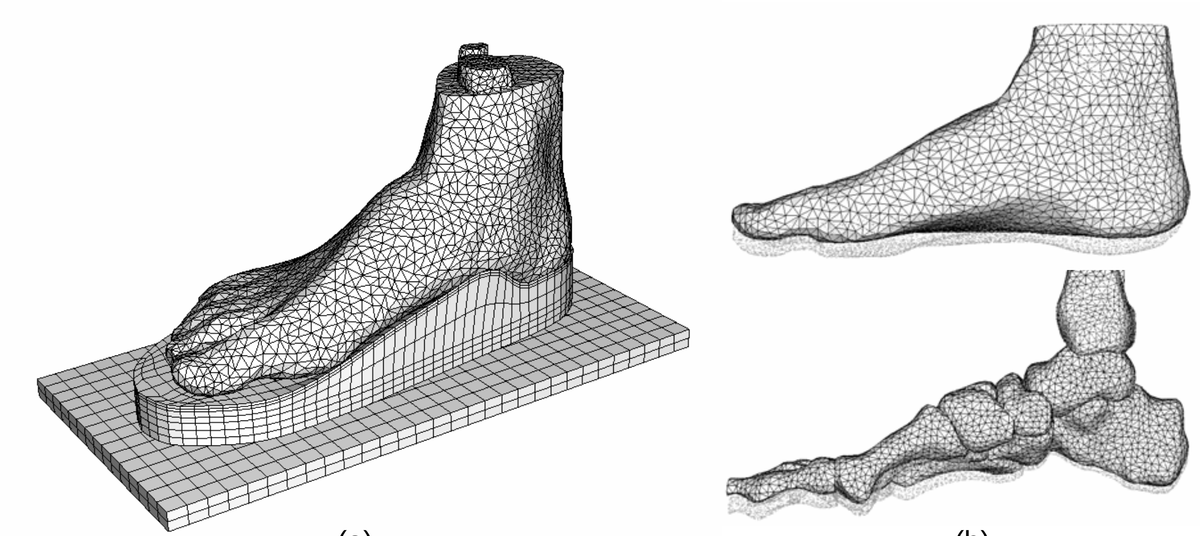

(a) (b)

Figure 4-27. The (a) foot-support interaction during simulated midstance and the (b) deformed plot of the soft tissue and bony structures during simulated midstance. Note: dotted lines represented unformed plot.

Figure 4-28 shows the typical FE predicted and F-scan measured plantar pressure distributions during simulated midstance. A pronounced increase in contact area especially at the midfoot was predicted with the use of an arch-supporting foot orthosis. From the F-scan measurement, it was found that the sensitivity of the F-scan system was too low to be able to pick up the signal of the low-pressure region at the midfoot especially with the use of arch-supporting foot orthosis. In additional, the inability of the material of the F-scan sensor to comform with the highly curved surface contour of the foot orthosis further affected the accuracy of the pressure measurements. Among all the simulated conditions, the highest plantar pressure was predicted at the forefoot, followed by the rearfoot and midfoot. Peak plantar pressure of the forefoot was found consistently beneath the second metatarsal head while peak plantar pressure of the rearfoot was found at the central heel region. For the midfoot, peak plantar pressure was predicted at the lateral midfoot. The predicted region of peak plantar pressure was consistent with the F-scan measurement of the subject.

The FE predicted peak plantar pressures with the 16 different orthotic configurations are tabulated in Table 4-3. The FE model predicted a pronounced decrease in peak plantar pressure at the forefoot and midfoot region with the use of an orthosis. The use of a softer insole material and an arch-supporting foot orthosis was found to be effective in the reduction of peak plantar pressure with the latter had a larger reducing effect.

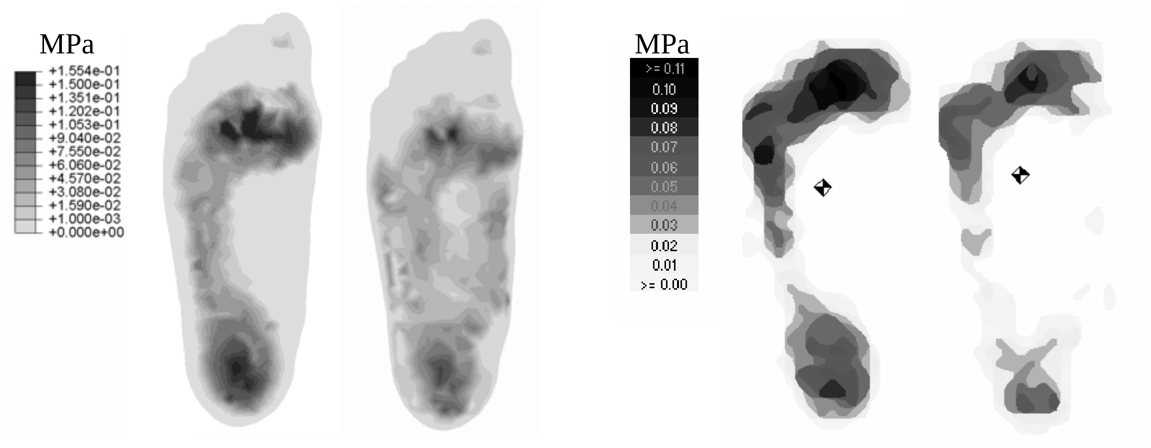


Flat Arch supported Flat Arch supported

(a) (b)

Figure 4-28. The typical (a) FE predicted and (c) F-scan measured plantar pressure distributions during midstance.

The mean effect of each design factor at each of the four levels can be found in Figure 4-29. The use of a foot orthosis was found to reduce the peak plantar pressure with the largest effect on the forefoot, followed by the rearfoot and a less obvious effect on the midfoot. In general, the use of a higher arch-support and softer and thicker material was found to have an increasing magnitude of peak pressure reduction. The degree of importance for each design factor can be further identified by comparing the sum of squares of predicted plantar pressure shown in Table 4-4 (Phadke MS, 1989).

Table 4-3. The FE predicted peak plantar pressure with different configurations of foot orthosis

| Trial number | FE predicted plantar pressure, MPa | | |
|---|---|---|---|
| | Forefoot | Midfoot | Rearfoot |
| 1 | 0.214 | 0.088 | 0.145 |
| 2 | 0.216 | 0.088 | 0.148 |
| 3 | 0.235 | 0.087 | 0.165 |
| 4 | 0.240 | 0.087 | 0.169 |
| | | | |
| 5 | 0.195 | 0.07 | 0.147 |
| 6 | 0.194 | 0.07 | 0.146 |
| 7 | 0.122 | 0.071 | 0.102 |
| 8 | 0.141 | 0.074 | 0.112 |
| | | | |
| 9 | 0.180 | 0.07 | 0.141 |
| 10 | 0.164 | 0.073 | 0.129 |
| 11 | 0.149 | 0.069 | 0.122 |
| 12 | 0.121 | 0.068 | 0.104 |
| | | | |
| 13 | 0.155 | 0.076 | 0.118 |
| 14 | 0.132 | 0.074 | 0.109 |
| 15 | 0.165 | 0.080 | 0.125 |
| 16 | 0.157 | 0.077 | 0.120 |

Among the five design factors, the use of an arch-supporting foot orthosis was found to be the most important design factor for peak plantar pressure reduction. The insole stiffness was found to be the second most important factor for peak pressure reduction. The rest of the design factors contributed to a much lesser extent in peak pressure reduction with a descending order from insole thickness, midsole stiffness and midsole thickness. The use of different combination of stiffness and material of the foot orthosis was insensitive to the change in peak plantar pressure of the midfoot.

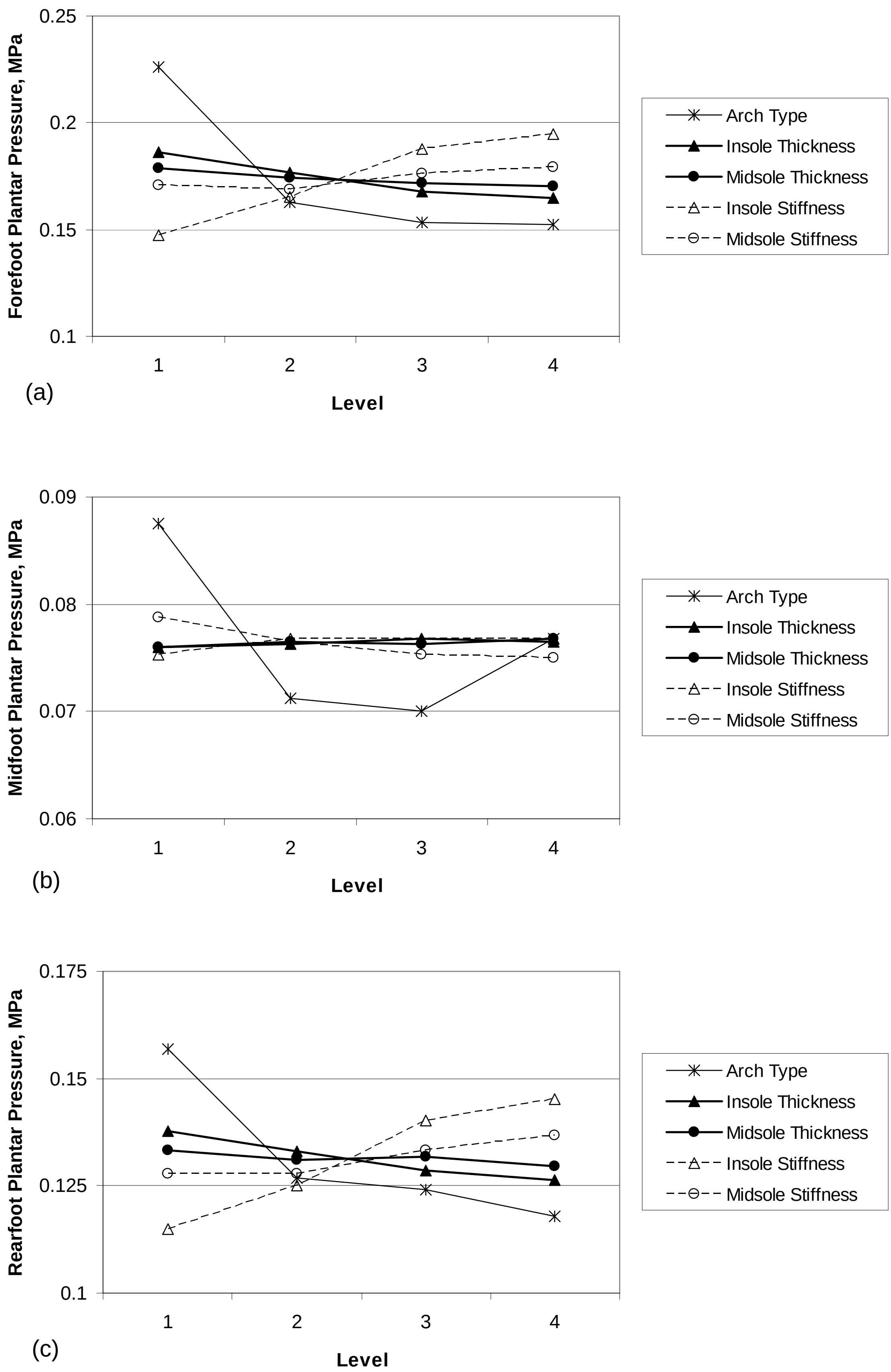


Figure 4-29. Mean effects of the five design factors at each level on the predicted (a) forefoot, (b) midfoot and (c) rearfoot plantar pressure.

Table 4-4. Analysis of variance of predicted plantar pressure in the forefoot, midfoot and rearfoot for 5-factor, 4 level fractional factorial.

| **Factor** | **Sum of squares for plantar pressure, MPa$^2$ (% of contribution)** | | |
|---|---|---|---|
| | Forefoot | Midfoot | Rearfoot |
| Arch Type | 0.0149765 (67.6%) | 0.00076325 (94.5%) | 0.00359425 (55.4%) |
| Insole Thickness | 0.0010985 (5.0%) | 0.00000125 (0.15%) | 0.00031125 (4.8%) |
| Midsole Thickness | 0.0001525 (0.7%) | 0.00000125 (0.15%) | 0.00002925 (0.45%) |
| Insole Stiffness | 0.0056460 (25.5%) | 0.00000675 (0.8%) | 0.00232025 (35.75%) |
| Midsole Stiffness | 0.0002655 (1.2%) | 0.00003525 (4.4%) | 0.00023475 (3.6%) |

Although the use of an arch-supporting foot orthosis was found to be the most important design factor for peak plantar pressure reduction (Fig. 4-29), small differences between the amount of plantar pressure reduction was predicted among the three arch-supporting conditions (level 2 to level 4). A decrease in insole stiffness was found to provide an increasing trend in magnitude of peak planar pressure reduction (Fig. 4-29). A pronounced reduction in forefoot and rearfoot peak plantar pressure was predicted with a change from the stiffer material (Nora_SLW) with hardness of $30^0$ to the softer material (Poron_L32) with hardness of $20^0$. A further reduction in peak plantar pressure was achieved with an even softer material (Poron_L24) with hardness of $10^0$. The trend in reduction of peak plantar pressure between the insole and midsole stiffness was similar (Fig. 4-29) but the performance for different midsole material was less obvious.

A general decrease in forefoot and rearfoot peak plantar pressure was predicted with an increasing insole and midsole thickness (Fig. 4-29), but the degree of reduction was less pronounced than the effect of orthotic material used. The difference in peak forefoot and rearfoot plantar pressure for an increasing midsole thickness was minimal. Except a slight reduction of peak pressure with an increasing midsole stiffness, the effect of insole stiffness, insole and midsole thickness on the peak pressure reduction of the midfoot was negligible.

The predicted peak plantar pressure with any combinations of levels among factors can be estimated using the superposition model. From the sensitivity analysis of the five design factors (Fig. 4-29), the predicted magnitude of peak pressure reduction would be the highest with the arch type, insole and midsole thickness assigned at level 4 and the insole and midsole stiffness assign at level 1. The FE predicted peak plantar pressure was 0.123, 0.078 and 0.096 MPa, respectively for the forefoot, midfoot and rearfoot. The FE predictions were slightly deviated from the corresponding peak pressure of 0.111, 0.0785 and 0.091 MPa estimated from the superposition model. Taking the same configurations except with a half weightbearing arch type, the estimated peak plantar pressure from the superposition model was 0.112, 0.0718 and 0.097 MPa for the forefoot, midfoot and rearfoot region. The estimations were comparable to the corresponding FE predictions of 0.115, 0.067, and 0.098 MPa.

### *Experimental Measurements*

The plantar pressure measurements of the same single subject for acquiring the geometrical properties of the FE model were used to validate the sensitivity analysis of the FE predictions. For the sake of simplification and because of the limitations of shoes to accommodate all the configurations of the foot orthosis, only the commonly used insole (Poron_L32) and midsole (Nora_SL) material and a total thickness of not more than 9 mm were considered. The average peak plantar pressures measured from three walking trials in different selected configurations of the foot orthosis are shown in Table 4-5. Owing to the low sensitivity and the limitation of the F-scan system to capture the low midfoot plantar pressure (Fig. 4-28b), a qualitative comparison in terms of pressure reduction was made between the FE predictions and the experimental measurements.

Table 4-5. The F-scan measured peak plantar pressure with different configurations of foot orthosis

| | Configurations of foot orthosis | | | | F-scan measurement, MPa | | |
|---|---|---|---|---|---|---|---|
| **Trial Number** | Arch Type | Insole (Poron_L32) Thickness, mm | Midsole (Nora_SL) Thickness, mm | | Forefoot | Midfoot | Rearfoot |
| 1 | F | 0 | 3 | | 0.133 | 0.077 | 0.1 |
| 2 | F | 3 | 3 | | 0.12 | 0.07 | 0.087 |
| 3 | F | 6 | 3 | | 0.113 | 0.073 | 0.09 |
| | | | | | | | |
| 4 | FWB | 0 | 3 | | 0.117 | 0.073 | 0.07 |
| 5 | FWB | 3 | 3 | | 0.097 | 0.053 | 0.06 |
| 6 | FWB | 6 | 3 | | 0.11 | 0.047 | 0.06 |
| | | | | | | | |
| 7 | HWB | 0 | 3 | | 0.103 | 0.06 | 0.07 |
| 8 | HWB | 3 | 3 | | 0.09 | 0.057 | 0.057 |
| 9 | HWB | 6 | 3 | | 0.1 | 0.06 | 0.06 |
| | | | | | | | |
| 10 | NWB | 0 | 3 | | 0.083 | 0.063 | 0.047 |
| 11 | NWB | 3 | 3 | | 0.073 | 0.047 | 0.047 |
| 12 | NWB | 6 | 3 | | 0.087 | 0.05 | 0.043 |

F: Flat, FWB: Full-weightbearing, HWB: Half-weightbearing, NWB: Non-weightbearing. Hardness values of 20 and 40 correspond to Poron_L32 and Nora_SL, respectively.

The F-scan measurements found a general reduction in peak plantar pressure with an increasing arch height of foot orthosis (Trial numbers. 1, 4, 7 and 10). The use of a 3 mm thick soft insole layer provided a consistent reduction of peak plantar pressure in forefoot, midfoot and rearfoot regions (Trial numbers. 2, 5, 8 and 11). However, the use of a thicker insole layer of 6 mm did not provide a further reduction plantar pressure (Trial numbers. 3, 6, 9 and 12). Instead, it resulted in a consistent in increase in the peak forefoot pressure. The increase in pressure was probably induced by the constrictive toe box of the shoes because of the limited in-depth of the footwear for accommodating the increased insole thickness.

# CHAPTER V DISCUSSION

## 5.1 Effects of Varying Bulk Soft Tissue Stiffness

Heel pain and ulceration of the diabetic foot are the most common complaints among patients with foot and ankle problems (Boyko et al., 1999; Holewski et al.,1989; Lavery et al., 2003; Pham et al., 2000; Selth and Francis, 2000). Patients with diabetes-related peripheral neuropathy are susceptible for developing ulcers on the plantar foot surface, which frequently leads to hospitalization and amputations of the lower extremities. One of the major causes of diabetic ulceration and painful heel syndrome is thought to be the presence of abnormally high plantar pressures (Boulton et al., 1987; Lavery et al., 2003; Mueller et al., 1994; Nigg and Bobbert, 1990; Onwuanyi, 2000; Pham et al., 2000; Reiber et al., 2002; Sage et al., 2001; Veves et al., 1992), which can be attributed from bony prominences, calluses, structural deformities or poor footwear fitting. Diabetic foot ulcers are highly associated with chronic pressure callus (Murray et al., 1996; Pitei et al., 1999; Sage et al., 2001), which is mainly a result of abnormal plantar tissue stiffening in patients with neuropathy. Recently, Charanya et al. (2004) studied the effects of foot sole hardness and thickness on the peak plantar pressure during barefoot walking and found a positive correlation of foot sole stiffness, peak plantar pressure and incidence of plantar ulcers in patients with diabetic neuropathy.

Knowledge on the effect of soft tissue compliance or other structural characteristic on the stress distribution of the plantar foot surface and bony structures is essential to achieve an appropriate individualized treatment strategy such as an orthotic design. The pressure distributions between the foot and different supports were measured experimentally with the use of in-shoe pressure sensors and pedobarograph (Cavanagh et al., 1987; Lavery et al., 1997; Lord and Hosein, 2000; Patil et al., 2002;

Raspovic et al., 2000). Due to the difficulties and lack of better technology for the experimental measurement, the load transfer mechanism and internal stress states within the soft tissues and the bony structures were not well addressed.

In order to supplement these experiments, researchers have turned to the computational methods. The models developed by Jacob and Patil (1999a) and Gefen (2003) were employed to investigate the biomechanical effects of soft tissue stiffening in the diabetic feet. These models predicted that an increase in soft tissue stiffness resulted in an increase in peak plantar pressure but with minimal effect on the bony structures. Gefen (2003) further speculated that the development of diabetic foot-related infection and injury was more likely initiated by micro-damage of tissue from intensified stress in the deeper subcutaneous layers rather than the skin surface. It has been shown in the literature that FE models can contribute in familiarizing the effects of thickness and stiffness of plantar soft tissue on plantar pressure distribution (Gefen, 2003; Jacob and Patil, 1999; Lemmon et al., 1997).

For the sake of convergence of solution and minimizing computational efforts, most of the linearly elastic FE foot models reported so far (Chen et al., 2001; Chu and Reddy, 1995; Chu et al., 1995; Jacob and Patil, 1999; Thomas et al., 2004) assigned relatively stiff mechanical properties for soft tissue, where the Young's moduli were selected as being 1 MPa or larger. These values of Young's moduli are much larger than those obtained from *in vivo* experimental measurements of plantar soft tissue, ranging from 0.05 to 0.3 MPa under strains of 10–35% (Gefen et al., 2001b; Zheng et al., 2000). For FE models using a nonlinear material model for plantar soft tissue (Gefen et al., 2000; Gefen, 2003; Nakamura et al., 1981; Lemmon et al., 1997), the adopted stress–strain behaviour varied as a result of the intrinsic variation of individual tissue, measurement techniques and environment.

The stress–strain response of plantar soft tissue was often obtained from either indentation or compression test of *in vivo* or cadaveric specimens (Gefen et al., 2001a; Klaesner et al., 2002; Lemmon et al., 1997; Miller-Young et al., 2002; Nakamura et al., 1981). In the literature, there is still a lack of material sensitivity study to quantify the effects of soft tissue stiffening on plantar pressure distribution using a geometrical accurate 3D foot model.

In this sensitivity study, the developed FE model was able to document the effect of varying bulk soft tissue stiffness on the plantar pressure distributions and stress of the bony structures during weightbearing of the foot. The predicted plantar pressure distribution was in general comparable to the F-scan measurement. With increased plantar soft tissue stiffness, the pressure tended to concentrate beneath the heel and the medial metatarsal heads especially for the second and third metatarsals. In all calculated cases, the peak plantar pressure was located at the centre of the heel and beneath the second and third metatarsal heads. This complies with the frequent observation of plantar foot ulcers at the medial forefoot and heel regions of diabetic patients (Mueller et al., 1994; Raspovic et al., 2000). The FE model implicated that stiff plantar soft tissue will decrease the ability of the foot to accommodate and assimilate the plantar pressures, which can be a possible factor for igniting plantar foot pain and further tissue breakdown and ulcer development. Besides, the predicted shear stress increased with tissue stiffening, which can also be a direct contribution of tissue breakdown of the diabetic feet (Lord and Hosein, 2000). In fact, the predicted percentage increase in plantar shear stress was more pronounced than the plantar pressure with stiffening of plantar soft tissue. Further investigations should be done to correlate the incidence of diabetic ulceration in terms of plantar shear stress.

As callus formation may act as a foreign body to elevate plantar pressure, it is therefore essential for diabetic patients to have regular callus removal (Pitei et al., 1999). There is also a need for subjects with high plantar tissue stiffness or neuropathic ulcer to redistribute the plantar foot pressure in a more uniform pattern in order to avoid local stress failure or relieve painful foot syndromes. This can be further elucidated by the clinical observation that patients with diabetic neuropathy and with a history of foot ulceration have abnormally high pressures under the feet and a high risk of recurrent ulceration because the high plantar pressures persist after healing of the ulcer.

From the FE prediction, the rate of increase in peak plantar pressure was found to be lower than the corresponding increase of soft tissue stiffness. A fivefold increase in soft tissue stiffness resulted in only about 1.33 and 1.35 times increase in peak plantar pressure of the heel and forefoot regions, respectively. The predicted peak pressure increases were comparable to other FE model predictions in the literature (Gefen, 2003; Jacob and Patil, 1999a). For instance, Gefen (2003) predicted 1.5 times increase in forefoot contact pressure of the standing foot with 5 times the stiffness of normal tissue. With 3 times the normal soft tissue stiffness, Jacob and Patil (1999a) predicted an average contact pressure increase of 1.2 and 1.7 times in the heel and forefoot region, respectively, during heel strike and push-off. From the FE predictions, the rate of peak pressure increase tended to decrease with stiffening of soft tissue.

Most of the linearly elastic FE models reported used a relatively large value of soft tissue stiffness in their analysis (Chen et al., 2001; Chu et al., 1995; Jacob and Patil, 1999a). These values overestimated the actual plantar soft tissue stiffness, and reduced the adapting ability of the plantar soft tissue to the supporting surface. This will lead to inaccuracy in predicting the plantar pressure and contact area especially when a geometrical accurate plantar foot contour is defined. The current FE analysis implicated that the soft tissue stiffness would have a noticeable effect on the plantar pressure distribution pattern. The material constants for the soft tissue should be measured or defined carefully and preferably using more accurate descriptions, such as nonlinear elasticity, in the FE analysis.

The predicted increases in peak plantar pressure in the simulated diabetic foot agreed with the reported range in the literature (Caselli et al., 2002; Luger et al., 2001). For instance, Luger et al. (2001) reported an average peak pressure increase of up to 1.2 and 2.2 times at the heel and forefoot regions, respectively, during barefoot walking from 75 normal and 328 diabetic patients. From the peak pressure measurement of 248 diabetic patients during barefoot walking, Caselli et al. (2002) found a 1.3 and 1.9 times increase in the heel and forefoot regions, respectively, between patients without neuropathy and in severe stages of neuropathy. It should be noted that the above plantar pressure measurement was done during walking while the current model simulates balanced standing. In fact, the effect of soft tissue stiffening on increased plantar pressure may be more pronounced during dynamic or full-weightbearing conditions.

From the FE predictions, it is clear that the increase in soft tissue stiffness will lead to an intensified peak plantar pressure. However, the rate of increase in peak plantar pressure was found to be much lower than the corresponding increase in soft tissue stiffness. The results speculated that screening of soft tissue stiffness might be an important procedure in addition to plantar pressure screening for early detection or implication of susceptible ulcerating sites.

The prediction of peak von Mises stress showed that the mid-shafts of the third and the second metatarsals sustained the highest bone stress. The confined positions, long and narrow shaft structures of these metatarsals and the high plantar pressure underneath the metatarsal heads are probably the direct cause of stress concentration and frequent sites of stress fracture. Because of its smaller shaft diameter, the mid-shaft of the third metatarsal sustained a higher bone stress than that of the second metatarsal in the current FE prediction. Apart from the mid-shaft of the metatarsals, the junction of the ankle, subtalar and calcaneal–cuboid joints together with the insertion areas of the plantar fascia also sustained high stresses under weightbearing. With stiffening of soft tissue, the load-bearing role of the encapsulated soft tissue increased while the flexibility of the foot reduced. As a result, some of the major foot bones especially the lateral cuneiform and the rearfoot bones were relatively unloaded, whereas other foot bones especially the cuboid and lateral metatarsals sustained increased stresses. With minimal increases in peak metatarsal stress, the FE predictions, however found no evidence on increasing the risk of stress failure of foot bones with stiffening of soft tissue.

It should be noticed that the effect of tissue stiffening considered in this simulation was simplified by a uniform increase of soft tissue modulus over the whole encapsulated tissue. In the real cases, the tissue stiffening may occur in discrete area of foot especially on the plantar foot and may exhibit different degrees of stiffening. The pathological conditions considered for diabetic patients were simplified as solely from the increase of soft tissue stiffness. The location of centre of pressure was assumed unchanged with the simulations of pathological conditions. The overall biomechanical behaviour of diabetic feet may be influenced by other structural changes, such as increased bone deformity, laxity of ligamentous structures or changes in muscular reaction. Besides, the effects of varying plantar soft tissue thickness on plantar pressure and internal stress distribution deserve further investigations. Owing to the use of geometrical accurate model, the generalization of the current FE prediction remains questionable. Simulations of various physiological loading conditions in addition to experimental validations are needed before a conclusion can be made.

## 5.2 Effects of Varying Plantar Fascia Stiffness

The plantar fascia, which originates from the medial tubercle of the calcaneus and inserts into the phalanges through a complex network of fibrous tissue (Hicks, 1954) is one of the major stabilizing structures of the longitudinal arch of the human foot, especially during the midstance phase of the gait cycle. Knowledge of its functional biomechanics is beneficial for establishing biomechanical rationale behind rehabilitation, orthotic and surgical plantar fasciitis. Plantar fasciotomy, a common surgical procedure to relieve chronic heel pain ignited by plantar fasciitis, was suggested to decrease the stiffness of the foot and create a more deformable foot arch (Davies et al., 1999). This biomechanical consequence raises concerns about the complication of decreased arch stability and biomechanical compensation of adjacent ligamentous structures such as the plantar ligaments. Alternatively, a stiff plantar fascia may lead to an overly rigid longitudinal arch and a reduced shock-absorbing capability. The tightness of the plantar fascia may overstress the insertion sites at the calcaneus and lead to the development of focal heel pain.

Cadaveric studies have been done to investigate the biomechanical consequence of plantar fascia release. Huang et al. (1993) reported that the average vertical displacements between the talar neck and supporting platform were 7.3 and 8.4 mm, respectively in 12 cadaveric feet with intact plantar fascia and fasciotomy under a load of 690 N. Murphy et al. (1998) reported a 29% increase in vertical displacement of the longitudinal arch in six cadaveric feet under a load of 682 N with plantar fascia release. Kitaoka et al. (1997c) studied the arch deformation (distance between the dorsal navicular and a line between the medial calcaneal tubercle and the plantar first metatarsal head) and relative joint rotation in the form of screw axis displacements in 12 fresh cadaveric feet under a load of 445 N. They found that the arch height was reduced with an average of 1.1 mm, and the mean talotibial, calcaneotalar and metatarsotalar rotations were increased after fasciotomy. Using implanted strain gauge, Crary et al. (2003) reported an increased strain of about 52% and 94% in the spring and long plantar ligaments, respectively at a load of 920 N with plantar fascia release in 11 cadaveric feet. Due to intrinsic variability of cadaveric specimens and experimental difficulties, a sensitivity analysis on the material stiffness of the plantar fascia was difficult using the cadaveric approach. In fact, most of the cadaveric studies in the literature focused on the biomechanical consequence of complete plantar fascia release and limited studies quantified the effect of partial release as well.

Computational models have been used to quantify the biomechanical role of plantar fascia in load bearing (Arangio et al., 1998; Gefen, 2002a). Using a 3D rigidly linked computational model (Arangio et al., 1998), the vertical displacement of the foot was found to increase with fasciotomy. A higher initial arch height was found to experience less vertical displacement of the foot with both the fascia intact and released. An increase in metatarsal stress and ligaments tension and a decrease in arch height following removal of the plantar fascia were predicted by Gefen (2002a), using a 2D FE model. In the literature, 3D geometrical detailed FE models have been developed (Camacho et al., 2002; Gefen et al., 2000; Jacob and Patil, 1999), but were not employed to quantify the biomechanical role of plantar fascia.

This sensitivity study is the first time in the literature to have a 3D FE model of the foot and ankle to investigate the effects of plantar fascia stiffness on the load-bearing characteristics of the plantar foot and the internal bony structures. The patterns of the predicted plantar pressure distribution and contact area were comparable to the F-scan measurement (Fig. 4-4). A relatively higher peak pressure was predicted compared with the measured value. The deviation may be a result of the differences in resolution of peak pressure measurement and prediction and the analytical stress concentration from the contact simulation between the plantar foot and support. The measured peak plantar pressure was therefore expected to be smaller than the FE predicted values. The increase in forefoot pressure and decrease in heel pressure with fasciotomy was a result of pronation of the midfoot and subsequent unloading of the lateral forefoot. The effect of varying fascia Young's modulus did not pose an obvious change in distribution of plantar pressure.

The predicted arch deformation (16.2%) was comparable to the subject measurement (18.3%). However, considerable amount of variation was found comparing to the experimental measurement in the literature, which may due to the individual variability of arch stiffness and the definition of arch height measurement. The FE model predicted 9.5 and 14.2 mm arch deformations with Young's modulus of fascia, E = 350 MPa and with fasciotomy (E = 0 MPa), corresponding to a 50% increase. Huang et al. (1993) and Murphy et al. (1998) reported averaged increases in arch deformation of about 15% and 29%, respectively after fasciotomy. Murphy et al. (1998) reported a drop of navicular bone level with an average of 4.05 mm after fasciotomy, which was comparable to the current FE prediction (4.7 mm). Zeroing the fascia Young's modulus led to a pronounced reduction of predicted arch height during load-bearing, but did not result in total collapse of the foot arch.

The model predicted that the fascia sustained about 45% of the applied load, which complied with the prediction (47%) reported in the literature (Wright and Rennels, 1964). The predicted value was larger than the predictions (25.5%) by Arangio et al. (1998). The high tension predicted in the plantar fascia suggested that it is one of the major stabilizers of the longitudinal arch during midstance of the gait cycle. With laceration or resection of this important structure, other ligamentous structures have to contribute to this stabilizing role. From the FE prediction, fasciotomy resulted in a pronounced increase in maximum tensile strain of 192%, 215% and 279% in the long plantar, short plantar and spring ligaments. Crary et al. (2003) measured an average increased strain of 52% and 94% in the spring and long plantar ligaments, respectively with fasciotomy. Gefen (2002a) predicted an increased tension of up to 200% in the long plantar ligaments with simulation of plantar fascia release using a 2D FE model. The deviation in strain measurement between the experimental and computational approaches may be the result of the variable nature of the measuring equipment, position and alignment of measurement and individualized structural strength. Although the long-term effect of increased strains of intrinsic ligaments cannot be predicted, it can be speculated that the involved plantar ligamentous structures may remodel with increased laxity and lead to further degradation of arch stability.

For Young's modulus of fascia equal or above one-eighth of reference value (E = 350 MPa), the peak von Mises stresses at the plantar mid-shafts of the third metatarsal intensified with increasing Young's modulus of fascia. With Young's modulus of fascia below one-eighth of reference value, the peak von Mises stresses shifted to the second metatarsal. The metatarsals stresses tended to be relatively relieved with reducing fascia stiffness. However, stress concentration occurred with further reduction of fascia stiffness and especially with fasciotomy, which was accompanied by pronation of the midfoot. The stress concentration in the centralised metatarsals and the plantar ligamentous attachment areas of the cuboid bone following fasciotomy, reflected the possible regions of stress failure. Gefen (2002) predicted that removal of the fascia elevated the dorsal compression stresses up to 65% and suggested the plantar fascia had a role in relieving metatarsal stresses. The current 3D model predicted similar increase in dorsal von Mises stress especially at the mid-shaft of the second and fourth metatarsals after fasciotomy. However, the effect of plantar fascia release on individual metatarsal bone stress distribution differed. Although a reduction of fascia stiffness may result in adverse biomechanical effect, it is able to relieve the focal stress at the calcaneal insertion, which is believed to be associated with heel pain. With simulation of fasciotomy, a von Mises stress reduction of 54% was predicted at the calcaneal insertion.

Stiffening of plantar fascia alone would not contribute to rigid arch structure such as a cavus foot, the rigid or restrained arch structure is probably a combination of intrinsic ligaments restraint, muscular contraction and orientation of articulating joints. Partial or total plantar fascia release may relieve the metatarsal and calcaneal stresses and the painful heel syndromes of plantar fasciitis. However, reduction of plantar fascia stiffness may cause a significant impact of arch stability, resulting in a more deformable longitudinal arch and a pronated foot. The intensified stresses in the centralised metatarsals, dorsal calcaneocuboid joint junction, plantar ligaments and their attachment bony areas after plantar fascia release may likely cause stress or fatigue failure and subsequent midfoot pain.

Pain development along the lateral column of the foot has been a common clinical observation following fasciotomy (Brugh et al., 2002). This post-operative syndrome complies with the current prediction of increased stress in the cuboid and increased straining of the plantar ligaments especially the spring ligament. From the FE prediction, reductions of plantar fascia stiffness beyond 50% were found to have a pronounced and increasing effect on load redistribution. To avoid the risk of surgical complication, the portion of released plantar fascia should thus be minimized and conservative treatment for plantar fasciitis or chronic heel pain should be the primary act in order to preserve the structural integrity of the ankle–foot complex.

To simplify the analysis in this study, homogeneous and linearly elastic material properties were assigned to the model. The ligaments within the toes and other connective tissue such as the joint capsules were not considered. The use of homogeneous and linearity of the encapsulated soft tissue stiffness and the ligamentous structures was a simplification of the real situation. Only the Achilles tendon loading was considered while other intrinsic and extrinsic muscle forces were not simulated. Balanced standing was simulated while the more complex and high load-bearing stance phases were not analysed. The location of centre of pressure was assumed unchanged with the simulations of different fascia stiffness. The developed model represented a normal arch configuration whilst the effect of varying plantar fascia stiffness is individualized with different foot structures (Arangio et al., 1998; Kitaoka et al., 1997b, c).

The plantar fascia was found to be an important stabilizing structure of the longitudinal arch of human foot during weightbearing. Decreasing the stiffness of plantar fascia would reduce the arch height, increase the strains of the long and short plantar and spring ligaments. Reduction of plantar fascia stiffness to beyond certain level may induce excessive strains or stresses in the ligamentous and bony structures. Surgical release of the plantar fascia, if necessary, should be well-planned to try to minimize the effect on its structural integrity.

## *5.3 Effects of Partial and Complete Plantar Fascia Release*

Insertional plantar fasciitis is a common diagnosis of chronic heel pain in athletes as well as the general population (Cornwall and McPoil, 1999; Onwuanyi, 2000; Woelffer et al., 2000) and is often suggested as a cause of excessive stretching of the plantar fascia. Plantar fasciotomy, a common surgical procedure to relieve chronic heel pain, was found to have an acceptable success rate in the literature (Brugh et al., 2002; Davies et al., 1999; Woelffer et al., 2000). However, plantar fascia release decreases the stiffness of the foot and creates a more deformable foot arch or a pes planus foot (Davies et al., 1999; Kitaoka et al., 1997b, c, 1998; Yu, et al., 1999). These biomechanical consequences raised concerns about the adverse effects of decreased arch stability and biomechanical compensation of adjacent ligamentous structures such as the plantar ligaments. Less than 50% of patients reported were satisfied with the surgical treatment (Davies et al., 1999). Postoperatively, patients may experience acute plantar fasciitis, forefoot stress fractures, calcaneal and cuboid fracture, and medial or lateral column foot pain (Brugh et al., 2002; Yu, et al., 1999). Various percentages of partial fascia release have been advocated for its preservation of structural integrity (Brugh et al., 2002; Davies et al., 1999; Woelffer et al., 2000). A systematic evaluation of the biomechanical effect of sequential plantar fascia release is essential before a plausible conclusion can be made.

A number of cadaver studies have been done to investigate the biomechanical consequence of partial and total plantar fascia release (Anderson et al., 2001; Crary et al., 2003; Huang et al., 1993; Kitaoka et al., 1997b, c, 1998; Murphy et al., 1998). In general, an increase in vertical displacement, elongation of the longitudinal arch and joint rotation were reported after fasciotomy (Huang et al., 1993; Kitaoka et al., 1997b, c; Murphy et al., 1998). Anderson et al. (2001) reported minimal changes in the position of the calcaneocuboid joint with plantar fascia release and suggested straining of the lateral ligaments around the sinus tarsi was the cause of postoperative midfoot pain. Crary et al. (2003) found an increase in average strains in the spring and long plantar ligaments after plantar fascia release, using implanted strain gauge.

Due to the intrinsic structural and material variability of cadaver specimens and experimental limitations, systematic evaluations of the load distribution of the ankle-foot complex following different degree of plantar fascia release are difficult to achieve. Some researchers have turned to the computational approach to acquire these biomechanical parameters (Arangio et al., 1998; Gefen, 2002a). Using a 3D rigidly linked computational model, Arangio et al. (1998) found that a higher initial arch height experienced less vertical displacement of the foot with both the fascia intact and released. Using a 2D FE model, Gefen (2002) predicted an increase in metatarsal stress and ligaments tension and a decrease in arch height following removal of the plantar fascia.

The sensitivity analysis in this study is the first attempt in the literature to quantify the biomechanical effects of partial and total plantar fascia release using a 3D FE model. From the FE predictions, plantar fascia release was not found to pose a tremendous impact on the load distribution of the plantar foot with sequential plantar fascia release. Sectioning of the plantar fascia led to a pronounced reduction of arch height during load-bearing, but did not necessary result in total collapse of the foot arch even with additional dissection of the long plantar ligament. This is complementary to the observation from cadaver studies in the literature (Kitaoka et al., 1997b, c).

The predicted strain (42.9%) of the plantar the fascia during balanced standing was within the range from computational predictions reported by Wright and Rennels (1964) (47%) and Arangio et al. (1998) (26%). The maximum strains (0.3%) predicted by the FE model agreed with the experimental measurements by Kogler et al. (1995). The high tension predicted in the plantar fascia suggested it as a major stabilizer of the longitudinal arch of the foot. With laceration or resection of the plantar fascia, other ligamentous structures have to contribute to its stabilizing role.

Partial or total plantar fascia release may relieve the metatarsal and calcaneal stresses and the painful heel syndromes of plantar fasciitis. However, reduction of plantar fascia stiffness may cause a significant impact of arch stability, resulting in a more deformable longitudinal arch and a pronated foot. There was a tremendous effect of load sharing in the plantar ligaments with different degree of sectioning of the plantar fascia. Complete fascia release resulted in a pronounced increase in maximum tensile strain of the long plantar ligaments, followed by the spring and short plantar ligaments.

The compensation by the plantar ligaments may lead to tensile failure of the spring, long and short plantar ligaments, which are the most longitudinally aligned.

The FE predicted ligamentous strain agreed qualitatively with the experimental finding and the deviation in strain measurement between the experimental (Crary et al., 2003) and computational (Gefen, 2002a) approaches may be the result of the variable nature of the measuring equipment, position and alignment of measurement and individualized structural strength. From the FE prediction, the maximum strains and total tensions of the long and short plantar ligaments experienced a general increase with sequential sectioning of the fascia. A pronounced increase in total tensions and maximum strains was predicted but the differences among the four cases of fascia release were small. Plantar fascia release may therefore overstretch the plantar ligaments and associated joint capsules, which may lead to subsequent midfoot pain.

Although the long term effect of increased strains of intrinsic ligaments cannot be predicted, it can be speculated that the involved plantar ligamentous structures may remodel with increased laxity and lead to further degradation of arch stability (Brugh et al., 2002). The increased straining of the plantar ligaments and stresses at the inferior plantar ligaments attachment area of the cuboid may cause focal stress failure and subsequent lateral midfoot pain. The current prediction complies with the commonly observed post-operative lateral foot pain syndrome following fasciotomy (Brugh et al., 2002; Yu et al., 1999).

The post-operative complications such as acute plantar fasciitis, midfoot syndrome and metatarsal stress fractures may cause symptoms that can be more painful than the initial heel pain (Brugh et al., 2002; Yu et al., 1999). Non-surgical treatment such as the use of stretching programs and orthoses should thus be done first for treating plantar fasciitis in order to preserve the normal biomechanics of the ankle-foot complex. If surgical release of the fascia is necessary, a partial releasing approach is advocated for its smaller effect on the plantar ligaments and joint capsules, which may reduce the risk of the post-operative midfoot syndrome.

The developed model represented a normal arch configuration while the effects of varying plantar fascia stiffness were individualized with different foot structures (Arangio et al., 1998; Kitaoka et al., 1997b, c). The simulation of partial plantar fascia release may be an exaggeration of the actual surgical outcomes because five discrete fascia sections rather than continuous and unified structures were considered. As only the calcaneal insertion of the fascia was dissected in the surgical procedure, total ignorance of the medial fascia section may have hindered its residual stiffening effect on the medial arch.

From the FE predictions and other experimental findings in the literature (Anderson et al., 2001; Crary et al., 2003; Huang et al., 1993; Kitaoka et al., 1997b, c, 1998; Murphy et al., 1998), surgical release of the plantar fascia will alter the normal foot biomechanics by increasing the longitudinal arch instability, straining of surrounding ligaments and joint capsules and may pose the risk of developing postoperative foot pain (Brugh et al., 2002; Yu et al., 1999). The FE model predicted that surgical release of the plantar fascia with around 40% may result in a pronounced increase in load-bearing of the centralized metatarsal bones, plantar ligaments and associated cuboidal joint capsules.

Load redistribution among the centralized metatarsal bones was predicted with different types of fasciotomy; however, the effects on the stress distribution of individual metatarsal bone were not systematic in nature and probably depended on the load sharing status of adjacent metatarsal bones in response to the dissected proportion of plantar fascia. From the FE prediction, the stress of the centralized metatarsals especially the second and third metatarsals intensified with plantar fascia release. The plantar fascia was found to be an important structure to maintain uniform stress distributions among the five metatarsals. Damage or sectioning of the fascia may alter this function and lead to metatarsal stress concentration. Using a 2D FE model, Gefen (2002a) predicted an increase in metatarsal stress and decrease of the arch height with fasciotomy. He reported that removal of the fascia elevated the dorsal compression stresses up to 65% and suggested the plantar fascia had a role in relieving metatarsal stresses.

With fascia release of 40% or more, a pronounced increase in maximum von Mises stresses was found in the cuboid bone around the attachment regions of the plantar ligaments. The stress concentration of the centralized metatarsal bones and the plantar ligamentous attachment areas of the cuboid bone were found to be the possible region of stress or fatigue failure following plantar fascia release.

Even though dissection of the plantar fascia may result in adverse biomechanical effect, it is able to relieve the focal stress at the calcaneal insertion, which is believed to be associated with heel pain. Comparing to the intact condition, a von Mises stress reduction of about 70% was predicted at the calcaneal insertion with complete plantar fascia release. Among the cases of partial fascia release, medial 20% release provided the largest stress reduction of about 17% at the calcaneal insertion.

Although 20% release of fascia led to a pronounced increase in spring ligament strain and metatarsal stress, the induced magnitude and the detrimental effects on other ligamentous and bony structures were relatively lower comparing to plantar fascia release of 40% or more. Among all the simulated cases of partial fascia release, a 20% release provided the largest stress reduction at the calcaneal insertion. From the FE predications, it was speculated that partial fascia release of less than 40% may be considered as a safer yet effective surgical approach for calcaneal insertional stress or pain relieve. However, large-scale prospective clinical trials are needed before a conclusion on the suggested safe portion for plantar fascia release can be made.

Using the FE analysis, the plantar fascia was found to sustain high tension during weightbearing, suggesting it as a major stabilizer of the longitudinal arch of the foot. Dissection of the plantar fascia led to a pronounced decrease in arch height during load-bearing. Plantar fascia release increased the strain of the plantar ligaments and associated joint capsules, which may be overstretched and lead to subsequent midfoot pain. The increase in metatarsals stress following plantar fascia release may be related to post-operative stress fracture. Therefore, the advantage of the surgical treatment to relieve the focal stress at the calcaneal insertion and the instep heel pain may be overwhelmed by its adverse biomechanical consequences on longitudinal arch instability and lateral midfoot pain. Surgical treatments for plantar fasciitis should only be regarded as a final resort when none of the non surgical treatments provide relieve or improvement of the patient's condition. If fasciotomy is necessary to relieve the painful heel syndrome, partial release of less than 40% of the fascia is recommended for its lesser disturbance to arch stability and normal foot biomechanics.

## *5.4 Effects of Varying Achilles Tendon Loading*

Insertional plantar fasciitis, which is common in athletes as well as the general population (Cornwall and McPoil, 1999; Warren, 1990), usually associates with a chronic painful syndrome at the inferior heel region. Excessive stretching, repetitive and abnormal stress induced in the plantar fascia and its calcaneal insertion may cause inflammation and injury, which are thought to be the major causes of plantar fasciitis (Cornwall and McPoil, 1999; Warren, 1990). Conditions that predispose the plantar fascia to increased tension during weightbearing such as excessive pronation, flat or high-arched foot structures and tight Achilles tendon are often suggested as implicating factors of plantar fasciitis (Warren, 1990).

Conservative treatment such as anti-inflammatory medication, stretching and strengthening exercise and foot orthoses has been used effectively to alleviate the painful syndrome of plantar fasciitis (Barry et al., 2002; Pfeffer et al., 1999; Probe et al., 1999). Stretching exercise and dorsiflexion night splints are often prescribed to help relieve the Achilles tendon tension with an attempt to reduce arch deformation, excessive pronation, rearfoot valgus and the tension of the plantar fascia. The dorsiflexion night splint was first described for use in the treatment of plantar fasciitis by Wapner and Sharkey in 1991 and has been proven to be beneficial by several prospective and randomised control studies (Barry et al., 2002; Probe et al., 1999).

Despite the success of Achilles tendon stress relief for treatment of plantar fasciitis, the biomechanical relationship between Achilles tendon loading and tension on the plantar fascia has not been well documented. A larger number of cadaveric studies (Crary et al., 2003; Donahue and Sharkey, 1999; Kitaoka et al., 1997b, c, 1998; Thordarson et al., 1995) and computational analyses (Gefen, 2002a; Giddings et al., 2000; Kim and Voloshin, 1995) have focused on the biomechanical response of the plantar fascia under different loading and supporting conditions and the biomechanical consequences of fasciotomy. Because of the difficulties and invasive nature of *in vivo* measurements of Achilles tendon tension (Finni et al., 1998), the biomechanical effect of varying Achilles tendon loading on plantar fascia has only been investigated by cadaveric studies. Thordarson et al. (1995) documented the arch-deforming effect of the Achilles tendon loading and the arch-supporting mechanism of the plantar fascia with toe extension via a 3D movement analysis on cadavers. Carlson et al. (2000) measured an increased plantar fascia strain with increasing loading on the Achilles tendon and with toe extension under static loading conditions of the foot. Erdemir et al. (2004)

found a positive correlation between plantar fascia tension and Achilles tendon force during simulations of the stance phase of gait in a cadaver model.

Although cadaveric studies (Carlson et al., 2000, Erdemir et al., 2004) have been done to investigate the effect of Achilles tendon loading on the loading response of the plantar fascia, these studies were subjected to certain limitations. For instance, physiological loading condition was not simulated by Carlson et al. (2000) because the body weight on the foot was not considered. Erdemir et al. (2004) measured the tension of the plantar fascia during simulated normal walking using a dynamic cadaveric model without a strict control on the effects of other extrinsic muscle forces, ground reaction forces and ankle-foot position. Therefore, their cadaveric simulation cannot provide a sensitivity analysis on the effects of Achilles tendon tension on the loading response of the plantar fascia. In this sensitivity study, a 3D FE foot model was used to quantify the biomechanical effect of varying Achilles tendon loading on the plantar fascia, longitudinal arch deformation and plantar pressure distribution of the standing foot.

*FE predictions and cadaveric foot measurements under pure compression*

Under pure compression, the FE model predicted a similar profile but a larger magnitude of vertical foot deformation than the cadaveric foot measurements. The discrepancy might probably be the results of neglecting the joint capsules and the stabilizing effects from the structural interactions between the joints and the ligamentous and muscular tissues, which reduced the joint stiffness of the ankle-foot structures. Besides, the effect of tissue desiccation upon loading and resulted from the process of freezing and thawing of the cadaveric specimens (Schafer and Kaufmann 1999) might alter the mechanical properties of the foot soft tissues and result in a stiffened foot structure.

The measured and FE-predicted straining profile of the plantar fascia with the foot under vertical compression agreed with the strain measurements in the literature (Kogler et al., 1995, 1996). Using an implanted displacement transducer, Kogler et al. (1995, 1996) reported average plantar fascia strains of 1.46% and 3.54% in the tested foot with vertical compression of 675 N. The average strain measurement from the cadaveric experiment in this study was comparable to the measurement by Kogler et al. (1995, 1996). The FE model predicted a relatively lower and linear response of increased fascia strain under vertical compression. The discrepancy was found to be related to the unstable ankle joint response, which resulted from the neglection of the aforementioned soft tissue restraint on the foot joints and the mass of the foot. During the initial phase of vertical compression on the foot, the ankle and subtalar joint was found to dorsiflex, resulting in shortening of the arch length between the metatarsal heads and the inferior calcaneal insertions of the plantar fascia. As a result, the increasing plantar fascia strain induced by the deforming arch was counterbalanced by an increasing dorsiflexion of the rearfoot bones. Besides, the assumption of linear material property and geometrical simplification of the plantar fascia as linear truss structures might also lead to an underestimation of predicted plantar fascia strain. The FE-predicted straining characteristic of plantar fascia agreed with the experimental measurements as the foot deformed under a larger magnitude of vertical compression.

### *FE predictions and subject measurements during balanced standing*

Computational analyses in the literature (Arangio et al., 2000; Gefen, 2002; Kim and Voloshin, 1995) usually assumed the Achilles tendon forces of the standing foot from analytical estimations. The analytical models employed by Kim and Voloshin, (1995) and Arangio et al. (2000) did not consider the plantar soft tissue structures and the foot-ground interface. Gefen (2002a) considered the bony, ligamentous and encapsulated soft tissue structures with their FE simulations of the standing foot;

however, the simulated loading conditions were not validated by experimental measurements. In this study, a geometrically accurate FE model was employed to investigate the effects of Achilles tendon load under half body weightbearing. The tension of the Achilles tendon during balanced standing was estimated from matching the FE-predicted and measured centre of pressure. The FE model predicted a larger Achilles tendon force of about 75% of the total weight on the standing foot (350 N) during balanced standing in comparison to the analytical assumptions (Arangio et al., 2000; Kim and Voloshin, 1995) which estimated Achilles tensions ranging from about half to two-third the weight on the foot. Without considering the geometrical constraints of the plantar soft tissue and its interaction with the plantar support, the computational analysis in the literature (Arangio et al., 2000; Gefen, 2002; Kim and Voloshin, 1995) likely underestimated the Achilles tendon forces during balanced standing.

Under simulated balanced standing, the five rays of plantar fascia segments sustained average and total tensions of 5.7% and 44% of the total weight on the foot. The FE predictions agreed with the reported loading percentage by Wright and Rennels (1964) (total: 47%) but were larger than the predictions by Arangio et al. (1998) (total: 26%, average: 5.3%) and Kim and Voloshin, (1995) (total: 14%). The discrepancy between studies resulted probably from the variations in nature and assumption of the models including the differences in material assignments, geometrical representation of the bony and ligamentous and other soft tissue structures. Using a 2D FE model, Giddings et al. (2000) predicted a relatively large plantar fascia tension of about 1.8 times and 3.7 times of body weight during walking and running, respectively.

All the computational analyses except the one from Giddings et al. (2000) provided a reasonable prediction of the plantar fascia tension during its functional weightbearing, which was within the physiological loading reported in experimental measurements (Erdemir et al., 2004; Kitaoka et al., 1994a). Erdemir et al. (2004) reported the failure loads of plantar fascia in the range of 916 to 1743 N, corresponding to about 2.15 to 2.80 times the body weight. Kitaoka et al. (1994a) reported significantly higher failure loads of plantar fascia for men (1540 N with a standard deviation of 246 N) than those for women (1002 N with a standard deviation of 101 N).

### *FE predictions of the effect of Achilles tendon tension on the standing foot*

Positive correlations between strain or loading of the plantar fascia and the Achilles tendon forces have been found in the literature (Carlson et al., 2000; Erdemir et al., 2004). Using a strain-gauged extensometer, Carlson et al. (2000) reported an increasing plantar fascia strain in the cadaver feet with increasing Achilles tendon force, consistent with the current FE predictions. The FE model predicted a lower strain value of 0.74% with an Achilles tendon force of 350 N than the experimental measurements (1.85%) by Carlson et al. (2000), who reported an increasing strain of up to 2.25% with an increasing Achilles tendon tension of up to 500 N. The current FE model predicted a similar straining profile but smaller values of plantar fascia strain, which resulted probably from the simplification of geometrical and material properties of the plantar fascia.

Using a pressure-sensitive optical gait platform and a radiographic fluoroscopy system, Gefen (2003b) reported an estimated *in vivo* deformation of the plantar fascia ranging from 9 to 12% during the contact phase of walking. The indirect strain measurement from lateral X-ray projections was subjected to certain approximations and limitations. The measured plantar fascia strain by Gefen (2003b) was likely overestimated because failure strains of less than 10% were reported from mechanical tests (Kitaoka et al., 1994a; Wright and Rennels, 1964).

Erdemir et al., (2004) established a correlation (r = 0.76) between plantar fascia tension and Achilles tendon force with simulations of the stance phase of gait in a cadaver model. The plantar fascia forces were found to increase gradually until it reached peak forces of about 538 N (96% of body weight) with a standard deviation of 193 N during the terminal stance phase. Erdemir et al., (2004) estimated the plantar fascia force ($F_f$) as a function of total weight on the foot ($F_w$) and Achilles tendon force ($F_a$) using the equation:

$$F_f = 0.041F_w + 0.474F_a \qquad (5\text{-}1).$$

According to the FE-predicted function (4-2) in this study, the estimated peak plantar fascia tension at the terminal stance was 430 N (77% of body weight), considering values of Achilles tendon tension (998 N) and ground reaction force (578 N) from the experimental data (Erdemir et al., 2004). The high tension predicted in the plantar fascia suggested it as a major stabilizer of the longitudinal arch of the foot. During the terminal instance, the plantar fascia is further tightened and strained according to a windlass mechanism (Hicks, 1954) in which the arch of the foot is elevated by winding of the plantar fascia around the heads of the metatarsals during toe extension. Because the current FE predictions did not account for the windlass mechanism, the predicted peak plantar fascia tension at the terminal stance was likely underestimated.

While sustaining a tension during weightbearing of the arch structures, the plantar fascia plays an important role in transmitting Achilles tendon forces to the forefoot especially during the terminal stance phase of walking (Carlson et al., 2000; Hicks, 1954). Carlson et al. (2000) reported an increasing plantar fascia strain with an increase of metatarsophalangeal extension under the same level of Achilles loading magnitude. Dorsiflexion of the toe activates the windlass mechanism and enhances the stability of the foot arch with an increasing tension and support from the plantar fascia. With the forefoot on the ground and the heel slightly elevated, contraction of the Achilles tendon tends to rotate the talus and calcaneus in the sagittal plane relative to the forefoot that tends to flatten the arch. Damage, weakening or surgical release of the plantar fascia may disturb this mechanism and thus compromise its stabilizing role for the transverse and longitudinal arches for efficient propulsion (Carlson et al., 2000). A number of cadaveric and computational studies have revealed that fasciotomy will reduce the arch height and stability (Arangio et al., 1998; Gefen, 2002a; Kim and Voloshin, 1995; Kitaoka et al., 1997b, c; Murphy et al., 1998), alter the load distribution of the forefoot (D'Ambrogi et al., 2003; Donahue and Sharkey, 1999; Gefen, 2002a), and increase the load-bearing of adjacent joint and soft tissue structures (Crary et al., 2003).

From the FE predictions, an increase in Achilles tendon load resulted in reductions of arch height and increases in plantar fascia tensions. The same magnitude of increase in Achilles tendon loading was found to produce about two times the tension of the plantar fascia produced by vertical compression on the standing foot. The average *in vivo* tension of the Achilles tendon during normal walking has been found to be 1430 N with a standard deviation of 500 N (Finni et al., 1998). The plantar fascia, which is substantially loaded by contraction of the plantar flexors and toe extensions during the stance phase of gait (Carlson et al., 2000; Thordarson et al., 1995), is expected to sustain an intensified tension in spite of the contribution of the intrinsic muscles in supporting the foot arch during dynamic activities.

Judging from the anterior shifting of centre of pressure with the increase of Achilles tendon loading in the balanced standing position, an extremely tight Achilles tendon that may cause an individual to stand on the forefoot without heel contact in the upright balanced standing posture may sustain a passive tension of magnitude more than the body weight. Individual with extreme tightness of the Achilles tendon will constantly sustain a high Achilles tendon tension. Therefore, it can be speculated from the FE predictions that overstretching of the Achilles tendon resulting from intense muscle contraction and passive stretching of tight Achilles tendon are plausible mechanical factors for overstraining of the plantar fascia. Lengthening or tension relief of the Achilles tendon especially in subjects with tight calf muscles and Achilles tendon may be beneficial in terms of plantar fascia stress relief.

To simplify the FE analysis, the FE model did not account for the surface interactions between bony, ligamentous and muscles structures. The structural simplification of the FE model would result in a reduction of joint stability of the ankle-foot structures and an increase in predictions of joint and arch deformation. Because of the use of linear truss elements to approximate the nonlinear profile of the plantar fascia structure, assumption of linear material property and the neglection of structural interface between the plantar fascia and surrounding tissue, the predicted plantar fascia strain in this study was likely underestimated.

## *5.5. Effects of Posterior Tibial Tendon Dysfunction*

The tibialis posterior is the deepest calf muscle, arising from the tibia, fibula and interosseous membrane. Distally, the tendon of the tibialis posterior turns forward below the medial malleolus and passes inferior to the spring ligament and inserts principally onto the tuberosity of the navicular. The tibialis posterior is a strong invertor and a weak plantarflexor of the foot (Kim et al., 2003) which supports the longitudinal arch of the foot. During the stance phase of gait especially at heel-off, the tibialis posterior stabilizes the calcaneocuboid, talonavicular and transverse tarsal joints and creates a rigid lever for the foot to facilitate propulsion.

The posterior tibial tendon dysfunction (PTTD) is a common pathological condition of foot (Kohls-Gatzoulis et al., 2004) which is painful and disabling. Posterior tibial tendon dysfunction usually begins with tendonitis. Without orthotic or surgical treatment, chronic posterior tibial tendon insufficiency will progressively worsen and lead to severe inflammation and dysfunction of the tendon. Failure of the PT tendon is highly associated with injuries of the surrounding soft tissue structures that are responsible for supporting the foot arch (Balen and Helms, 2001; Deland et al., 2005). A gradual increase in deformities associated with attenuation of the PT tendon and other arch-supporting soft tissue structures may ultimately lead to rigid flatfoot deformity, peritalar dislocation, and degenerative joint diseases (Mosier et al., 1999). Acquired flatfoot deformity may gradually progress into a severe disability and can only be treated by surgical corrections and associated postoperative rehabilitation, which are costly and may lead to possible post-surgical complications (Kohls-Gatzoulis et al., 2004).

Apart from the dynamic support provided by extrinsic muscles to the foot, the shapes of the interlocking tarsal joints, ligaments (spring ligament, ligaments of the sinus tarsi), joint capsules, and plantar fascia are responsible for maintaining the arch of the foot (Balen and Helms, 2001; Deland et al., 2005). During upright standing, the effect of the extrinsic muscles to the foot is limited, indicating the importance of these static structures in maintaining the foot arch (Basmajian and Stecko, 1963). Tear of the posterior tibial tendon is highly associated with the injury of the spring ligament (Balen and Helms, 2001) and patients presented with both injuries have severe abnormalities of the hindfoot. The talocalcaneal interosseus ligament and the cervical ligament in the sinus tarsi, which assist the posterior tibial tendon and spring ligament to maintain the longitudinal arch and stability of the calcaneus and the talus and to prevent talar flexion or rotation on the calcaneus (Balen and Helms, 2001).

A number of cadaveric studies have been done to evaluate the pathomechanics and biomechanical consequence of PTTD (Hansen et al., 2001; Imhauser et al., 2004; Kitaoka et al., 1997d; Niki et al., 2001; Thordarson et al. 1995). Thordarson et al. (1995) quantified the effect of PTTD on ten foot specimens in the presence of vertical compressive load of 350 N and 700 N by measuring the sagittal rotation between the first metatarsal and talus and the transverse rotation between the navicular and talus using a 3D digitizer. The PTT was found to have important arch-supporting function, which also act to adduct the forefoot. Kitaoka et al. (1997d) determined the effect of the posterior tibial tendon (PTT) on the bone movements of 13 cadaveric foot specimens in simulated midstance phase of gait using a magnetic tracking device. Significant arch flattening effect and tarsal bone movements were observed at the metatarsotalar, calcaneotalar, and talotibial joints with the application of tendon loads. Removal of PTT loading resulted in a further decrease in arch height and PTT was suggested as an important stabilizer of the arch of the foot. Using similar magnetic tracking system, Niki et al. (2001) investigated the role of PTT in acquired flatfoot deformity in eight cadaveric foot specimens. The 3D bone movements of the hindfoot complex were measured during simulated heel strike, midstance, heel off. The effect of PTT loading on the change in the angular orientation of the hindfoot was found to be small in both the intact and acquired flatfoot specimens with partially dissected spring ligament. The effect of PTT loading was the most significant during simulated heel rise. The arch supporting effect of PTT loading was found to be less pronounced than the osteoligamentous structures of the foot.

Imhauser et al. (2004) studied the effect of PTTD on the arch position, hindfoot position and plantar pressure distribution in five cadaveric foot specimens during simulated heel off using an infrared movement analysis system. The effect of PTTD was found to be more significant in the intact condition than the acquired flatfoot condition. A posterior shift in the centre of pressure and increased load on medial foot structures was found in both the intact and acquired flatfoot specimens with PTT unloaded. Simulated PTTD resulted in decreases in height of the talus, navicular and medial cuneiform in the intact condition. However, releasing the PTT with a flatfoot deformity only decreased the height of the medial cuneiform. Unloading the PTT caused the angle of the talus to increase with respect to the calcaneus. Simulated PTTD caused the navicular to evert in the intact condition, but not in the acquired flatfoot condition. The PTT exhibited no significant effect on either the height or the orientation of the cuboid in the intact or flatfoot conditions. Imhauser et al. (2004) suggested from their findings that the PTT was a strong invertor of the subtalar joint when the ligaments are intact.

Hansen et al. (2001) study the effect of PTTD in 15 cadaveric foot specimens during simulated heel off using a closed-loop feedback control on position and external muscle and ground reaction forces. The posterior tibialis tendon force required to maintain the intact condition generally increased with increasing peroneus loads. The Achilles force increased with PTTD compared to the intact condition. A significant amount of eversion was measured with PTTD, which resulted in eversion and abduction of the navicular and an increase in strain of the spring ligament. In general, PTTD was found to result in a change in bone and joint motion, ligaments strain. PTTD decreased arch height and may result in increased strain of the adjacent ligaments. Loss of PTT function, combined with the continuing function of its neutral antagonist (peroneus brevis), impose unbalanced loads on the static osteoligamentous hindfoot constraints. The lack of support beneath the talonavicular joint is thought to lead to gradual elongation of the soft tissues around the hindfoot, loss of the longitudinal arch, and eventually a progressive flatfoot deformity. The anatomical features commonly associated with PTTD and associated acquired flatfoot deformity are primarily a rotational malalignment with metatarsal-talar eversion, dorsiflexion, and abduction; calcaneal-talar eversion and abduction; talar-tibial plantar flexion; and loss of arch height (Kitaoka et al., 1997d; Niki et al., 2001).

Three-dimensional FE models have been used to analyses the biomechanical effect of muscular dysfunction on the human foot in the literature (Gefen et al., 2001; Gefen, 2002b; Jacob and Patil 1999b); however, the effect of PTTD had not yet been investigated. In this study, the developed 3D FE model of the human foot and ankle was used to quantify the biomechanical effect of PTTD on the foot during simulated midstance.

With PFR or PTTD, a medial shift of plantar pressure at the metatarsal region was measured in the cadaveric specimens and fasciotomy consistently produced a more pronounced effect. The FE predicted and experimentally measured changes in the plantar pressure characteristics agreed qualitatively with the cadaveric experiments (Imhauser et al., 2004) and clinical observations (Baumhauer, 1997) in the literature that PTT dysfunction causes abnormal forces on the midfoot and stretching of the associated ligamentous structures of the arch.

The FE predicted arch deformation (0.8 mm) after unloading the PTT was within the range of experimental measurements in the literature. Kitaoka et al. (1997d) and Imhauser et al. (2004) reported that the height of the navicular decreased by 0.5 mm and 2.24 mm after unloading the PTT.

From the FE predictions, the strains of the plantar fascia and plantar ligaments increased with PTTD. The predicted increase in strain of the spring ligament (3.4%) and the plantar fascia (5.6%) with PTTD was larger than the experimental measurements by Hansen et al. (2001) (1.82%) and in the current study (2.4%), respectively. The discrepancies between the FE predictions and experimental measurements may be due to the more deformable arch response predicted by the FE model because of the inadequacy in modeling the stabilizing soft tissue structures of the foot joints.

The larger increase in predicted tension of the spring ligament and plantar fascia with PTTD was consistent with the frequent clinical observations (Kohls-Gatzoulis et al. 2004) of spring ligament injury and plantar fasciitis with PTT injury. Unlike PFR which resulted in a larger increase in the long and short plantar ligaments, PTTD induced a larger straining effect on the spring ligament. This is comparable to the clinical findings by Deland et al. (2005) who identified the pattern of ligament involvement using MRI in 31 consecutive patients diagnosed with PTTD compared to an age matched control group. They found that ligament involvement was extensive with PTTD and that the spring ligaments were the most frequently and severely involved. Therefore, it can be speculated that PTTD will produce a larger reduction in the medial longitudinal arch and prolonged straining of the medial arch may result in further attenuation of the spring ligament and other ligamentous structures such as the plantar fascia and lead to subsequent pronated or flat foot deformity. In addition to treatment for posterior tibial tendinopathy or dysfunction, proper treatment is necessary to protect or prevent progressive failure of PTTD involved ligamentous structures.

The larger arch-flattening effect of PFR than that of PTTD predicted by the FE model was consistent with the experimental findings by Hansen et al. (2001), who showed that the directional changes of the hindfoot bones associated with unloaded PTT were consistent but were much smaller in magnitude than the effect of acquired flatfoot deformity. From the FE predictions, PFR resulted in a larger plantarflexed talotibial joint, dorsiflexed and inverted metatarsonavicular and metatarsotalar joints. From the FE predictions and experimental measurements, the most significant arch-flattening effect of PFR as compared to PTTD was the plantarflexed calcaneotalar joint and dorsiflexed and inverted metatarsonavicular and metatarsotalar joints, which represented a flattened longitudinal arch. The difference in experimental measurements between the PTTD and PFR were not significant. From the FE predictions, the pattern of joint motions in the sagittal and transverse planes produced by unloading the PTT in the intact condition and with PRF was consistent. The induced magnitude of sagittal rotations by PTTD was more pronounced with the PFR condition.

Several experimental studies (Hansen et al., 2001; Imhauser et al., 2004; Kitaoka et al., 1997d, 1998; Niki et al., 2001) have quantified the joint rotation of the foot with PTTD and PFR during simulated midstance positions. Because of the variation in structural and material properties of individual specimen as well as the differences in loading conditions and experimental setup, large variations in measured responses were found within and between the experimental studies. For the sake of comparison, a qualitative approach was used to compare the FE predictions to the experimental measurements in terms of the directional changes of joint motion. Table 5-1 shows the comparison between the FE predicted and experimentally measured joint motion during simulated midstance. The FE predictions were generally agreed with the experimental measurement in this study and from the literature. Discrepancies between the FE predictions and experimental measurements were found mainly in the transverse plane of motion.

As observed from the changes in joint motion especially at the foot arch upon unloading the PTT, both the FE predictions and experimental measurements suggested that the PTT provides stability to the longitudinal arch. Other experimental studies (Imhauser et al. 2004; Kitaoka et al, 1997d; Hansen et al. 2001; Niki et al. 2001; Thordarson et al. 1995) also provided a consistent agreement on the stabilizing role of PTT on the longitudinal arch of the foot. Hansen et al. (2001) and Imhauser et al. (2004) further suggested that the PTT was a strong invertor of the subtalar joint when the ligaments are intact. Imhauser et al. (2004) and Niki et al. (2001) suggested that the passive support from the ligamentous structures was important for the proper functioning of PTT in maintaining the normal joint position for the foot progression especially during the heel off phase. They further suggested that reconstruction for

PTTD might not be able to restore normal arch and hindfoot kinematics when a flatfoot deformity was present. These findings were comparable to the current FE predictions that sectioning the static structure such as the plantar fascia produced a more detrimental effect to the normal foot mechanics than PTTD alone. In additional, our experimental measurements showed that the arch-supporting function of PTT was reduced with an acquired flatfoot deformity. Therefore, conservative or surgical treatments for PTTD should consider restoring the PT function as well as reconstruction of any ligamentous structures involved.

Table 5-1. Comparison of the FE predicted and experimentally measured joint motion with posterior tibial tendon dysfunction (PTTD) and plantar fascia release (PFR) during simulated midstance.

| **Relative Bones** | **Relative Conditions** | **FE Predicted Joint Motion** | | |
|---|---|---|---|---|
| | | Sagittal | Coronal | Transverse |
| Talus to Tibia | PTTD / Intact | Plantarflexion (4/4) | Eversion (4/4) | External Rotation (2/4) |
| | PFR / Intact | Plantarflexion (1/1) | Eversion (0/1) | Internal Rotation (0/1) |
| | PFR+PTTD / PFR | Plantarflexion (2/2) | Eversion (2/2) | Internal Rotation (1/2) |
| | | | | |
| Calcaneus to Talus | PTTD / Intact | Dorsiflexion (3/3) | Eversion (3/3) | External Rotation (3/3) |
| | PFR / Intact | Plantarflexion (0/1) | Eversion (1/1) | External Rotation (1/1) |
| | PFR+PTTD / PFR | Dorsiflexion (1/1) | Inversion (0/1) | External Rotation (1/1) |
| | | | | |
| Navicular To Talus | PTTD / Intact | Dorsiflexion (1/1) | Eversion (1/1) | Internal Rotation (0/1) |
| | PFR / Intact | Dorsiflexion (1/1) | Eversion (1/1) | External Rotation (1/1) |
| | PFR+PTTD / PFR | Dorsiflexion (0/0) | Eversion (0/0) | External Rotation (0/0) |
| | | | | |
| 1st Metatarsal to Talus | PTTD / Intact | Dorsiflexion (1/1) | Eversion (0/1) | External Rotation (1/1) |
| | PFR / Intact | Dorsiflexion (1/1) | Inversion (0/1) | Internal Rotation (0/1) |
| | PFR+PTTD / PFR | Dorsiflexion (0/0) | Eversion (0/0) | External Rotation (0/0) |
| Ratio of Agreement | | 15/16 | 12/16 | 10/16 |

The ratio in bracket shows the number of agreements per the number of compared experimental studies in the literature (Hansen et al., 2001; Imhauser et al., 2004; Kitaoka et al., 1997d, 1998; Niki et al., 2001)

Although PTTD alone might not result in significant load redistribution of the foot bones and soft tissue structures, it might lead to progressive flattening of the longitudinal arch and subsequent acquired flatfoot deformity as a result of increased straining and attenuation of the arch-supporting soft tissue. From the cadaveric measurements, PTTD was found to increase the load on the medial foot structures and the strain of the plantar fascia. The role of PTTD in producing a more deformable and pronated foot structure was further supported by the FE predictions, which showed an increase in navicular stress and straining of the plantar fascia and ligamentous structures especially the spring ligament with PTTD. Therefore, possible degenerative joint symptoms, overstraining of the arch-supporting ligamentous structures and subsequent midfoot painful syndrome might arise with progressive PTTD related flatfoot deformity. The current FE prediction complies with the commonly observed clinical painful foot syndrome with diagnosed PTTD associated acquired flatfoot deformities (Brugh et al., 2002; Baumhauer, 1997). Orthotic (Kulig et al., 2006; Wapner and Chao, 1999) and surgical treatment must be prescribed to compensate, strengthen and restore the function of PTT in order to preserve the normal biomechanics of the longitudinal arch of the foot.

Apart from the simplifications of the structural and material properties of the defined bony and soft tissue structures, the following assumptions made for the FE simulations would affect the FE predicted response of simulated PTTD. First of all, the joint capsules and the tendon-bone surface interaction were neglected and the stabilizing role provided by these structures cannot be considered. Secondly, the tibia and fibula motion was constrained and the tibia rotations involved during weightbearing of the foot cannot be considered. Imhauser et al. (2004) suggested that constraining tibial rotation will stiffen the ankle and subtalar joints and reduced the associate effect of the PTT loading and result in larger rotational response of the navicular. Thirdly, the assumption of linear EMG-muscle force relationship for determining the tendon forces might result in large variations with the actual physiological tendon loads. In this study, a high (10-1) loading ratio between Achilles and PT tendons was used in this studies while different loading ratio including 7.5-1 (Thordarson et al. 1995), 6-1 (Niki et al., 2001; Kitaoka et al., 1997d), 3-1 (Imhauser et al., 2004) and 1.25-1 (Hansen et al., 2001) were used. The small or inconsistent joint movements recorded in the current study and other studies in the literature (Niki et al., 2001; Kitaoka et al., 1997d; Thordarson et al., 1995) may be attributed to this high loading ratio between the Achilles and PT tendons.

Besides the variations in the above assumptions made in different studies, the differences in order of tendon loading, which were not specified in many of the studies might result in discrepancy of results between studies. Imhauser et al. (2004) suggested that proper order of tendon loading was an important parameter for cadaveric foot simulations. In addition, some of the cadaveric studies on PTTD (Imhauser et al. 2004; Kitaoka et al, 1997d; Niki et al. 2001) employed a scale-down approach for simulation of multiple muscular loading and ground reaction forces because of the limitations in applying high tension forces via wiring and suture or other clamping techniques. As a result, the accuracy of these experimental studies to document the normal and physiological behaviour of the ankle-foot complex was unknown. Hansen et al. (2001) reported from their experiments that PTT forces of up to 1000 N and Achilles tendon forces of up to 1300 N were required at heel off with 75% body weight. The serrated plastic jaw clamp in this study was able to facilitate the application of physiological human tendon loading without slippage and damage of the clamped tendon.

## *5.6. Effects of Foot Orthoses*

### 5.6.1 Effects of Foot Orthosis on the Loading Response of the Foot

Rheumatoid foot pain and diabetic ulceration are closely related to abnormal plantar pressure distributions (Boyko et al., 1999; Charanya et al. 2004; Frykberg et al., 1998; Hodge et al., 1999; Lavery et al., 1998, 2003; Stess et al., 1997; Veves et al., 1992; Woodburn et al., 2002). Increasing evidence suggests that these painful foot syndromes or diseases can be successfully resolved or relieved by fitting a proper foot insole, helping to relieve elevated plantar pressures (Charanya et al. 2004; Hodge et al., 1999; Kato et al., 1996; Novick et al., 1993; Raspovic et al., 2000; Woodburn et al., 2002). To achieve an optimal foot support design for subjects with a specific foot deformity or functional requirement, it is essential to explore stress distribution across the plantar foot surface and bony structures. Pressure distributions between the foot and different supports have been measured by experimental methods with the use of in-shoe pressure sensors and a pedobarograph (Cavanagh et al., 1987; Charanya et al. 2004; Hodge et al., 1999; Hosein and Lord, 2000; Kato et al., 1996; Novick et al., 1993; Raspovic et al., 2000). Because of inherent difficulties and lack of better technology for that measurement, the load transfer mechanism and internal stress states within the soft tissues and the bony structures were not well addressed. Previous rationales behind the insole’s functional role load distribution and foot stabilization depended merely on subjective views or interfacial pressure measurements.

Today, computational modeling, such as the FE method, is a complementary tool to enhance our knowledge of foot biomechanics. Finite element analyses can predict the load distribution between the foot and supports, and provide information on the internal stress/strain states of the ankle-foot complex. The FE analyses enable efficient parametric evaluations to be made for the outcomes of insole shape and material modifications, without needing to fabricate and test orthoses in a series of patient trials.

Previous FE analyses have contributed to the understanding of biomechanical behaviour and performance of foot supports (Chen et al., 2003; Chu and Reddy, 1995; Chu et al., 1995; Erdemir et al., 2005; Goske et al., 2006; Lemmon et al., 1997; Shiang, 1997; Syngellakis et al., 2000). Researchers have used it to study what effects orthotic thickness and stiffness have on plantar soft tissue and plantar pressure distribution. In general, custom-molded, thicker and softer orthoses have been shown to reduce the peak plantar pressure and redistribute it in a more uniform pattern. However, a more detailed model of the human foot and ankle, incorporating realistic geometric and material properties of both bony and soft tissue components, is needed to enhance the reliability of the quantitative evaluations of different orthotic designs (Camacho et al., 2002; Kirby, 2001).

In this preliminary study, the ability of the developed FE model of the human foot and foot support to quantify the plantar pressure and the internal stress/strain in the bony and soft tissue structures during weightbearing was demonstrated. The predicted plantar pressure distribution pattern was, in general, comparable to the F-scan measurement. However, the predicted values of peak pressure were higher than the F-scan measurements. The difference may be caused by resolution differences between the F-scan measurement and the FE analysis. Having a spatial resolution of about 4 sensors per $cm^2$, the F-scan sensors recorded an average pressure for an area of 25 $mm^2$. By contrast, the FE analysis provided solutions of nodal contact pressure rather than an average pressure calculated from nodal force per element surface area. The measured peak plantar pressure was therefore expected to be smaller than the predicted values.

The predicted peak von Mises stress showed that the midshaft of the second and third metatarsals sustained the highest bone stress. The high plantar pressures beneath the metatarsal heads and the confined positions of these metatarsals, especially with tissue stiffening, are probably the cause of stress concentration. Apart from the midshaft of the metatarsals, the junctions of the subtalar and calcaneocuboid joints also sustained high bone stresses under weightbearing. The use of softer insole, especially the custom-molded insoles, is effective in reducing the bone stress in the forefoot and midfoot regions.

From the FE prediction, the change in supporting conditions would strongly affect the pressure distribution of the plantar foot. This hypothesis is supported by experimental findings (Kato et al., 1996; McPoil and Cornwall, 1992; Novick et al., 1993). Kato et al. (1996) reported a range of 19% to 80% mean peak plantar pressure reduction with the use of foot orthoses in 13 diabetic patients. Novick et al. (1993) reported mean peak plantar pressures of 0.164, 0.011, and 0.142 MPa for the heel, midfoot, and metatarsal regions, respectively, during walking with a flat, soft insole. The corresponding values for the custom-molded, rigid insole were 0.18, 0.019, and 0.143 MPa. These measurements were consistent with the FE prediction, reflecting the corresponding pressure-relieving and pressure-redistributing abilities of the soft, custom-molded insole. Kato et al. (1996) reported a mean increase in postorthotic contact area of about 63%, which was comparable to the FE prediction (59.7%). Both a softer material and a custom-molded shape were found to have a role in the reduction of peak plantar pressure. These insoles aided in assimilating the plantar pressure in a more uniform manner than a rigid, flat insole, which tended to concentrate the load at the heel and beneath the first and second metatarsal heads. The custom-molded insoles enabled a more uniform distribution of pressures, whereas soft, flat insoles provide localized pressure relief. The custom-molded insoles were more effective in redistributing the plantar pressure to the midfoot region than the soft, flat insole. The FE prediction indicated that an appropriate insole can reduce high plantar pressure and may relieve pressure related foot pain, especially for persons with stiff plantar tissue. The FE model may help researchers design an optimal foot support with appropriate insole shape and material properties to suit patients' individual needs.

In addition to providing a more uniform plantar pressure pattern, use of custom-molded insoles reduced the strain of the plantar fascia. The arch support provided by the custom insoles reduced foot lengthening and tension on the fascia during load bearing. The results thus suggested a possible therapeutic effect of custom orthoses in terms of stress relief of the plantar fascia and relief of associated foot problems, such as plantar fasciitis or insertional painful heel syndrome. The plantar fascia strains (0.37-0.49%) predicted by FE analysis were consistent with the strain of about 0.5% reported by Kogler et al. (1995), who used a microstrain transducer to measure the plantar fascia strain of cadaveric specimens with a similar magnitude of compressive loading.

Finite element analysis supports the use of soft, custom-molded insoles for redistributing plantar foot pressure. Particular care should be taken in prescribing the insoles to avoid complications from redistributed pressures. In fact, the foot's soft-tissue compliance should be among the factors used to decide which type of orthosis and the material prescribed. For instance, diabetic patients with neuropathic ulcers may need a semi-rigid, custom-fitted insole to redistribute the localized pressures, whereas an elderly patient with a lack of plantar fatty pads may require use of a softer insole. Localized tissue sensitivity of the plantar foot should be inspected and the insole should be modified and evaluated as appropriate. To achieve a balance between pressure relief and control of foot motion, it may be necessary to provide a properly rigid functional orthosis that can achieve optimal efficacy. This consideration particularly applies to patients requiring multipurpose treatments.

To simplify the analysis in this study, we assigned homogeneous and linearly elastic material properties to the model. The ligaments within the toes and other connective tissue, such as the joint capsules, were not considered. Use of homogeneous material and linearity of the encapsulated soft tissue stiffness was a simplification of the real situation. Only the Achilles' tendon loading was considered, whereas other intrinsic and extrinsic muscle forces were not simulated. The location of centre of pressure was assumed unchanged with the simulations of different insole supports.

Although the dynamic response during walking was not considered in the present model, the pain experienced during standing might be related to that experienced while walking (Hodge et al., 1999). The static pressure response of the plantar foot, which is more readily available in most clinical settings, can thus be a possible indicator of the plantar foot pain that patients experience during gait. With further improvements and appropriate simulations, the FE model may aid in developing and prescribing a pressure-relieving orthosis pertinent to individual needs.

The FE analysis indicated that the insole's custom-molded shape is more important in reducing peak plantar pressure than the stiffness of the material from which it is made. A comprehensive FE ankle-foot model makes monitoring the parametric effect of different insole shapes and material properties more efficient. The FE model is an ideal clinical tool to investigate foot behaviour under different supports and to explore the design of various forms of foot support.

### 5.6.2 Parametrical Analysis on Pressure Relieving Foot Orthoses

Therapeutic footwear and custom-molded foot orthosis are frequently prescribed in routine clinical practice to prevent or treat plantar ulcers in diabetes by reducing the peak plantar pressures. However, the fabrication and design of insoles and footwear vary among clinical practitioners and industries and little information about the parametrical effects of different combinations of design factors is available. A large number of studies in the literature (Brown et al. 1996; Busch and Chantelau, 2003; Lavery et al., 1997; Linge, 1996; Lobmann et al., 2001; Viswanathan et al., 2004; Windle et al., 1999) focused on the performance of off-the-shelf footwear, orthosis and material without comprehensive quantifications of their structural and material characteristics. For the fabrication of custom foot orthosis, the principles and techniques currently used in prescribing an orthosis are largely based on the theoretical model proposed by Root (Root et al., 1971) for functional foot orthoses. Owing to the large variations of prescribed footwear and uncertainty in reliability and validity of the assessment and intervention methods, consistent outcomes can yet be achieved and conflicting results are common in terms of functionality of footwear (McPoil and Hunt, 1995; Nawoczenski et al. 1995; Reiber et al., 2002; Stacoff et al., 2000).

Although the use of therapeutic footwear has been found to be beneficial in plantar pressure relief and effective in the prevention of foot ulceration in diabetes (Busch and Chantelau, 2003; Hodge et al., 1999; Kato et al., 1996; Lavery et al., 1997; Lobmann et al., 2001; Novick et al., 1993; Raspovic et al., 2000; Viswanathan et al., 2004), there is no clear understanding of the design factors which contribute most to reduction of pressure and thus the approach to treatment and relief of symptoms is often largely empirical. The design and modification of a foot pressure-relieving orthosis relies mainly on subjective views and interfacial pressure measurements. Many suggested there was still a lack of consensus on the appropriate application of shape, material properties and placement of foot orthoses for different foot types or injuries (Ball and Afheldt, 2002; Landorf and Keenan, 2000; Nigg et al., 1999; Razeghi and Batt, 2000; Stacoff et al., 2000).

In fact, ulcer recurrence is still common among diabetes (Mantey et al., 1999; Reiber et al., 2002) in spite of the use of therapeutic footwear and the rationale behind the functional performance and prescription of therapeutic footwear has been challenged (McPoil and Hunt, 1995; Reiber et al., 2002). A review on randomized studies on pressure relieving interventions for preventing and treating diabetic foot ulcers conducted by Spencer (2000) found that the evidence of the effectiveness of orthotic interventions and therapeutic shoes is still limited and controversial. Reiber et al. (2002) further suggested from their randomized clinical studies that careful attention to foot care by health care professionals might be more important than therapeutic footwear.

Currently, limited well-controlled studies evaluating the efficiency and functional mechanism of variety designs of foot orthosis are available and the biomechanical rationale behind the optimal or appropriate design of foot orthosis is still unclear. More in-depth and comprehensive studies are needed to evaluate and analyze the effect of various orthotic interventions on biomechanical effects of the ankle-foot complex under various loading and supporting conditions. As an alternative to the experimental approach, a comprehensive FE model of the foot and footwear can provide efficient sensitivity analysis on the effect of different combinations of structural and material design factors on peak pressure reduction.

In this study, the pressure-relieving capability of different material and structural configurations of foot orthosis were quantified using the developed FE model of the human foot and foot support. Among the five design factors (arch type, insole material, insole thickness, midsole material and midsole thickness) considered in this study, the use of an arch-conforming foot orthosis and a softer insole material was found to be effective in the reduction of peak plantar pressure with the former provided a larger pressure reduction. Insole thickness, midsole stiffness and midsole thickness were found to contribute to less pronounced roles in peak pressure reduction.

It should be noted from the deviations of predicted peak plantar pressure using the optimized configurations of the foot orthosis between the superposition method and the FE model that there might be an interaction of design factors at particular configurations that may outweigh the individual effect of the design factor on pressure reduction. There might also be a limit in peak pressure reduction considering merely the combination of the current five design factors of foot orthosis. For instance, further decreasing the stiffness of the orthotic material or increasing the thickness might have a diminished effect on peak pressure reduction.

Depending on the purpose of the foot orthosis such as the target region of pressure relief and its confounding conditions of the actual situations such as the overall height of the foot orthosis and size or in-depth of the shoes, the optimized design of the pressure-relieving foot orthosis may be highly individualized. Therefore, the optimized configurations may need to have further adjustments according to the degree of importance and predicted responses for each design factor in order to a achieve the best overall performance for individual foot structure and requirement.

In general, the plantar pressure measurement agreed with FE predictions that the use of a softer insole material and an arch-supporting foot orthosis was effective in the reduction of peak plantar pressure with the latter had a larger reducing effect. However, the measured trend and magnitude of peak plantar pressure reduction was less pronounced and consistent comparing to the FE predictions. The discrepancy was probably due to the differences in the effect of interaction between the foot orthosis and the footwear. It might also be due to a change in pattern and speed of walking in different orthotic conditions and with different trials. The effect of an increasing insole thickness and the optimal combinations of insole and midsole thickness deserve further experimental justifications of different configurations of foot orthosis with standardized extra-depth footwear.

Apart from the structural and material simplifications of the FE model, certain simplifications and assumptions of the FE simulations might affect the accuracy of the results. First of all, the interaction between the foot and the shoe surface was not considered. This would result in a less confined foot position and larger foot deformation. Secondly, only the midstance position was considered whereas peak plantar pressure and shear occurred during heel strike and push-off might be more relevant to the cause of diabetic ulceration. Thirdly, the current simulation considered only the static condition while the inertia effect and loading response of the foot during dynamic walking were not addressed. Fourthly, the same loading and boundary conditions as well as the frictional properties of the foot-support interface for simulations of different design configurations of foot orthosis was assumed. Finally, the current simulations considered only the response of a normal foot structures. The effect of the same foot orthosis on other foot types or structures such as flatfoot, high-arched and with other deformities was not addressed and deserved further investigations.

The developed FE model could allow efficient parametric evaluations for the outcomes of the shape modifications and other design parameters of the orthosis without the prerequisite of fabricated orthosis and replicating patient trials to series of orthoses. This will certainly simplify the decision process as to which specific foot orthosis may be best suited for each patient. The emergence of computer-aided design can therefore lead to an effective manufacture process and better design by providing a parametrical analysis to determine an appropriate shape and stiffness of the orthosis for specific functional requirements so as to provide an effective and optimal load distribution and stabilization to maximize the subject comfort and gait performance.

### 5.6.3 Guidelines on the Design of Pressure-Relieving Foot Orthosis

Footwear and orthotics play an important role in reduction of peak plantar pressure related foot ulceration in people with diabetes especially for those with neuropathy, or lack of sensation. Poorly fitted shoes often lead to ulceration and subsequent amputations in diabetes. While proper footwear provides the primary element for diabetic foot care and pressure relief, the use of foot orthotics maximizes the functional role of the therapeutic footwear as a whole. The functionality of a foot orthosis depends on the availability of proper footwear for the accommodation of the prescribed foot orthosis. Footwear should therefore be properly fitted to provide comfort and protection of the diabetic foot by providing adequate room in the toe area, over the instep, and across the ball of the foot, and around the heel, which should also provide extra in-depth for the accommodation of foot orthotics.

According to Tyrrell (1999), foot orthosis for diabetes should increase cushioning for shock absorption. Foot orthosis should also redistribute and reduce the excessive plantar pressure or shear from the vulnerable areas to those tolerable areas by enabling total contact with the plantar foot of the patient. In addition, foot orthosis should support and align the joints of the foot in proper position for weightbearing and propulsion and to accommodate or correct foot deformities.

From the FE parametrical analysis of the foot orthosis, the use of a custom arch support was found to be an important design factor for peak plantar pressure reduction. The FE predictions agreed with the experimental findings by Tsung et al. (2004) and Bus et al. (2004) who found that the use of custom-molded insoles was significantly better than flat insoles in terms of peak pressure reduction. Among the three insole conditions (non-weightbearing, semi-weightbearing, full-weightbearing) in the study by Tsung et al. (2004), the insole with the semi-weightbearing foot shape was found to provide the greatest peak pressure reduction, especially for patients with peak pressure located at the second to third metatarsal heads. It should however be noted that the use of the same custom design may result in significant differences in performance for individual foot structure. For instance, Bus et al. (2004) found considerable variability in the efficiency for the same custom design between individuals although most pressure redistribution occurred from the lateral heel to the medial midfoot regions.

In addition, custom-molded orthoses with an additional metatarsal pad or rearfoot wedges were found to be more effective for pressure relief than the use of custom-molded orthosis alone in some studies (Hodge et al., 1999; Kato et al., 1996; Redmond et al. 2000) while other studies (Armstrong et al., 1995; Ashry et al. 1997; Van Gheluwe and Dananberg, 2004) found that additional arch support, metatarsal padding or insole wedging produced negligible or adverse effects on pressure distribution. These findings further suggested that the efficiency of a custom-molded foot orthosis for pressure relief was highly individualized with the differences in foot structure or arch type.

For the use of additional padding or support, knowledge on the proper use of different dimensions and placements of additional padding was important to achieve a better orthotic treatment for pressure relief. For instance, Hayda et al. (1994) reported that the differences in placement and size of metatarsal pad resulted in a variation in plantar pressure distribution. In general, smaller pad caused the greatest and most consistent decrease in metatarsal plantar pressure while a more distal positioning of the pad cause the greatest decreases in pressure for all pad types. Another study by Chang et al. (1994) further suggested that redistribution of plantar pressures related not only to the dimensions of the metatarsal pads, but also to foot size, anatomic foot configuration, and pad location. Therefore, determination of an optimized custom-molded shape to fit the dynamic foot response during gait might be important in maximize the functional performance of foot orthosis. Depending on the flexibility of individual foot arch structures, the optimal arch type/height of the foot orthosis may vary. For instance, patient will a more deformable foot arch may require a full- or half-weightbearing arch type for the custom orthosis. Alternatively, patent with a rigid arch structure may require a non-weightbearing of an even higher arch type or an additional padding for foot arch support and pressure redistribution. It should also be reminded from other experimental studies (Brown et al., 1996) that pressure relief in certain area provided by the arch-supporting foot orthosis might be compromised with an increasing pressure in other areas of the plantar foot.

From the FE predictions, the second important factor for peak pressure reduction is the use of a soft cushioning insole material. The FE predictions suggested that the stiffness of the insole layer should of hardness value less than $20^0$ in order to maximise its pressure-relieving capability. It should however be noted that the optimal insole stiffness would depend on the expected pressure on the insole, which is determined from the body weight, and activities involved of the patient. The FE model predicted a pronounced inverse relationship between insole thickness and peak plantar pressure, consistent with the experimental findings in the literature (Birke et al., 1994; Linge, 1996). Depending on the in-depth of the footwear, a cushioning insole layer of no less than 9 mm was suggested from the FE predictions. However, the optimal or possible insole thickness for use in actual situation would need to consider the issue of reduced proprioception and propulsion efficiency, which deserves further investigation.

Comparing to the insole layer, the material and thickness of the midsole layer were found to contribute to a much lesser extent in peak pressure reduction. This finding agrees with the common clinical practice that the midsole layer is for use with foot support or motion control. From the FE predictions, the change in peak plantar pressure of the midfoot was insensitive further reduction of midsole stiffness below hardness value of $30^0$. Besides, the predicted change in peak plantar pressure was not sensitive to the midsole thickness. Therefore, a relatively stiffer and thinner midsole layer made from a more durable material was suggested for fabricating the foot orthosis. The midsole layer should consist of material of hardness value no less than $30^0$ to achieve its supporting purpose. Experimental measurements by Linge (1996) showed that the addition of a shank to control insole rigidity reduced the overall peak pressures under the foot. In addition, clinical studies in the literature (Chalmers et al., 2000) reported that semi-rigid orthoses was more effective than soft orthoses in terms of pain relief. Again, to what extent the midsole stiffness would be needed to achieve the necessary function on foot support and motion control deserves further investigation.

By and large, a custom pressure-relieving foot orthosis should provide the best total contact fit of the plantar foot of the patient during weightbearing. The cushioning insole layer should contribute majority of the thickness of the foot orthosis to maximise peak pressure reduction. The use of extra-depth footwear in diabetes was highly recommended for the accommodation of custom foot orthosis consisting of a thick, cushioning insole layer. The FE predictions suggested that the custom-molded total-contact foot orthosis was effective in peak plantar pressures and would play an important role in the prevention of foot ulceration in diabetes.

It should be noted that the design guidelines for pressure-relieving foot orthosis established from the FE simulations and validation of a single subject, representing individual geometrical properties. In addition, only a single instance of the stance phase of gait was simulated in a static condition and the influence of the shoe-orthosis-foot interface was not considered. Therefore, the orthotic performance during different load bearing and dynamic conditions and the generalization of the current FE simulations for the response of the general population deserve further computational and experimental investigations.

The ability of the developed FE model for the parametrical designs of foot orthosis was justified in this study. Further investigations on the biomechanical effects of different types of foot orthosis can be used to refine the design principles of orthosis in the CAD/CAM process in terms of appropriate shape and material of the orthosis in order to fit specific functional requirements of the subject and individual foot structure. The ultimate goal of the developed computational system is to establish the knowledge-based criteria to provide systemic guidelines for clinician to prescribe and fabricate an optimized orthosis to maximize the functions of the foot orthoses as well as the subjects' comfort and gait performance.

## *5.7 Limitations of the Finite Element Simulation*

To simplify the FE analysis, homogeneous and linearly elastic material properties were assigned to the bony and ligamentous structures and the ligaments within the toes and other connective tissues such as the joint capsules were not considered. Besides, the use of linear truss elements to approximate the nonlinear profile of the plantar fascia and other ligamentous structures was a gross assumption. The current FE model did not account for the surface interactions between bony, ligamentous and musculotendon structures and the stabilizing role provided by these structural interactions cannot be considered. These structural simplifications of the FE model would probably result in a reduction of joint stability of the ankle-foot structures and an increase in predictions of joint and arch deformation.

Apart from the simplifications of the structural and material properties of the defined bony and soft tissue structures, the following assumptions on the loading and boundary conditions made for the FE simulations would affect the accuracy of the FE predictions. First of all, only the major extrinsic musculotendon forces were considered while other intrinsic muscle forces were not simulated. Fiolkowski et al. (2003) reported a drop in navicular height of the standing subjects after decreasing the activity of the intrinsic muscles by injection of lidocaine to block the tibial nerve, indicating that the intrinsic muscles might play an important role in supporting the medial longitudinal arch. Therefore, the predicted foot responses from the current FE simulations likely underestimated the stiffness of the actual foot structure.

In addition, the variations in the loading or walking pattern of the subject such as the changes in location of centre of pressure and muscular reaction under different simulated pathological and orthotic conditions were assumed the same. Besides, the relationship between the EMG signals and muscle forces output are nonlinear in nature, which varies with individual muscle structures, joint positions, amplitudes of muscular forces and loading conditions, etc. Therefore, the assumption of linear EMG-muscle force relationship for determining the tendon forces might result in large variations with the actual physiological tendon loads. The tibia and fibula motion was constrained and the coupling between the lower leg and the rearfoot especially the tibia rotations involved during weightbearing of the foot cannot be considered.

In this study, only balanced standing and the midstance position were simulated while the more complex and high load-bearing stance phases such as push-off and heel strike were not analysed. Static condition was considered in all simulations and the biomechanical effects of inertial forces and history of loading during the dynamic conditions cannot be addressed.

The developed model represented a normal arch configuration whilst the arch stability or stiffness is individualized with different foot structures. Owing to the use of geometrical accurate model, the generalization of the current FE prediction remains questionable. Improvement on certain aspects of the FE model and more comprehensive simulations of various physiological loading conditions on different foot types in addition to experimental validations are needed to obtain a more representative and generalized solution.

Owing to the limitations of automatic meshing algorithm in ABAQUS, the geometrically complex bony and soft tissue structures were meshed using the tetrahedral elements. The accuracy of the FE predictions can be increased with the use of hexahedral elements, which provide better accuracy under larger deformation. To what extent the accuracy of the current FE mesh could provide was not yet known and rigorous convergence and sensitivity tests on the element types and mesh density should be conducted before a conclusion can be made.

# CHAPTER VI CONCLUSIONS AND FUTURE WORK

## *6.1 Conclusions*

Because of the difficulties to understand the biomechanics of the complicated human foot and ankle structures from experimental studies alone, computational model is needed to provide a viable alternative to predict their biomechanical behaviour. In this study, a 3D FE model of the human foot and ankle was developed from 3D reconstruction of MR images from the right foot of a male adult subject. The developed FE model, which took into consideration the nonlinearities from material properties, large deformations and interfacial slip/friction conditions consisted of 28 contacting bony structures, 72 ligaments and the plantar fascia embedded in a volume of encapsulated soft tissue. The developed geometrically accurate 3D FE models of the foot and ankle considered the first time in the literature the relative motion of all the major foot joints by a surface-to-surface contact approach. The FE model considered realistic nonlinear material properties of the encapsulated soft tissue reported from the experimental studies in the literature. The loading response of the FE model was validated by experimental measurements of the same subject who underwent the MR scanning and the experimental studies in the literature. The FE predictions were found to be reasonably complied with the experimental measurements and certain aspects for improving the accuracy of the FE model were identified

In the parametrical analyses of the FE foot model, the biomechanical effects of varying stiffness of the encapsulated bulk soft tissue and the plantar fascia were investigated. An increase in bulk soft tissue stiffness from 2 and up to 5 times the normal values was used to approximate the pathologically stiffened tissue behaviour with increasing stages of diabetic neuropathy. The results showed that increasing soft tissue stiffness led to a decrease in the total contact area between the plantar foot and the horizontal support surface and pronounced increases in peak plantar pressure at the forefoot and rearfoot regions. The effect of bulk soft tissue stiffening on bone stress was found to be minimal. A sensitivity study was conducted to evaluate the biomechanical effects of varying elastic modulus (0–700 MPa) of the plantar fascia. The plantar fascia was found to be an important stabilizing structure of the longitudinal arch of human foot during weightbearing and decreasing the stiffness of plantar fascia would reduce the arch height, increase the strains of the long and short plantar and spring ligaments. In addition, surgical releases of partial and the entire plantar fascia were simulated. Plantar fascia release (PFR) increased the strains of the plantar ligaments and intensified stress in the midfoot and metatarsal bones. Partial and total PFR decreased arch height and resulted in midfoot pronation but did not lead to the total collapse of foot arch even with additional dissection of the long plantar ligaments. The FE model implicated that PFR may provide relief of focal stresses and associated heel pain. However, these surgical procedures may pose a risk of developing arch instability and clinically may produce lateral midfoot pain. For surgical treatments of plantar fasciitis, partial release of less than 40% of the fascia was found to induce the least disturbance to arch stability and normal foot biomechanics. The FE predictions suggested that the initial strategy for treating plantar fasciitis should be nonoperative. Surgical release of the plantar fascia, if necessary, should consider only partial release of the plantar fascia to minimize the effect on its structural integrity.

The biomechanical effects of Achilles and posterior tibial tendon loading were investigated. A positive correlation between Achilles tendon loading and plantar fascia tension was found. With the total ground reaction forces of one foot maintained at 350 N to represent half body weight, an increase in Achilles tendon load from (0-700 N) resulted in a general increase in total force and peak plantar pressure at the forefoot. There was a lateral and anterior shift of the centre of pressure and a reduction in the arch height with an increasing Achilles tendon load. From the FE predictions of simulated balanced standing, Achilles tendon forces of 75% of the total weight on the foot (350 N) were found to provide the closest match of the measured centre of pressure of the subject during balanced standing. Both the weight on the foot and Achilles tendon loading resulted in an increase in tension of the plantar fascia with the latter showing a two-times larger straining effect. From the FE predictions, overstretching of the Achilles tendon and tight Achilles tendon are plausible mechanical factors for overstraining of the plantar fascia and subsequent development of plantar fasciitis or heel pain. The effect of posterior tibial tendon dysfunction (PTTD) on intact and flat-arched foot structures was investigated during simulated midstance. Unloading the posterior tibial tendon increased the arch deformation and strains of the plantar ligaments especially the spring ligament. The arch-flattening effect of PTTD was smaller than that from PFR. The lack of foot arch support with PFR and PTTD may lead to attenuation of surrounding soft tissue structures and elongation of foot arch, resulting in a progressive acquired flatfoot deformity.

The developed FE model can be used in clinical applications to investigate the foot behaviour of different gait pattern and to design a good foot support. Because of the ability of the FE model to identify vulnerable skeletal and soft tissue components of the foot, it can be used not only for understanding the development mechanisms of some common disorders like diabetes, arthritis and stress fractures, etc, but also to serve as a tool for development of novel clinical decision making and foot treatment approaches. In terms of orthotic/footwear design, the FE model could allow efficient parametric evaluations for the outcomes of the shape modifications and other design parameters of the orthosis without the prerequisite of fabricated orthosis and replicating patient trials.

From the parametrical analyses of the FE model, the custom-molded shape was found to be a more important design factor in reducing peak plantar pressure than the stiffness of the orthotic material. Besides the use of an arch-supporting foot orthosis, the insole stiffness was found to be the second most important factor for peak pressure reduction. Other design factors contributed to a less pronounced role in peak pressure reduction in the order of insole thickness, midsole stiffness and midsole thickness. Custom pressure-relieving foot orthosis providing total contact fit of the plantar foot of the diabetic patients during weightbearing was an important treatment strategy for plantar pressure related diabetic ulceration. A custom orthotic device and extra-depth footwear should be prescribed to diabetic patients at risk of plantar ulceration whenever possible and available.

With further improvement and development of the FE model, the FE predictions on the biomechanical effect of different types of foot orthosis can be used to refine the design principles of orthosis in the CAD/CAM process in terms of appropriate shape and material of the orthosis in order to fit specific functional requirements of the subject and individual foot structure. Comprehensive knowledge-based criteria for designing foot orthoses can be established to provide systemic guidelines for clinicians to prescribe and fabricate an optimized orthosis to maximize the functions of the foot orthoses as well as the subjects' comfort and gait performance.

## *6.2 Directions of Further Studies*

A number of further studies can be done, which are directed to the improvement of the current FE model. These include refinements and improvements of certain simplifications and assumptions of the current FE model as follows:

1. Advanced material model such as hyperelastic, orthotropic, and viscoelastic models can be incorporated in the FE model to enable a realistic simulation of the mechanical behaviour of the foot soft tissue.

2. Material testing can be done to extract the soft tissue properties of foot in order to establish the aforementioned material models for the FE model. This may include compression test on the plantar soft tissue, tensile test on the plantar fascia and other ligamentous structures (Fig. 6-1).

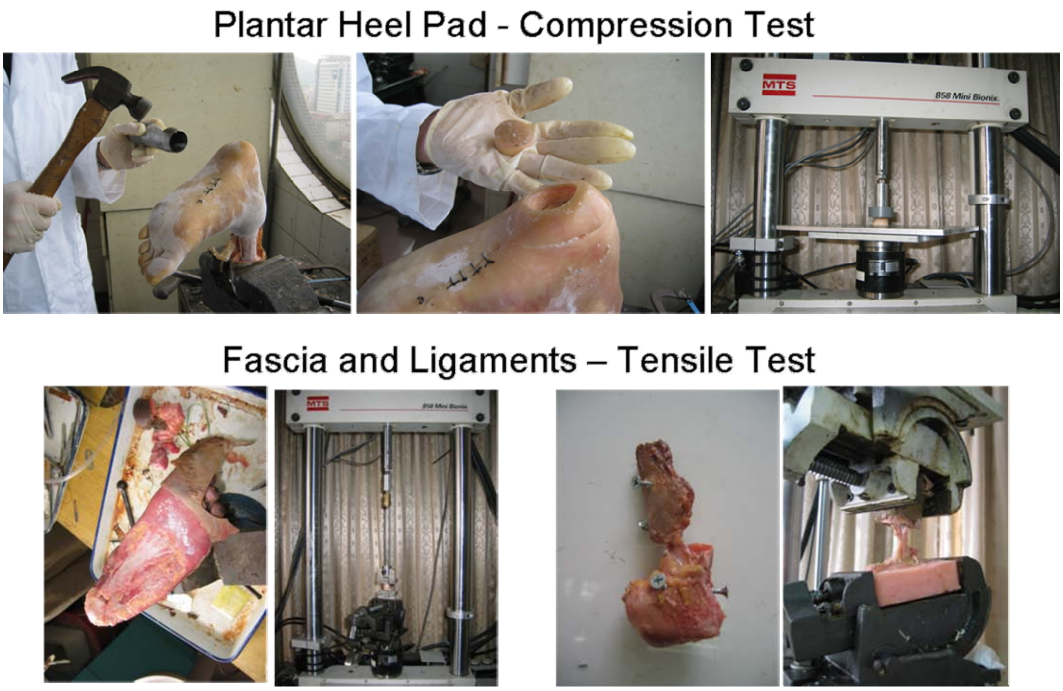


Figure 6-1. Mechanical testing of foot soft tissue.

3. Three-dimensional structural modeling of the ligamentous and musculotendon structures can be incorporated to simulate more accurately the stabilizing role provided by these structures and the interactions with the bony and encapsulated soft tissue structures.

4. Refinements on simulating the foot joints can be done by incorporating the structures of the hyaline cartilage of the contacting joint surfaces and associated joint capsules.

5. Further investigations on other design factors of foot orthosis such as different custom-molded shapes, shank and arch profiles, metatarsal paddings, forefoot and rearfoot wedges, magnitudes of heel elevation and distributions of material stiffness can be done (Fig. 6.2).

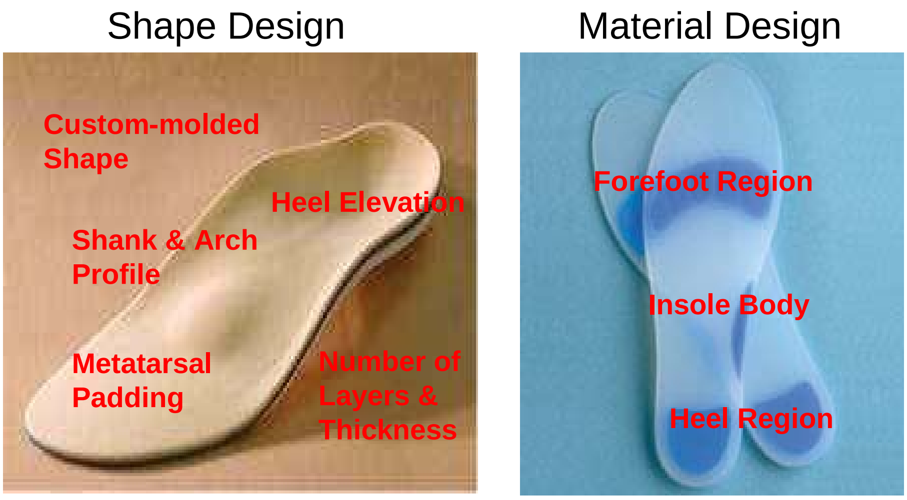


Figure 6-2. Design factors of foot orthosis.

6. The interactions between the foot and shoe structures can be incorporated (Fig. 6-3).

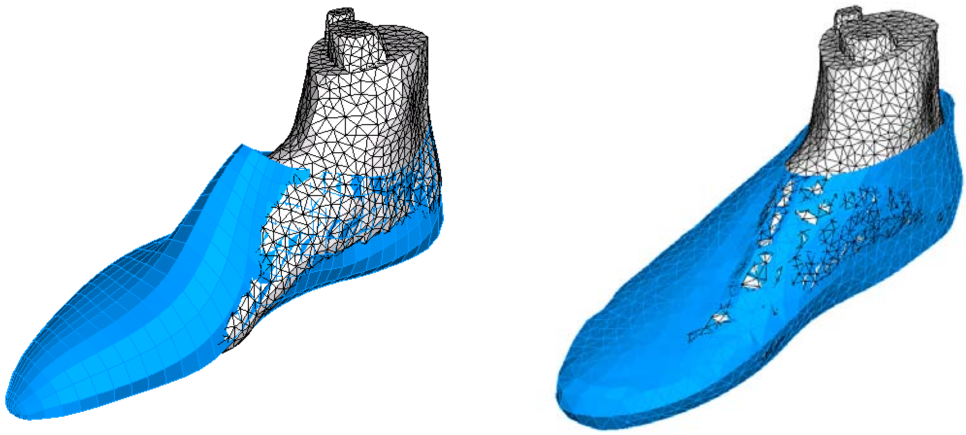

Figure 6-3. Finite element models for simulating foot-shoe interface.

7. The current FE model can be extended to the knee joint level (Fig. 6-4).

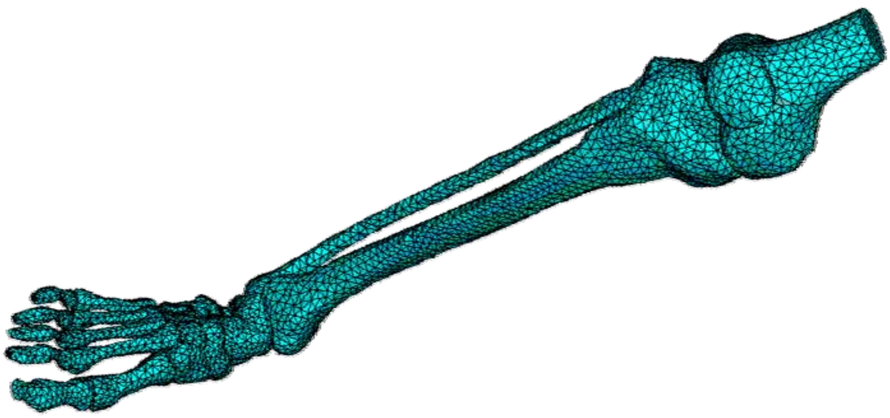

Figure 6-4. Finite element model of the knee-ankle-foot structures.

# APPENDIX

## *A serrated jaw clamp for tendon gripping*

Application of muscular tendon forces in cadaveric studies (Erdemir et al., 2004; Imhauser et al., 2004; Kitaoka et al., 1997d) requires the use of a clamp to hold the tendon rigidly at high loads without damaging it. Because of the low friction between the material of the devices and wet soft collagenous tissues, difficulties are encountered in gripping the tendon ends effectively to avoid tendon slippage. One of the solutions to increase the friction of the tendon clamp interface is to compress the tendon using serrated jaws. In this study, a custom-made, serrated jaw clamp was fabricated to apply tendon forces for the cadaveric foot simulation.

Plastic racks (Kohara Gear Industry Co., Ltd., Japan) made of molded nylon resin (Fig. 1a) of hardness, HRR115-120 were used to fabricate the tendon clamp. The plastics are able to work with the heat generated from machining. The pitch of the plastic rack is about 5 mm with the indentations of about 3.5 mm deep at an angle of 20 degrees (Fig. A-1a). The two parallel serrated clamp plate (Fig. A-1b) can be pressed together with four M6/M4 screws.

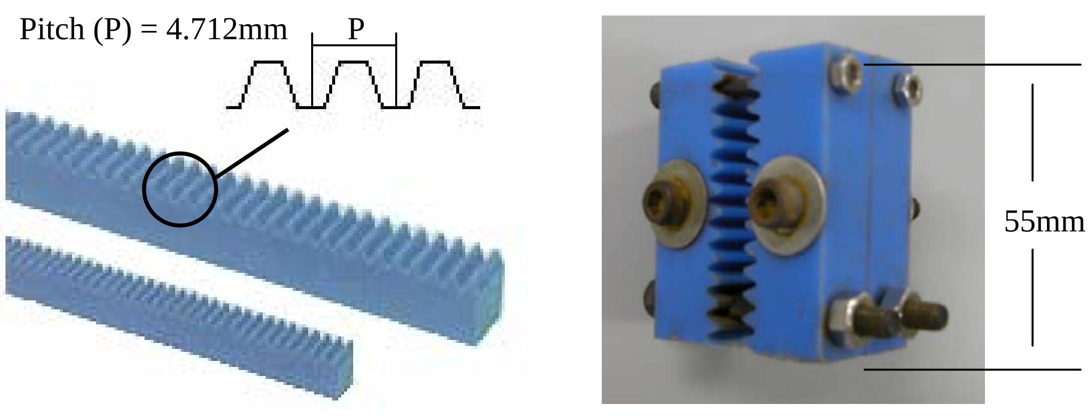


(a) (b)

Figure A-1. (a) Plastic racks of different sizes and (b) the custom-made serrated jaw clamp.

The capacity of the tendon clamp was tested in uniaxial tension using a Hounsfield material testing machine (Model H10KM, Hounsfield Test Equipment, UK) with a 10 kN load cell (Fig. A-2a). The tested bovine tendon had width and thickness of about 16 mm and 7.5 mm, respectively. The initial grip-to-grip distance was about 60 mm for the tests. The serrated jaw clamp was able sustain tension forces of more than 2500 N and strain of about 30% without slippage and cutting of the bovine tendon (Fig. A-3).

(a) (b)

Figure A-2. (a) Tensile testing of the bovine tendon being mounted by the custom-made serrated jaw clamps on the Hounsfield material testing machine. (b) Tendon clamp test on the human Achilles tendon via deadweight of 1800 N.

The ability of the tendon clamp to hold the Achilles tendon of human foot was evaluated by applying deadweight (Fig. A-2b). A cadaveric foot was mounted in an inverted position with the plantar foot in contact with a ground support. The clamp was successfully used to apply a static weight of about 1800 N for more than 30 minutes to the human Achilles tendon without slipping and cutting of the tendon (Fig. A-2b). The applied deadweight corresponded to measured vertical ground reaction forces of about 800 N on the plantar forefoot. Visual slippage of the tendon was monitored and the vertical ground reaction force was measured by F-scan pressure sensors (Tekscan Inc., Boston, USA).

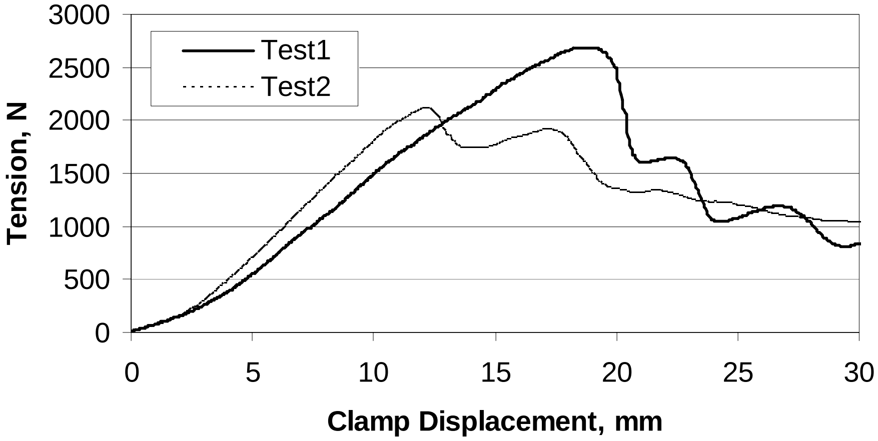


Figure A-3. The tension versus clamp displacement plot of the bovine tendon in two consecutive tests. Test 2 was done immediately after tendon slippage occurred in test 1.

Many of the cadaver studies in the literature have not considered the contributions of the investing muscles because of the difficulties in applying high tension forces via wiring and suture or other clamping techniques (Imhauser et al., 2004; Kitaoka et al., 1997d). These cadaveric studies employed a scale-down approach for simulation of multiple muscular loading and ground reaction forces because of the limitations in simulating muscle activity in the laboratory. As a result, the accuracy of their experimental set-up to document the normal and physiological behaviour of the musculoskeletal system, especially the shoulder and ankle-foot complex, where muscular contraction is an important stabilizing factor during human locomotion, was unknown.

The plastic serrated jaw clamp designed in this study was able to apply physiological human tendon loading without slippage and damage of the clamped tendon. Therefore, the actual tendon loading on the foot can be applied to provide a more physiological simulation of the loading response of the foot.

# REFERENCES


ABAQUS theory and user's manual, version 6.4, 2004. Hibbitt, Karlsson and Sorensen Inc., Pawtucket, RI, USA.

Ahn TK, Kitaoka HB, Luo ZP, An KN, 1997. Kinematics and contact characteristics of the first metatarsophalangeal joint. Foot Ankle Int. 18, 170-174.

American Diabetes Association, 2005. (http://www.diabetes.org).

Anderson DJ, Fallat LM, Savoy-Moore T, 2001. Computer-assisted assessment of lateral column movement following plantar fascial release: a cadaveric study. J Foot Ankle Surg. 40, 62-70.

Arangio GA, Chen C, Salathe EP, 1998. Effect of varying arch height with and without the plantar fascia on the mechanical properties of the foot. Foot Ankle Int. 19, 705-709.

Arangio GA, Phillippy DC, Xiao D, Gu WK, Salathe EP, 2000. Subtalar pronation-relationship to the medial longitudinal arch loading in the normal foot. Foot Ankle Int. 21, 216-220.

Armstrong DG, Liswood PJ, Todd WF, 1995. Potential risks of accommodative padding in the treatment of neuropathic ulcerations. Ostomy Wound Manage. 41, 44-46, 48-49.

Ashry HR, Lavery LA, Murdoch DP, Frolich M, Lavery DC, 1997. Effectiveness of diabetic insoles to reduce foot pressures. J Foot Ankle Surg. 36, 268-271.

Athanasiou KA, Liu GT, Lavery LA, Lanctot DR, Schenck RC, 1998. Biomechanical topography of human articular cartilage in the first metatarsophalangeal joint. Clin Orthop. 348, 269–281.

Ball KA, Afheldt MJ, 2002. Evolution of foot orthotics-part 1: coherent theory or coherent practice? J Manipulative Physiol Ther. 25, 116-124.

Bandak FA, Tannous RE, Toridis T, 2001. On the development of an osseo-ligamentous finite element model of the human ankle joint. Int J Solids Struct. 38, 1681-1697.

Barani Z, Haghpanahi M, Katoozian H, 2005. Three dimensional stress analysis of diabetic insole: a finite element approach. Technol Health Care. 13, 185-192.

Barry LD, Barry AN, Chen Y, 2002. A retrospective study of standing gastrocnemius-soleus stretching versus night splinting in the treatment of plantar fasciitis. J Foot Ankle Surg. 41, 221-227.

Basmajian JV, Stecko G, 1963. The role of muscles in arch support of the foot. J Bone Joint Surg Am. 45, 1184-1190.

Birke JA, Foto JG, Deepak S, Watson J, 1994. Measurement of pressure walking in footwear used in leprosy. Lepr Rev. 65, 262-271.

Boulton AJ, 2000. The diabetic foot: a global view. Diabetes Metab Res Rev. 16 Suppl 1, S2-5.

Boulton AJ, Betts RP, Franks CI, Ward JD, Duckworth T, 1987. The natural history of foot pressure abnormalities in neuropathic diabetic subjects. Diabetes Res. 5, 73-77.

Boyko EJ, Ahroni JH, Smith DG, Davignon D, 1996. Increased mortality associated with diabetic foot ulcer. Diabet Med. 13, 967-972.

Boyko EJ, Ahroni JH, Stensel V, Forsberg RC, Davignon DR, Smith DG, 1999. A prospective study of risk factors for diabetic foot ulcer. The Seattle Diabetic Foot Study. Diabetes Care. 22, 1036-1042.

Brown GP, Donatelli R, Catlin PA, Wooden MJ, 1995. The effect of two types of foot orthoses on rearfoot mechanics. J Orthop Sports Phys Ther. 21, 258-267.

Brown M, Rudicel S, Esquenazi A, 1996. Measurement of dynamic pressures at the shoe-foot interface during normal walking with various foot orthoses using the FSCAN system. Foot Ankle Int. 17, 152-156.

Brugh AM, Fallat LM, Savoy-Moore RT, 2002. Lateral column symptomatology following plantar fascial release: a prospective study. J Foot Ankle Surg. 41, 365-371.

Bus SA, Lange AD, 2005. A comparison of the 1-step, 2-step, and 3-step protocols for obtaining barefoot plantar pressure data in the diabetic neuropathic foot. Clin Biomech. 20, 892-899.

Bus SA, Ulbrecht JS, Cavanagh PR, 2004. Pressure relief and load redistribution by custom-made insoles in diabetic patients with neuropathy and foot deformity. Clin Biomech. 19, 629-638.

Busch K, Chantelau E, 2003. Effectiveness of a new brand of stock 'diabetic' shoes to protect against diabetic foot ulcer relapse. A prospective cohort study. Diabet Med. 20, 665-669.

Camacho DLA, Ledoux WR, Rohr ES, Sangeorzan BJ, Ching RP, 2002. A three-dimensional, anatomically detailed foot model: A foundation for a finite element simulation and means of quantifying foot-bone position. J Rehabil Res Dev. 39, 401-410.

Carlson RE, Fleming LL, Hutton WC, 2000. The biomechanical relationship between the tendoachilles, plantar fascia and metatarsophalangeal joint dorsiflexion angle. Foot Ankle Int. 21, 18-25.

Caselli A, Pham H, Giurini JM, Armstrong DG, Veves A, 2002. The forefoot-to-rearfoot plantar pressure ratio is increased in severe diabetic neuropathy and can predict foot ulceration. Diabetes Care. 25, 1066–1071.

Cavanagh PR, Rodgers MM, Iiboshi A, 1987. Pressure distribution under symptom-free feet during barefoot standing. Foot Ankle. 7, 262-276.

Chalmers AC, Busby C, Goyert J, Porter B, Schulzer M, 2000. Metatarsalgia and rheumatoid arthritis-a randomized, single blind, sequential trial comparing 2 types of foot orthoses and supportive shoes. J Rheumatol. 27, 1643-1647.

Chang AH, Abu-Faraj ZU, Harris GF, Nery J, Shereff MJ, 1994. Multistep measurement of plantar pressure alterations using metatarsal pads. Foot Ankle Int. 5, 654-660.

Charanya G, Patil KM, Narayanamurthy VB, Parivalavan R, Visvanathan K, 2004. Effect of foot sole hardness, thickness and footwear on foot pressure distribution parameters in diabetic neuropathy. Proc Inst Mech Eng [H]. 218, 431-443.

Chen WP, Ju CW, Tang FT, 2003. Effects of total contact insoles on the plantar stress redistribution: a finite element analysis. Clin Biomech. 18, S17-24.

Chen WP, Tang FT, Ju CW, 2001. Stress distribution of the foot during mid-stance to push-off in barefoot gait: a 3-D finite element analysis. Clin Biomech. 16, 614-620.

Chu TM, Reddy NP, 1995. Stress distribution in the ankle-foot orthosis used to correct pathological gait. J Rehabil Res Dev. 32, 349-360.

Chu TM, Reddy NP, Padovan J, 1995. Three-dimensional finite element stress analysis of the polypropylene, ankle-foot orthosis: static analysis. Med Eng Phys. 17, 372-379.

Cockram CS, 2000. The epidemiology of diabetes mellitus in the Asia-Pacific region. Hong Kong Med J. 6, 43-52.

Cornwall MW, McPoil TG, 1999. Plantar fasciitis: etiology and treatment. J Orthop Sports Phys Ther. 29, 756-760.

Crary JL, Hollis JM, Manoli A, 2003. The effect of plantar fascia release on strain in the spring and long plantar ligaments. Foot Ankle Int. 24, 245–250.

D'Ambrogi E, Giurato L, D'Agostino MA, Giacomozzi C, Macellari V, Caselli A, Uccioli L, 2003. Contribution of plantar fascia to the increased forefoot pressures in diabetic patients. Diabetes Care. 26, 1525-1529.

Davies MS, Weiss GA, Saxby TS, 1999. Plantar fasciitis: how successful is surgical intervention? Foot Ankle Int. 20, 803–807.

Deland JT, de Asla RJ, Sung IH, Ernberg LA, Potter HG. 2005. Posterior tibial tendon insufficiency: which ligaments are involved? Foot Ankle Int. 26, 427-435.

Donahue SW, Sharkey NA, 1999. Strains in the metatarsals during the stance phase of gait: implications for stress fractures. J Bone Joint Surg Am. 81, 1236-1244.

Dul J, 1983. Development of a minimum-fatigue optimization technique for predicting individual muscle forces during human posture and movement with application to the ankle musculature during standing and walking. Ph.D. thesis, Vanderbilt University.

Eng JJ, Pierrynowski MR, 1994. The effect of soft foot orthotics on three-dimensional lower-limb kinematics during walking and running. Phys Ther. 74, 836-844.

Erdemir A, Hamel AJ, Fauth AR, Piazza SJ, Sharkey NA, 2004. Dynamic loading of the plantar aponeurosis in walking. J Bone Joint Surg Am. 86, 546–552.

Erdemir A, Saucerman JJ, Lemmon D, Loppnow B, Turso B, Ulbrecht JS, Cavanagh PR, 2005. Local plantar pressure relief in therapeutic footwear: design guidelines from finite element models. J Biomech. 38, 1798-1806.

Erdemir A, Viveiros ML, Ulbrecht JS, Cavanagh PR, 2006. An inverse finite-element model of heel-pad indentation. J Biomech. in press.

Finni T, Komi PV, Lukkariniemi J, 1998. Achilles tendon loading during walking: application of a novel optic fiber technique. Eur J Appl Physiol Occup Physiol. 77, 289-291.

Fiolkowski P, Brunt D, Bishop M, Woo R, Horodyski M, 2003. Intrinsic pedal musculature support of the medial longitudinal arch: an electromyography study. J Foot Ankle Surg. 42, 327-333.

Frykberg RG, Lavery LA, Pham H, Harvey C, Harkless L, Veves A, 1998. Role of neuropathy and high foot pressures in diabetic foot ulceration. Diabetes Care. 21, 1714-1719.

Gefen A, 2001. Simulations of foot stability during gait characteristic of ankle dorsiflexor weakness in the elderly. IEEE Trans Neural Syst Rehabil Eng. 9, 333-337.

Gefen A, 2002a. Stress analysis of the standing foot following surgical plantar fascia release. J Biomech. 35, 629–637.

Gefen A, 2002b. Biomechanical analysis of fatigue-related foot injury mechanisms in athletes and recruits during intensive marching. Med Biol Eng Comput. 40, 302-310.

Gefen A, 2003a. Plantar soft tissue loading under the medial metatarsals in the standing diabetic foot. Med Eng Phys. 25, 491-499.

Gefen A, 2003b. The in vivo elastic properties of the plantar fascia during the contact phase of walking. Foot Ankle Int. 24, 238-244.

Gefen A, Megido-Ravid M, Azariah M, Itzchak Y, Arcan M, 2001a. Integration of plantar soft tissue stiffness measurements in routine MRI of the diabetic foot. Clin Biomech. 16, 921–925.

Gefen A, Megido-Ravid M, Itzchak Y, 2001b. In vivo biomechanical behaviour of the human heel pad during the stance phase of gait. J Biomech. 34, 1661–1665.

Gefen A, Megido-Ravid M, Itzchak Y, Arcan M, 2000. Biomechanical analysis of the three-dimensional foot structure during gait: a basic tool for clinical applications. J Biomech. Eng. 122, 630–639.

Giddings VL, Beaupre GS, Whalen RT, Carter DR, 2000. Calcaneal loading during walking and running. Med Sci Sports Exerc. 32, 627-634.

Gordois A, Scuffham P, Shearer A, Oglesby A, Tobian JA, 2003. The health care costs of diabetic peripheral neuropathy in the US. Diabetes Care. 26, 1790-1795.

Goske S, Erdemir A, Petre M, Budhabhatti S, Cavanagh PR, 2006. Reduction of plantar heel pressures: Insole design using finite element analysis. J Biomech. In press.

Group TG, 2000. Epidemiology of lower extremity amputation in centres in Europe, North America and East Asia. The global lower extremity amputation study group. Br J Surg. 87, 328-337.

Hansen ML, Otis JC, Kenneally SM, Deland JT, 2001. A closed-loop cadaveric foot and ankle loading model. J Biomech. 34, 551-555.

Harrington C, Zagari MJ, Corea J, Klitenic J, 2000. A cost analysis of diabetic lower-extremity ulcers. Diabetes Care. 23, 1333-1338.

Hayda R, Tremaine MD, Tremaine K, Banco S, Teed K, 1994. Effect of metatarsal pads and their positioning: a quantitative assessment. Foot Ankle Int. 5, 561-566.

Healthcommunities.com, Inc., 2005. (http://www.podiatrychannel.com/anatomy)

Hicks JH, 1954. The mechanics of the foot. II. The plantar aponeurosis and the arch. J Anat. 88, 25-30.

Hodge MC, Bach TM, Carter GM, 1999. Orthotic management of plantar pressure and pain in rheumatoid arthritis. Clin Biomech. 14, 567-575.

Hogan P, Dall T, Nikolov P, 2003. American Diabetes Association. Economic costs of diabetes in the US in 2002. Diabetes Care. 26, 917-932.

Holewski JJ, Moss KM, Stess RM, Graf PM, Grunfeld C, 1989. Prevalence of foot pathology and lower extremity complications in a diabetic outpatient clinic. J Rehabil Res Dev. 26, 35-44.

Hosein R, Lord M, 2000. A study of in-shoe plantar shear in normals. Clin Biomech. 15, 46-53.

Huang CK, Kitaoka HB, An KN, Chao EY, 1993. Biomechanical evaluation of longitudinal arch stability. Foot Ankle. 14, 353–357.

Humphrey AR, Dowse GK, Thoma K, Zimmet PZ, 1996. Diabetes and nontraumatic lower extremity amputations. Incidence, risk factors, and prevention-a 12-year follow-up study in Nauru. Diabetes Care. 19, 710-714.

Imhauser CW, Abidi NA, Frankel DZ, Gavin K, Siegler S, 2002. Biomechanical evaluation of the efficacy of external stabilizers in the conservative treatment of acquired flatfoot deformity. Foot Ankle Int. 23, 727-737.

Imhauser CW, Siegler S, Abidi NA, Frankel DZ, 2004. The effect of posterior tibialis tendon dysfunction on the plantar pressure characteristics and the kinematics of the arch and the hindfoot. Clin Biomech. 19, 161-169.

Interaction foot and ankle, 1999. Primal Picture Ltd., London, UK.

Jacob S, Patil MK, 1999a. Stress analysis in three-dimensional foot models of normal and diabetic neuropathy. Front Med Biol Eng. 9, 211-227.

Jacob S, Patil MK, 1999b. Three-dimensional foot modeling and analysis of stresses in normal and early stage Hansen's disease with muscle paralysis. J Rehabil Res Dev. 36, 252-263.

Johanson MA, Donatelli R, Wooden MJ, Andrew PD, Cummings GS, 1994. Effects of three different posting methods on controlling abnormal subtalar pronation. Phys Ther. 74, 149-158.

Jordan C, Bartlett R, 1995. Pressure distribution and perceived comfort in casual footwear. Gait Posture. 3, 215-220.

Kato H, Takada T, Kawamura T, Hotta N, Torii S, 1996. The reduction and redistribution of plantar pressures using foot orthoses in diabetic patients. Diabetes Res Clin Pract. 31, 115-118.

Kelaher D, Mirka GA, Dudziak KQ, 2000. Effects of semi-rigid arch-support orthotics: an investigation with potential ergonomic implications. Appl Ergon. 31, 515-522.

KHK Stock Gears, 1996. Product Guide and Technical Data, Kohara Gear Industry Co. Ltd., Japan. (http://www.khkgears.co.jp/english/)

Kim KJ, Kitaoka HB, Luo ZP, Ozeki S, Berglund LJ, Kaufman KR, An KN, 2001. An in vitro simulation of the stance phase in human gait. J Musculoskeletal Res. 5, 113-121.

Kim KJ, Uchiyama E, Kitaoka HB, An KN, 2003. An in vitro study of individual ankle muscle actions on the center of pressure. Gait Posture. 17, 125-131.

Kim W, Voloshin AS, 1995. Role of plantar fascia in the load bearing capacity of the human foot. J Biomech. 28, 1025-1033.

Kirby KA, 2001. What future direction should podiatric biomechanics take? Clin Podiatr Med Surg. 18, 719-723.

Kitagawa Y, Ichikawa H, King AI, Begeman PC, 2000. Development of a human ankle/foot model. In: Kajzer J, Tanaka E, Yamada H, (Eds.), Human Biomechanics and Injury Prevention. Springer: Tokyo. pp. 117–122.

Kitaoka HB, Luo ZP, Growney ES, Berglund LJ, An KN, 1994a. Material properties of the plantar aponeurosis. Foot Ankle Int. 15, 557-560.

Kitaoka HB, Schaap EJ, Chao EY, An KN, 1994b. Displaced intra-articular fractures of the calcaneus treated non-operatively. Clinical results and analysis of motion and ground-reaction and temporal forces. J Bone Joint Surg Am. 76, 1531-1540.

Kitaoka HB, Lundberg A, Luo ZP, An KN, 1995. Kinematics of the normal arch of the foot and ankle under physiologic loading. Foot Ankle Int. 16, 492-429.

Kitaoka HB, Luo ZP, An KN, 1997a. Subtalar arthrodesis versus flexor digitorum longus tendon transfer for severe flatfoot deformity: an in vitro biomechanical analysis. Foot Ankle Int. 18, 710-715.

Kitaoka HB, Luo ZP, An KN, 1997b. Effect of plantar fasciotomy on stability of arch of foot. Clin Orthop. 344, 307–312.

Kitaoka HB, Luo ZP, An KN, 1997c. Mechanical behavior of the foot and ankle after plantar fascia release in the unstable foot. Foot Ankle Int. 18, 8-15.

Kitaoka HB, Luo ZP, An KN, 1997d. Effect of the posterior tibial tendon on the arch of the foot during simulated weightbearing: biomechanical analysis. Foot Ankle Int. 18, 43-46.

Kitaoka HB, Luo ZP, An KN, 1998. Three-dimensional analysis of flatfoot deformity: cadaver study. Foot Ankle Int. 19, 447-451.

Kitaoka HB, Kura H, Luo ZP, An KN, 2000. Calcaneocuboid distraction arthrodesis for posterior tibial tendon dysfunction and flatfoot: a cadaveric study. Clin Orthop. 381, 241-247.

Kitaoka HB, Luo ZP, Kura H, An KN, 2002. Effect of foot orthoses on 3-dimensional kinematics of flatfoot: a cadaveric study. Arch Phys Med Rehabil. 83, 876-879.

Klaesner JW, Hastings MK, Zou D, Lewis C, Mueller MJ, 2002. Plantar tissue stiffness in patients with diabetes mellitus and peripheral neuropathy. Arch Phys Med Rehabil. 83, 1796-1801.

Kogler GF, Solomonidis SE, Paul JP, 1995. In vitro method for quantifying the effectiveness of the longitudinal arch support mechanism of a foot orthosis. Clin biomech. 10, 245-252.

Kogler GF, Solomonidis SE, Paul JP, 1996. Biomechanics of longitudinal arch support mechanisms in foot orthoses and their effect on plantar aponeurosis strain. Clin biomech. 11, 243-252.

Kogler GF, Veer FB, Solomonidis SE, Paul J, Illisois S, 1999. The influence of medial and lateral placement of orthotic wedges loading of the plantar aponeurosis. J Bone Joints Surg. 81, 1404-1413.

Kohls-Gatzoulis J, Angel JC, Singh D, Haddad F, Livingstone J, Berry G, 2004. Tibialis posterior dysfunction: a common and treatable cause of adult acquired flatfoot. BMJ. 329, 1328-1333.

Kulig K, Burnfield JM, Reischl S, Requejo SM, Blanco CE, Thordarson DB, 2006. Effect of foot orthoses on tibialis posterior activation in persons with pes planus. Med Sci Sports Exerc. in press

Landorf KB, Keenan AM, 2000. Efficacy of foot orthoses. What does the literature tell us? J Am Podiatr Med Assoc. 90, 149-158.

Lavery LA, Armstrong DG, Vela SA, Quebedeaux TL, Fleischli JG, 1998. Practical criteria for screening patients at high risk for diabetic foot ulceration. Arch Intern Med. 158, 157-162.

Lavery LA, Armstrong DG, Wunderlich RP, Tredwell J, Boulton AJ, 2003. Predictive value of foot pressure assessment as part of a population-based diabetes disease management program. Diabetes Care. 26, 1069-1073.

Lavery LA, Vela SA, Fleischli JG, Armstrong DG, Lavery DC, 1997. Reducing plantar pressure in the neuropathic foot. A comparison of footwear. Diabetes Care. 20, 1706-1710.

Lemmon D, Shiang TY, Hashmi A, Ulbrecht JS, Cavanagh PR, 1997. The effect of insoles in therapeutic footwear: a finite-element approach. J Biomech. 30, 615-620.

Leung AK, Mak AF, Evans JH, 1998. Biomedical gait evaluation of the immediate effect of orthotic treatment for flexible flat foot. Prosthet Orthot Int. 22, 25-34.

Leung HB, Ho YC, Carnett J, Lam PK, Wong WC, 2001. Diabetic foot ulcers in the Hong Kong Chinese population: retrospective study. Hong Kong Med J. 7, 350-355.

Lewis G, 2003. Finite element analysis of a model of a therapeutic shoe: effect of material selection for the outsole. Biomed Mater Eng. 13, 75-81.

Linge K, 1996. A preliminary objective evaluation of leprosy footwear using in-shoe pressure measurement. Acta Orthop Belg., 62, S18-22.

Lobmann R, Kasten G, Kasten U, Lehnert H, 2002. Association of increased plantar pressures with peripheral sensorimotor and peripheral autonomic neuropathy in Type 2 diabetic patients. Diabetes Nutr Metab. 15, 165-168.

Lobmann R, Kayser R, Kasten G, Kasten U, Kluge K, Neumann W, Lehnert H, 2001. Effects of preventative footwear on foot pressure as determined by pedobarography in diabetic patients: a prospective study. Diabet Med. 18, 314-319.

Lord M, Hosein R, 2000. A study of in-shoe plantar shear in patients with diabetic neuropathy. Clin Biomech. 15, 278-283.

Luger E, Nissan M, Karpf A, Steinberg E, Dekel S, 2001. Dynamic pressures on the diabetic foot. Foot Ankle Int. 22, 715-719.

Luo ZP, Kitaoka HB, Hsu HC, Kura H, An KN, 1997. Physiological elongation of ligamentous complex surrounding the hindfoot joints: in vitro biomechanical study. Foot Ankle Int. 18, 277-283.

Lusardi M, Nielsen C, 2000. Orthotics and prosthetics in rehabilitation, Boston, Butterworth-Heinemann.

Mantey I, Foster AV, Spencer S, Edmonds ME, 1999. Why do foot ulcers recur in diabetic patients? Diabet Med. 16, 245-249.

McCulloch MU, Brunt D, Vander Linden D, 1993. The effect of foot orthotics and gait velocity on lower limb kinematics and temporal events of stance. J Orthop Sports Phys Ther. 17, 2-10.

McPoil TG, Cornwall MW, 1992. Effect of insole material on force and plantar pressures during walking. J Am Podiatr Med Assoc. 82, 412-416.

McPoil TG, Cornwall MW, 2000. The effect of foot orthoses on transverse tibial rotation during walking. J Am Podiatr Med Assoc. 90, 2-11.

McPoil TG, Hunt GC, 1995. Evaluation and management of foot and ankle disorders: present problems and future directions. J Orthop Sports Phys Ther. 21, 381-388.

Miller JE, Nigg BM, Liu W, Stefanyshyn DJ, Nurse MA, 2000. Influence of foot, leg and shoe characteristics on subjective comfort. Foot Ankle Int. 21, 759-767.

Miller-Young JE, Duncan NA, Baroud G, 2002. Material properties of the human calcaneal fat pad in compression: experiment and theory. J Biomech. 35, 1523–1531.

Mosier SM, Pomeroy G, Manoli A, 1999. Pathoanatomy and etiology of posterior tibial tendon dysfunction. Clin Orthop. 365, 12-22.

Moss SE, Klein R, Klein BE, 1999. The 14-year incidence of lower-extremity amputations in a diabetic population. The Wisconsin Epidemiologic Study of Diabetic Retinopathy. Diabetes Care. 22, 951-959.

Mueller MJ, Sinacore DR, Hoogstrate S, Daly L, 1994. Hip and ankle walking strategies: effect on peak plantar pressures and implications for neuropathic ulceration. Arch Phys Med Rehabil. 75, 1196-1200.

Mundermann A, Nigg BM, Humble RN, Stefanyshyn DJ, 2003. Orthotic comfort is related to kinematics, kinetics, and EMG in recreational runners. Med Sci Sports Exerc. 35, 1710-1719.

Mundermann A, Stefanyshyn DJ, Nigg BM, 2001. Relationship between footwear comfort of shoe inserts and anthropometric and sensory factors. Med Sci Sports Exerc. 33, 1939-1945.

Murphy GA, Pneumaticos SG, Kamaric E, Noble PC, Trevino SG, Baxter DE, 1998. Biomechanical consequences of sequential plantar fascia release. Foot Ankle Int. 19, 149-152.

Murray HJ, Young MJ, Hollis S, Boulton AJ, 1996. The association between callus formation, high pressures and neuropathy in diabetic foot ulceration. Diabet Med. 13, 979-982.

Nakamura S, Crowninshield RD, Cooper RR, 1981. An analysis of soft tissue loading in the foot—a preliminary report. Bull Prosthet Res. 18, 27-34.

Nawoczenski DA, Cook TM, Saltzman CL, 1995. The effect of foot orthotics on three-dimensional kinematics of the leg and rearfoot during running. J Orthop Sports Phys Ther. 21, 317-327.

Nester CJ. Hutchins S. Bowker P, 2001. Effect of foot orthoses on rearfoot complex kinematics during walking gait. Foot Ankle Int. 22, 133-139.

Neumann DA, 2002, Kinesiology of the musculoskeletal system: foundations for physical rehabilitation, Publisher St. Louis: Mosby.

Nigg BM, Bobbert M, 1990. On the potential of various approaches in load analysis to reduce the frequency of sports injuries. J Biomech. 23, Suppl 1, 3-12.

Nigg BM, Khan A, Fisher V, Stefanyshyn D, 1998. Effect of shoe insert construction on foot and leg movement. Med Sci Sports Exerc. 30, 550-555.

Nigg BM, Nurse MA, Stefanyshyn DJ, 1999. Shoe inserts and orthotics for sport and physical activities. Med Sci Sports Exerc. 31, S421-428.

Nigg BM, Stergiou P, Cole G, Stefanyshyn D, Mundermann A, Humble N, 2003. Effect of shoe inserts on kinematics, center of pressure, and leg joint moments during running. Med Sci Sports Exerc. 35, 314-319.

Niki H, Ching RP, Kiser P, Sangeorzan BJ, 2001. The effect of posterior tibial tendon dysfunction on hindfoot kinematics.Foot Ankle Int. 22, 292-300.

Novick A, Stone J, Birke JA, Brasseaux DM, Broussard JB, Hoard AS, Hawkins ES, 1993. Reduction of plantar pressure with the rigid relief orthosis. J Am Podiatr Med Assoc. 83, 115-122.

Oatis CA, 2004. Kinesiology: the mechanics and pathomechanics of human movement, Baltimore, MD: Lippincott Williams and Wilkins, Edition 1st ed.

Onwuanyi ON, 2000. Calcaneal spurs and plantar heel pad pain. Foot. 10, 182–185.

Opila KA, Wagner SS, Schiowitz S, Chen J, 1988. Postural alignment in barefoot and high-heeled stance. Spine. 13, 542-547.

Patil KM, Charanya G, Prabhu GK, 2002. Optical pedobarography for assessing neuropathic feet in diabetic patients—a review. Int J Low Extrem Wounds. 1, 93-103.

Perry J, 1992. Gait analysis: normal and pathological function. Publisher Thorofare, N.J.: SLACK.

Pfeffer G, Bacchetti P, Deland J, Lewis A, Anderson R, Davis W, Alvarez R, Brodsky J, Cooper P, Frey C, Herrick R, Myerson M, Sammarco J, Janecki C, Ross S, Bowman M, Smith R, 1999. Comparison of custom and prefabricated orthoses in the initial treatment of proximal plantar fasciitis. Foot Ankle Int. 20, 214-221.

Phadke MS, 1989. Quality engineering using robust design. Publisher Englewood Cliffs, N.J.: Prentice Hall.

Pham H, Armstrong DG, Harvey C, Harkless LB, Giurini JM, Veves A, 2000. Screening techniques to identify people at high risk for diabetic foot ulceration: a prospective multicenter trial. Diabetes Care. 23, 606-611.

Pitei DL, Foster A, Edmonds M, 1999. The effect of regular callus removal on foot pressures. J Foot Ankle Surg. 38, 251-255.

Probe RA, Baca M, Adams R, Preece C, 1999. Night splint treatment for plantar fasciitis. A prospective randomized study. Clin Orthop. 368, 190-195.

Raspovic A, Newcombe L, Lloyd J, Dalton E, 2000. Effect of customized insoles on vertical plantar pressures in sites of previous neuropathic ulceration in the diabetic foot. Foot, 10, 133-138.

Razeghi M, Batt ME, 2000. Biomechanical analysis of the effect of orthotic shoe inserts: a review of the literature. Sports Med. 29, 425-438.

Redmond A, Lumb PS, Landorf K, 2000. Effect of cast and noncast foot orthoses on plantar pressure and force during normal gait. J Am Podiatr Med Assoc. 90, 441-449.

Reiber GE, Smith DG, Wallace C, Sullivan K, Hayes S, Vath C, Maciejewski ML, Yu O, Heagerty PJ, LeMaster J, 2002. Effect of therapeutic footwear on foot reulceration in patients with diabetes: a randomized controlled trial. JAMA. 287, 2552-2558.

Root ML, Orien WP, Weed JH, 1971. Biomechanical Examination of the Foot: Clinical Biomechanics Vol. 1. Los Angels, CA: Clinical Biomechanics Corp.

Sage RA, Webster JK, Fisher SG, 2001. Outpatient care and morbidity reduction in diabetic foot ulcers associated with chronic pressure callus. J Am Podiatr Med Assoc. 91, 275–279.

Salathe EP, Arangio GA, 2002. A biomechanical model of the foot: the role of muscles, tendons, and ligaments. J Biomech Eng. 124, 281-287.

Schafer AT, Kaufmann JD, 1999. What happens in freezing bodies? Experimental study of histological tissue change caused by freezing injuries. Forensic Sci Int. 102, 149-158.

Scott SH, Winter DA, 1993. Biomechanical model of the human foot: kinematics and kinetics during the stance phase of walking. J Biomech. 26, 1091-1104.

Selth CA, Francis BE, 2000. Review of non-functional plantar heel pain. Foot. 10, 97-104.

Shiang TY, 1997. The nonlinear finite element analysis and plantar pressure measurement for various shoe soles in heel region. Proc Natl Sci Counc Repub China B. 21, 168-174.

Siegler S, Block J, Schneck CD, 1988. The mechanical characteristics of the collateral ligaments of the human ankle joint. Foot Ankle. 8, 234-242.

Simkin A, 1982. Structural analysis of the human foot in standing posture, Ph.D. thesis, Tel Aviv University, Tel Aviv, Israel.

Sorensen TI, 2000. The changing lifestyle in the world. Body weight and what else? Diabetes Care. 23, Suppl 2:B1-4.

Spears IR, Miller-Young JE, Waters M, Rome K, 2005. The effect of loading conditions on stress in the barefooted heel pad.Med Sci Sports Exerc. 37, 1030-1036.

Spencer S, 2000. Pressure relieving interventions for preventing and treating diabetic foot ulcers. Cochrane Database Syst Rev. 3, CD002302.

Stacoff A, Reinschmidt C, Nigg BM, van den Bogert AJ, Lundberg A, Denoth J, Stussi E, 2000. Effects of foot orthoses on skeletal motion during running. Clin Biomech. 15, 54-64.

Stess RM, Jensen SR, Mirmiran R, 1997. The role of dynamic plantar pressures in diabetic foot ulcers. Diabetes Care. 20, 855-858.

Syngellakis S, Arnold MA, Rassoulian H, 2000. Assessment of the non-linear behaviour of plastic ankle foot orthoses by the finite element method. Proc Inst Mech Eng [H]. 214, 527-539.

Taguchi G, 2005. Taguchi's quality engineering handbook. Publisher Hoboken, New Jersey: Wiley.

Thomas VJ, Patil KM, Radhakrishnan S, 2004. Three-dimensional stress analysis for the mechanics of plantar ulcers in diabetic neuropathy. Med Biol Eng Comput. 42, 230-235.

Thordarson DB, Schmotzer H, Chon J, Peters J, 1995. Dynamic support of the human longitudinal arch. A biomechanical evaluation. Clin Orthop. 316, 165-172.

Tochigi Y, 2003. Effect of arch supports on ankle-subtalar complex instability: A biomechanical experimental study. Foot Ankle Int. 24, 634-639.

Tseng CH, 2003. Prevalence and risk factors of diabetic foot problems in Taiwan: a cross-sectional survey of non-type 1 diabetic patients from a nationally representative sample. Diabetes Care. 26, 3351.

Tsung BY, Zhang M, Mak AF, Wong MW, 2004. Effectiveness of insoles on plantar pressure redistribution. J Rehabil Res Dev. 41, 767-774.

Tyrrell W, 1999. Orthotic intervention in patients with diabetic foot ulceration. J Wound Care. 8, 530-532.

Van Gheluwe B, Dananberg HJ, 2004. Changes in plantar foot pressure with in-shoe varus or valgus wedging. J Am Podiatr Med Assoc. 94, 1-11.

Verdejo R, Mills NJ, 2004. Heel-shoe interactions and the durability of EVA foam running-shoe midsoles. J Biomech. 37, 1379-1386.

Veves A, Murray HJ, Young MJ, Boulton AJ, 1992. The risk of foot ulceration in diabetic patients with high foot pressure: a prospective study. Diabetologia. 35, 660-663.

Viswanathan V, Madhavan S, Gnanasundaram S, Gopalakrishna G, Das BN, Rajasekar S, Ramachandran A, 2004. Effectiveness of different types of footwear insoles for the diabetic neuropathic foot: a follow-up study. Diabetes Care. 27, 474-477.

Wapner KL, Chao W, 1999. Nonoperative treatment of posterior tibial tendon dysfunction. Clin Orthop. 365, 39-45.

Wapner KL, Sharkey PF, 1991. The use of night splints for treatment of recalcitrant plantar fasciitis. Foot Ankle. 12, 135-137.

Warren BL, 1990. Plantar fasciitis in runners. Treatment and prevention. Sports Med. 10, 338-345.

Wild S, Roglic G, Green A, Sicree R, King H, 2004. Global prevalence of diabetes: estimates for the year 2000 and projections for 2030. Diabetes Care. 27, 1047-1053.

Windle CM, Gregory SM, Dixon SJ, 1999. The shock attenuation characteristics of four different insoles when worn in a military boot during running and marching. Gait Posture. 9, 31-37.

Woelffer KE, Figura MA, Sandberg NS, Snyder NS, 2000. Five-year follow-up results of instep plantar fasciotomy for chronic heel pain. J Foot Ankle Surg. 39, 218-223.

Woodburn J, Barker S, Helliwell PS, 2002. A randomized controlled trial of foot orthoses in rheumatoid arthritis. J Rheumatol. 29, 1377-1383.

World Health Organization, 2004. Diabetes Action Now: An initiative of the World Health Organization and the International Diabetes Federation, by: World Health Organization, 20 Avenue Appia, 1211 Geneva 27, Switzerland.

World Health Organization, 2005. (http://www.who.int/diabetes).

Wright D, Rennels D, 1964. A study of the elastic properties of plantar fascia. J Bone Joint Surg Am. 46, 482-492.

Wu G, Siegler S, Allard P, Kirtley C, Leardini A, Rosenbaum D, Whittle M, D'Lima DD, Cristofolini L, Witte H, Schmid O, Stokes I; Standardization and Terminology Committee of the International Society of Biomechanics, 2002. ISB recommendation on definitions of joint coordinate system of various joints for the reporting of human joint motion-part I: ankle, hip, and spine. J Biomech. 35, 543-548.

Young MJ, Boulton AJ, MacLeod AF, Williams DR, Sonksen PH, 1993. A multicentre study of the prevalence of diabetic peripheral neuropathy in the United Kingdom hospital clinic population. Diabetologia. 36, 150-154.

Yu JS, Spigos D, Tomczak R, 1999. Foot pain after a plantar fasciotomy: an MR analysis to determine potential causes. J Comput Assist Tomogr. 23, 707-712.

Zhang M, Mak AF, 1999. In vivo skin frictional properties. Prosthet Orthot Int. 23, 135-141.

Zheng YP, Choi YK, Wong K, Chan S, Mak AF, 2000. Biomechanical assessment of plantar foot tissue in diabetic patients using an ultrasound indentation system. Ultrasound Med Biol. 26, 451-456.